OPTIMAL AND NEAR-OPTIMAL MEDIUM RANGE AIR-TO-AIR MISSILE GUIDANCE AGAINST MANEUVERING TARGETS

by

Renjith R. Kumar

Dissertation submitted to the Faculty of the

Virginia Polytechnic Institute and State University

in partial fulfillment of the requirements for the degree of

Doctor of Philosophy

in

Aerospace and Ocean Engineering

APPROVED:

E.M. Cliff, Chairman

F.H. Lutze

J.A. Burns

L.G. Kraige

W.H. Mason

June 19, 1989

Blacksburg, Virginia

OPTIMAL AND NEAR-OPTIMAL MEDIUM RANGE AIR-TO-AIR MISSILE GUIDANCE AGAINST MANEUVERING TARGETS

by

Renjith R. Kumar

E.M. Cliff, Chairman

Aerospace and Ocean Engineering

(ABSTRACT)

Optimal intercept trajectories for a boost-sustain-coast medium-range air-to-air missile are synthesized using optimal control theory. Optimality in time/range/energy at intercept of a target is the main objective. Attainable sets and their boundaries are obtained and used to generate optimal intercept points in a three-dimensional scenario.

A three-phase closed-loop guidance scheme is used to generate an efficient guidance law against a maneuvering target. In the present study, target maneuvers are restricted to the horizontal plane.

An initial boost-phase with near-optimal guidance in the presence of active control constraints and thrust switches is simulated. Target maneuvers are neglected during this phase. A new method of gain evaluation is detailed. A midcourse guidance scheme with neighboring guidance, transversal comparisons, and chasing center-of-attainability of target to augment performance is studied. Modifications in terminal guidance using proportional navigation, such as

chasing the center-of-attainability of target, altitude shaping, and drag-resolution schemes are used to attempt better performance at intercept.

A composite guidance strategy using a combination of neighboring guidance and proportional navigation for the midcourse guidance is introduced. The excellent performance of this guidance strategy and the improvement in storage requirements for on-board use make it a very special scheme.

Acknowledgements

I am deeply indebted to Dr. Cliff who took me under his wings after the sudden and untimely demise of my dear teacher and guide Dr. Kelley. The sincerity and constant encouragement I have enjoyed under them is deeply appreciated. I shall be eternally obliged to them.

I wish to thank Dr. Burns, first for his class on calculus-of-variations - a real eye-opener and for all the support during the blues in early spring 1988. Dr. Lutze has been a steady and constant support all through my stay at VPI and I thank him for all the help given to me in this venture. I would like to thank Dr. Kraige and Dr. Mason for serving on my committee.

I would love to take this opportunity to thank , a great friend, a wonderful thinker - hats off for all the arguments and discussions! I greatly appreciate all my friends and colleagues, one too many, for all the insight given to me.

This research was supported in part by the Air Force Armament Laboratory, Eglin AFB under contract F08635-86-K-0390 and in part by DARPA under contract (ACMP) F49620-87-C-0116.

Finally let me acknowledge all the help given to me by my wife in the last two hectic years and my parents and brother who keep waving the banner for me!

Dedication

To my wonderful parents and to the loving memory of Dr. Kelley

1.0 Table of Contents

2.0 List of Figures

3.0 List of Tables

Chapter 1: Introduction

While efficient intercept has been of interest at least since the time of Sir Francis Drake and his 'manouevre board', it was the requirements of the Second World War that prompted serious study of the problem of guidance against a maneuvering target. **Pure-pursuit , command to line-of-sight, collision course**, and **proportion navigation** (pro-nav) were some developments from this interest [1]. Pro-nav guidance was developed in the U.S. by Yuan [2], Newell [3] and Spitz [4]. Murtaugh and Criel [5] in their study closed the classic approach era to pro-nav. Later studies demonstrated that pro-nav guidance produced a control that was optimal, in a specified sense, for certain linear models [6-9]. By incorporating additional features in the system model, it was possible to extend classical pro-nav and improve the end-game performance [10]. Even today, the guidance for most short-range air-to-air missiles is based on pro-nav or one of its variants.

While the historical development has been focused on short-range intercept problems, it is clear that medium-range and long-range missiles presently in

vogue require an energy/time/range efficient guidance algorithm. Most of the missiles currently under research, like the **EMRAAT**, employ advanced guidance schemes based on optimal control theory with optimized parameters typically being time-to-intercept, range, and average velocity.

There are three phases of medium or long-range missile flight and their characteristics are sufficiently different so as to require the use of more than one guidance scheme [1]. A typical flight would include boost, midcourse, and terminal guidance phases.

The **boost phase** is from initial firing to the time when the boost motor shuts down (and possibly initiates staging). The missile continues in flight either under sustained power or coasting. The character of range/time optimal flight during this early boost phase is in general radically different from the **midcourse phase.** During **terminal guidance** the shortened time-line generally requires autonomous guidance of the missile. In association with the intercept of a target, there are three classical methods of **homing** - active homing, semi-active homing and passive homing [1], the choice being left to the mission-at-hand and capabilities of the missile.

Much of the research in the area of midcourse guidance has employed **reduced-order** modelling to obtain near-optimal feedback laws [11,12]. Such models are based on the mathematical theory of **singular perturbation** ; applications in the broad area of flight control were pioneered by Kelley [13].

Recently it has been shown [14,15] that for vertical plane motions, the control histories produced by various reduced-order models do not provide very accurate approximations of the corresponding control for a point-mass model. It is expected that the three-dimensional flight would also exhibit these differences.

For this reason the major purpose of this study has been to obtain a range/energy/time efficient guidance law for an interceptor missile modelled as a **point-mass in three-dimensional atmospheric flight**, using the principles of optimal control theory. The model of the missile used has a **boost-sustain-coast** propulsion system. The control variables are the horizontal and vertical load-factors. Extremal fields and neighboring extremal ideas [16] are used hand in hand with the nominal solutions to develop a closed-loop guidance scheme.

The basic concept of developing a guidance algorithm for optimal or near-optimal intercept involves **flooding** the state space with extremals and selecting the right extremal for real-time on-board use. Each extremal is solved via the Pontryagin's Minimum Principle [17,18] leading to a two-point-boundary-value-problem (**TPBVP**). These are solved using a multiple-shooting algorithm **BOUNDSCO** [19] and the solutions give open-loop trajectories. Storage of nominal trajectories and associated gains for all permutations of end-conditions is impossible. Suitable discretization of the state-space is required such that on-board storage is feasible. The accuracy of linearization about reference trajectory for large perturbations in state or terminal target set is to be studied.

The down-range and cross-range space is flooded with optimal intercept points for fixed final time. Optimality implies maximum/minimum down-range for a given cross-range or vice-versa. The final energy and altitude; initial energy, altitude, and heading of the missile are specified equalities or inequalities. The study shows possible appearances of **holes** in the attainability sets (defined in Chapter 4) of the missile. Homotopy or continuation methods to obtain the boundary of the attainability sets are interesting and are discussed in detail. Families of down-range - cross-range charts with various end-conditions can be stored and used for real-time on-board guidance.

The nominal optimal control problem solved to obtain the attainable set boundary is one of maximizing/minimizing range for fixed time-of-flight. The attainable set boundary corresponding to maximum range is of real significance in the guidance scheme. However, the entire attainability set is developed to picture the capabilities of the missile. Once the missile is launched, the real motive is no longer to maximize range at the given time. This can be seen clearly in the case of a target turn away. Assuming that the nominal is based on a head-on engagement, if the target turns away, the predicted intercept time and range will increase markedly. The nominal optimal control solutions used for reference is a reciprocal problem : minimum-time to intercept. This nominal solution is a scaled version of the maximum-range solution, except for pathological cases.

The optimality of minimizing regular or **regularized** extremals is checked for conjugate points [20,21,22] and in this connection, a new matrix and its governing matrix differential equation has been derived with suitable boundary conditions. The new matrix satisfies a Riccati-type differential equation and its finiteness is checked for **no conjugate point** along the test extremal.

The guidance scheme as explained earlier is divided into three segments. In the first boost/injection phase, target maneuvering is neglected and the guidance takes into consideration only the perturbations in missile's state from the nominal. A simple efficient method of gain evaluation is discussed which has not been found in literature. A comparison of this method with other forms of gain evaluation is also presented. High lofting and turning are essential features of this part of the trajectory. Hence guidance in presence of active control constraints and associated switching structures are simulated and compared with optimal trajectories.

The second phase, namely, midcourse guidance is longest in duration. Target maneuvers and state perturbations are both considered in this analysis. Gain-indexing using performance-index-to-go [23,24] and clock-time are compared. Performance augmentation using **center-of-attainability** of the target as a pseudo-target is realized to take care of all possible target maneuvers. This is used to prevent sudden large changes in the terminal target set.

The final or terminal phase is a well researched area. However, variations of proportional-navigation has been used to check and validate the results at the end of midcourse guidance. **Pure** and **true** pro-nav schemes are simulated for the terminal guidance. Morover, classical three-dimensional pro-nav [25] using the same idea of pseudo-target chasing (with the pseudo-target fairing to the real target as time-to-go becomes smaller) is discussed. Improvement of pro-nav is attempted using **drag-resolution** schemes and **altitude shaping** .

Simulation of the missile guidance is performed with different target maneuvers. However, for simplicity, only target maneuvers in the horizontal plane are considered. A model of a constant velocity target whose center-of-attainability is chased is the first model. Even-though the target model is simple, it requires updating of the change in terminal surface at every instant of time. Secondly, a constant velocity target which is initially advancing towards the missile, turning away at some point (continues turning at maximum load-factor until the line-of-sight projection in the horizontal plane culminates in a tail-chase) followed by fleeing in a straight line is simulated. Finally, a more realistic target model (in horizontal plane) using Shinar's **missile avoidance maneuvers of longer duration** [26] is used. The target model has acceleration and turning capabilities and uses feed-back control for the turning load-factor. This target model uses the principles of singular perturbation theory [27] applied to a zero-sum differential game [28].

Missile strategies using near-optimal perturbation guidance against these target models reveal a new strategy christened as **half-pn** which increases the versatility of the medium range missile. The improvement in storage requirements for on-board applications, the simplicity of the algorithm and the total enhancement of the guidance scheme against maneuvering targets is understood. The deficiency of near-optimal schemes using linearization about a reference trajectory, in the sense that the linearization becomes inaccurate for large perturbations from the nominal and the inability to perform guidance until final time due to unbounded gains etc., yields the idea of **half-pn** - a very special scheme. Extension of target maneuvers in three-dimensions with suitable definitions for its center-of attainability can also be envisioned.

The material in the following sections are arranged as follows: Chapter 2 contains the missile model and the problem formulation. The aerodynamic and propulsive models are discussed in detail with numerics in Appendix A. In Chapter 3, the synthesis of the optimal trajectory, numerical examples, and necessary conditions for optimality is explained. In Chapter 4, the homotopy methods in constructing the boundary of attainable sets and the nature of the attainable sets are dealt with. Regularization of extremals and sufficiency conditions for optimality, including conjugate point testing is detailed. Appendix B contains the derivation of suitable matrix differential equations for the same. In Chapter 5, the neighboring guidance scheme for the boost-phase, including new methods of efficient gain evaluation and guidance with active control constraints is investigated. Chapter 6 similarly contains guidance during

midcourse. This also includes comparisons of gain-indexing and pseudo-target chasing for performance augmentation. In the next chapter, terminal guidance is treated carefully with its variants and modifications. An introduction to a composite strategy called half-pn and its feasibility is discussed in Chapter 8. In the last section, Chapter 9, the study is concluded with remarks, inferences, and suggestions.

Chapter 2: Modelling and Problem Formulation

2.1: Overview

This chapter introduces the problem formulation, discussing the system dynamics and the relevant differential equations. The point-mass model of the air-to-air missile capable of maneuvers in three-dimensional space, the associated state and control variables, and the algebraic constraints are presented. The nominal optimal control problem and its variants to construct reference trajectories for the guidance scheme are detailed.

2.2: Missile Model

The air-to-air missile model is usually a nonlinear system. This can be most generally written as:

$$\dot{X} = f(X,u,t) \tag{2.1}$$

where X is a vector denoting the state variables, u a vector of control variables and t showing possible time-dependency of the system model. The differential equations are valid during the time $t_0 \leq t \leq t_f$, where t_0 indicates initial time and t_f the terminal or final time, which may be fixed or free.

The boundary conditions for the state variables are initial conditions $X(t_0) = X_0$ and the target set $[X(t_f), t_f] \in \Theta_f$. The control vector is selected from a control constraint set $u(t) \in \Omega$.

For the specific missile model to study range/time/energy efficient intercept, we assume six states and two control variables, i.e.,

$X = [x,y,h,E,\gamma,\chi]^T$ and $u = [n_v, n_h]^T$.

The state variables are the down-range x, the cross-range y, altitude h, specific energy denoted by E, the flight-path angle γ as defined in standard literature and χ, the heading angle measured from the down-range axis. The control variables are n_v and n_h ; the vertical load-factor and the horizontal load-factor respectively. The control variables used above are algebraically related to n , the resultant load-factor and μ_b , the bank-angle by the formulae, $n_v = n \cos(\mu_b)$ and $n_h = n \sin(\mu_b)$.

The following assumptions are made in deriving the three-dimensional point-mass model of the missile.

- Flat earth model.
- Gravitational acceleration is independent of altitude.

- Air-density variation with altitude is realistic.

The first-order ordinary differential equations governing the three-dimensional motion of the missile are:

$$\dot{x} = V \cos\gamma \cos\chi \tag{2.2}$$

$$\dot{y} = V \cos\gamma \sin\chi \tag{2.3}$$

$$\dot{h} = V \sin\gamma \tag{2.4}$$

$$\dot{E} = \frac{V}{W(t)} (T(t) - D(h,M,n)) \tag{2.5}$$

$$\dot{\gamma} = \frac{g}{V} (n_v - \cos\gamma) \tag{2.6}$$

$$\dot{\chi} = \frac{g}{V} \left(\frac{n_h}{\cos\gamma}\right) \tag{2.7}$$

The specific energy, which is the sum of the specific kinetic energy and specific potential energy, was first introduced by Kaiser [29] in the singular perturbation analysis of flight performance of aircrafts. The specific energy has been used here instead of the magnitude of velocity V for no special reason. It is important to note here that the characteristics of the solution will not change due to this choice of variable. The velocity at any instant is obtained from the algebraic equation:

$$V = \sqrt{2g\,(E - h)} \tag{2.8}$$

Here n denotes the resultant load-factor, which is related to the horizontal and vertical load-factors by the simple relation $n = \sqrt{(n_v^2 + n_h^2)}$.

n is always a positive quantity. g denotes the acceleration due to gravity at sea-level. The aerodynamic and propulsive model used for the missile is detailed in Appendix A. The functional dependence of thrust T and drag D is as given in Eq. (2.5).

The propulsion is of **boost-sustain-coast** type. The thrust and weight histories of the missile are specified functions of time. The time histories of the above are shown in Fig. {A.1,A.2}. These imply the explicit dependence of time in the differential equations. The graphs of energy and velocity can exhibit slope discontinuities at the switching points.

The control variables n_v and n_h are constrained by two limits as shown in Appendix A. These are the structural limit corresponding to maximum control surface deflection and the aerodynamic limit which is a function of speed and atmospheric properties indicating a possible stall limit.

2.3: Problem Formulation

The basic idea behind this study is to obtain an "efficient" intercept of a maneuvering target. The term "efficient" indicates time/range/energy optimality. The guidance scheme for the efficient intercept involves flooding the state space with extremals and then applying neighboring near-optimal guidance.

Generation of extremals for the above requires the solution of suitably formulated optimal control problems. The variants of the optimal control problems used are carefully detailed in this section.

The general optimal control problem to be considered is a Bolza type problem with a performance index to be minimized of the form:

$$\mathcal{J} = [\phi\,(X(t_f), t_f)\,] + \int_{t_0}^{t_f} L(X, u, t)\,dt \tag{2.9}$$

where, $\phi\,(X(t_f), t_f)$ is a scalar terminal cost function and $L\,(X, u, t)$ denotes a scalar integral cost function. The equivalence of the Bolza problem to the Mayer or Lagrange formulation [30] can be easily seen.

The optimal control $u(t) \in \Omega$ is to be determined which drives the p-dimensional ($p = 6$) system of the form given in Eq. (2.1) from initial conditions $X\,(t_0) = X_0$ to a terminal surface or target set Θ_f of the form:

$$[\psi\,(X(t_f), t_f)\,] = \bar{0} \tag{2.10}$$

Here, $\psi\,(X(t_f), t_f)$ is a q-dimensional vector function and $\bar{0}$ indicates a zero vector of same order.

The launcher aircraft is assumed to be cruising at a prescribed altitude with a given velocity. It is also assumed that no pre-launch maneuver is performed. The initial flight-path-angle and the heading-angle are assumed to be zero. The initial velocity of the missile is the same as the initial velocity of the launcher. The

control parameter histories are to be determined to obtain the attainable set boundary points in the $x-y$ plane for given final time at the nominal final altitude of the target. The intercept is to be achieved with a prescribed lower bound on final energy, so that, during real-time guidance, there is enough velocity in the missile for end-game maneuvers. The final orientation angles of the velocity vector are not prescribed.

In connection with the optimal control problem at hand, the problem can be stated as to obtain the attainable set boundary of the missile in $x-y$ plane, with other states prescribed or free at initial and final time (to be discussed later). This implies, $x(t_f)$ is maximized or minimized for fixed $y(t_f)$ or vice-versa. The particular choice of the performance index depends on the terminal conditions of intercept and the ease in solving the associated TPBVP. The choice is easily seen as detailed in Chapter 4. Hence, $\phi\,(X(t_f), t_f) = \pm x\,(t_f)$ or $\pm y\,(t_f)$ and $L\,(X, u, t)$ is identically zero for the entire time interval. It should be noted here that for motion in the vertical plane, range-optimization of the same missile model was performed [14,15] with various initial and end conditions. The relevant boundary conditions for the intercept problem without pre-launch maneuvers of launching aircraft are as follows:

Initial conditions	*Final conditions*
$x(t_0) = 0$	$x(t_f) = x_{\max\,/\,\min}$ or x_{fixed}
$y(t_0) = 0$	$y(t_f) = y_{fixed}$ or $y_{\max\,/\,\min}$
$h(t_0) = h_0$ *(specified)*	$h(t_f) = h_f$ (specified)

$E(t_0) = E_0$ *(specified)*	$E(t_f) \geq E_f$ (specified inequality)
$\gamma(t_0) = 0$	$\gamma(t_f) = \gamma_{free}$ (unspecified)
$\chi(t_0) = 0$	$\chi(t_f) = \chi_{free}$ (unspecified)

The above boundary conditions indicate range maximization/minimization in all directions in the $x-y$ plane for other states specified or free. This problem is denoted as problem p1. The above orientation angle specifications for the missile at initial and final time can be used for nearly all real-time scenarios. The initial conditions of down-range and cross-range can always be chosen as zero, since these do not appear in the right-hand-side of the differential equations. Hence the flooding of state space requires a seven-parameter ($h_0, h_f, E_0, E_f, x(t_f), y(t_f), t_f$) family of solutions. The solutions of the above optimal control problem for fixed initial and final values of altitude and energy is termed as a **range-chart** which contains max/min-range intercept points for various final times. Thus it is clear that a four-parameter (h_0, h_f, E_0, E_f) family of such charts are to be generated for flooding the entire state space.

The initial and final altitudes of the missile can vary from 0 ft to approximately 50000 ft, since these are the nominal flying altitude corridors for aircrafts. The study [14] indicates that neighboring guidance in the vertical plane can be achieved with large initial altitude perturbations (in the order of 5000 ft). This implies that the discretization mesh for initial and final altitudes can be made coarse. Similar results for the initial and final energy of the missile (or the

launcher velocity and end-game velocity requirements) reduces the number of "range-charts" required for real-time on-board guidance.

Once the range-charts are obtained for all possible scenarios, a possible mode of selection of the reference extremal is as discussed below:
The target is viewed at a given instant of time by the launcher aircraft. The selection of the right range-chart is decided by the pilot of the launching aircraft depending upon the launcher altitude and speed and the altitude and speed of the target. The (x,y) intercept co-ordinates obtained from the range-chart and the corresponding final time t_f are arranged in tabular form $(x,y;t_f)$. Given the current target position and an estimated intercept time t_f, the target position can be extrapolated in the velocity direction linearly (The target is assumed to travel in the horizontal plane). This gives an ordered pair (x_T, y_T) . The value of t_f is iteratively adjusted so that (x_T, y_T) is within some prescribed tolerance of the point (x,y) interpolated from the tabular data. In short, the missile co-ordinates at final time must be equal to the extrapolated target position at final time. Once the nominal intercept co-ordinate is located, the " closest " nominal solution is used as the reference trajectory.

The nominal optimal control problem with the performance index as the range [problem p1] cannot be used as such in the generation of a near-optimal neighboring guidance scheme. This is easily understood from the following facts. In general intercept does not occur at a predicted fixed final time and hence a neighboring guidance scheme with final time fixed would be catastrophic!

Morover, for the cases when the target turns away, maximizing range makes the problem impractical with a missile chasing a target as far as it can without intercept. These problems make the choice of the above performance index and boundary conditions unsuitable for developing neighboring guidance. However, it should be noted that the above scheme is used for predicting the intercept point and storing the reference state and control histories.

The problem encountered above is solved by considering an equivalent time-optimal control problem [problem p2]. Once the reference trajectory has been identified, an equivalent minimum-time to intercept problem is considered. This scheme does not have the disadvantages of the previous method. Even if the target turns away, the missile tries to intercept it as soon as possible. The performance index to be minimized is final time. Hence, $\phi\,(X(t_f), t_f) = t_f$ and $L\,(X, u, t)$ is identically zero for the entire time interval. Equivalently, for given initial time, one may write $\phi\,(X(t_f), t_f) = 0$ and $L\,(X, u, t)$ identically unity for the entire time interval. The boundary conditions are similar to the problem p1 except for the final conditions on the down-range and/or cross-range, as the case may be. The initial and final conditions on the six state variables are as follows:

Initial conditions	*Final conditions*
$x(t_0) = 0$	$x(t_f) = x_{fixed}$ (specified)
$y(t_0) = 0$	$y(t_f) = y_{fixed}$ (specified)
$h(t_0) = h_0$ *(specified)*	$h(t_f) = h_f$ (specified)
$E(t_0) = E_0$ *(specified)*	$E(t_f) \geq E_f$ (specified inequality)
$\gamma(t_0) = 0$	$\gamma(t_f) = \gamma_{free}$ (unspecified)

$\chi(t_0) = 0$ $\chi(t_f) = \chi_{free}$ (unspecified)

The equivalence of the two nominal problems via the **Mayer reciprocity** and the solutions are discussed in the next chapter.

To study the guidance of the missile with possible thrust deficiency during real flight, it may be essential to include an artificial throttle-setting parameter in the energy equation (2.5) of the form:

$$\dot{E} = \frac{V}{W(t)} (\eta\, T(t) - D(h,M,n)) \tag{2.11}$$

The parameter η is from the set $\eta \in [0, 1]$. A differential equation for η of the form $\dot{\eta} = 0$ is used for the nominal problem, with initial condition $\eta(t_0) = 1$. Thus η is elevated to the status of a state variable. During real-time guidance the state η may undergo perturbation and the neighboring guidance scheme can be used to obtain a near-optimal guidance. However, in the present study simulations with possible thrust deficiencies were not performed.

Chapter 3: Synthesis of Optimal Trajectory

3.1: Overview

This chapter discusses the existence of optimal solutions and necessary conditions for optimality based on Pontryagin's minimum principle [17,18] for the nominal optimal control problem introduced in the previous chapter. The nature of optimal solutions and the equivalence of optimal control problems discussed in the previous chapter are also examined. Numerical solutions of the associated TPBVPs are presented in this chapter.

3.2: Existence of Optimal Solution

The usual variational-based approach to these problems proceeds with the construction of a pre-Hamiltonian function and the application of the Minimum principle [17,18]. However, before proceeding with such a theory of necessary conditions, it is prudent to establish the existence of a solution for the given

optimal control problem. One key condition in the existence theory [31] is the convexity of the **hodograph** figure or **velocity set** in the state-rate space [32,33]. The following theorem, which is an adaptation of the existence theorem from [31] is used to establish the existence of an optimal control:

Consider the following non-linear process,

$$\dot{X} = f(X,u,t) \tag{3.1}$$

in a time interval $[t_0, t_f]$ *with initial conditions* $X(t_0) = X_0$, *a target set* $X(t_f) \in \Theta_f$, *a nonempty compact continuously varying control constraint set* $u(t) \in \Omega$ *and with the cost for each* $u(t) \in \Omega$ *is* $C(u)$. *Assume that there exists a uniform bound for all responses* $X(t)$, *(i.e.,* $|x(t)| < b$ *) to controllers* $u(t) \in \Omega$ *and that the velocity set*

$$V(X,t) = \{f(X,u,t) \mid u \in \Omega(X,t)\} \tag{3.2}$$

is convex for each fixed (X,t)

Then there exists an optimal controller $u^*(t)$ *on* $[t_0, t_f]$ *in* Ω *minimizing* $C(u)$.

The proof of existence of an optimal control for the specific problem at hand is done by checking the convexity of the hodograph space. To construct a hodograph space, one should first freeze the states and time at some fixed value. The controls are chosen from the allowed control constraint set and the maneuverability domain or the instantaneously useable domain in the hodograph space is obtained.

The controls appear in the differential equations of energy, flight-path-angle, and the heading-angle. Thus the hodograph space is only three-dimensional. The following functional dependence of the relevant state-rates on the controls is obtained from Eq. (2.5)-(2.7).

$$\dot{E} = a_1 + a_2 [n_v^2 + n_h^2]^{\frac{k}{2}} \tag{3.3}$$

$$\dot{\gamma} = a_3 + a_4 n_v \tag{3.4}$$

$$\dot{\chi} = a_5 n_h \tag{3.5}$$

a_1 through a_5 are constants for fixed states and time and $k = 1.8$, a constant. The hodograph space can be constructed using the relation $\dot{E} = \hat{f}(\dot{\gamma}, \dot{\chi})$, where $\hat{f}$ is function of the form:

$$\hat{f} = a_1 + a_2 [(\frac{\dot{\gamma} - a_3}{a_4})^2 + (\frac{\dot{\chi}}{a_5})^2]^{\frac{k}{2}} \tag{3.6}$$

with the controls varied inside the control constraint set. It is clear that for the above described function the domain is not convex. However, the non-convexity can be overcome by **relaxation** of the controls [31,32,33], i.e., by adding points to the maneuverability domain to obtain the convex hull. Operation in the convex hull implies usage of chattering control. Operation in these regions becomes essential only for certain special cases of the optimal control problem at hand. An easy method of convexizing the hodograph for the specific problem would be

to introduce an additional control in the differential equations similar in physical nature to **speed-brakes** . This may be modelled in the energy equation as follows:

$$\dot{E} = \frac{V}{W(t)} \left[T(t) - \kappa\{D - D_{\max}\} - D_{\max} \right] \tag{3.7}$$

where κ is the additional control variable in the form of a speed-brake. Here, $D_{\max}$ is the maximum drag possible and is a function of altitude and velocity of the missile while D is a function of altitude, velocity, and the control variables. $\kappa \in [0,1]$ convexizes the hodograph. $\kappa = 1$ indicates the original hodograph surface, and $\kappa = 0$ "closes the lid" or forms the convex hull. Any other value of κ denotes a point inside the convexized hodograph. Values of κ not equal to unity are singular solutions of the relaxed problems. These singular solutions correspond to chattering solutions of the original non-relaxed problem. It should be mentioned here that operation in the non-convex regions of the hodograph space for this specific range-optimization problem is analogous to operating at high drag (waste of energy) which is clearly of little interest. The above phenomenon is analyzed later in this chapter following the definition of adjoint variables and transversality conditions.

Fig. {3.1 & 3.2} give two views of a three-dimensional hodograph space for this problem for some specified states and time. The surface alone is the hodograph space of the unrelaxed problem, while the entire volume becomes the hodograph space for the relaxed problem. It should be noted here that the hodograph is independent of the down-range, cross-range, and the heading-angle. The

elliptical base indicates the nature of the control constraint set. For the specific example the other states used are as follows:

$h = 20Kft$, $E = 140Kft$, and $\gamma = -1.0149\ radians$. The time is chosen such that the thrust is zero. The control is chosen from the constraint set $n \leq n_{\max}$.

3.3: Necessary Conditions

In this section the necessary conditions for optimality including the Euler-Lagrange equations, extremal controls with and without active constraints, and the transversality conditions are detailed.

The variational-Hamiltonian $\mathscr{H}$ is defined in the usual way as follows:

$$\mathscr{H}(\lambda_X, X, u, t) = \lambda_X^T . f(X,u,t) + L(X,u,t) \tag{3.8}$$

where, λ_X is the co-state or adjoint variable vector of the form:

$\lambda_X = [\lambda_x \lambda_y \lambda_h \lambda_E \lambda_\gamma \lambda_\chi]^T$

The variational-Hamiltonian for the range-maximization problem at hand takes the following form:

$$\mathscr{H} = \lambda_x V(h,E) \cos\gamma \cos\chi + \lambda_y V(h,E) \cos\gamma \sin\chi + \lambda_h V(h,E) \sin\gamma \tag{3.9}$$

$$+ \lambda_E \frac{V(h,E)}{W(t)} [T(t) - D(h,E,n_v,n_h)] + \lambda_\gamma \frac{g}{V(h,E)} [n_v - \cos\gamma]$$

$$+ \lambda_\chi \frac{g}{V(h,E)} \frac{n_h}{\cos\gamma}$$

3.3.1: Euler-Lagrange Equations

The necessary conditions for optimality of the optimal control problem requires that the adjoint variables satisfy the Euler-Lagrange equations. These are equivalent to the classical Euler equations for the familiar calculus of variations problems. The Euler-Lagrange equations are as follows:

$$\dot{\lambda}_X = -\frac{\partial \mathcal{H}}{\partial X} \tag{3.10}$$

For the missile example one gets:

$$\dot{\lambda}_x = 0 \tag{3.11}$$

$$\dot{\lambda}_y = 0 \tag{3.12}$$

$$\dot{\lambda}_h = -\left[\lambda_x \cos\gamma\cos\chi + \lambda_y \cos\gamma\sin\chi + \lambda_h \sin\gamma\right]\frac{\partial V}{\partial h} \tag{3.13}$$

$$+ \left[\lambda_\gamma (n_v - \cos\gamma)\frac{g}{V^2}\right]\frac{\partial V}{\partial h} + \left[\lambda_\chi \left(\frac{n_h}{\cos\gamma}\right)\frac{g}{V^2}\right]\frac{\partial V}{\partial h}$$

$$- \lambda_E \frac{(T-D)}{W}\frac{\partial V}{\partial h} - \lambda_E \frac{V}{W}\left(-\frac{\partial D}{\partial h}\right)$$

$$\dot{\lambda}_E = -\left[\lambda_x \cos\gamma\cos\chi + \lambda_y \cos\gamma\sin\chi + \lambda_h \sin\gamma\right]\frac{\partial V}{\partial E} \tag{3.14}$$

$$+ \left[\lambda_\gamma (n_v - \cos\gamma)\frac{g}{V^2}\right]\frac{\partial V}{\partial E} + \left[\lambda_\chi \left(\frac{n_h}{\cos\gamma}\right)\frac{g}{V^2}\right]\frac{\partial V}{\partial E}$$

$$- \lambda_E \frac{(T-D)}{W}\frac{\partial V}{\partial E} - \lambda_E \frac{V}{W}\left(-\frac{\partial D}{\partial E}\right)$$

$$\dot{\lambda}_\gamma = \lambda_x V \sin\gamma \cos\chi + \lambda_y V \sin\gamma \sin\chi - \lambda_\gamma \frac{g}{V} \sin\gamma \qquad (3.15)$$

$$- \lambda_\chi \frac{g}{V} \tan\gamma \sec\gamma$$

$$\dot{\lambda}_\chi = \lambda_x V \cos\gamma \sin\chi - \lambda_y V \cos\gamma \cos\chi \qquad (3.16)$$

The above system of co-state equations is homogeneous of order one. Some of the partials with respect to altitude and energy of drag, air density etc. are evaluated numerically from the spline interpolations. Numerical differentiation is performed using a central difference scheme.

3.3.2: Extremal Control

The minimum principle requires that an optimal control must minimize the variational-Hamiltonian with respect to the controls subject to the control constraint. This implies that if the controls are in the interior of the constraint set Ω, then:

$$\frac{\partial \mathcal{H}}{\partial n_v} = 0 \qquad (3.17)$$

and

$$\frac{\partial \mathcal{H}}{\partial n_h} = 0 \qquad (3.18)$$

These equations yield the extremal controls n_v^* and n_h^* given by:

$$n_v^* = -sgn(\lambda_\gamma)\,[abs(\frac{\lambda_\gamma\, g}{\lambda_E\, D_i\ V^2\, k})]^{\frac{1}{k-1}}\ \text{x} \tag{3.19}$$

$$[1 + \{\frac{\lambda_\chi}{\lambda_\gamma\ \cos\gamma}\}^2]^{(1-\frac{k}{2})/(k-1)}$$

and

$$n_h^* = -sgn(\lambda_\chi)\,[abs(\frac{\lambda_\chi\, g}{\lambda_E\, D_i\ V^2\, k\ \cos\gamma})]^{\frac{1}{k-1}}\ \text{x} \tag{3.20}$$

$$[1 + \{\frac{\lambda_\gamma\ \cos\gamma}{\lambda_\chi}\}^2]^{(1-\frac{k}{2})/(k-1)}$$

The *sgn* appearing in the above equations can be seen by close examination of Eq. (3.17) and (3.18). The weakened form of the classical Legendre-Clebsch condition for the minimizing extremal implies that

$$[\mathscr{H}_{uu}] \geq 0 \tag{3.21}$$

i.e., the matrix be positive semi-definite. This implies that the diagonal elements must be positive semi-definite, i.e.,

$$\frac{\partial^2 \mathscr{H}}{\partial n_v^2} \geq 0 \tag{3.22}$$

and

$$\frac{\partial^2 \mathscr{H}}{\partial n_h^2} \geq 0 \tag{3.23}$$

The above equations yield the necessary condition that $\lambda_E \leq 0$ for n_v and n_h not zero simultaneously. It can also be seen that the determinant of the matrix $\mathscr{H}_{uu}$, i.e.,

$$\mathscr{H}_{n_v n_v}\ \mathscr{H}_{n_h n_h} - \mathscr{H}_{n_v n_h}\ \mathscr{H}_{n_h n_v}$$

is also positive semi-definite.

In this connection one traces back to the hodograph space. It is clear that a unique controller can be obtained for the optimal control problem using minimum principle, except when $\lambda_E \geq 0$ and λ_γ and λ_χ are simultaneously equal to zero for a finite interval of time. If λ_E is equal to zero along with the other two co-states λ_γ and λ_χ, it implies a completely singular solution and the minimum principle is vacuous. If $\lambda_E > 0$ with λ_γ and λ_χ both zero, the plane of constant minimizing Hamiltonian becomes parallel to the elliptical base of the convexized hodograph space. The relaxed problem would give a singular control solution for the load-factors which would correspond to chattering nature of the original unrelaxed problem. Thus for non-chattering phenomena for all possible λ_γ and λ_χ, one must operate only in the domain of a negative λ_E. This corresponds to an energy conservative system. The κ parameter in the speed-brake modelling would be zero, if the energy multiplier is positive, corresponding to increased drag operation.

The control constraint limits are incorporated in the minimum principle using the idea of an augmented Hamiltonian with constraint multipliers or "Valentine multipliers" μ_1 and μ_2. Thus the augmented Hamiltonian denoted by $\overline{\mathscr{H}}$ is:

$$\overline{\mathcal{H}} = \mathcal{H} + \mu_1 \beta_1 + \mu_2 \beta_2 \tag{3.24}$$

where, β_1 corresponds to the inequality constraint $(n - n_{max}) \leq 0$ and β_2 denotes the second inequality constraint $(n - n_L) \leq 0$. The extremal controls obtained from stationary values of $\overline{\mathcal{H}}$ is as below:

$$n_v^* = - \frac{\lambda_\gamma}{[\lambda_\gamma^2 + (\frac{\lambda_\chi}{\cos\gamma})^2]^{0.5}} \quad infimum(n_L, n_{max}) \tag{3.25}$$

and

$$n_h^* = - \frac{\lambda_\chi}{\cos\gamma\,[\lambda_\gamma^2 + (\frac{\lambda_\chi}{\cos\gamma})^2]^{0.5}} \quad infimum(n_L, n_{max}) \tag{3.26}$$

where, *infimum* denotes infimum of the two control limits when active. The multipliers μ_1 and μ_2 are always greater than or equal to zero. A particular multiplier is equal to zero if the respective constraint is inactive and may be greater than or equal to zero if the respective constraint is active. This nature of the multipliers results from the usual Kuhn-Tucker conditions [21].

The co-state equations are obtained from the following:

$$\dot{\lambda}_X = - \frac{\partial \overline{\mathcal{H}}}{\partial X} \tag{3.27}$$

i.e.,

$$\dot{\lambda}_X = - \frac{\partial \mathcal{H}}{\partial X} - \mu_2 \frac{\partial \beta_2}{\partial X} \tag{3.28}$$

The Euler-Lagrange equations are different from the unconstrained case only for equations of the co-states of altitude and energy. It should be noted that the continuity of the controls at the junction of constrained and unconstrained arcs depends on the continuity of λ_X , $\mathscr{H}$, and $\frac{\partial \mathscr{H}}{\partial u}$.

3.3.3: Transversality Conditions

For the optimal control problem as stated in Chapter 2 in the form of Bolza, one gets the transversality conditions of the form:

$$\lambda_X(t_f) = [\frac{\partial \phi(X(t_f), t_f)}{\partial X(t_f)} + \nu^T \frac{\partial \psi(X(t_f), t_f)}{\partial X(t_f)}]_{t_f} \tag{3.29}$$

where ν is a multiplier vector. This provides the necessary boundary conditions for the co-state vector to obtain a TPBVP.

Using (3.29) for the boundary conditions for range maximization problem p1, one obtains the following end-conditions for some of the co-states.

$$\lambda_\gamma(t_f) = 0 \quad (\gamma(t_f) \textit{ free}) \tag{3.30}$$

$$\lambda_\chi(t_f) = 0 \quad (\chi(t_f) \textit{ free}) \tag{3.31}$$

$$\lambda_x(t_f) = \pm 1 \quad (\min / \max \ x(t_f) \ \textit{and} \ y(t_f) \ \textit{specified}) \tag{3.32}$$

or

$$\lambda_y(t_f) = \pm 1 \quad (\min / \max \ y(t_f) \ \textit{and} \ x(t_f) \ \textit{specified}) \tag{3.33}$$

whichever be the relevant boundary condition.

It is to be noted here that the boundary condition for energy is in the form of an inequality. This is treated in the following manner. The final energy is fixed as an equality and the boundary value problem is solved with $E(t_f) = E_f$. The corresponding co-state $\lambda_E(t_f)$ is checked. If this is negative then the solution of the TPBVP is regarded as an extremal. Otherwise, one must re-solve the problem with the boundary condition $\lambda_E(t_f) = 0$, called the **natural** boundary condition. This arises if the specified bound E_f is less than the natural value of $E(t_f)$. Strict negativity of the energy multiplier throughout the trajectory confirms the energy conservative nature of the problem and bars the possibility of high-drag chattering controls.

The transversality condition for the Hamiltonian at final time is given as:

$$\mathcal{H}(t_f) = -\left[\frac{\partial \phi(X(t_f), t_f)}{\partial t_f} + \nu^T \frac{\partial \psi(X(t_f), t_f)}{\partial t_f}\right]_{t_f} \tag{3.34}$$

For problem p1 corresponding to fixed final time this reduces to the fact that the $\mathcal{H}(t_f)$ is some unknown number which is obtained after the solution of the TPBVP. Hence this condition yields no additional information. The fixed final time is used as the boundary condition. For the problem p2, one obtains the condition $\mathcal{H}(t_f)$ = -1 from the transversality condition. This is used as one of the conditions for determining the unknown final time t_f.

3.3.4 Mayer Reciprocity

It is clear that the nominal solutions obtained from solving p1 cannot be used as reference trajectories due to the fact that range-maximization for fixed final time is not always the motive. The nominal solutions obtained from solving p1 is equivalent to solving a minimum-time to intercept problem, namely p2. The equivalence is seen as follows:

The transversality conditions for p2 implies that $\mathcal{H}(t_f) = -1$ with final time t_f to be minimized. All other boundary conditions remain the same except that the co-state variables $\lambda_x(t_f)$ and $\lambda_y(t_f)$ are unspecified (because the down-range and cross-range are specified values). Thus the nominal intercept solution is obtained from solving p1 and all the co-state variables are divided by $|\mathcal{H}(t_f)|$ corresponding to p1 solution. This scaled co-state solution is a solution of p2 with the down-range and cross-range at final time, specified as the same values obtained from the optimal solution of p1. The final optimized time of p2 would be equal to the fixed final time of p1. The state and control histories remain the same for both the problems.

In the above analysis it is to be noted that the value of $\mathcal{H}(t_f)$ must be less than zero. Otherwise the two problems are not equivalent. Morover, if $\mathcal{H}(t_f) = 0$, then the scaling cannot be performed. However, this corresponds to a final time equal to the natural time of p1. This is just a pathological case.

The problem p1 is solved and its co-state vector is scaled as above and stored as **reference** trajectory. Neighboring guidance is performed with linearizations about such reference trajectories.

3.4 Numerical Solution

Once the initial state variables, the initial co-state variables, all switching times and any associated multiplier values (for example, in junctions of constrained and unconstrained arcs) are known, the non-linear system of differential equations can be integrated forward and the solution obtained. The difficulty in solving optimal control problems arises due to the need for solving two-point boundary value problems or in general multi-point boundary value problems.

The solution is attempted by using a simple Newton method to find roots of a function of finite parameters. In a simple shooting algorithm one has an input vector of the form $\overline{X}$ containing guess values of the parameters to be determined which would make a vector-valued function $\overline{Y}(\overline{X})$ containing the boundary and interior point conditions, equal to zero. The number of parameters should be equal to the number of boundary conditions and interior point conditions prescribed in $\overline{Y}$. The function evaluation generally requires an integrator. Perturbations are made independently in each parameter in the $\overline{X}$ vector and a Jacobian $[\overline{J}]$ is obtained by suitably evaluating the sensitivity in the output vector $\overline{Y}$ due to the perturbations. The input vector $\overline{X}_{n+1}$ for the next iteration is obtained from the expression:

$$\overline{X}_{n+1} = \overline{X}_n - [\overline{J}]_n^{-1} \quad \overline{Y}_n \tag{3.35}$$

This is repeated until some error criterion is satisfied. The above description is a simple illustration of the general approach used to solve the formulated TPBVPs.

It is sometimes essential to employ multiple shooting algorithm for long flight times, due to stability problems in integrating the differential equations. This is performed by insertion of nodes along the independent variable axis and demanding continuity of the dependent variables at these knot-points within prescribed tolerance. This is the idea used in the software code called **BOUNDSCO** synonymous with **BOUNDSOL** . The above software is used for solving the TPBVPs.

Initial guesses of the state and co-state vector for the flight in a vertical plane were obtained from [14], which in turn were obtained from simplified reduced-order models [15] with induced drag approximated with a constant load-factor. The next chapter explains the continuation method used for extending the optimal solutions to obtain three-dimensional flight of the missile.

The solutions of the TPBVP with the following boundary conditions are shown in Figs. {3.3-3.18}.

Initial conditions	*Final conditions*
$x(t_0) = 0$	$x(t_f) = x_{maximized}$
$y(t_0) = 0$	$y(t_f) = 200000\,ft$

$h(t_0) = 20000\,ft$ $\qquad$ $h(t_f) = 20000\,ft$

$E(t_0) = 52800\,ft$ $\qquad$ $E(t_f) = 140000\,ft$

$\gamma(t_0) = 0$ $\qquad$ $\gamma(t_f) = \gamma_{free}$

$\chi(t_0) = 0$ $\qquad$ $\chi(t_f) = \chi_{free}$

The final time t_f is specified as 150 seconds. The boundary conditions in E and h correspond to an initial launcher velocity of about 1448 ft/sec and final missile velocity of 2767 ft/sec respectively.

The extremal trajectory shows high amount of lofting - Fig. {3.8} and turning - Fig. {3.9} during the thrust phase. This can also be seen from the control histories in Figs. {3.10 & 3.11}. The missile directs its heading towards the target point quickly as seen from the χ history in Fig. {3.9}. The change in heading angle is nearly zero after about 10 percent of the time of flight. The flight is nearly ballistic for much of the trajectory (n_v is nearly zero) as seen in Fig. {3.10}. The transversality conditions impose that the control variables must be zero at final time. The transient at the final time to meet the boundary conditions of energy and altitude is interesting. The energy and the velocity diagrams {3.6 & 3.7} respectively, shows the rapid increase during the thrust phase (with slope discontinuities in both). The energy decreases steadily followed by a steep reduction as a result of drag rise during the final descent.

The variational-Hamiltonian as in Fig. {3.12}, is discontinuous at the switching points of thrust. However, during the final coast phase, it is constant as expected since there is no explicit time dependence. The co-state of energy as in Fig. {3.16}

can be seen to lie below the zero threshold, indicating that the solution is indeed an extremal. The controls are within the control bounds specified for the missile model.

The final energy for the same flight time of 150 seconds was varied from 106.1 Kft to about 150 Kft. The lower energy bound came as a result of the natural energy limit, for which the energy multiplier at final time just became zero. The upper limit, of course, comes due to the limitation of available energy for the given time for the assumed thrust-weight configuration. If the final energy E_f is increased, the performance index, i.e., the range, is reduced. The final time was also varied from 100 seconds to about 223 seconds. The former time indicates an adhoc threshold value for medium range operations and the upper bound denotes the natural time corresponding to Hamiltonian at final time becoming zero as discussed in the section on Mayer reciprocity. Only medium range intercept scenarios in these time zones are considered.

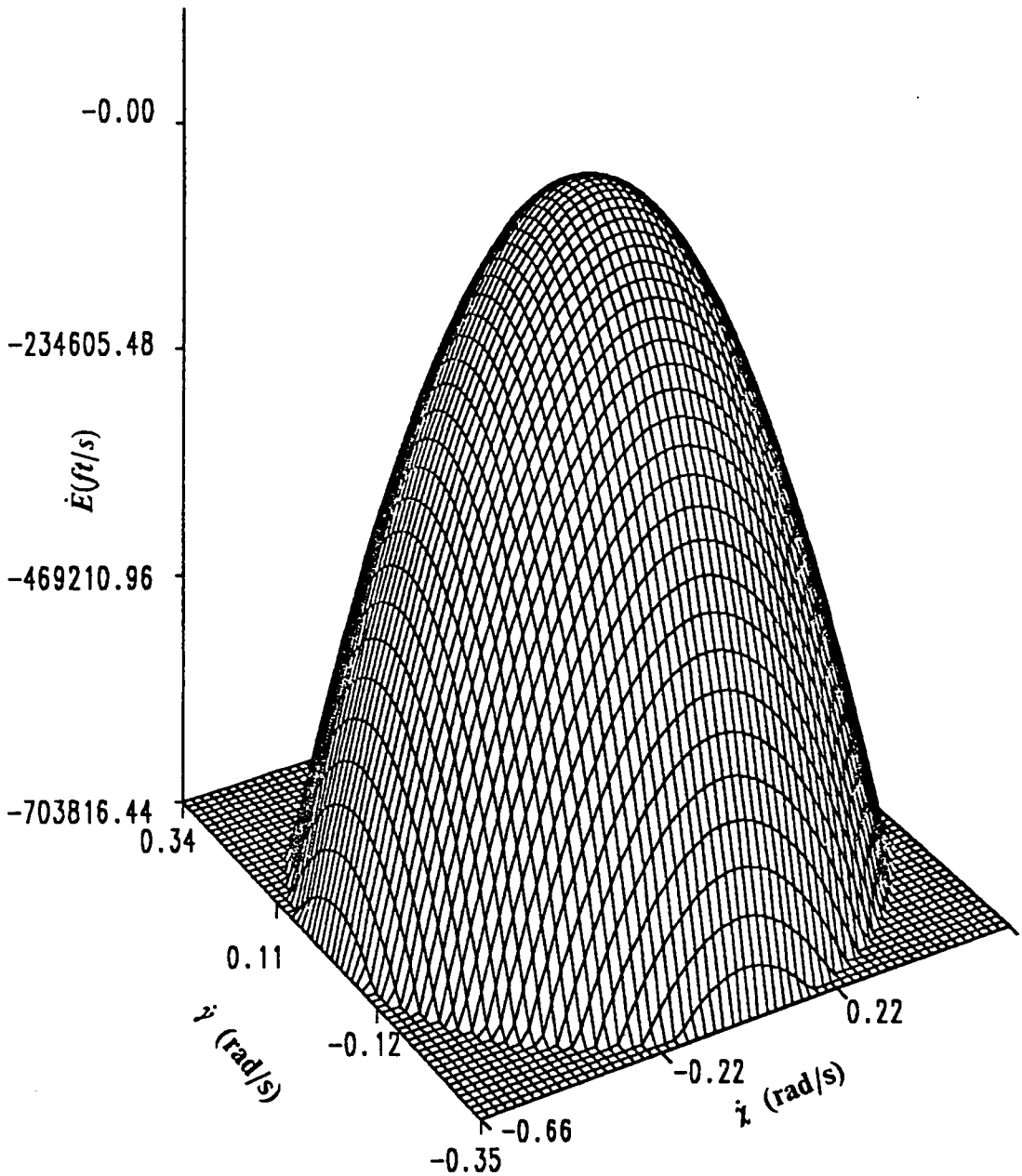

Fig. 3.1: Side-view of hodograph space for specified states

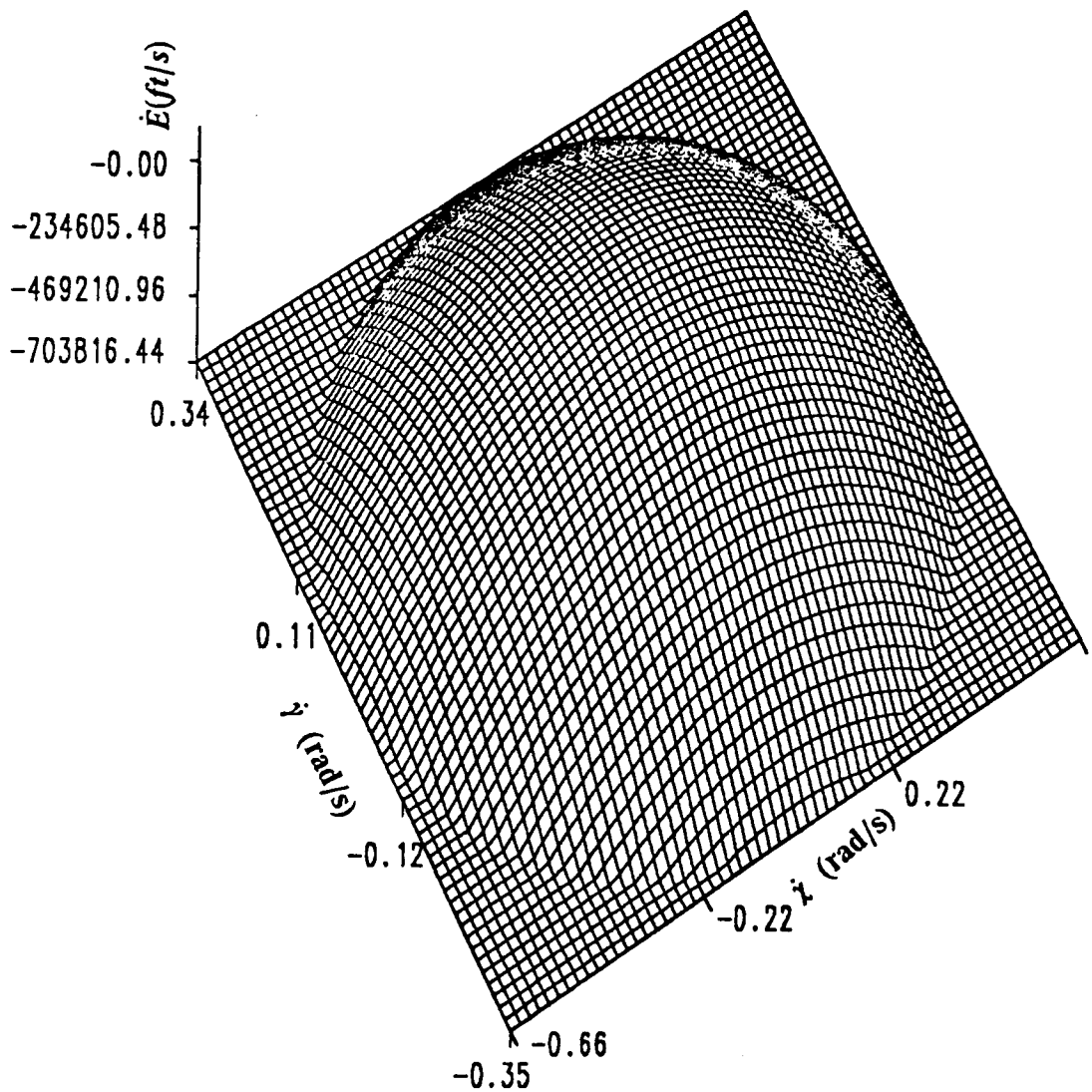

Fig. 3.2: Top-view of hodograph space for specified states

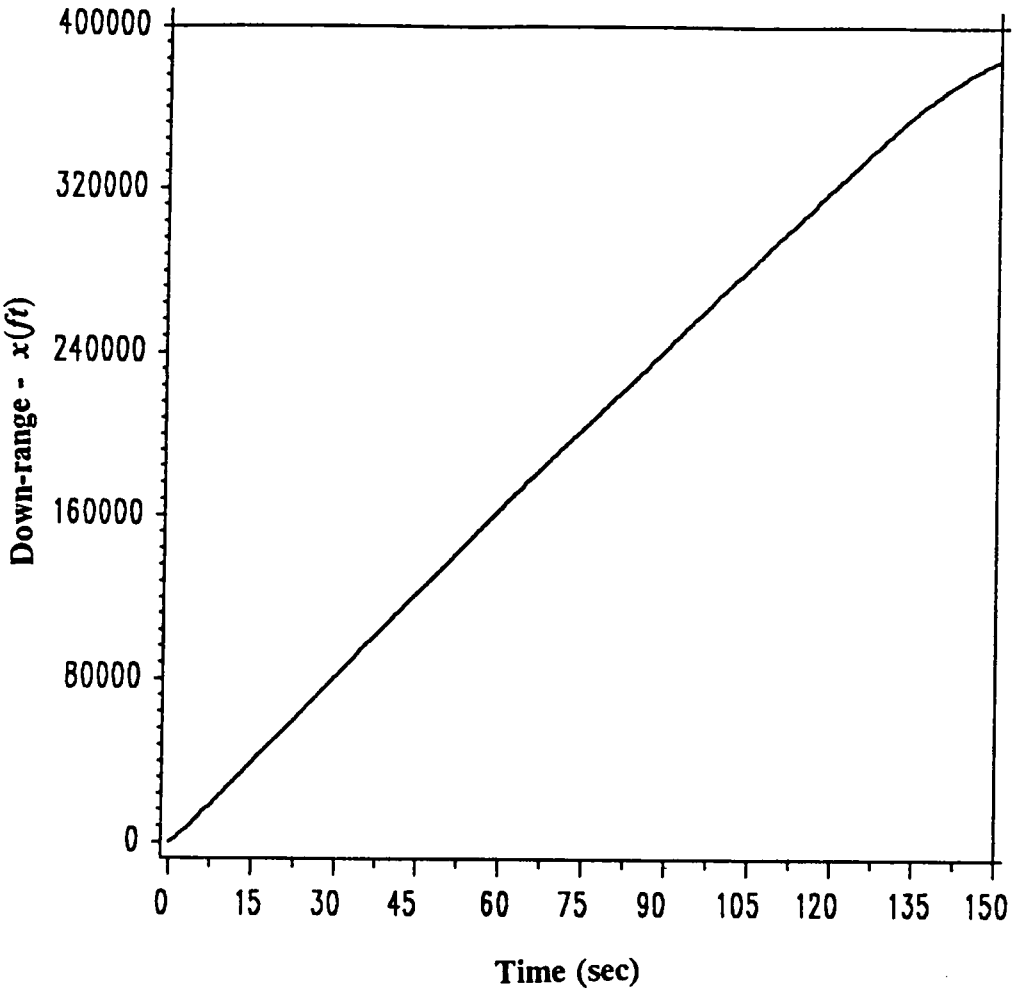

Fig. 3.3: Down-range time history for $t_f = 150s$

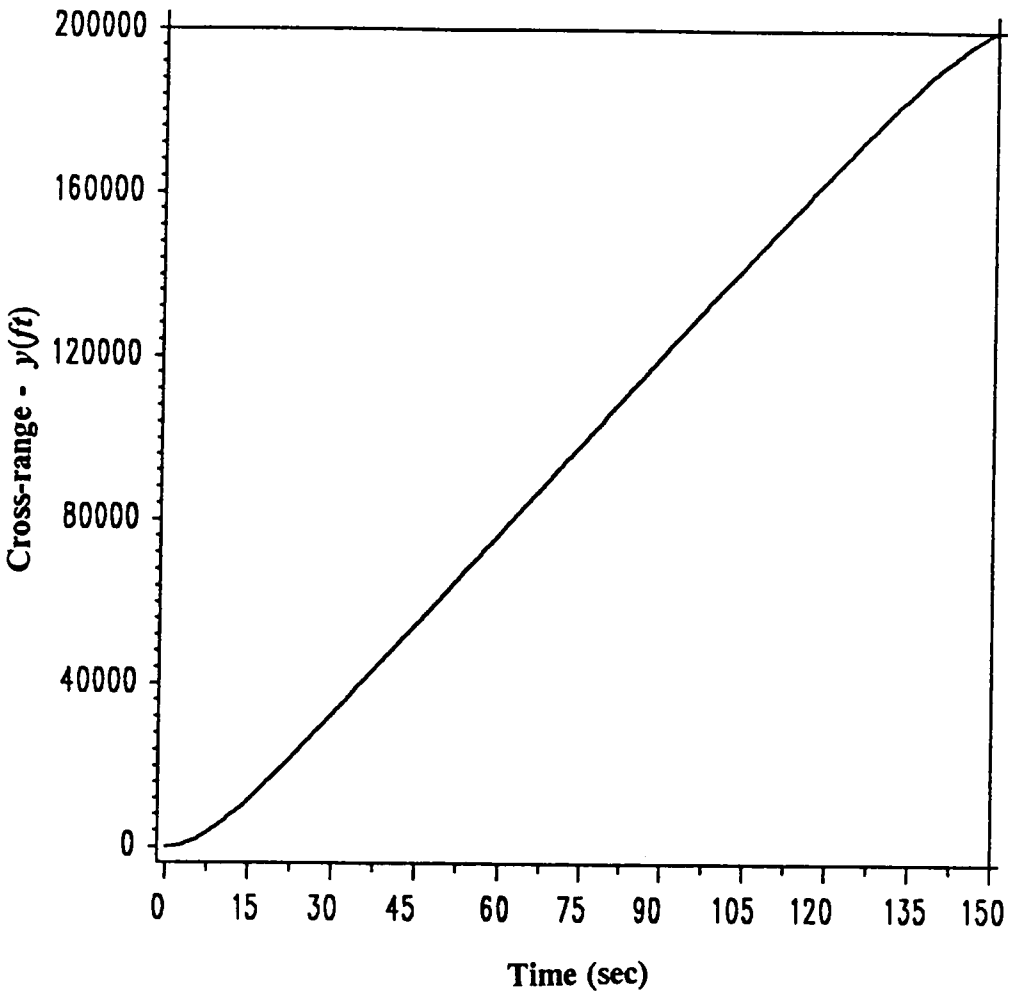

Fig. 3.4: Cross-range time history for $t_f = 150s$

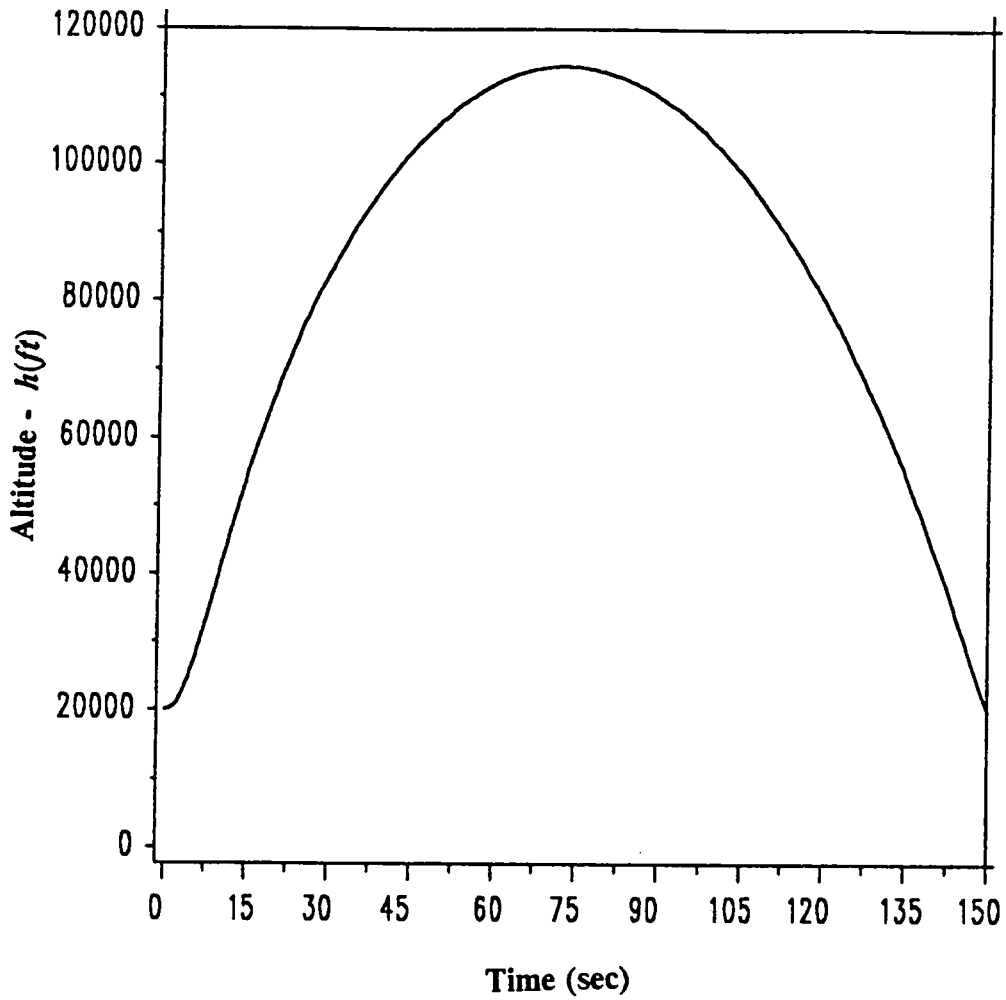

Fig. 3.5: Altitude time history for $t_f = 150s$

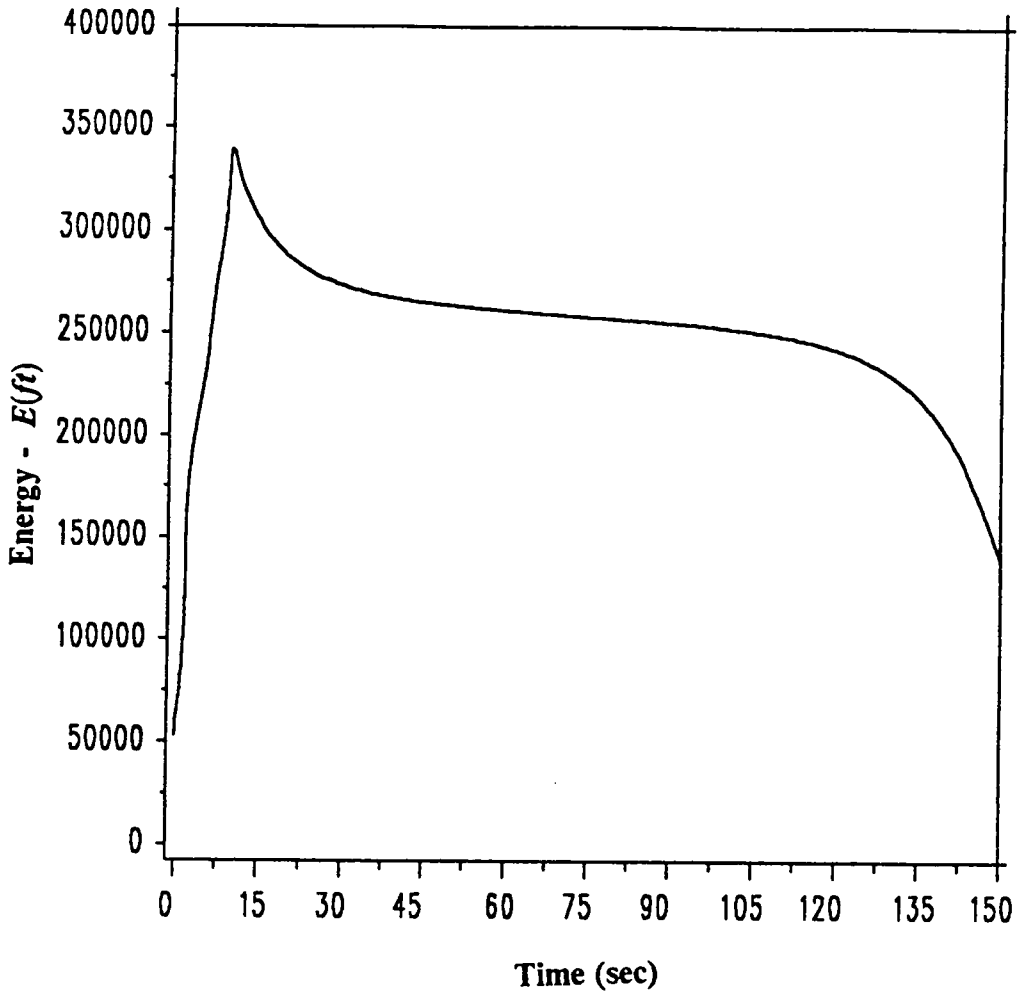

Fig. 3.6: Energy time history for $t_f = 150s$

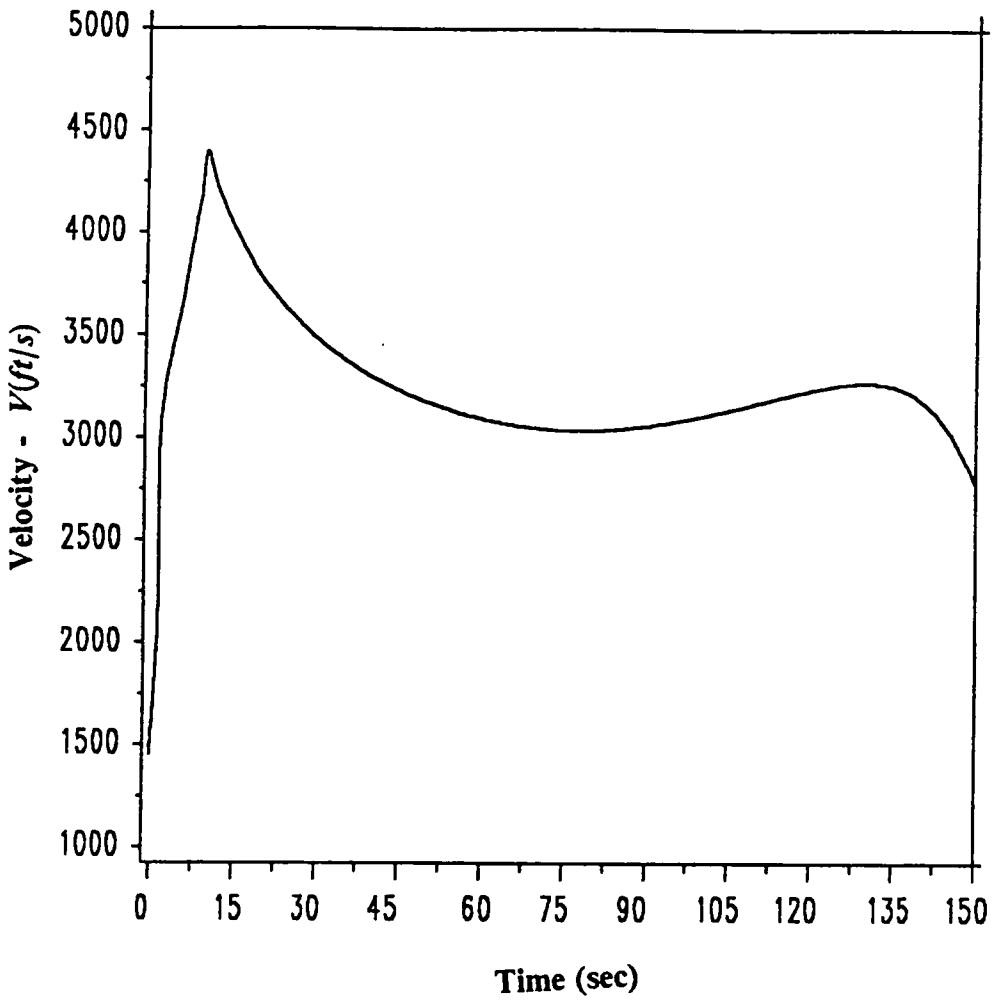

Fig. 3.7: Velocity time history for $t_f = 150s$

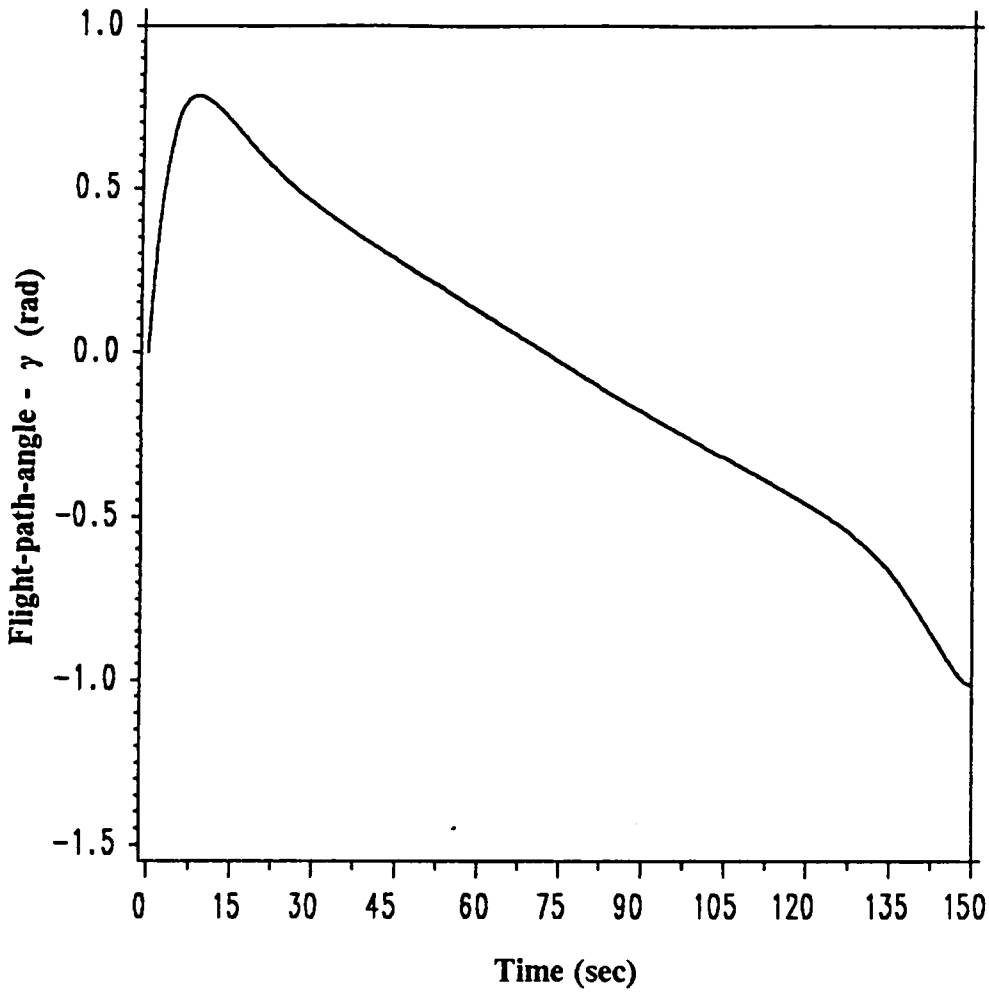

Fig. 3.8: Flight-path-angle time history for $t_f = 150s$

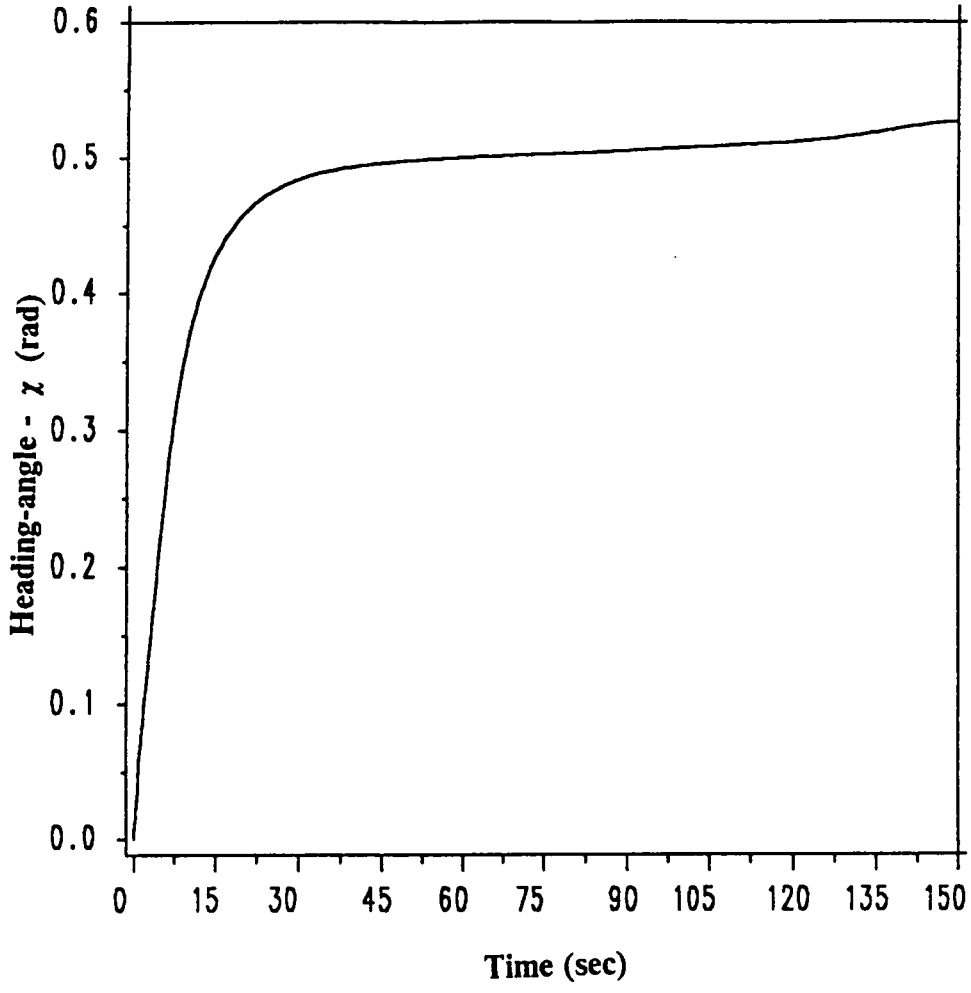

Fig. 3.9: Heading-angle time history for $t_f = 150s$

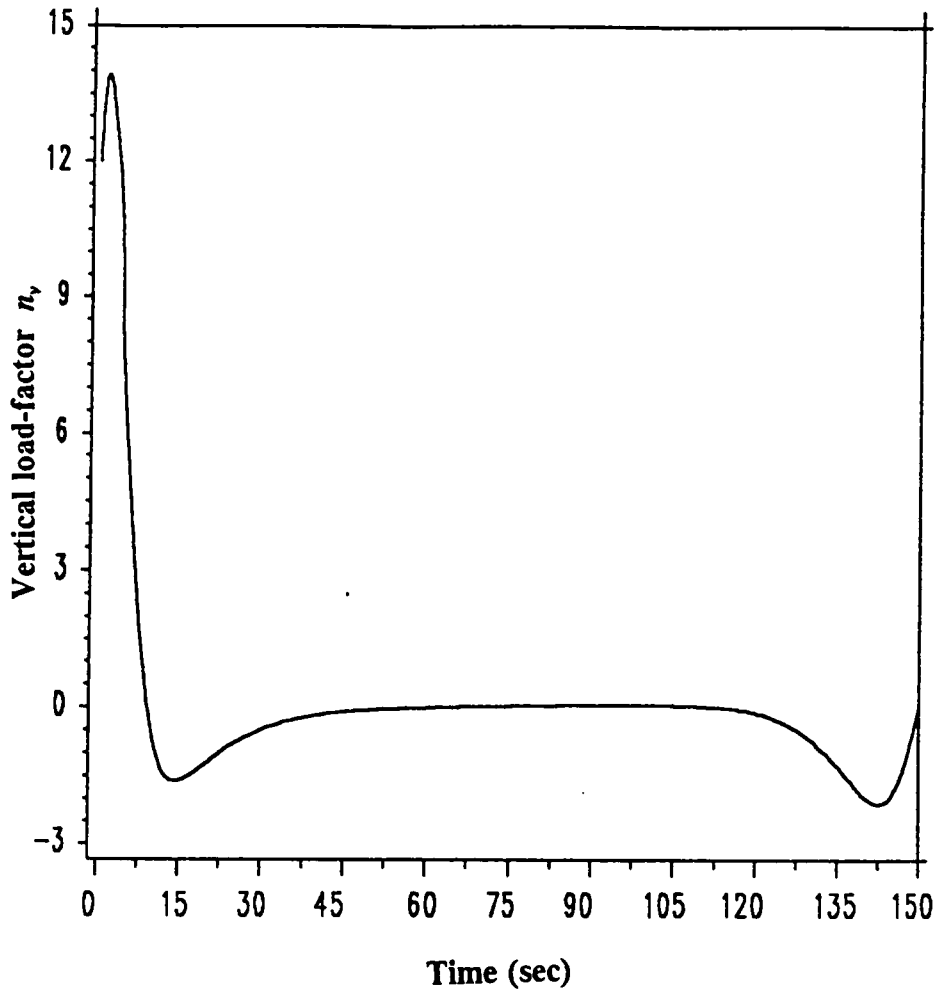

Fig. 3.10: Vertical load-factor time history for $t_f = 150s$

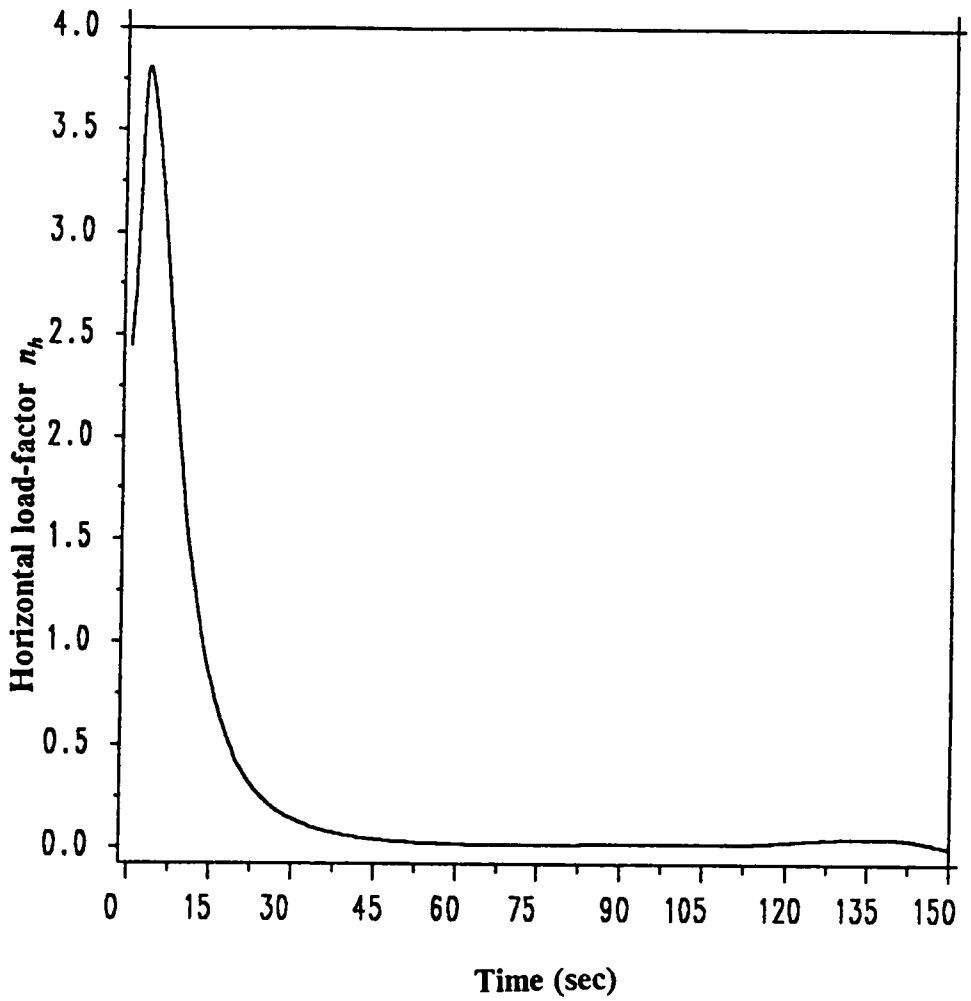

Fig. 3.11: Horizontal load-factor time history for $t_f = 150s$

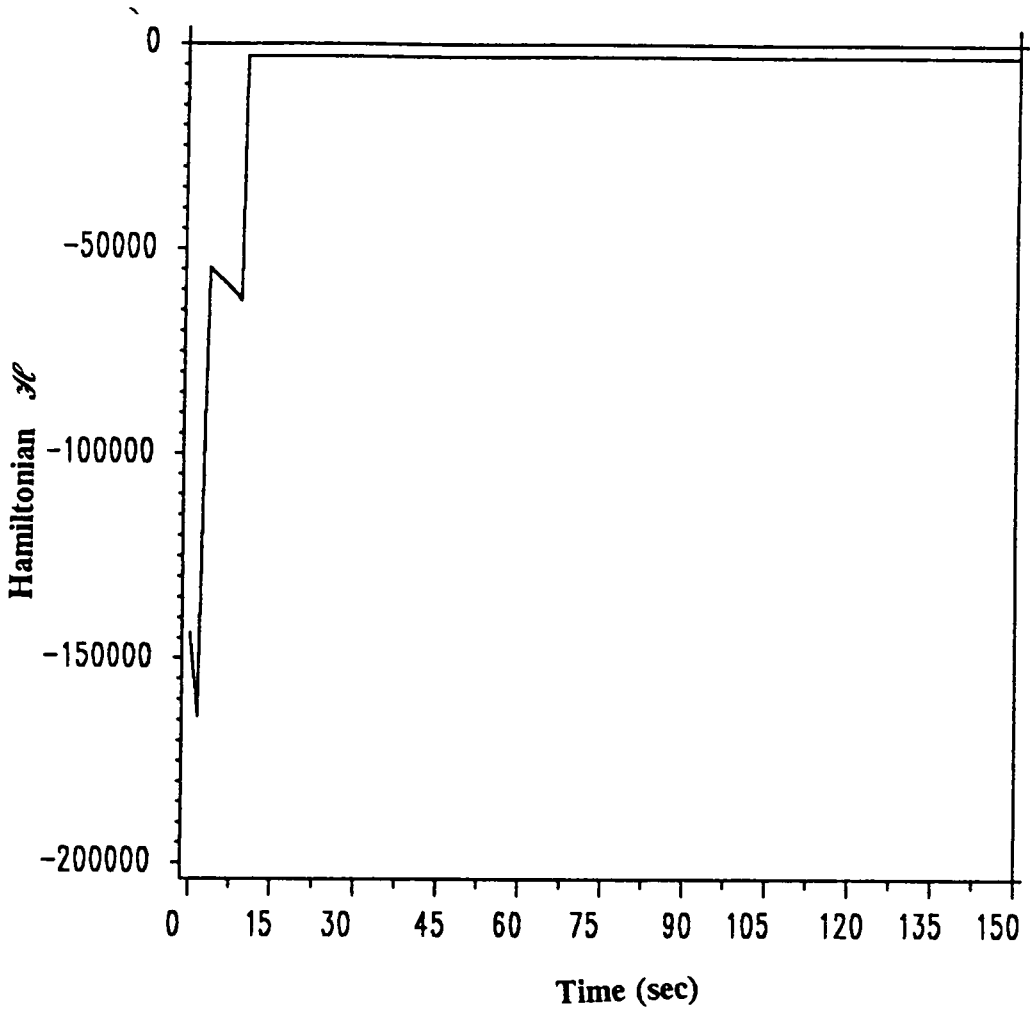

Fig. 3.12: Variational-Hamiltonian time history for $t_f = 150s$

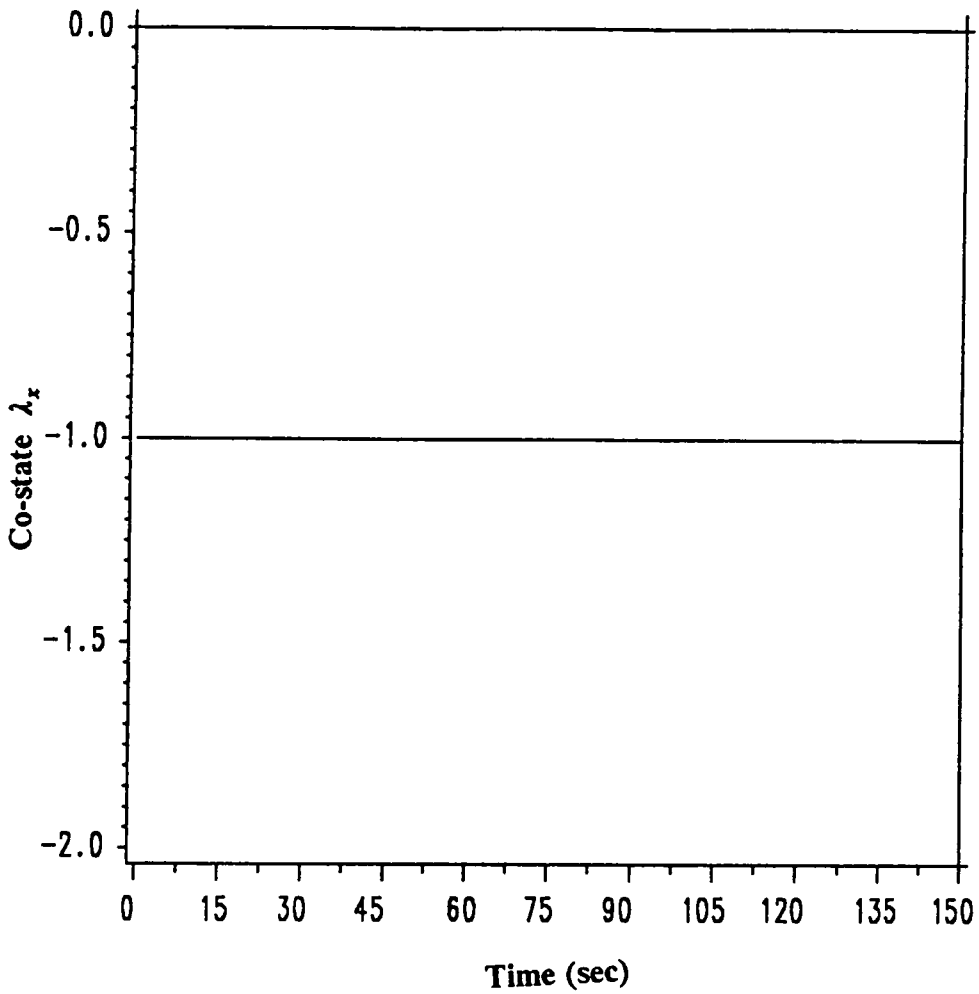

Fig. 3.13: Co-state λ_x time history for $t_f = 150s$

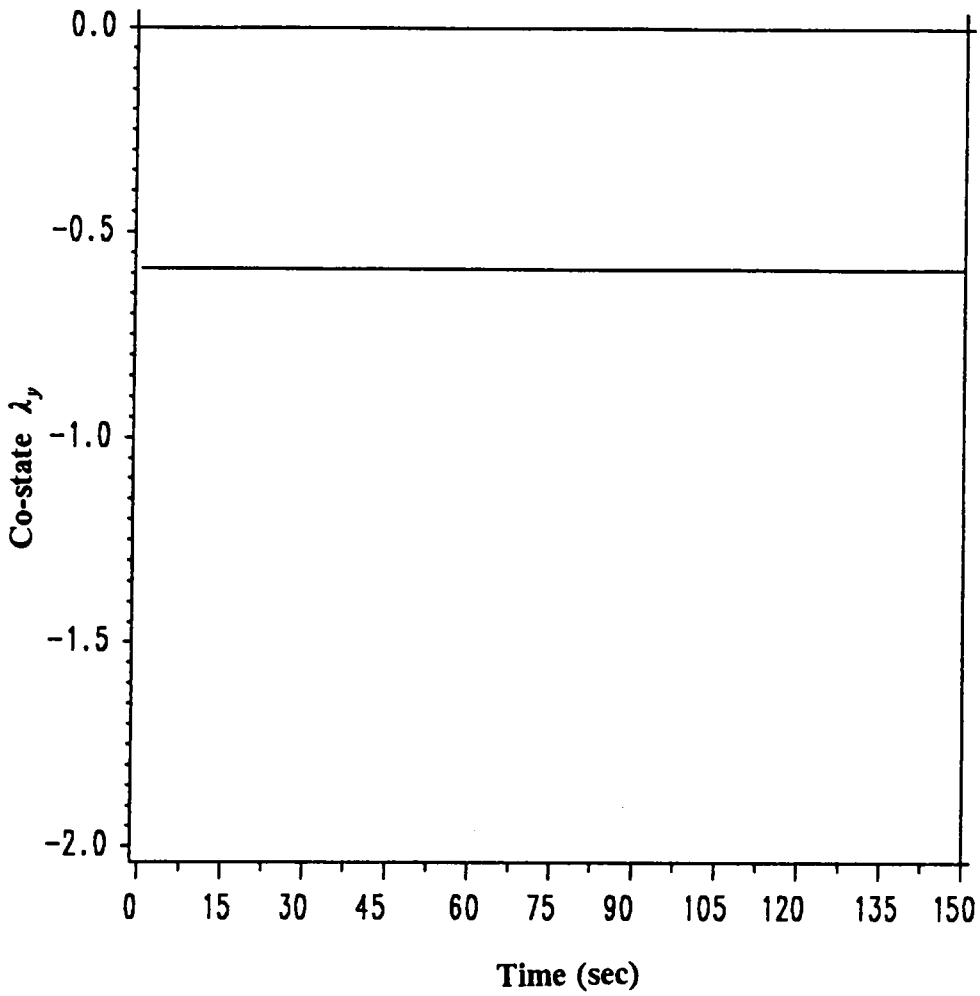

Fig. 3.14: Co-state λ_y time history for $t_f = 150s$

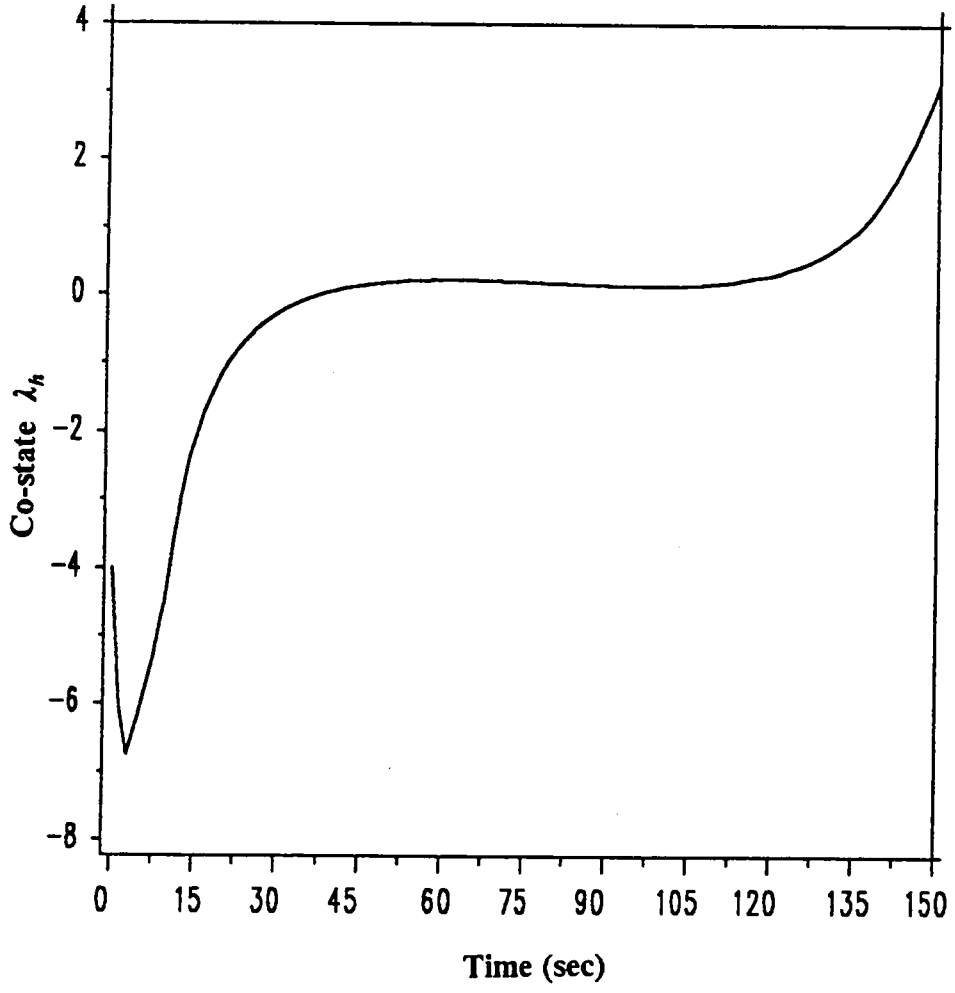

Fig. 3.15: Co-state λ_h time history for $t_f = 150s$

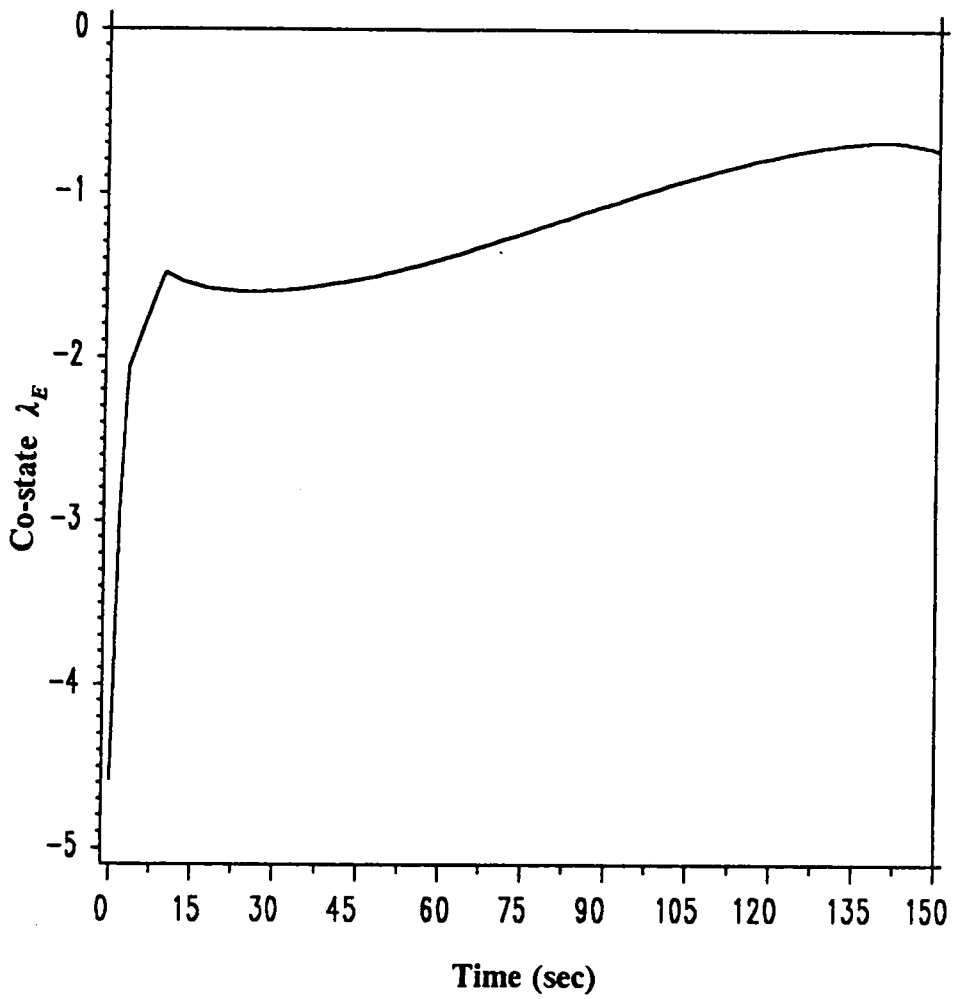

Fig. 3.16: Co-state λ_E time history for $t_f = 150s$

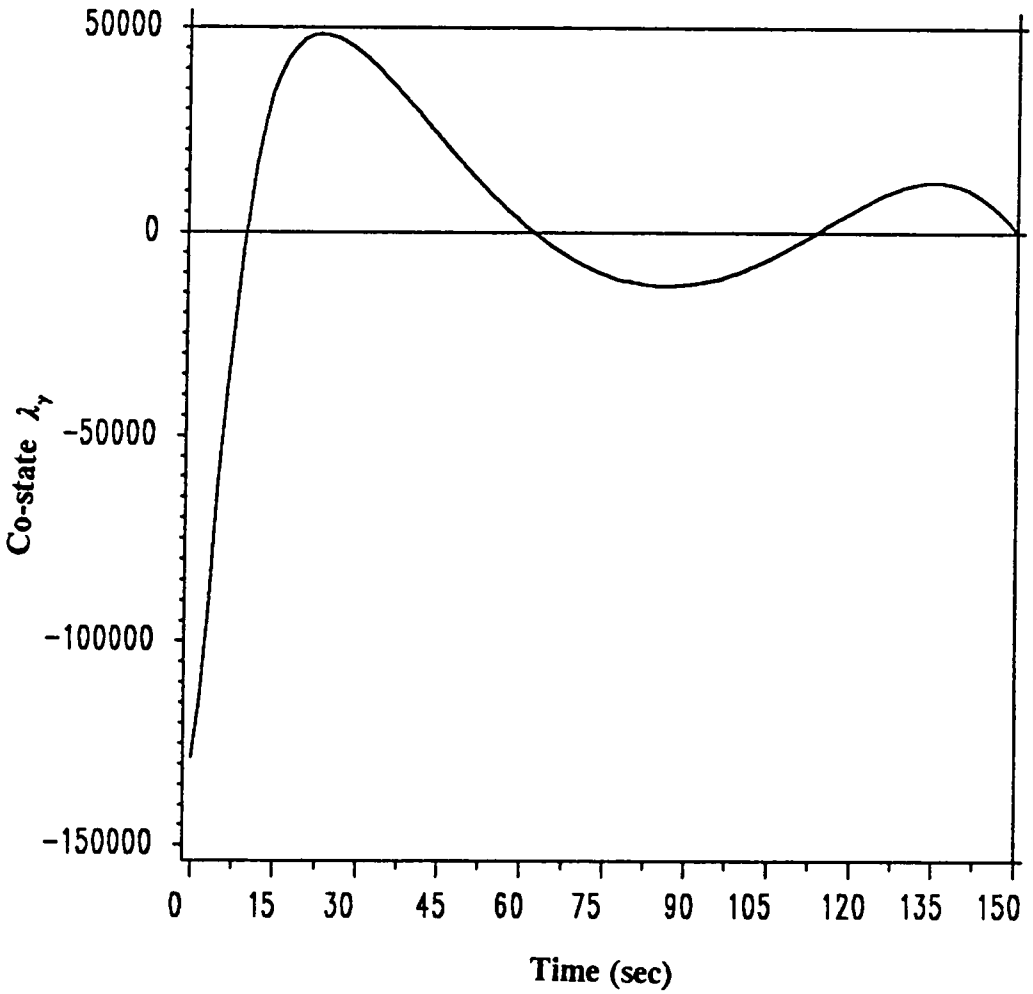

Fig. 3.17: Co-state λ_γ time history for $t_f = 150s$

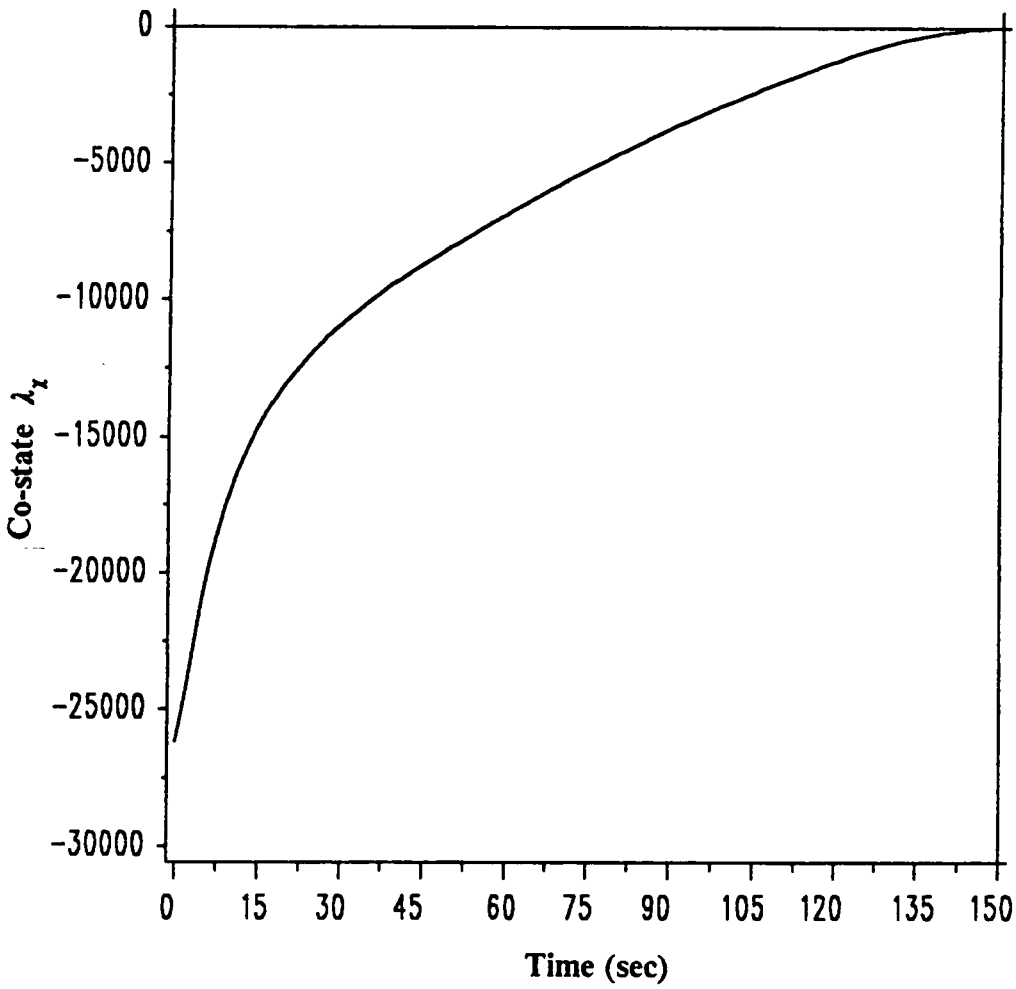

Fig. 3.18: Co-state λ_x time history for $t_f = 150s$

Chapter 4: Attainability Sets and Sufficiency Conditions

4.1: Overview

The chapter opens with a discussion of the continuation method and the homotopy parameters used to generate the boundaries of attainable sets [31]. The term attainable set is the set of all points that can be attained at a given final time when starting from a prescribed state at given initial time. In this study, "attainable set" would be considered as the projection of the six-dimensional attainable set in the state-space on the $x-y$ state-space. The nature of the attainability sets and the characteristics of the trajectories leading to the boundary points are interesting. Sufficiency conditions for optimality for regular or regularized extremals are detailed and a new matrix differential equation governing a test matrix to check **conjugate points** is also introduced.

4.2: Continuation Method

In the previous chapter it has been noted that solutions for vertical plane trajectories without three-dimensional maneuvers has been obtained from [14]. The three-dimensional model is in fact an augmented two-dimensional model with two extra states y and χ and an extra control n_h. The solution obtained from the two-dimensional model is used as an initial guess. The guess values for the heading angle and its associated co-state is assumed to be zero identically from initial time to final time. The cross-range and its co-state is also chosen as zero identically all along the trajectory. The other boundary conditions are as corresponding to p1 for maximizing $x(t_f)$.

The extremal trajectories with boundary conditions as given earlier is obtained by solving the associated TPBVP. The maximum range is indicated by point 1 in Fig. {4.1}. This figure shows the boundary of attainability for a final time of 150 seconds with the initial and final altitude and energy fixed at prescribed values. To obtain the boundary one has to obtain the maximum range and minimum range intercept points for all directions in the $x-y$ plane. This implies either maximizing or minimizing $x(t_f)$ for given $y(t_f)$ or vice-versa. The following paragraphs explain the method of solution for different $x-y$ values.

The cross-range $y(t_f)$ is used as the initial homotopy parameter. $y(t_f)$ is increased from zero to higer values. Negative values of $y(t_f)$ give symmetric solutions about the down-range axis. The down-range at final time $x(t_f)$ is maximized and hence

its co-state is fixed at negative unity. Homotopy with $y(t_f)$ is continued until point 2 in Fig. {4.1}. This point corresponds to the terminal surface which yields $\lambda_y \simeq -1$. Continuation of homotopy with $y(t_f)$ would considerably slow the convergence of the continuation technique and would eventually halt the convergence at point 3, corresponding to $\lambda_y \to \infty$. Thus at point 2, the homotopy parameter is changed from $y(t_f)$ to $x(t_f)$. This implies maximizing $y(t_f)$ with $x(t_f)$ fixed. This helps to re-scale the multipliers to keep the co-state of cross-range bounded. From point 2 to point 3, the co-state $\lambda_y = -1$ and λ_x changes from $\simeq -1$ to zero at point 3. From point 3 to point 4 the multiplier λ_x increases from zero to unity. Point 4 is characterized by $\lambda_x = +1$ and $\lambda_y = -1$. If the attainable set is strictly convex, then there exists a unique support plane with a unique outward normal at every point on the boundary [34]. The multipliers λ_x and λ_y are related to the slope of the outward normal at each point on the boundary of attainability [34]. This gives a general idea as to the boundedness of each co-state multiplier along the homotopy procedure.

It should be noted here that homotopy in a given state is also equivalent **locally** to a homotopy in its co-state. At point 4, the homotopy parameter is changed to λ_y (or $y(t_f)$). This change is to enhance convergence, anticipating the boundary of attainability to become parallel to the cross-range axis, which happens at point 5. This corresponds to $\lambda_x = +1$ and $\lambda_y = 0$.

From point 5 the homotopy was continued with $y(t_f)$, with λ_y increasing from zero to positive quantity and λ_x scaled to $+1$. It was observed that the

continuation method failed between point 5 and point 6 due to the sudden transition of λ_y from zero at point 5 to $+\infty$ at point 6. A change in homotopy parameter to cross-range or its co-state did not alter the situation. This cul-de-sac was circumvented by using the Mayer reciprocity discussed in Chapter 3. A minimum-time problem (p2) is solved, fixing $x(t_f)$ and $y(t_f)$. The re-scaling of the original problem (p1) is performed such that $\mathscr{H}(t_f) = -1$. Then for fixed final down-range, $y(t_f)$ is varied in such fashion that the final time corresponding to the isochrone being completed is enclosed within a lower and upper bound of final time. These bounds are squeezed as much as needed and the resulting solutions (suitably re-scaled) are used as initial guesses to obtain solutions to fixed final time problem p1. This method is used from point 5 to point 6.

Continuation of the attainability set boundary is performed by varying $x(t_f)$ from point 6 to point 8. Point 7 indicates $\lambda_x = 0$. Point 8 suggests a change in homotopy parameter to $y(t_f)$ to ease the convergence until point 9. The boundary of attainability shown in Fig. {4.1} has a mirror image about the x axis. Once the boundary is obtained for one isochrone, the procedure can be repeated for different final times as shown in Fig. {4.2}. It is to be noted that the homotopy can also be performed with cartesian co-ordinates x and y replaced by polar co-ordinates R and θ, by maximizing or minimizing range R for fixed values of θ. The maximum range and minimum range arcs would meet at a point beyond which one cannot increase θ for the homotopy. This would indicate an **abnormal** point.

4.3: Attainability set

The attainable sets and the boundary are shown for different final times in Fig. {4.2}. For a final time of 150 seconds, the attainability set is closed, non-convex and does not indicate presence of **holes** within the set. This set is for a fixed value of initial and final altitudes and energy. Simulation results indicate that if the final energy requirement is decreased, the maximum range is increased and the minimum-range is decreased, thus increasing the area enclosed by the set of attainability. At a given point on the boundary, the local effect of a change in the $E(t_f)$ is predicted by the sign of $\lambda_E(t_f)$ ($\lambda_E(t_f) < 0$ implies an expanding boundary as $E(t_f)$ is decreased). The energy bound at t_f is active for all points on the t_f = 150 sec. boundary. The final energy requirement specification depends upon the target data and the thrust-to-weight ratio of the missile.

The set of attainability for longer flight time of 160 seconds also shows similar characteristics as the above with an increased area. The same structure of the attainability can be observed for flight times until 169.8 seconds. These numerics are for initial and final altitudes and energy as specified numerically in Chapter 3. For flight time above 169.8 seconds the set of maximum range intercept points and the set of minimum range intercept points are "separated". The attainability set is non-convex and closed but shows the presence of a hole within the set. The area of this hole reduces for larger prescribed flight times.

It should be noted that the open-loop trajectory for the straight-back flight of missile along the negative down-range axis encounters a singularity in the differential equation for heading angle. This is due to the fact that $\gamma = 90$ degrees ($\cos\gamma = 0$) corresponds to a singularity for Eq. (2.7). This phenomenon is a deficiency of the model chosen. This problem is solved by using a two-dimensional model and verifying this solution to be a candidate for the three-dimensional model with $y = 0$ and $\chi = 0$ or π radians, depending upon the missile heading.

This structure of the attainability sets is only true for long flight times as used by a medium-range missile. It is clearly understood that if the missile travels co-altitude with the target, as it would if guided by proportional navigation, the final energy would be attained in very short time (in the order of 25 seconds) due to high-drag operation. Thus, for very short times there would exist another family of solutions drastically different in nature. However, the interest here is in medium range intercepts and these short range trajectories are not considered.

The set of attainability is only used to obtain the nature and capabilities of the missile. The maximum range boundaries are of clear interest and the trajectories leading to them are to be stored for near-optimal neighboring guidance.

Comparison between two trajectories, one maximizing down-range and other minimizing the same for fixed final value of cross-range is made. Figs. {4.3-4.11} show the state and control histories for p1 with numerical data as prescribed in

Chapter 3. The cross-range and heading-angle histories shown in Figs. {4.4 & 4.9} show the missile turning left initially followed by a right turn for the minimum range trajectory. The missile climbs to higher altitudes so that the velocity component in the horizontal plane is reduced, still maintaining sufficient energy. The minimum-range trajectories must not be misinterpreted as energy-wasting trajectories. The co-state λ_E remains negative for all the minimum-range trajectories; hence these are energy conservative.

As one completes the attainability set, maximizing $x(t_f)$ for varying values of $y(t_f)$ for the minimum-range boundary, for values of $\hat{y}(t_f) < 15$ (where $\hat{y} = y/20Kft$ is a non-dimensionalized distance) the missile starts turning left followed by a right turn. The peak heading excursion in the negative cross-range direction initially increases with reduced $y(t_f)$ and then decreases to zero, corresponding to $y(t_f) = 0$, as seen in Fig. {4.12}.

4.4: Sufficiency Conditions

The second-order necessary conditions for a weak local minima are:

- Weakened form of the Legendre-Clebsch condition, i.e., for a minimizing extremal, $\mathscr{H}_{uu} \geq 0$ for all $t_0 \leq t \leq t_f$.
- If the former is true all along the the candidate trajectory in the strengthened form , then the Jacobi condition in the weakened form must be satisfied; i.e., the interval $t_0 < t < t_f$ must not contain any point conjugate to $X(t_f)$.

It should be noted here that the above necessary conditions are applied to extremals without corners. From [22], the "necessary condition that the regular extremal must have no-conjugate-points" is only true for regular extremals without corners. The continuity of certain matrices for the accessory minimum problem is required in proving the necessary conditions; in the presence of corners, this continuity is not guarenteed. It is however necessary that no-conjugate points (with respect to t_f) exist from final time to the time where the first corner appears, i.e., the thrust switch from sustain to coast.

The conditions above, in strengthened form, are sufficient to guarantee a weak-local minimum assuming the problem to be normal. Normality simply shows that the Euler-Lagrange equations satisfying the boundary conditions are not the **only** solution to the dynamical system (then, the solution is not really a minimizer in the sense that there is no competition). For a regular extremal (an extremal along which the strengthened Legendre-Clebsch condition holds) with corners, it can be shown that the sufficiency conditions hold in the same sense as for a smooth extremal. This is due to the lemma (and Eq. (15)) in [22] being unchanged for the special case with corners (corners for the specific problem have continuity of the co-state multipliers at fixed corner time) as due to thrust switching.

For a regular test extremal, a procedure as in [21] is used to check sufficiency for a weak-local minimum.

The following scalars, vectors and matrices are defined as in [21]. For the general problem of Bolza considered in Chapter 2, define Φ and Ω as follows:

$$\Phi(X, \nu, t) = \phi(X,t) + \nu^T \psi(X,t) \tag{4.1}$$

$$\Omega(X,u, \nu, t)\,|_{t=t_f} = \left(\frac{d\Phi}{dt} + L(X,u,t)\right)_{t=t_f} \tag{4.2}$$

To check for conjugate points for a regular extremal, one can check for the problem p1 or its equivalent problem p2. To obtain a closed-loop guidance using neighboring guidance scheme with p2 as the reference solution, one has to obtain gains to predict intercept time and to provide control corrections. Since the procedure to check optimality and to evaluate gains are identical, conjugate point testing is performed on problem p2, i.e., the final time being minimized. The matrices S $(p \times p)$, R $(p \times q)$, Q $(q \times q)$ and the vectors m $(p \times 1)$, n $(q \times 1)$ and the scalar α are constructed as in [21] and the differential equations and boundary conditions governing them are given as follows:

$$\dot{S} = -S A - A^T S + S B S - C \qquad S(t_f) = \left(\frac{\partial^2 \Phi}{\partial X^2}\right)_{t=t_f} \tag{4.3}$$

$$\dot{R} = - A^T R + S B R \qquad R(t_f) = \left(\frac{\partial \psi}{\partial X}\right)^T_{t=t_f} \tag{4.4}$$

$$\dot{Q} = R^T B R \qquad Q(t_f) = [0] \tag{4.5}$$

$$\dot{m} = - A^T m + S B m \qquad m(t_f) = \left(\frac{\partial \Omega}{\partial X}\right)^T_{t=t_f} \tag{4.6}$$

$$\dot{n} = R^T B m \qquad n(t_f) = \left(\frac{d\psi}{dt}\right)_{t=t_f} \tag{4.7}$$

$$\dot{\alpha} = m^T B\, m \qquad \alpha(t_f) = \left(\frac{d\Omega}{dt}\right)_{t=t_f} \tag{4.8}$$

where the matrices A, B and C are of order $(p \times p)$ and are defined as follows:

$$A = f_X - f_u\ \mathscr{H}_{uu}^{-1}\ \mathscr{H}_{uX} \tag{4.9}$$

$$B = f_u\ \mathscr{H}_{uu}^{-1}\ f_u^T \tag{4.10}$$

$$C = \mathscr{H}_{XX} - \mathscr{H}_{Xu}\ \mathscr{H}_{uu}^{-1}\ \mathscr{H}_{uX} \tag{4.11}$$

Matrices $\overline{S}$, $\overline{R}$ and $\overline{Q}$ are defined as:

$$\overline{S} = S - \frac{m\, m^T}{\alpha} \tag{4.12}$$

$$\overline{R} = R - \frac{m\, n^T}{\alpha} \tag{4.13}$$

$$\overline{Q} = Q - \frac{n\, n^T}{\alpha} \tag{4.14}$$

The above differential equations are integrated backwards, all matrices being evaluated along the test extremal. The sufficiency conditions for a weak-local minima are:

$$\mathscr{H}_{uu} > 0 \qquad for \qquad t_0 \le t \le t_f \tag{4.15}$$

$$\overline{Q} < 0\,,\ \alpha > 0 \qquad for \qquad t_0 \le t < t_f \tag{4.16}$$

$$\overline{S} - \overline{R}\,\overline{Q}^{-1}\,\overline{R}^T \ finite, \qquad for \qquad t_0 \le t < t_f \tag{4.17}$$

These correspond to the strengthened Legendre-Clebsch condition, normality condition and the "no-conjugate point" condition, respectively. In this connection, note that for a fixed final time problem, the conditions are similar as given below:

$$\mathscr{H}_{uu} > 0 \qquad for \qquad t_0 \le t \le t_f \tag{4.18}$$

$$Q < 0, \qquad for \qquad t_0 \le t < t_f \tag{4.19}$$

$$S - R\,Q^{-1}\,R^T \ finite, \qquad for \qquad t_0 \le t < t_f \tag{4.20}$$

For the fixed final time problem, $S \to \infty$ does not necessarily imply that $(S - R\,Q^{-1}\,R^T) \to \infty$. Similarly for the terminal time unspecified problem, one can observe that $\overline{S} \to \infty$ does not necessarily imply that $(\overline{S} - \overline{R}\,\overline{Q}^{-1}\,\overline{R}^T) \to \infty$.

It is observed that for some test extremals, during the backward integration, S became unbounded and checking for conjugate points for smaller times became impossible. This problem is avoided by using the derivations detailed in Appendix B. A matrix $\overline{H} = \overline{S} - \overline{R}\,\overline{Q}^{-1}\,\overline{R}^T$, its governing differential equation, and an associated boundary conditions are derived. A similar matrix H and associated differential equation and boundary conditions are also derived for fixed terminal time problems. Hence, this equation can be integrated backwards in time to check for conjugate points. The conjugate point corresponds to the point where $\overline{H} \to \infty$ or $H \to \infty$, for p2 and p1 respectively.

4.5: Regularization

It is observed that sufficiency conditions require the Legendre-Clebsch condition in the strengthened form all along the extremal for $t_0 \leq t \leq t_f$. For extremals corresponding to the problem of range maximization/minimization or the equivalent minimum-time problem, if the final heading angle and flight-path-angle at final time are unspecified, then the associated co-state variables at final time is zero by transversality conditions as given in Eqs. (3.30 & 3.31). This requires that both the controls n_v and n_h are simultaneously zero at final time. The elements of the $\mathscr{H}_{uu}$ matrix become identically zero yielding it singular, and making the extremal non-regular. For such extremals, the conjugate-point testing cannot be performed in the usual sense and a weak local minima cannot be established.

In a trial to overcome this problem, regularization of extremals is attempted by augmenting the performance index of the original problem p1 as follows:

$$\mathscr{J} = x(t_f) + \varepsilon_1 \gamma(t_f) + \varepsilon_2 \chi(t_f) \tag{4.21}$$

where, $\varepsilon_i \quad i = 1, 2$ are **small** quantities, not both zero. The term $x(t_f)$ may also be replaced by $y(t_f)$ depending upon the region of homotopy. This ensures that at least one of the controls is non-zero at final time, yielding $\mathscr{H}_{uu}$ matrix positive definite at final time, irrespective of the sign of ε_i. It is observed that for the flight in the vertical plane [14], the vanishing of the matrix $\mathscr{H}_{uu}$ can also happen for $t_0 \leq t < t_f$. These problems can be regularized by using $\varepsilon_2 \neq 0$. It has also

been observed, that for three-dimensional flight, the vanishing of the matrix $\mathscr{H}_{uu}$ in the interior of the time domain requires that two continuously varying co-state variables λ_γ and λ_χ changes sign at the same time. If this happens then, the cross-over can be made non-simultaneous by a careful selection of ε_i .

Once the problem is regularized, then one checks the Jacobi condition using the method detailed earlier. It has been observed that the non-regular TPBVP solved using BOUNDSCO yields a solution within prescribed error tolerance. The transversality conditions $\lambda_\gamma(t_f) = 0$ and $\lambda_\chi(t_f) = 0$ are used for the problem with the final angles free. The numerical solution yields values $\lambda_\gamma(t_f) = \delta_1$ and $\lambda_\chi(t_f) = \delta_2$, the δ_i of order 10^{-14}. If these values of δ_i are used as the ε_i, $i = 1, 2$, for the regularized problem and if the regularized TPBVP re-solved it would yield the same range ($x(t_f)$ or $y(t_f)$) within prescribed tolerance. This is due to the limitation of numerical precision in computations. The conjugate point test can be performed for this extremal and one can establish a weak-local minimum for the regularized extremal. Thus, one can abandon the "old" non-regular extremal in favor of the "new" regularized extremal, with identical (numerically) cost of range and check sufficiency conditions. It is clear that the sufficiency holds only for the regularized extremal and not the original non-regular extremal. Numerical tests for trajectories leading to the boundary of attainability were performed and absence of conjugate points established for regular and regularized extremals.

In theory, for the regular or regularized problem, the sufficiency conditions imply the existence of a **local** field about the test extremal. The existence of such a field about an non-regular extremal using classical theory is not proven. Even though one can show that there exists a field about the extremal with some $\varepsilon_i \to 0$ with $\varepsilon_i \neq 0$, one has to prove that this field does not collapse onto the extremal for both $\varepsilon_i = 0$. Conjugate-point testing for non-regular extremals may be performed by using computational Jacobi procedures as in [35]. However the absence of conjugate-points along the test extremal does not imply the existence of a local field about the non-regular extremal.

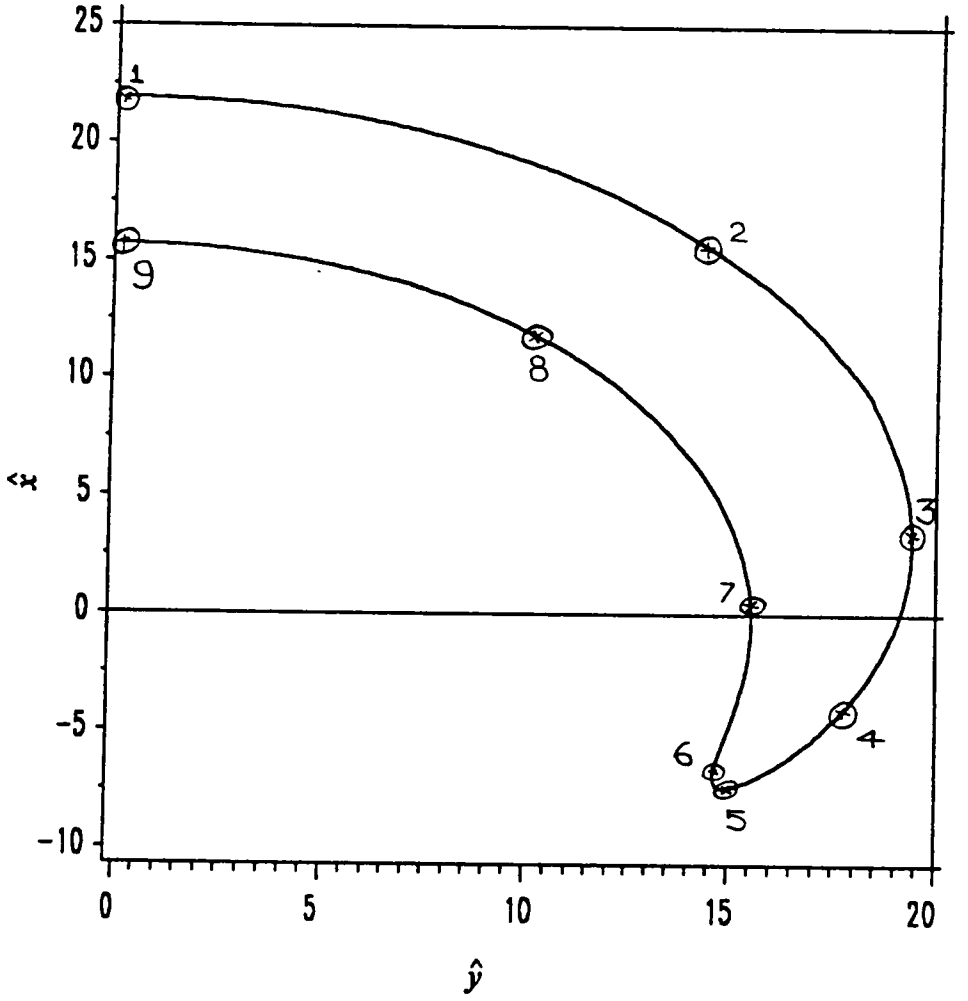

Fig. 4.1: Attainability set boundary and homotopy phases for $t_f = 150$ seconds

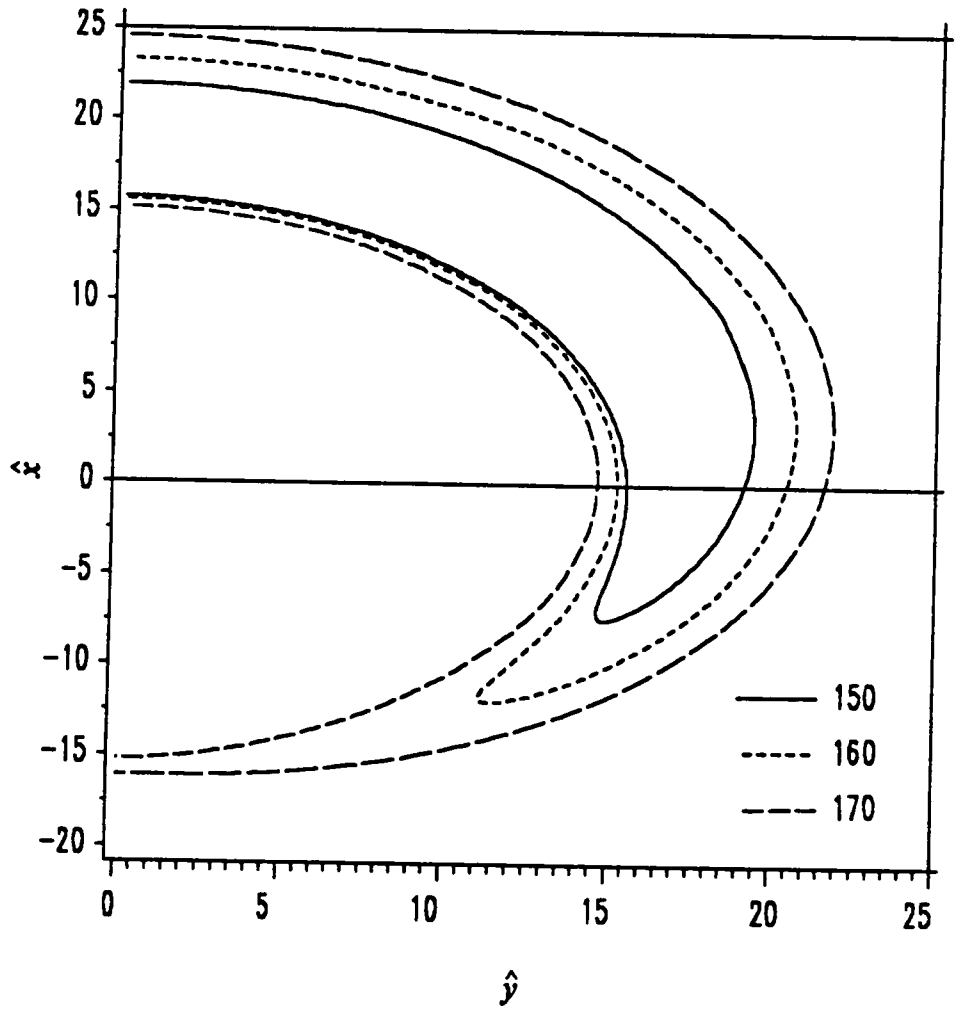

Fig. 4.2: Attainability sets for final times $t_f = 150, 160, 170$ seconds

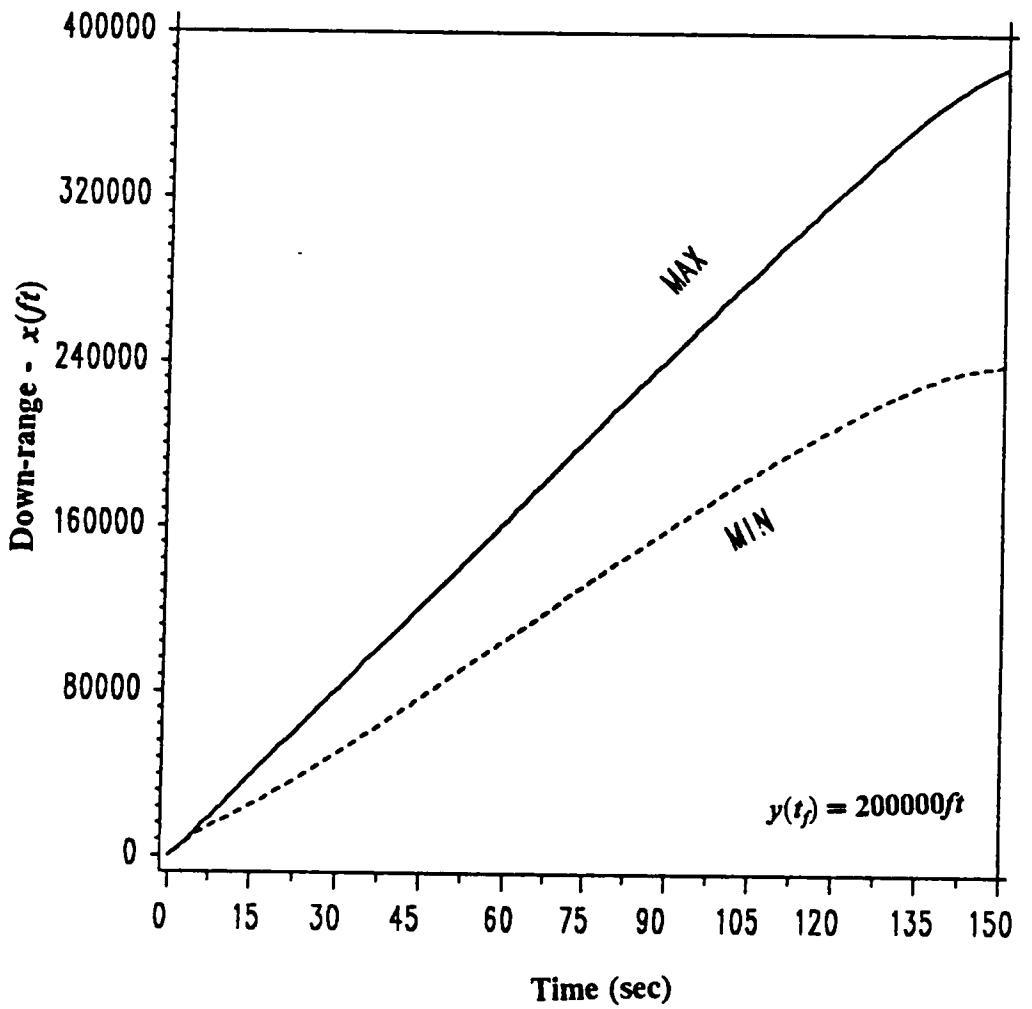

Fig. 4.3: Comparison of down-range x for maximum and minimum down-range extremals

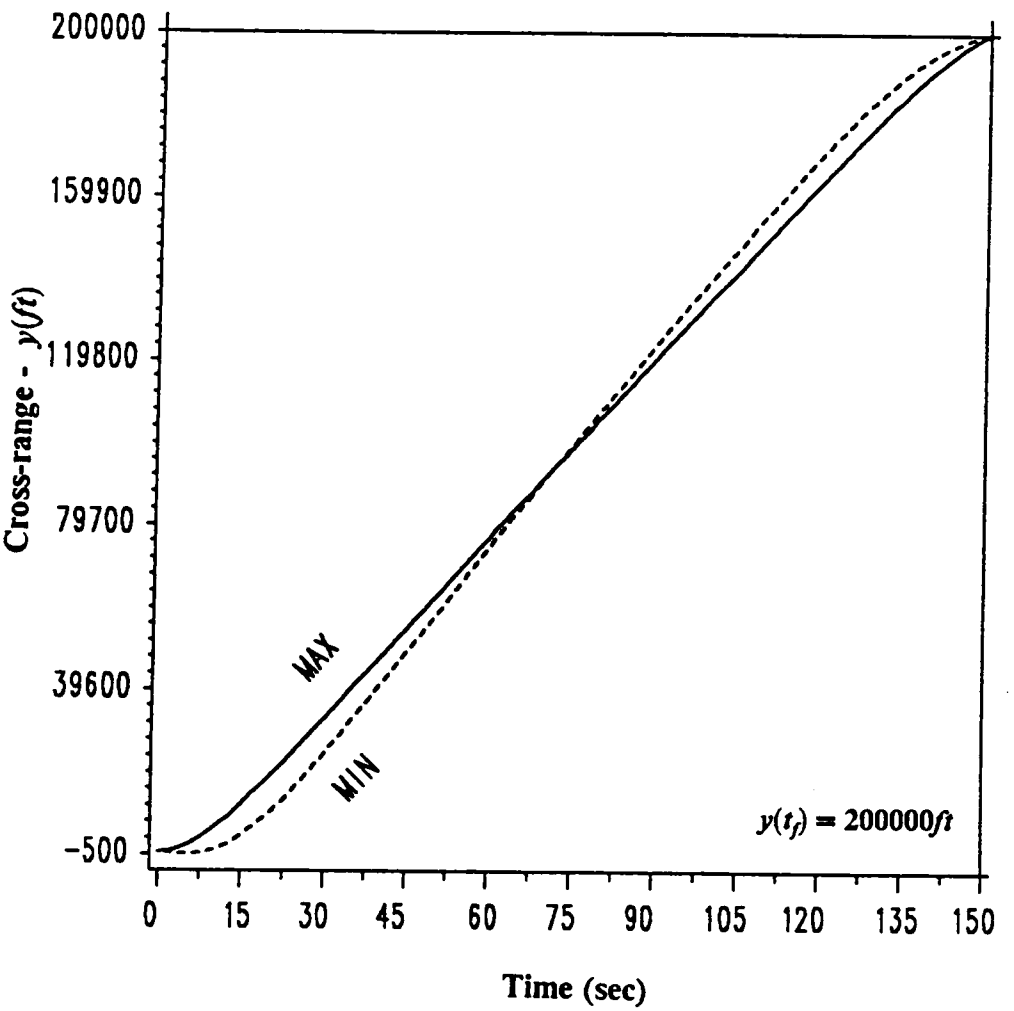

Fig. 4.4: Comparison of cross-range y for maximum and minimum down-range extremals

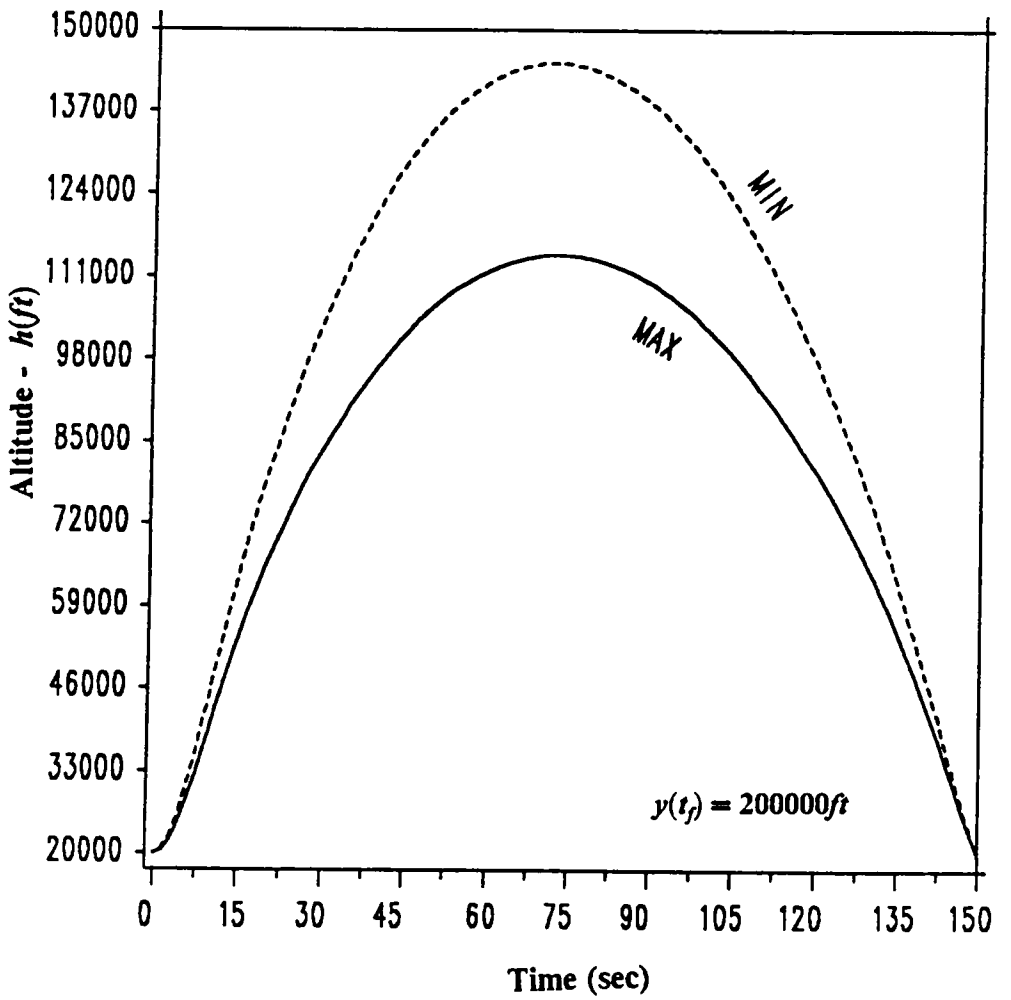

Fig. 4.5: Comparison of altitude h for maximum and minimum down-range extremals

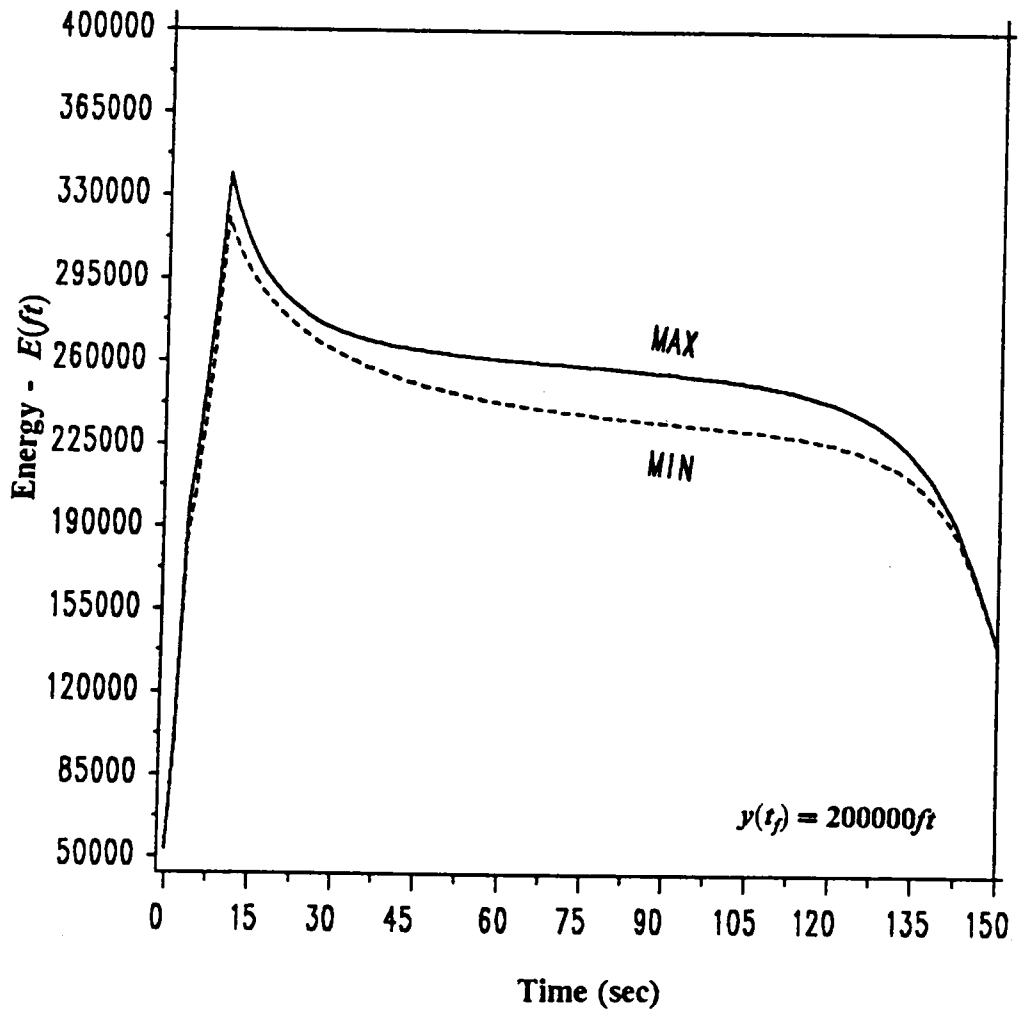

Fig. 4.6: Comparison of energy E for maximum and minimum down-range extremals

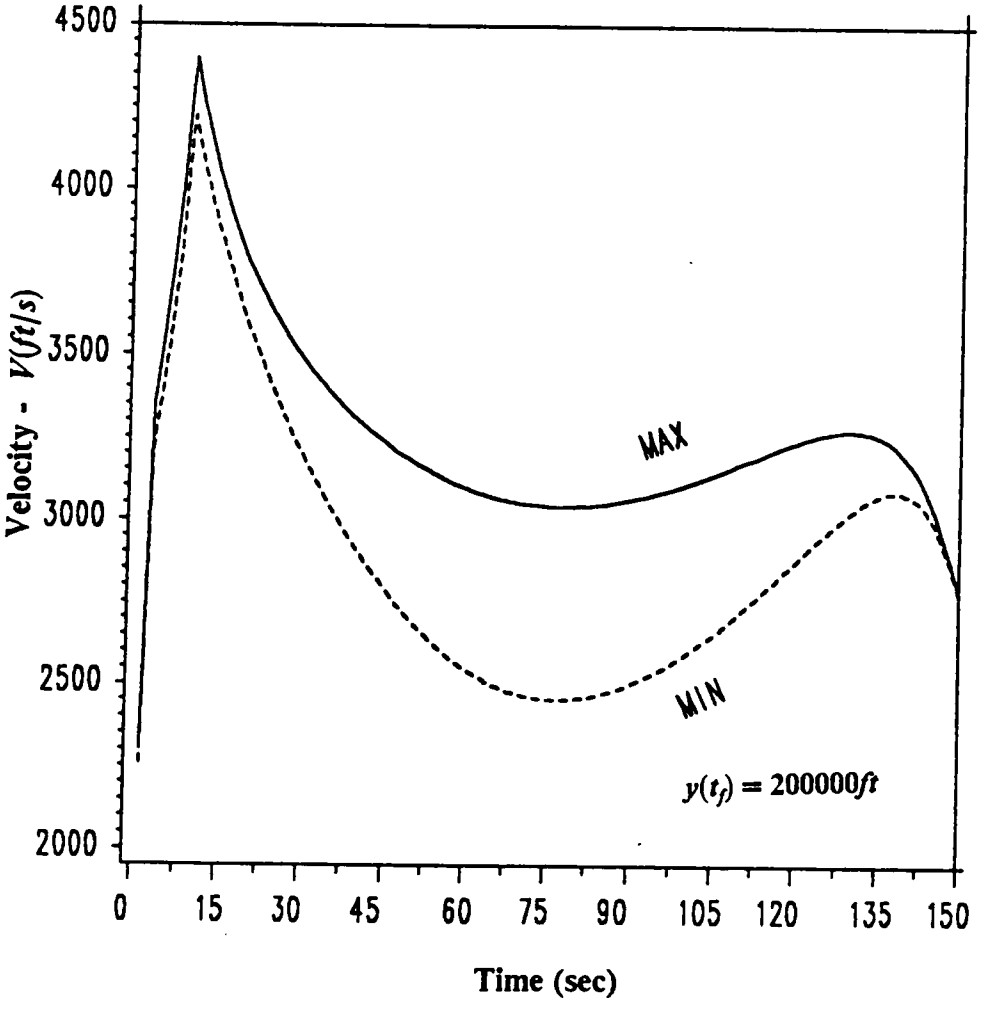

Fig. 4.7: Comparison of velocity V for maximum and minimum down-range extremals

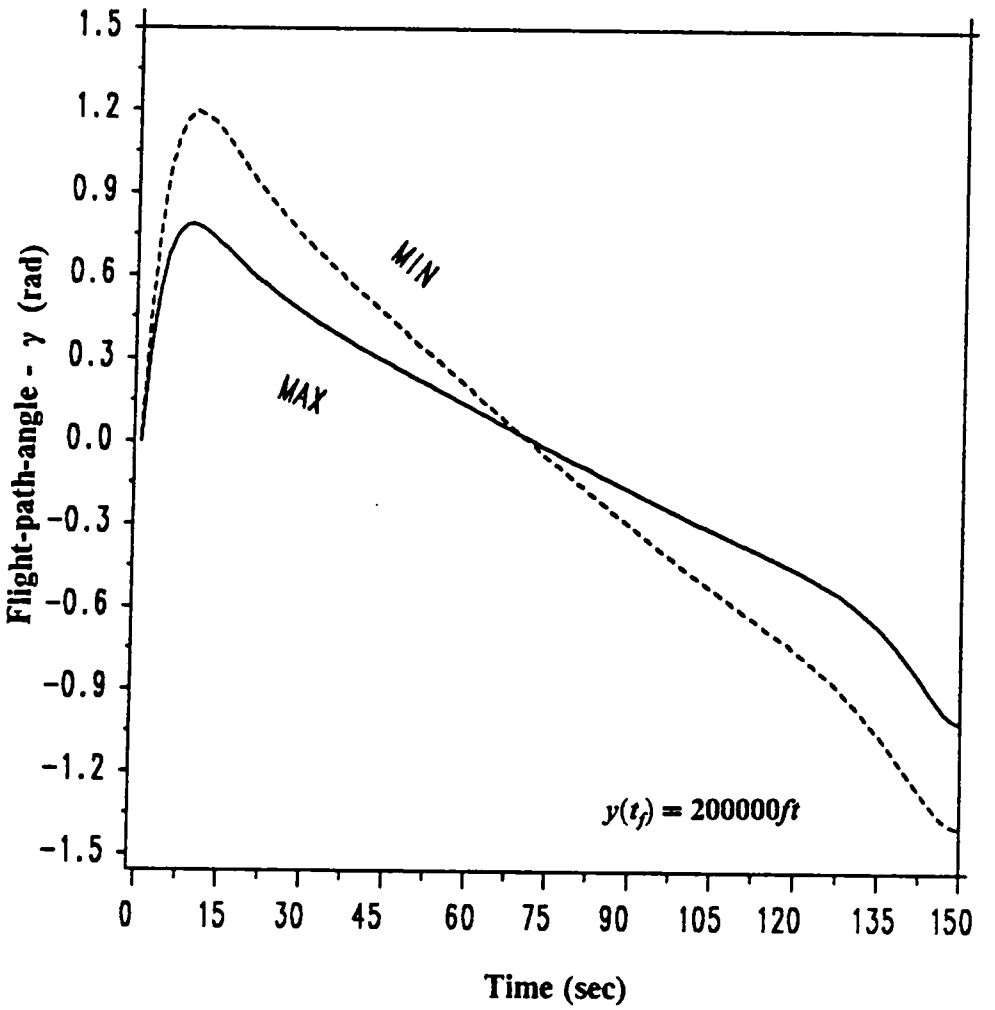

Fig. 4.8: Comparison of flight-path-angle γ for maximum and minimum down-range extremals

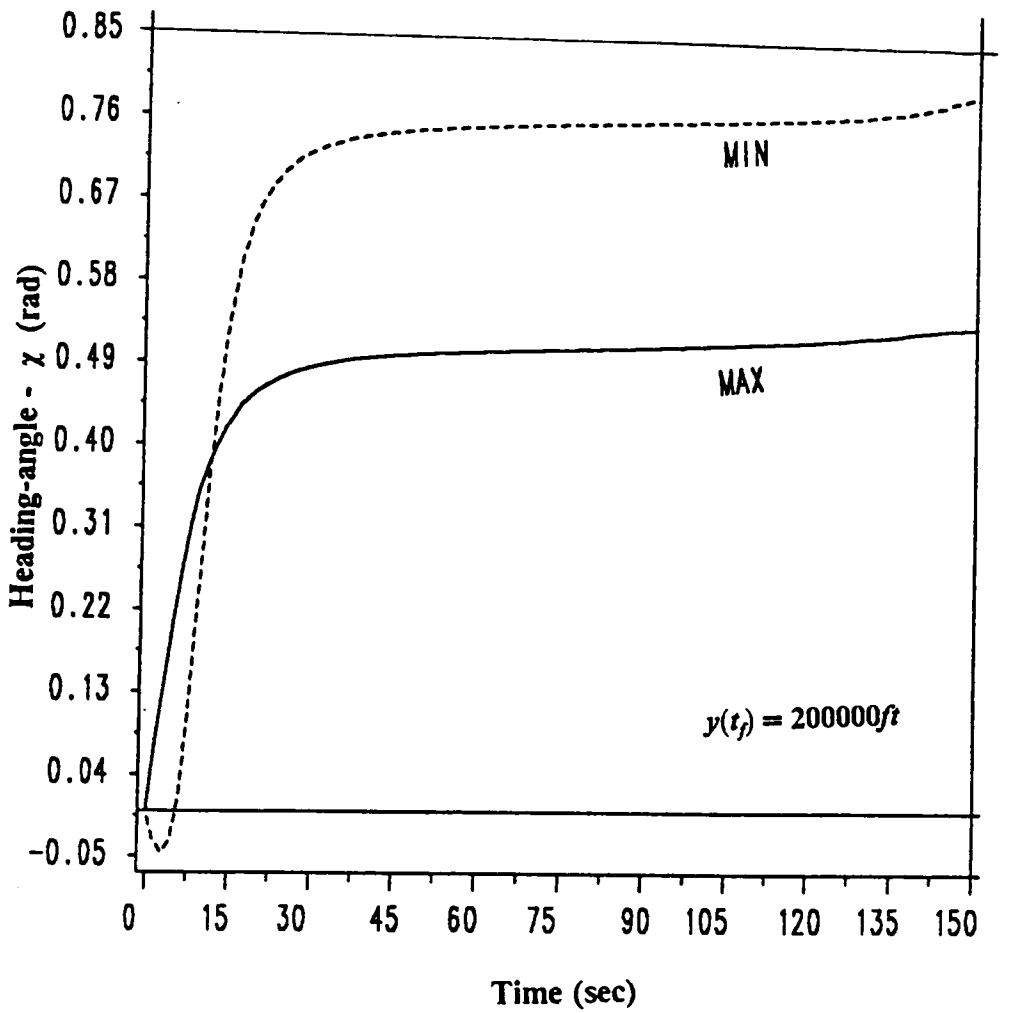

Fig. 4.9: Comparison of heading-angle χ for maximum and minimum down-range extremals

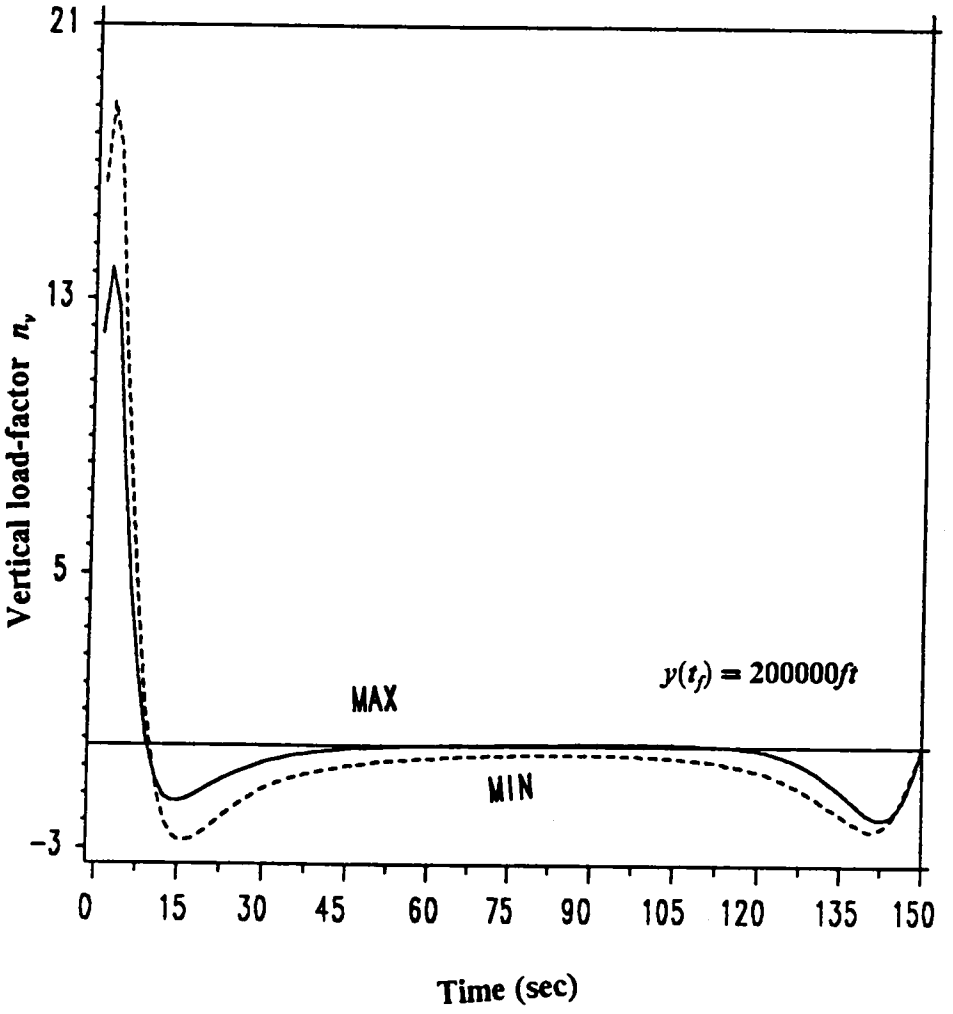

Fig. 4.10: Comparison of vertical load-factor n_v for maximum and minimum down-range extremals

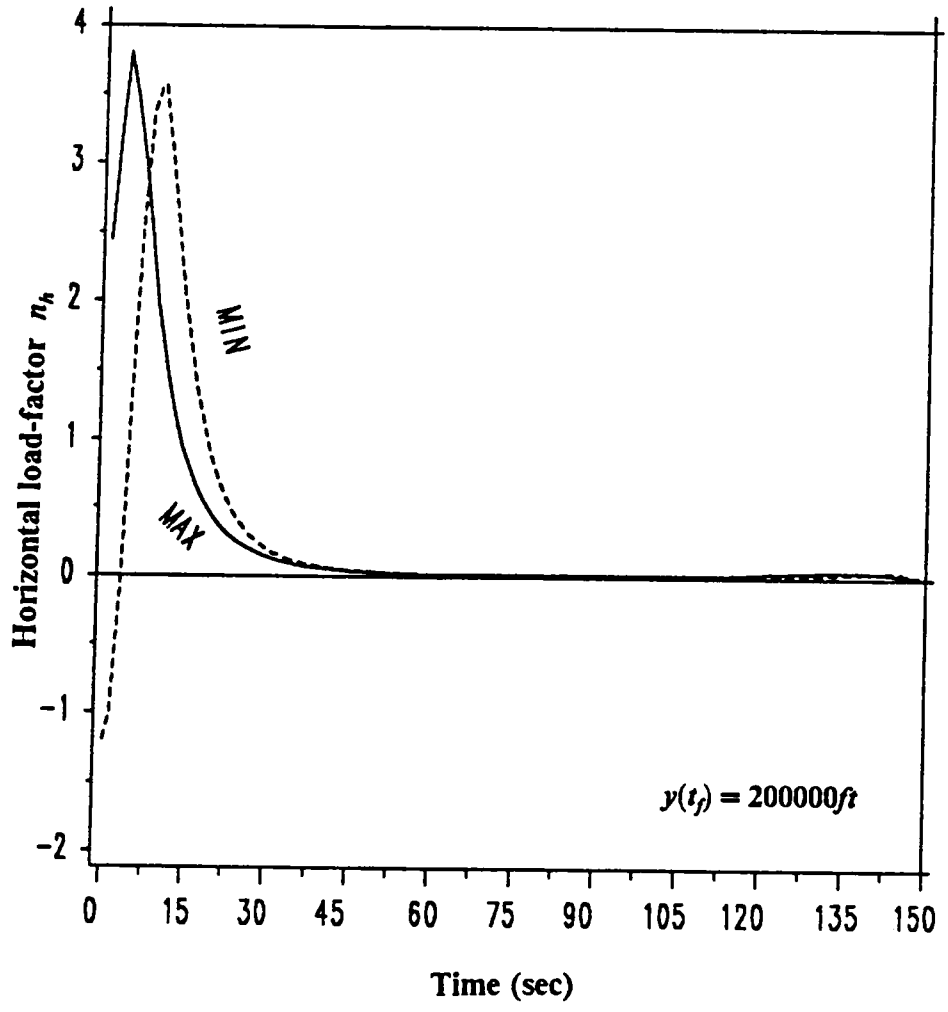

Fig. 4.11: Comparison of horizontal load-factor n_h for maximum and minimum down-range extremals

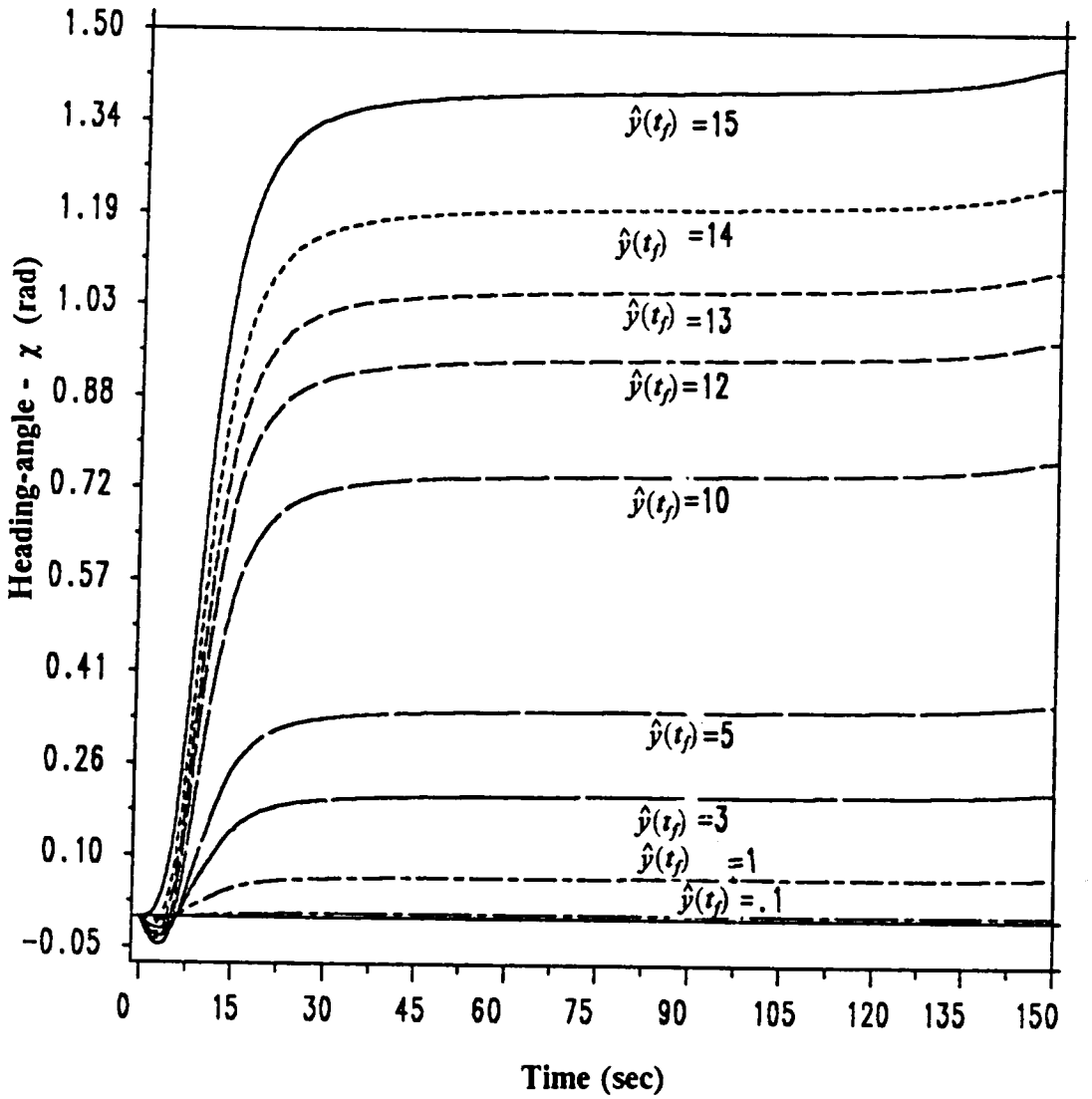

Fig. 4.12: Heading-angle history for trajectories leading to minimum range boundaries

Chapter 5: Boost-phase Guidance

5.1: Overview

This chapter is devoted to the development of a guidance scheme for the initial boost-sustain thrusting phase of the missile in flight. The term **boost-phase** is used for the time period during the thrust-phase with high magnitudes of control efforts. This phase is radically different from the rest of the trajectory in that the control variables show transient behavior of high magnitudes and hence guidance in presence of an active control constraint is considered. An efficient method of gain evaluation is also considered in detail.

5.2: Guidance Algorithm

The nominal intercept point is chosen as explained in Chapter 2, i.e., the extrapolated target position intersects the expanding (for increasing final time) maximum range boundary of attainability. Once the nominal intercept

co-ordinate is located, the "closest" nominal solution is used as a reference trajectory. The reference trajectory which is a solution of problem p2 for the above intercept scenario is obtained from stored data for on-board use. Near-optimal closed-loop guidance is performed about this reference trajectory.

The initial maneuver performed by the air-to-air missile is a combination of high lofting to reach high altitudes during the thrust phase and simultaneous horizontal plane maneuvers to align head-on with the predicted intercept point (PIP). The horizontal and vertical load-factors are of high magnitudes. The structural and aerodynamic limits of the missile constrain the control efforts. In this section of the guidance scheme, the problem of near optimal guidance with an active control constraint is considered. A discussion of neighboring trajectories in the presence of constraints can be found in [36,37].

The possibility of an active normal acceleration limit during this phase was simulated with a nominal problem with an active structural limit. The resultant load factor for the nominal intercept problem solved by using the TPBVP solver hits the constraint and remains on it for a finite period of time before leaving it. The nominal solution for the optimal control problem as formulated earlier uses n_v and n_h as the two control variables. The same problem and solution can be easily transformed with resultant load factor n and bank angle μ_b as the two new control variables. This eases the development of the neighboring optimal guidance scheme. The two new controls are related to the old ones by the usual formulae: $n_v = n\ \cos(\mu_b)$ and $n_h = n\ \sin(\mu_b)$.

Fig. {5.1} shows the nominal time history of the resultant load-factor. Let t_1 be the time of entry of n into the control constraint and let t_2 be the time of exit of n from the control constraint. Fig. {5.2} shows the nominal bank-angle history and Fig. {5.3} shows the control constraint multiplier μ (also called the Valentine multiplier used to augment the Hamiltonian) [21]. The continuity of the multiplier across the junctions is noted.

While developing gains for the closed-loop guidance, we assume the following:

- Neighboring extremals have the same switching structure as regards to the control constraint and the thrust switching.
- The perturbations in state variables are "small".

The gains required for the closed-loop guidance are obtained as follows:
At initial time t_0 a small perturbation is made in one of the states and the new optimal control intercept problem is solved via the TPBVP. The new state and control at t_0 is noted. The scheme is redone for the same perturbation in the reverse direction. The gain at t_0 for the required control-state pair is evaluated using a central difference. This is then performed for all other individual state perturbations. Once the gains are evaluated at initial time, this is repeated at different time nodes [38]. If there are p states and r nodes at which gains are required, it necessitates the solution of the TPBVP at least $p\,r$ times for a foward or backward difference method.

A more efficient, but possibly less accurate method is discussed below:

At initial time t_0 a small perturbation is made in one of the states as before and the new intercept problem resolved. The state and control values of the new TPBVP is stored at a number of sample points. The changes in controls and states from the nominal solution are recorded as a function of time. Next, a perturbation in the second state is made and the change in controls and states from nominal is recorded. This is continued for all six states and yields a set of six linear equations which when solved gives the required gains for the first control.

The set of equations are as follows:

$$\begin{bmatrix} \delta n_1(t) \\ \delta n_2(t) \\ \delta n_3(t) \\ \delta n_4(t) \\ \delta n_5(t) \\ \delta n_6(t) \end{bmatrix} = \begin{bmatrix} \delta x_1(t) & \delta y_1(t) & \delta h_1(t) & \delta E_1(t) & \delta \gamma_1(t) & \delta \chi_1(t) \\ \delta x_2(t) & \delta y_2(t) & \delta h_2(t) & \delta E_2(t) & \delta \gamma_2(t) & \delta \chi_2(t) \\ \delta x_3(t) & \delta y_3(t) & \delta h_3(t) & \delta E_3(t) & \delta \gamma_3(t) & \delta \chi_3(t) \\ \delta x_4(t) & \delta y_4(t) & \delta h_4(t) & \delta E_4(t) & \delta \gamma_4(t) & \delta \chi_4(t) \\ \delta x_5(t) & \delta y_5(t) & \delta h_5(t). & \delta E_5(t) & \delta \gamma_5(t) & \delta \chi_5(t) \\ \delta x_6(t) & \delta y_6(t) & \delta h_6(t) & \delta E_6(t) & \delta \gamma_6(t) & \delta \chi_6(t) \end{bmatrix} \begin{bmatrix} \frac{\partial n}{\partial x}(t) \\ \frac{\partial n}{\partial y}(t) \\ \frac{\partial n}{\partial h}(t) \\ \frac{\partial n}{\partial E}(t) \\ \frac{\partial n}{\partial \gamma}(t) \\ \frac{\partial n}{\partial \chi}(t) \end{bmatrix} \tag{5.1}$$

where, the unknowns are $\frac{\partial n}{\partial x}(t)$ etc. corresponding to the gains. $\delta n_i(t)$ is the difference in load-factor between nominal and the perturbed solutions with perturbation at initial time done to the i^{th} state (i=1 corresponds to down-range, x, and so on). Another such set of six equations exists for the second control μ_b.

The advantage of the second method of gain evaluation is that new optimal control problems need not be solved at different times. The TPBVP need be only redone p times, if there are p states. Inaccuracies arising due to solving an ill-conditioned set of linear equations is a possible disadvantage. The fundamental matrix obtained by linearizing the original system about the reference trajectory and expressing in a closed-loop form is a first order approximation of the transpose of the time-varying matrix in Eq. (5.1). Theoretically, the fundamental matrix cannot be singular. Neglecting second-order errors one can presume the non-singularity of the above matrix if six independent perturbation vectors are used at initial time. Thus one expects that for sufficiently small initial perturbations, the matrix will not be singular, though it may be badly conditioned for inversion.

The Riccati approach [Chapter 6;21] to obtain feedback gains was not implemented for this phase of the guidance because the constrained arc complicates the analysis. The gains obtained by the above method are meaningful only from time t_0 to t_1^- , t_1^+ to t_2^- and t_2^+ to t_f ; where, t_1^- is the earliest time at which the load-factor control gets saturated due to state perturbations at initial time for gain evaluations. Similarly, t_1^+ is the latest time at which the load-factor control gets saturated due to state perturbations at initial time for gain evaluation. The times t_2^- and t_2^+ correspond to the earliest and latest times for exit from the control constraint. Subscripts $(t)_-$ and $(t)_+$ denote values just to the left and right of (t).

The feedback control for neighboring solutions are obtained as described below: Let δt_1 be the shift in entry time as compared to t_1 of the nominal solution. This is known only during real flight and is not predicted earlier. The closed loop guidance is initiated from initial time and the closed-loop load-factor control, generated by the usual linear feedback law, is closely tracked. The closed-loop controls for some special regions are described below.

If n is unconstrained at t_1 , then from time t_1 to $(t_1 + \delta t_1)$ we use extrapolated controls and gains given by:

$$u_{CL}(t) = u_N(t_1) + \dot{u}_N(t_1)_- \; [t - t_1] + G(t_1^-) \; \delta X(t) \tag{5.2}$$

If n encounters the constraint earlier than t_1 , then $\delta t_1 < 0$ and :

$$u_{CL}(t) = u_N(t_1) + \dot{u}_N(t_1)_+ \; [t - t_1] + G(t_1^+) \; \delta X(t) \tag{5.3}$$

The suffix N denotes the reference values. $G(.)$ denotes the feedback gain vector and $\delta X(t)$ denotes the perturbation in states from the nominal. In the time zones $t_1^- < t < t_1^+$, $t_2^- < t < t_2^+$ and at times when the nominal and the closed-loop trajectories exhibit conflicting nature (one constrained and the other unconstrained), constant extrapolated gains are used. It can be easily shown that only second-order errors of the form $\delta X \, \delta t$ are introduced by this extrapolation, and these are neglected. The bank-angle control should also be extrapolated due to the fact that the change in control with respect to state perturbations exhibits a kink at the switching points yielding the linearization across the switching point to be inaccurate.

Once the load-factor control is riding the constraint, the feedback control for bank-angle is evaluated using the respective gains. The exit time from the constraint arc is decided by comparing the two competitive controls:

$$n_{CL}(t) = n_N(t_2) + \dot{n}_N(t_2)_+ \; [t - t_2] + G(t_2^+) \; \delta X(t) \tag{5.4}$$

and

$$n_{CL}(t) = n_{constrained}$$

When the former is lesser than the latter, the exit from the control constraint is made.

Small perturbations in each of the six states were used to obtain the gains. Test cases of closed-loop guidance were performed with different perturbations. The perturbed optimal control problem was re-solved (via BOUNDSCO) and results compared. The closed-loop solutions behave close to the exact optimal solutions of the perturbed problem. Fig. {5.12-5.23} shows typical gain histories stored for the boost-phase. The figures do not show the extrapolated gains. The discontinuities in the gains at entry and exit points are clearly seen for the load-factor control. Note the zero load-factor gains along the active control constraint.

Large perturbations at initial time were made and the closed-loop guidance was studied. The reference nominal trajectory used had an active structural limit of 13.4 g. Note that this value is much lower than expected for this type of missile, and was used only to illustrate the control limit phenomena. The simulations

were performed for different errors in initial states. The specific perturbation simulated is for $\delta h(t_0) = -2000 ft$. Fig. {5.4} show the nominal, perturbed optimal and the closed-loop load-factor solutions. Fig. {5.5} similarly exhibits the bank-angle history. Figs. {5.6-5.11} compares the state histories between the optimal and the closed-loop guidance scheme, exhibiting the accuracy of linearization. For larger initial perturbations it is generally observed that the linearization is inaccurate and this can be particularly noticed with bank-angle control jump at switching points, due to the increasing magnitude of second-order errors.

The assumptions made before for evaluating the gains for a feedback strategy required that the switching structure remain the same for the perturbed trajectory. This implies that the exit from the control constraint and the thrust switch from boost to sustain phase cannot change order. It may happen that the exit from the control constraint for the nominal solution be "very close" to the first thrust switching time t_b . This is a quite likely scenario. If this happens, the earlier guidance scheme would perform poorly, due to the fact that the gains are invalid for a changed switching structure.

A new guidance scheme is detailed for the case when the nominal control switch occurs "close" to the thrust switch and possible change in switching structure may occur. Assume the following:

- Neighboring extremals have the same switching structure as regards to the control constraint only.
- The perturbations in state variables are "small".

Assume a nominal load-factor control reference solution 1 as shown in Fig. {5.24}. The states and the control variables are stored as usual. The load-factor control exit time from the constraint, denoted by t_{s1}, is greater than the thrust switching time denoted by t_b from boost to sustain phase. A second back-up reference trajectory is also stored, obtained by solving a perturbed problem with a perturbation $\Delta X(t_0)$ in any one or more of the states at initial time, such that the control exit from the constraint is made before t_b. That such a solution exists is observed for the typical problem at hand. This trajectory is indicated by the index 2. The back-up trajectory is in general non-unique.

Let $G_1(t)$ be the gain matrix associated with trajectory 1 obtained by the schemes proposed earlier. The perturbations used to obtain these gains must be such that the neighboring solutions have the same switching structure regards to the control and thrust. Another set of gains $K_1(t) = \frac{\partial t_{s1}}{\partial X}$, is evaluated for trajectory 1. This gain is valid for the region $t > t_b$. Similar gains $G_2(t)$ and $K_2(t)$ are evaluated about the back-up trajectory and stored.

The closed-loop guidance is performed as follows:

An any time t, the perturbation of the actual measured state from the trajectory 1 is obtained. Let this be denoted by δX_1 vector. The change in switching time

t_{s1} is predicted using the formula $dt_{s1} = K_1(t)\,\delta X_1(t)$. If this is such that the predicted switching time is greater than t_b, guidance is performed in the usual sense with the reference trajectory continuing to be trajectory 1. If dt_{s1} is such that the predicted switching point is to the left of t_b, then the guidance is performed about the back-up reference trajectory 2. The directional property of dt_{s1} is not lost if for a given state perturbation one uses K_1 even for $t < t_b$. The exact switching time is not required. The only information needed is whether the switching is to the left or right of t_b. The closed-loop control is evaluated as usual and the exit from the control constraint made using similar logic as in Eq. (5.4), the reference trajectory, being either 1 or 2, depending on the state perturbations.

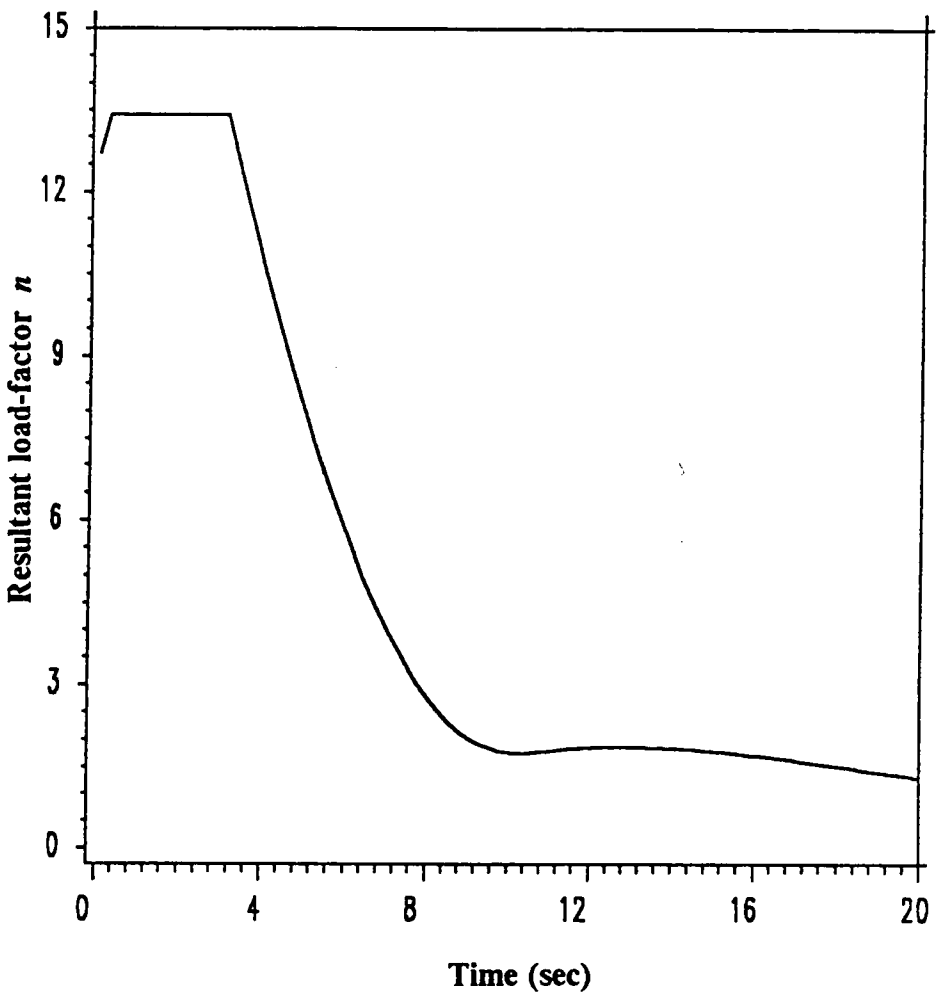

Fig. 5.1: Resultant load-factor time history of reference trajectory in presence of active control constraint

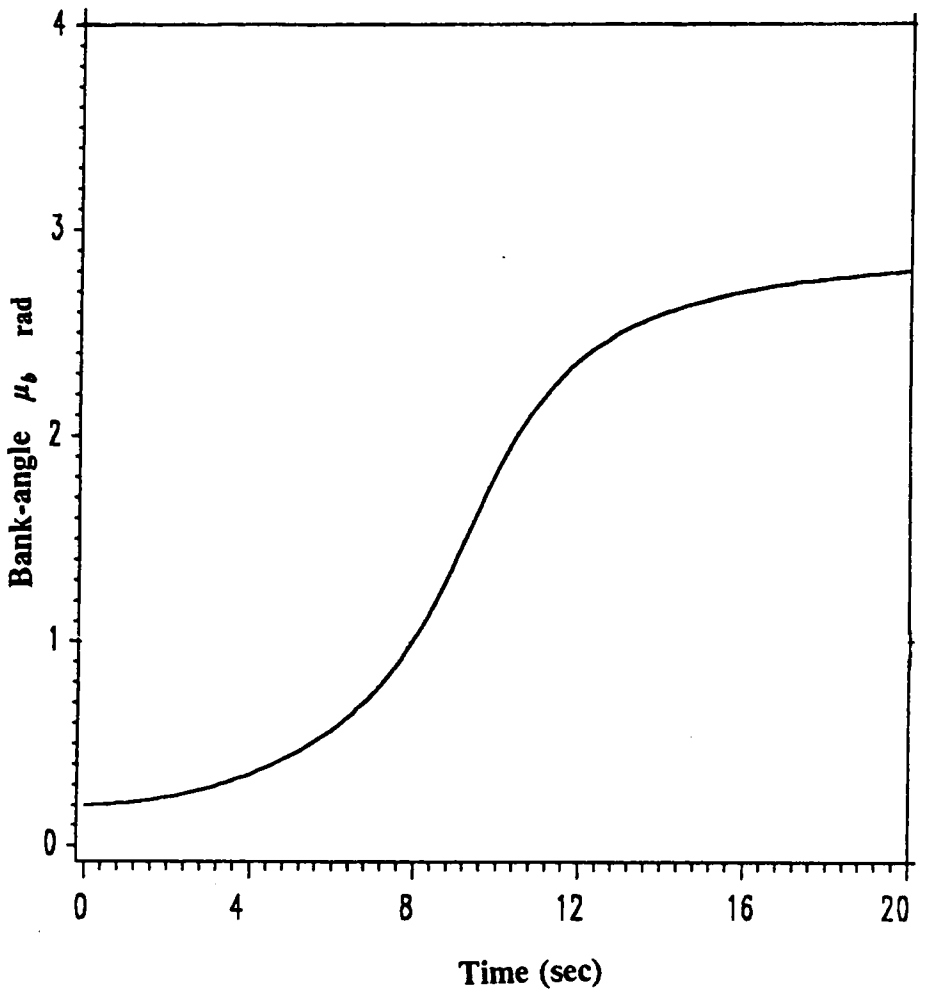

Fig. 5.2: Bank-angle time history of reference trajectory in presence of active control constraint

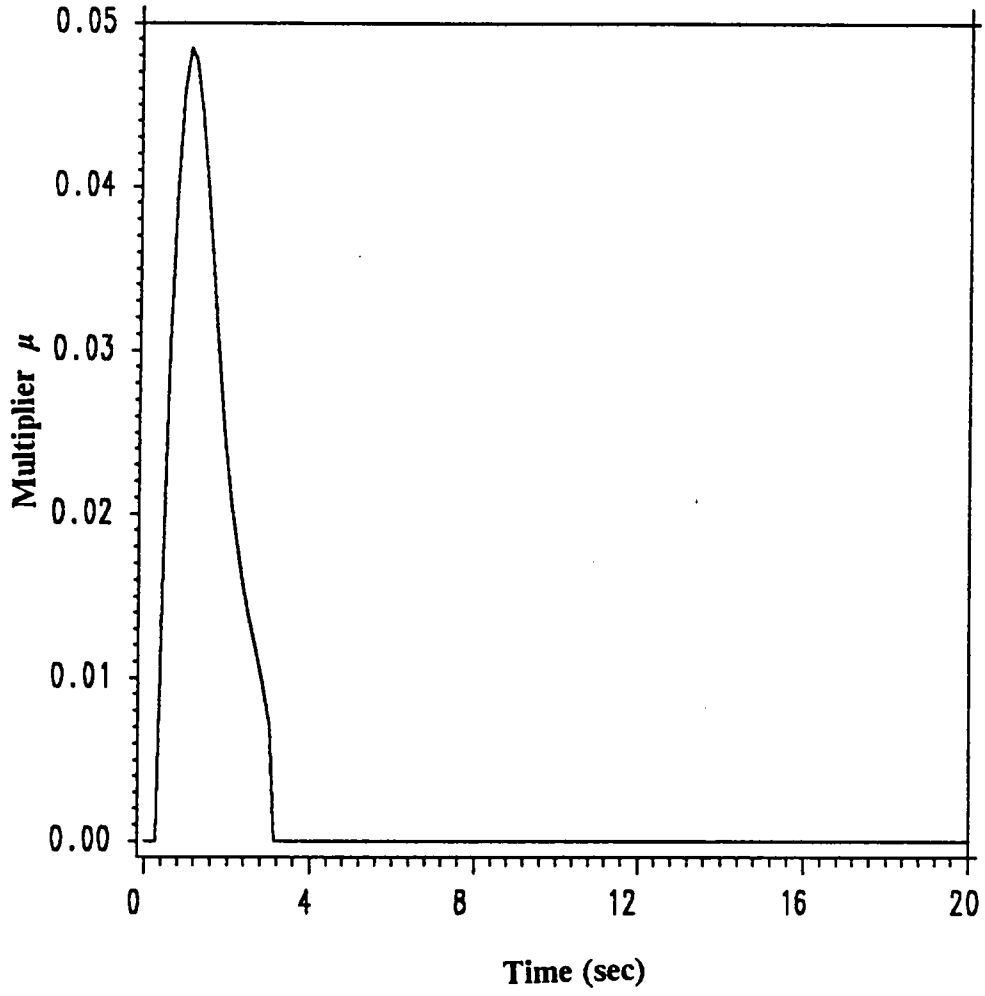

Fig. 5.3: Control constraint multiplier time history

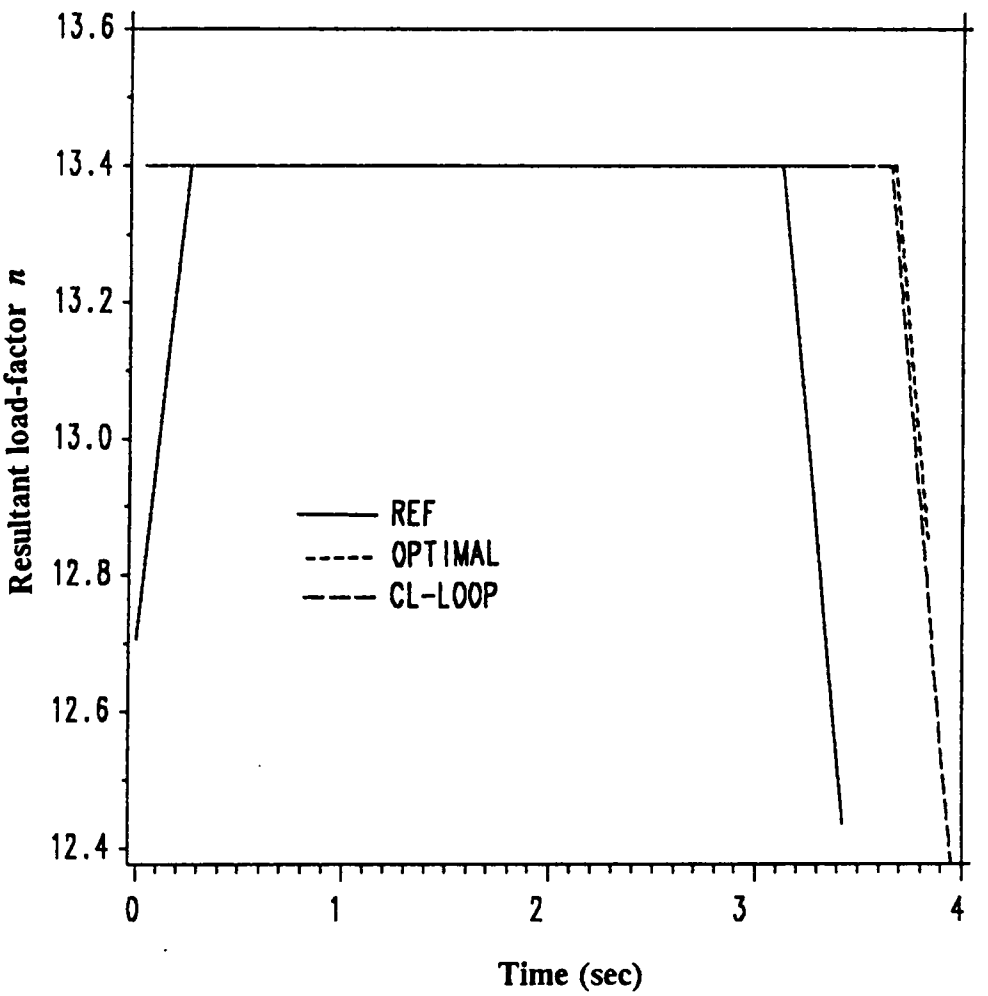

Fig. 5.4: Resultant load-factor time history - reference, optimal and closed-loop

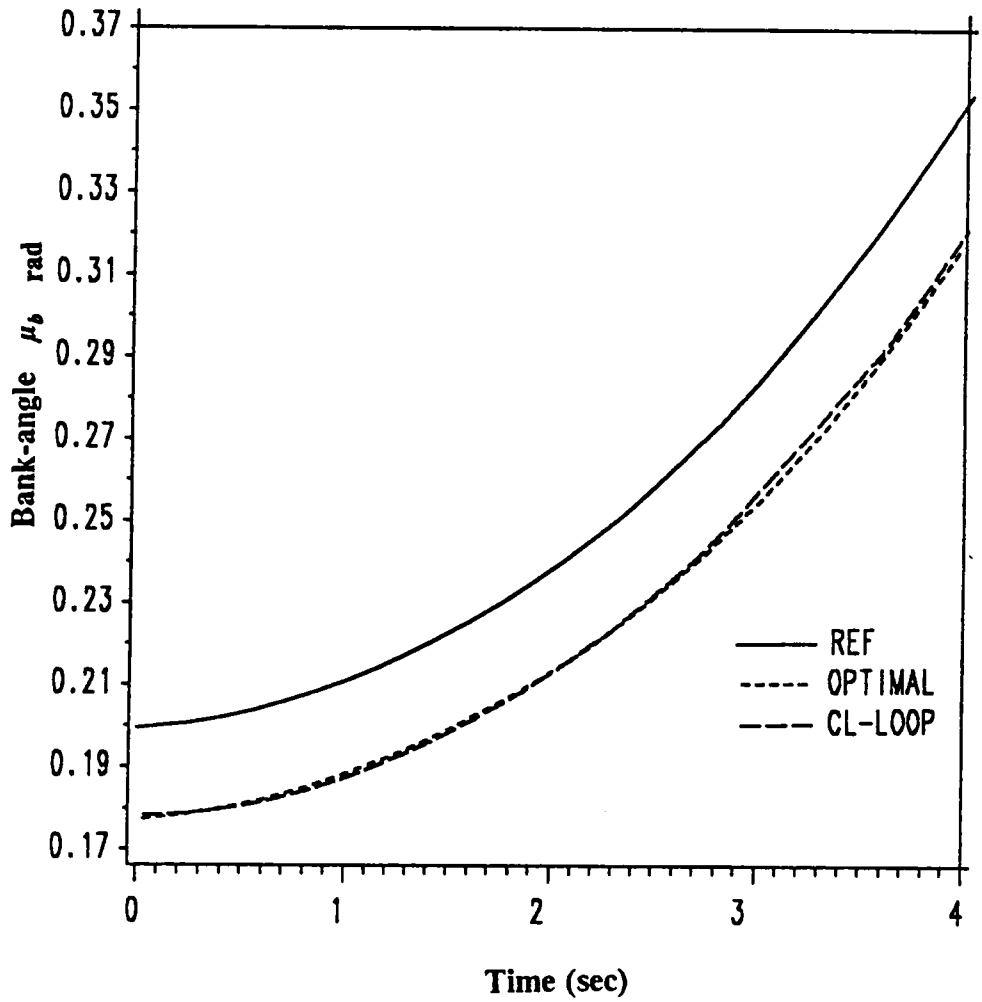

Fig. 5.5: Bank-angle time history - reference, optimal and closed-loop

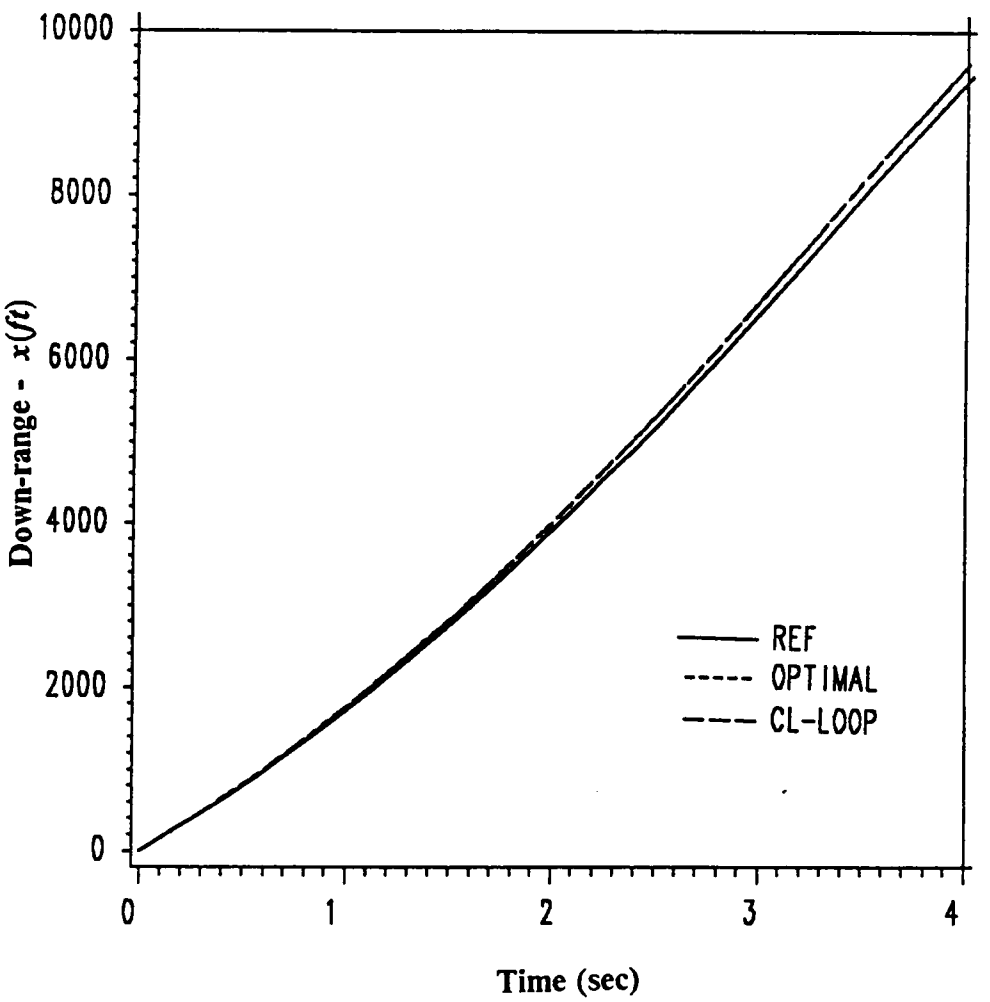

Fig. 5.6: Down-range time history - reference, optimal and closed-loop

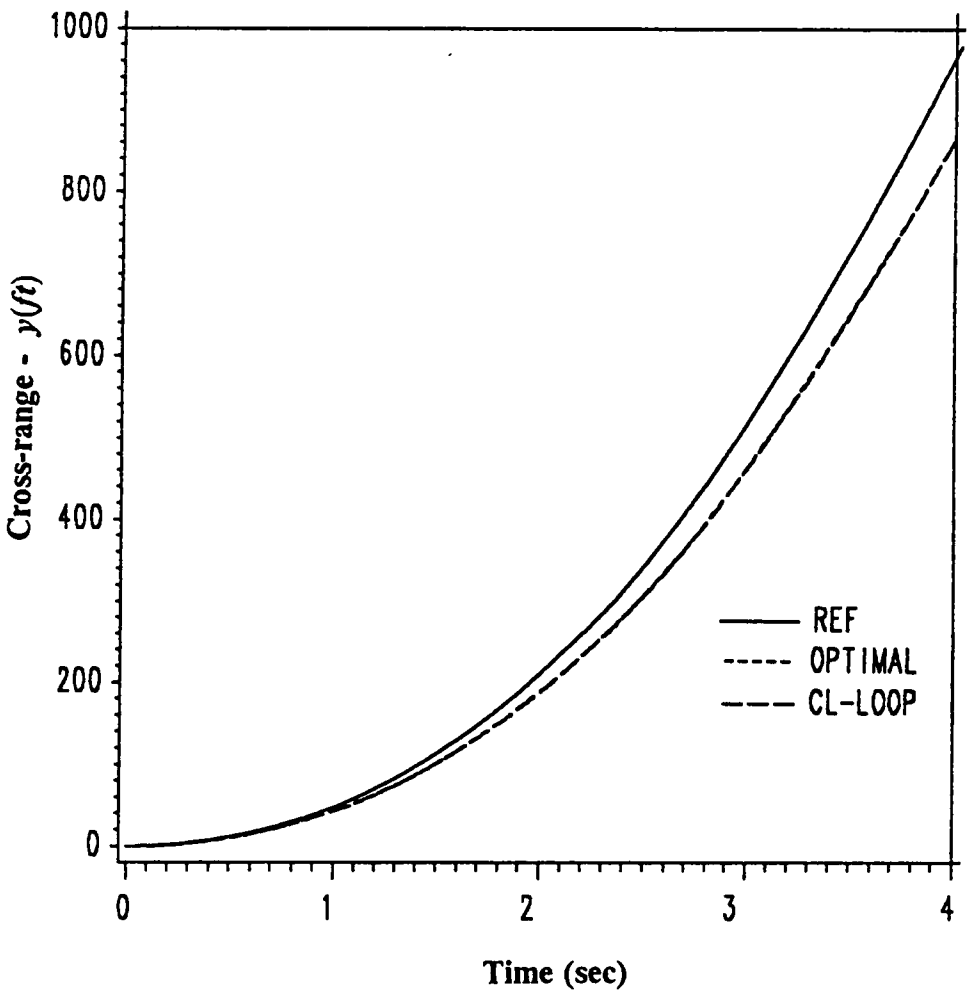

Fig. 5.7: Cross-range time history - reference, optimal and closed-loop

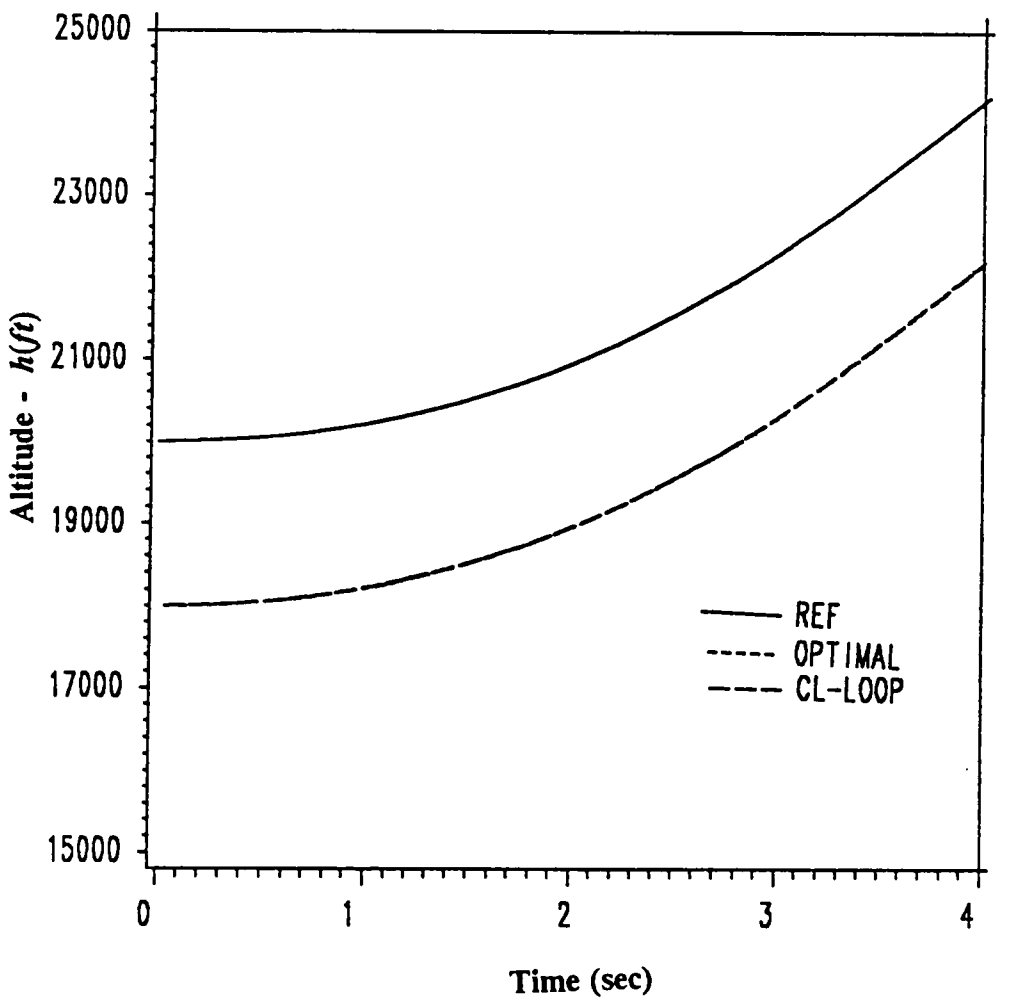

Fig. 5.8: Altitude time history - reference, optimal and closed-loop

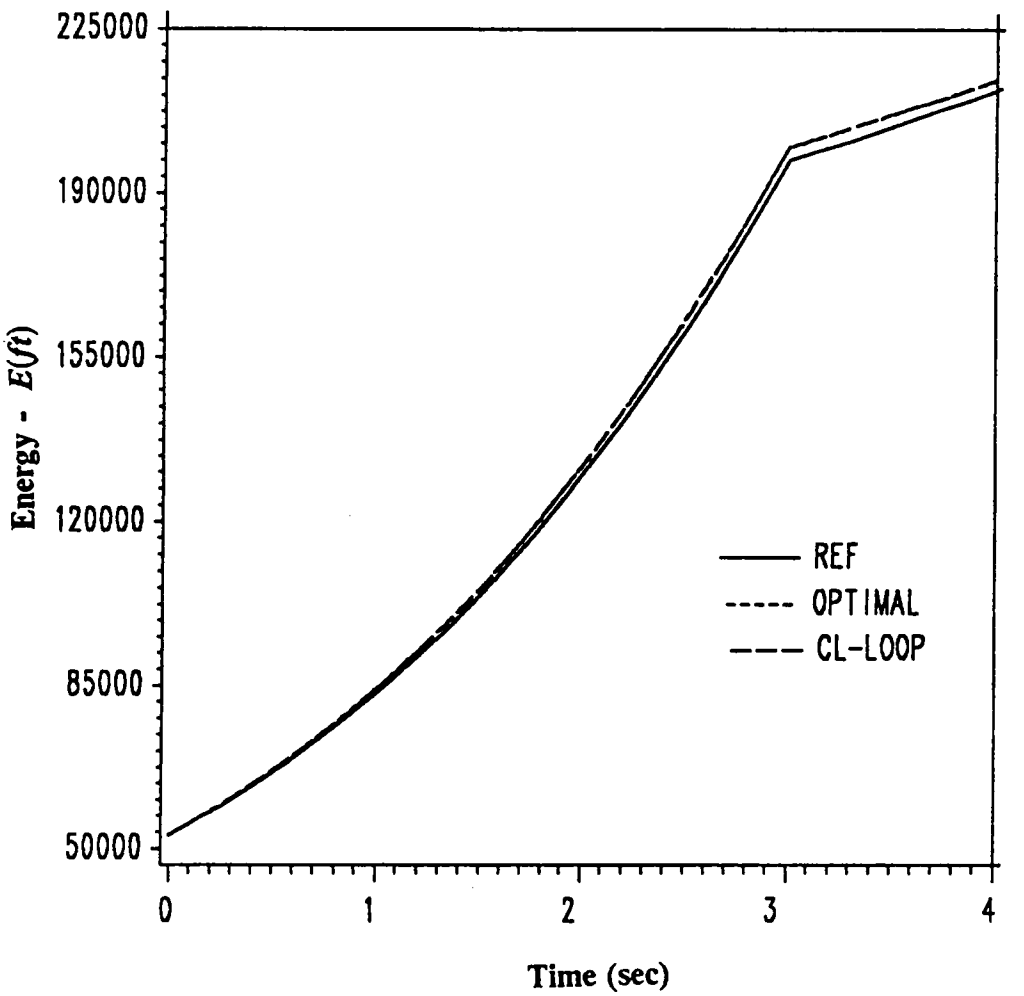

Fig. 5.9: Energy time history - reference, optimal and closed-loop

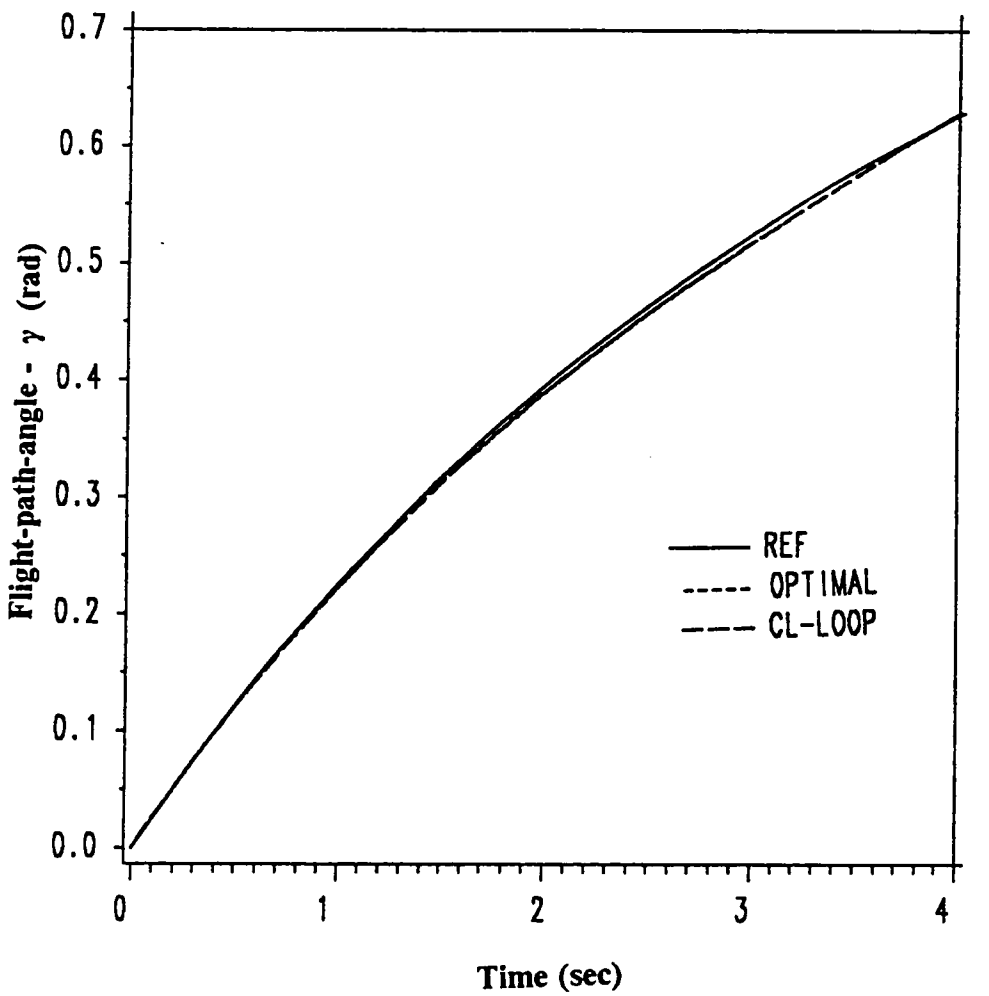

Fig. 5.10: Flight-path-angle time history - reference, optimal and closed-loop

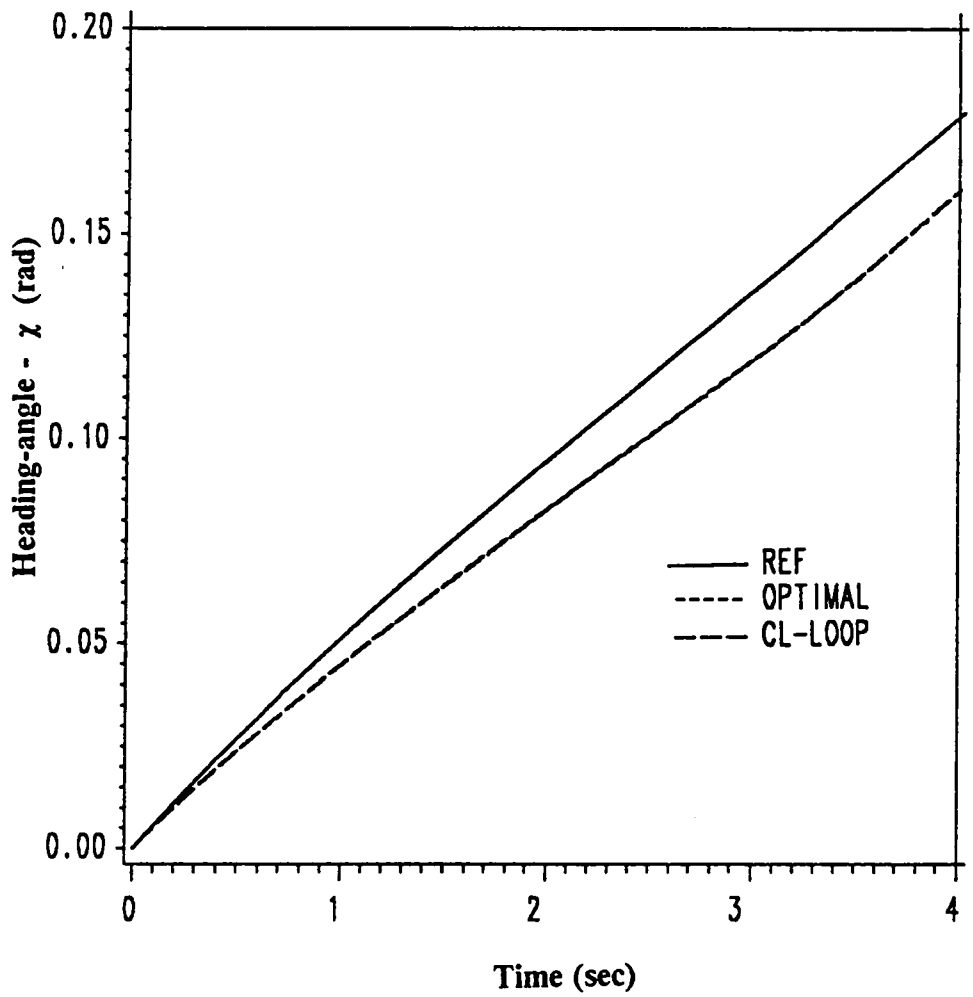

Fig. 5.11: Heading-angle time history - reference, optimal and closed-loop

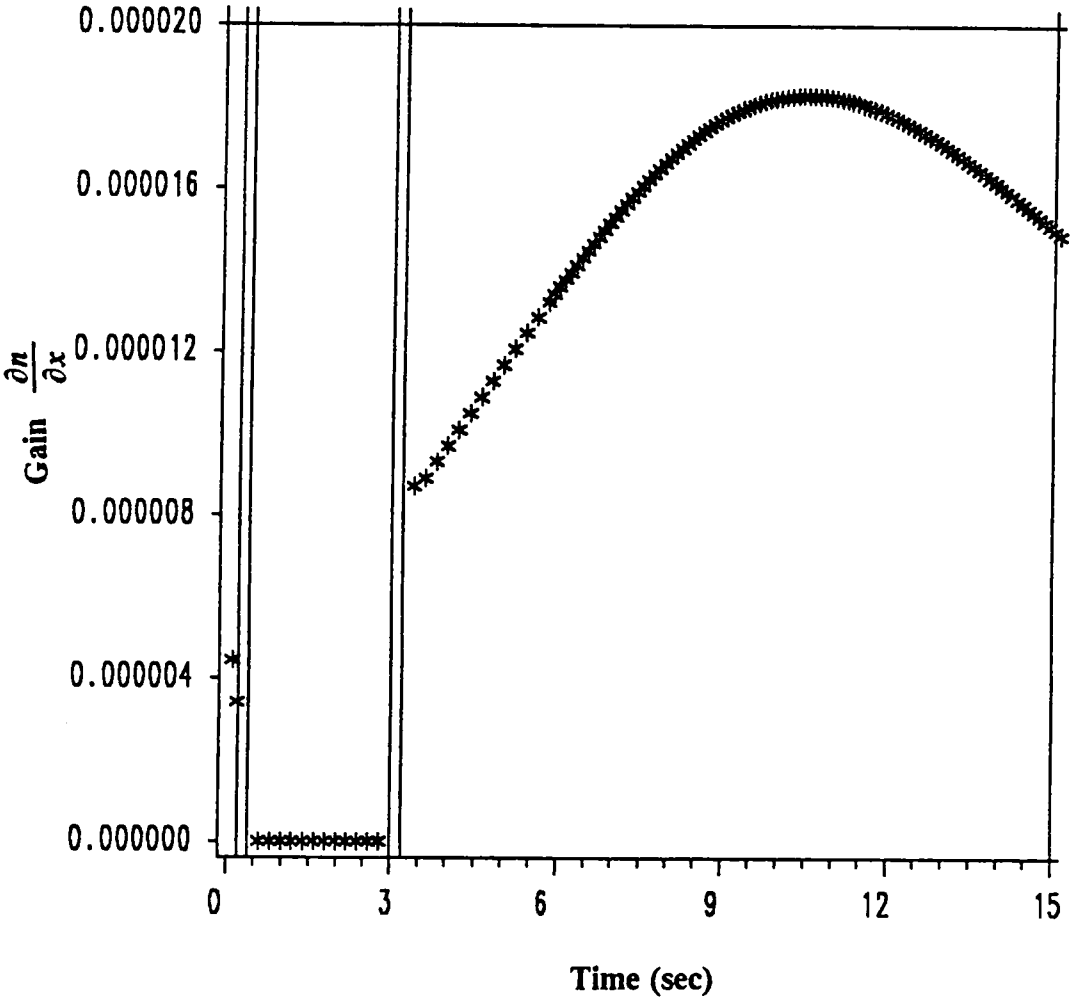

Fig. 5.12: Gain $\frac{\partial n}{\partial x}$ history - boost phase with active control constraint

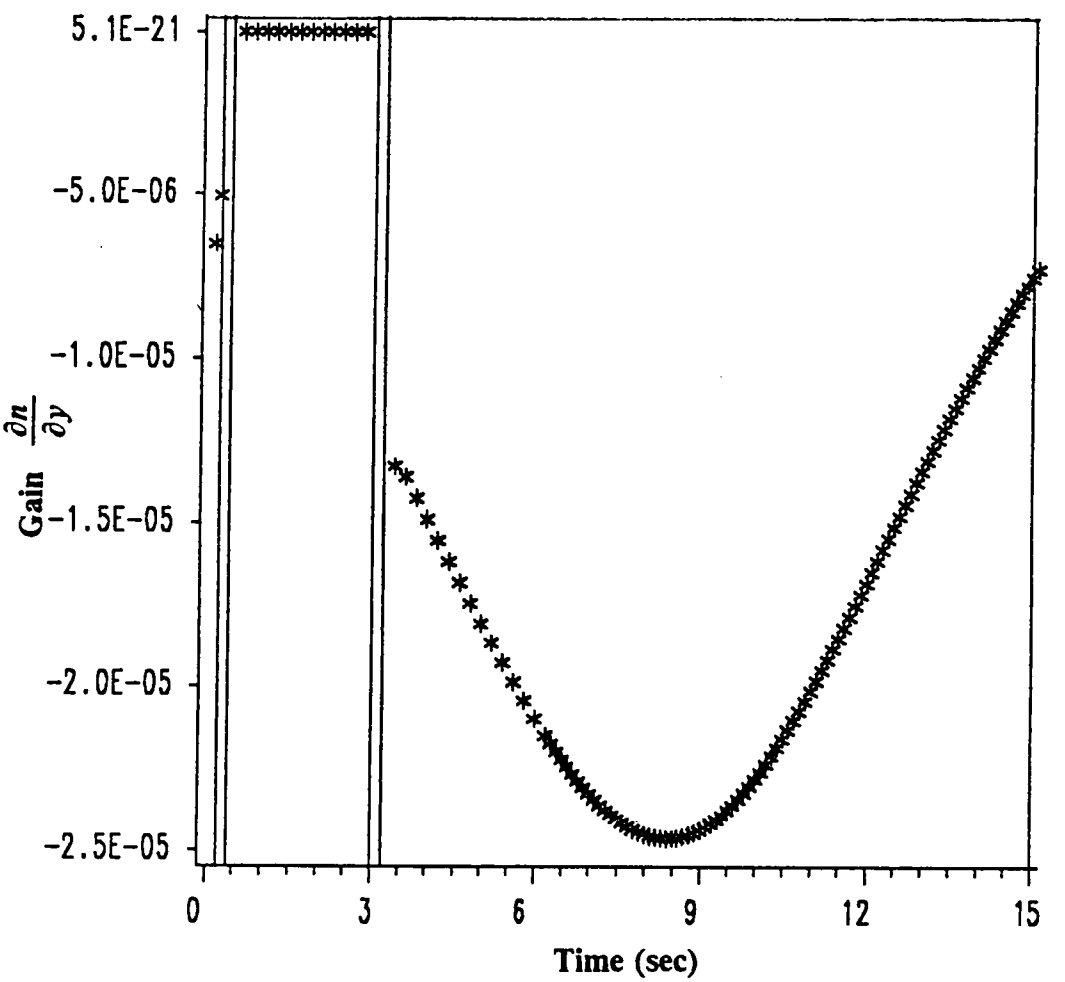

Fig. 5.13: Gain $\frac{\partial n}{\partial y}$ history - boost phase with active control constraint

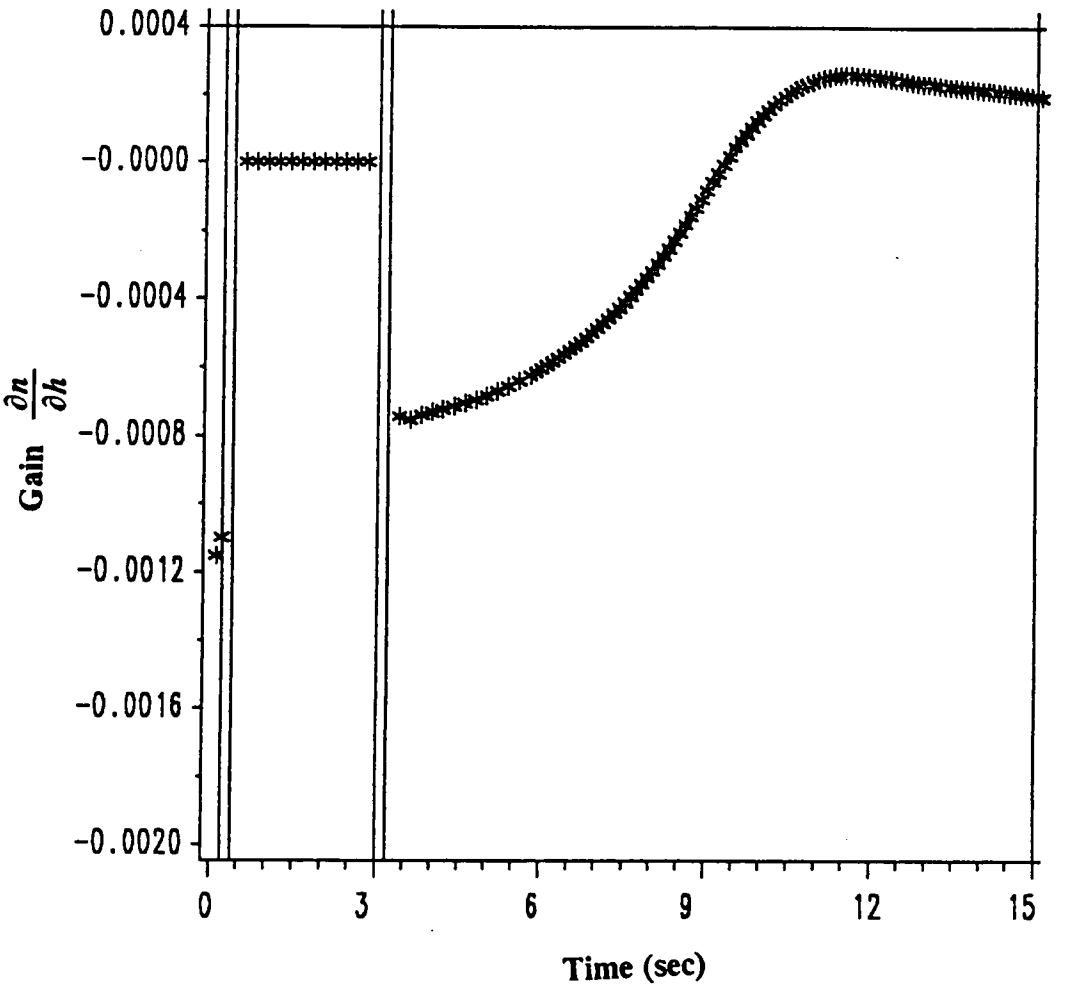

Fig. 5.14: Gain $\frac{\partial n}{\partial h}$ history - boost phase with active control constraint

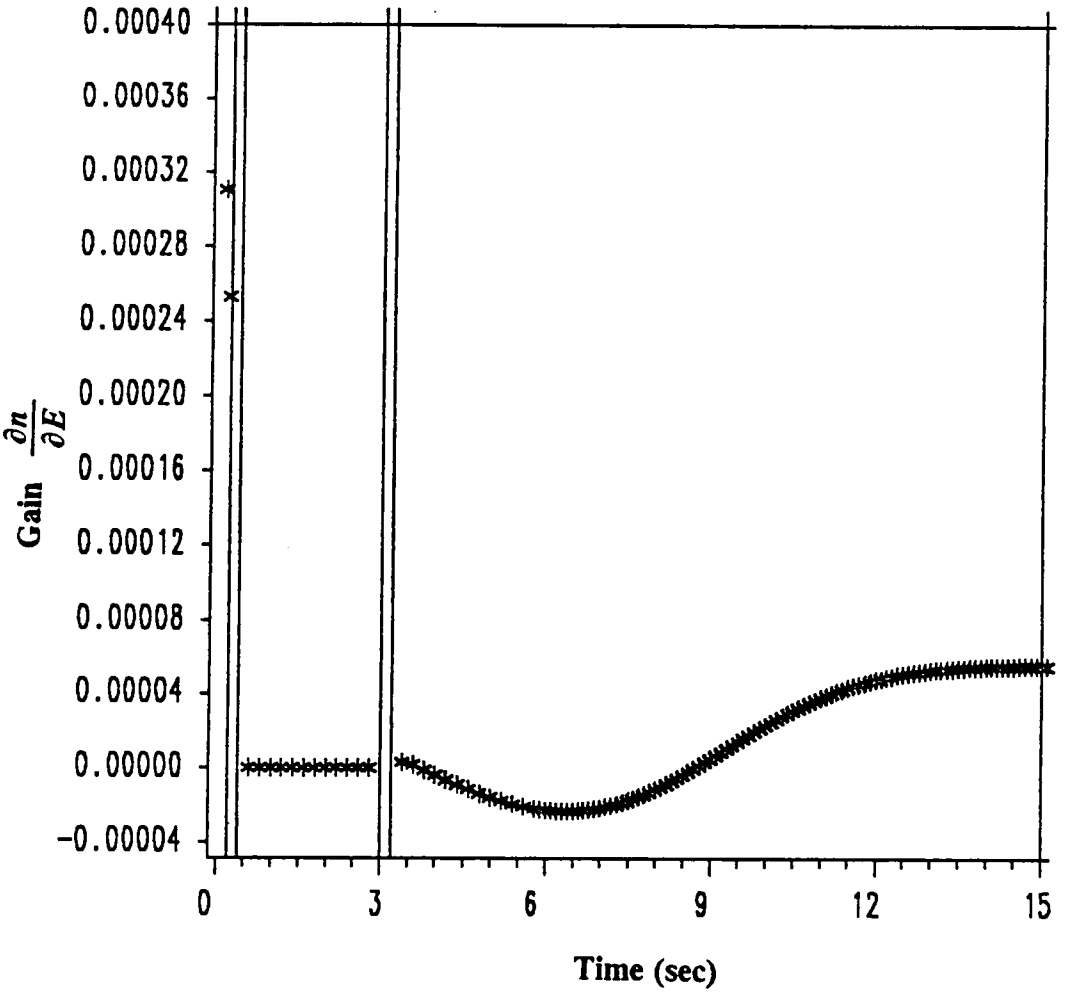

Fig. 5.15: Gain $\frac{\partial n}{\partial E}$ history - boost phase with active control constraint

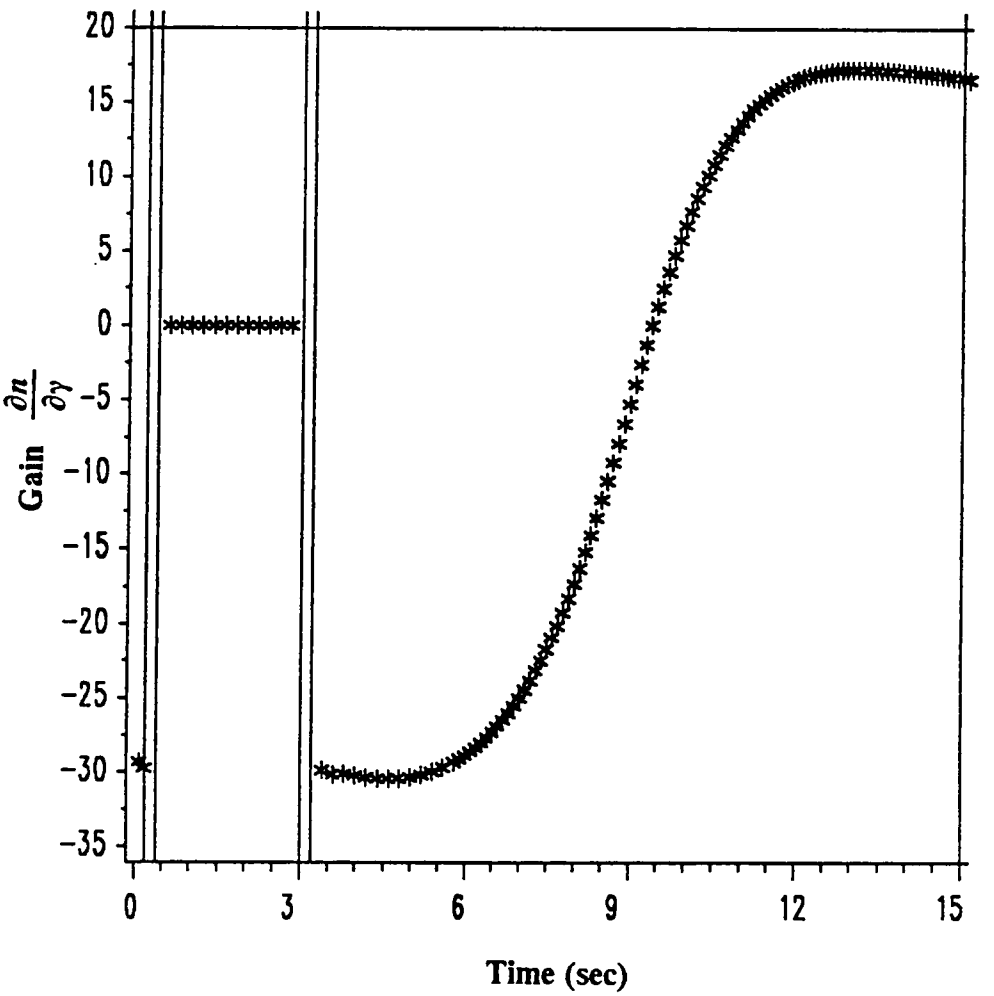

Fig. 5.16: Gain $\frac{\partial n}{\partial \gamma}$ history - boost phase with active control constraint

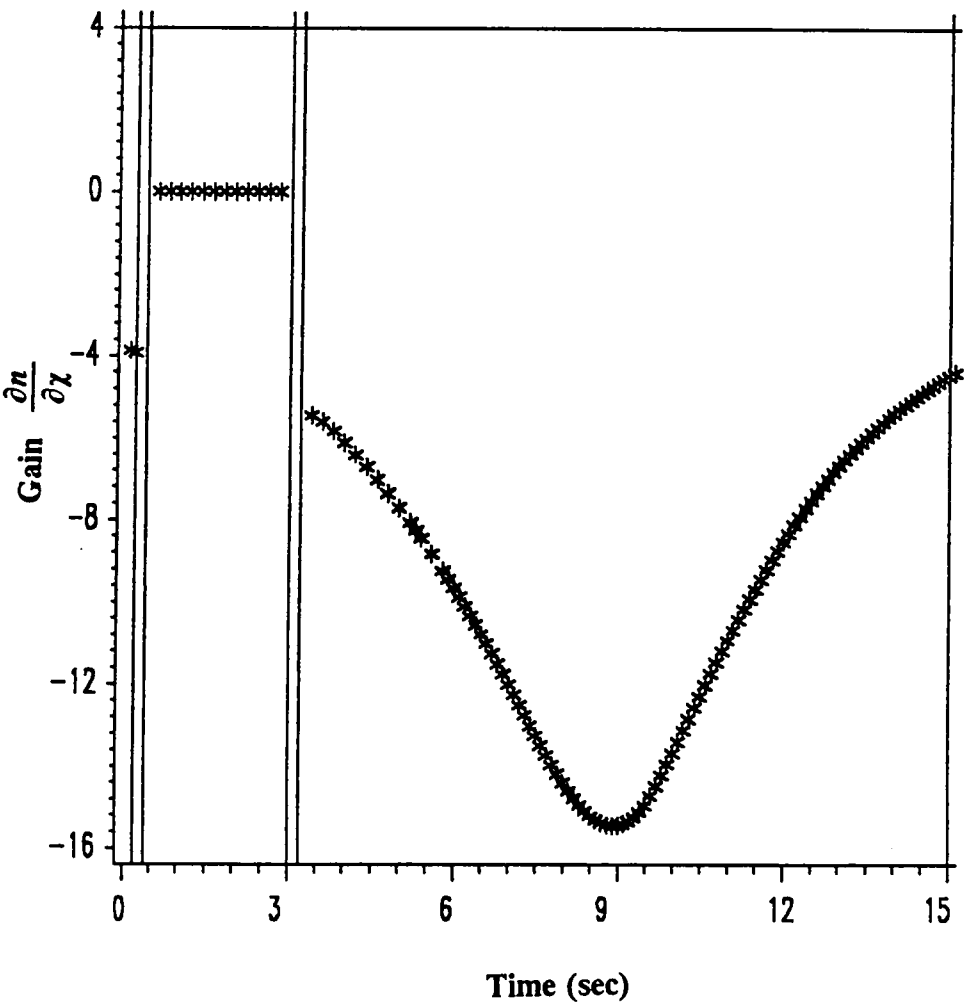

Fig. 5.17: Gain $\frac{\partial n}{\partial \chi}$ history - boost phase with active control constraint

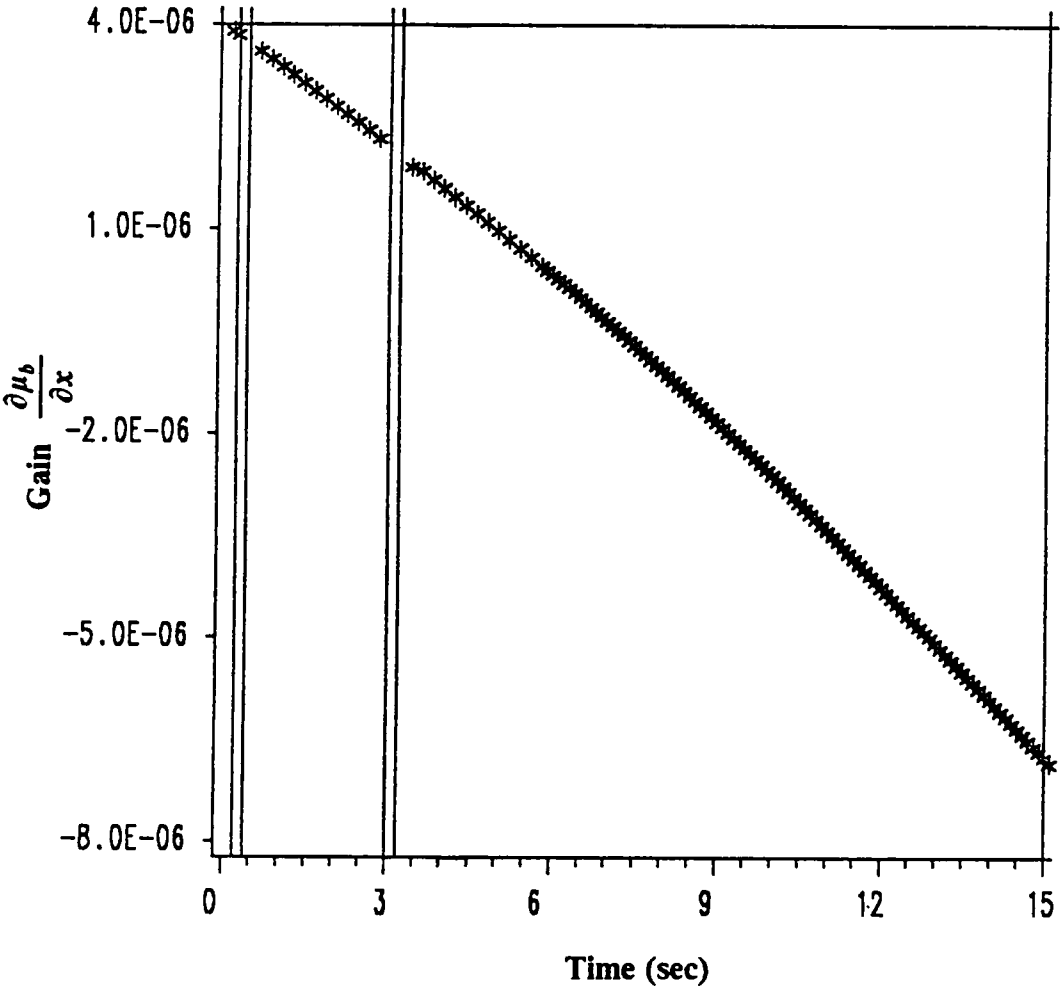

Fig. 5.18: Gain $\frac{\partial \mu_b}{\partial x}$ history - boost phase with active control constraint

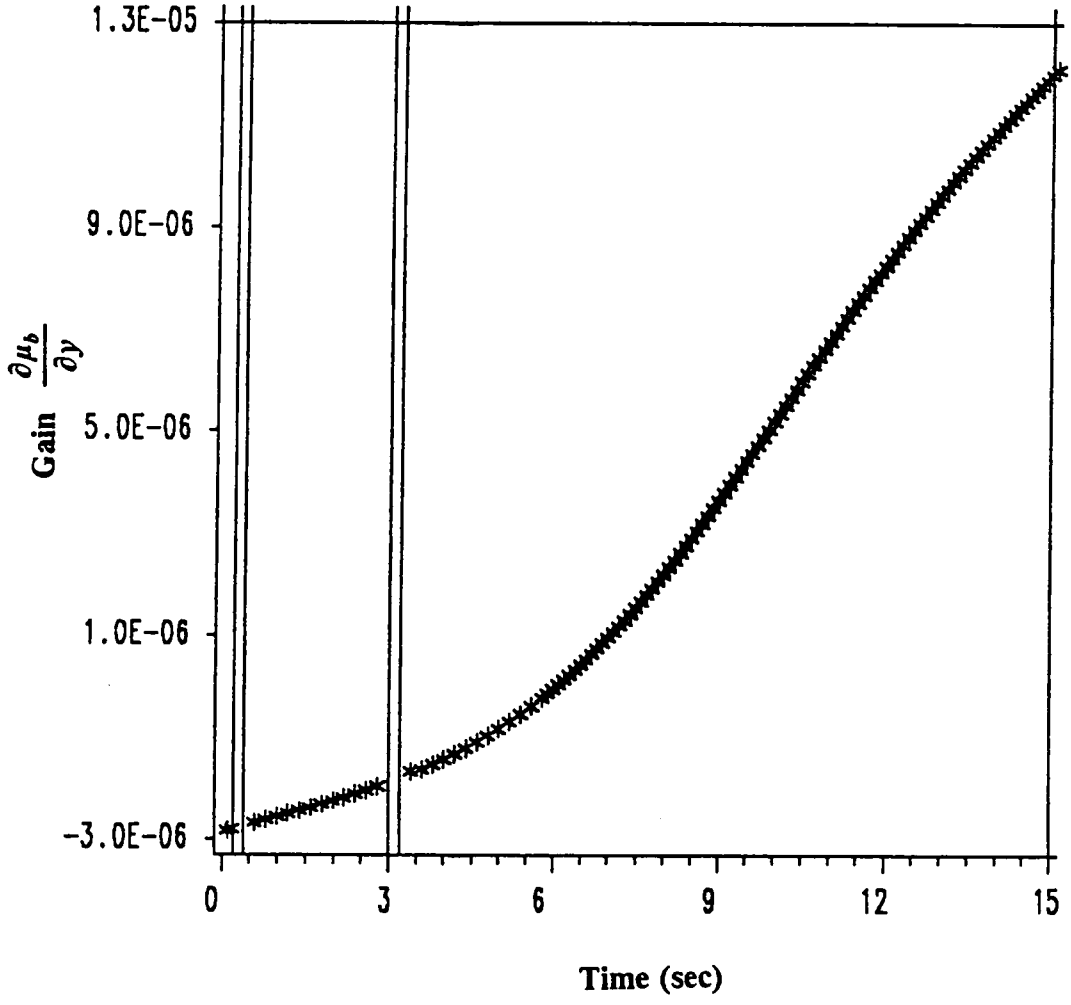

Fig. 5.19: Gain $\frac{\partial \mu_b}{\partial y}$ history - boost phase with active control constraint

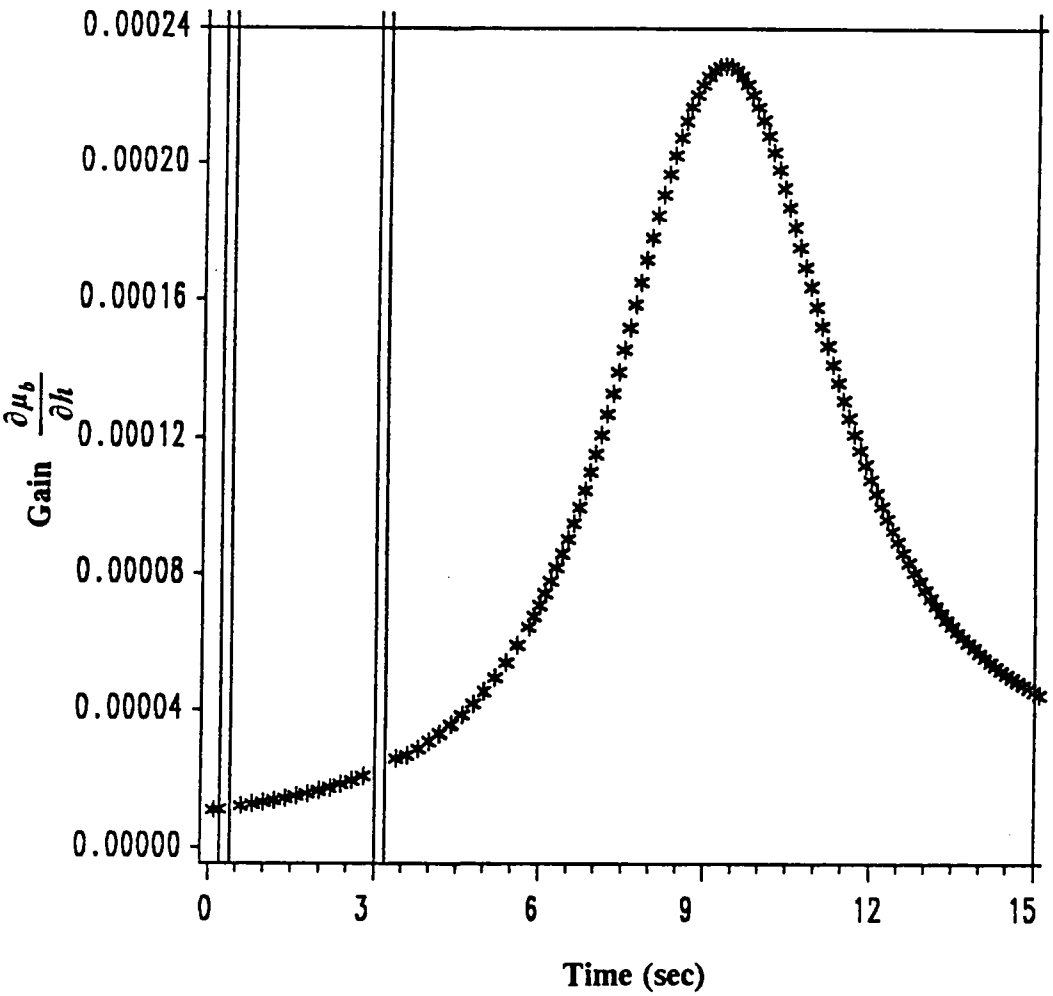

Fig. 5.20: Gain $\frac{\partial \mu_b}{\partial h}$ history - boost phase with active control constraint

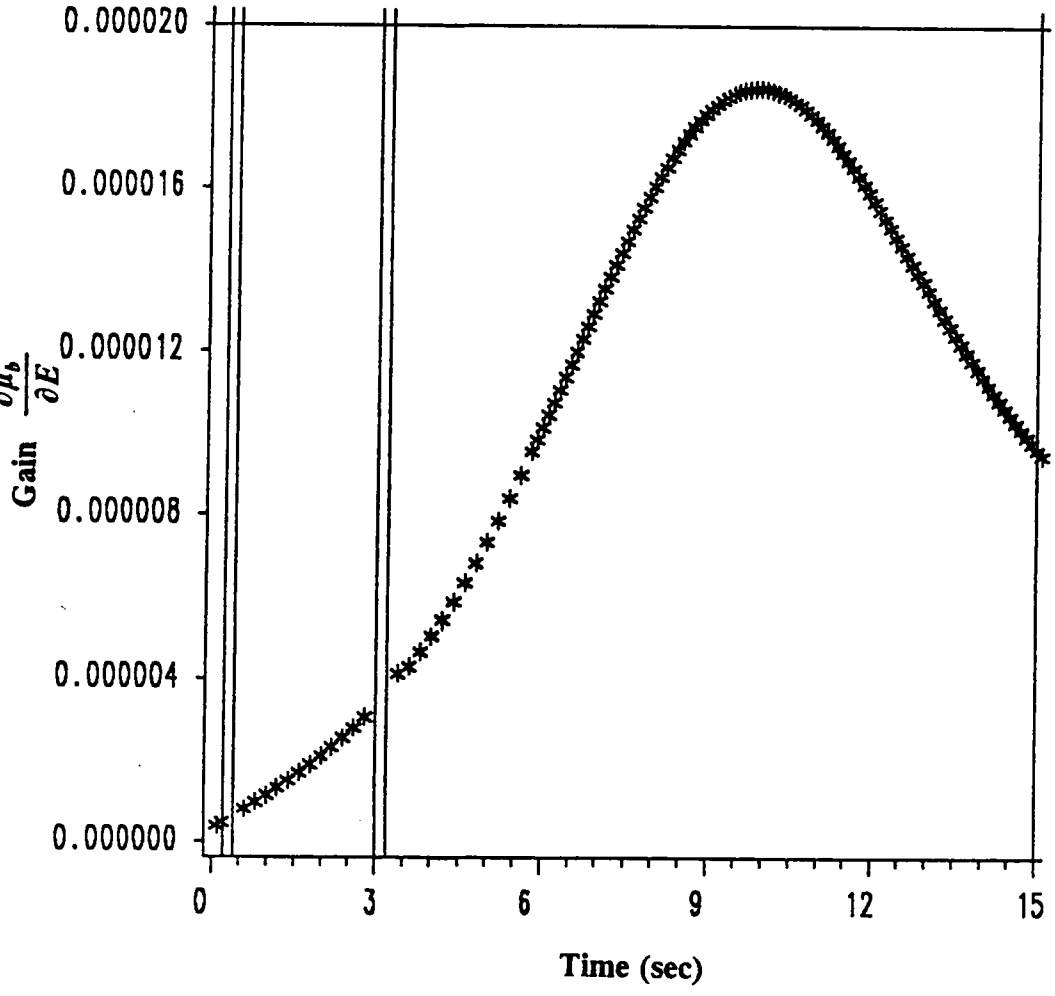

Fig. 5.21: Gain $\frac{\partial \mu_b}{\partial E}$ history - boost phase with active control constraint

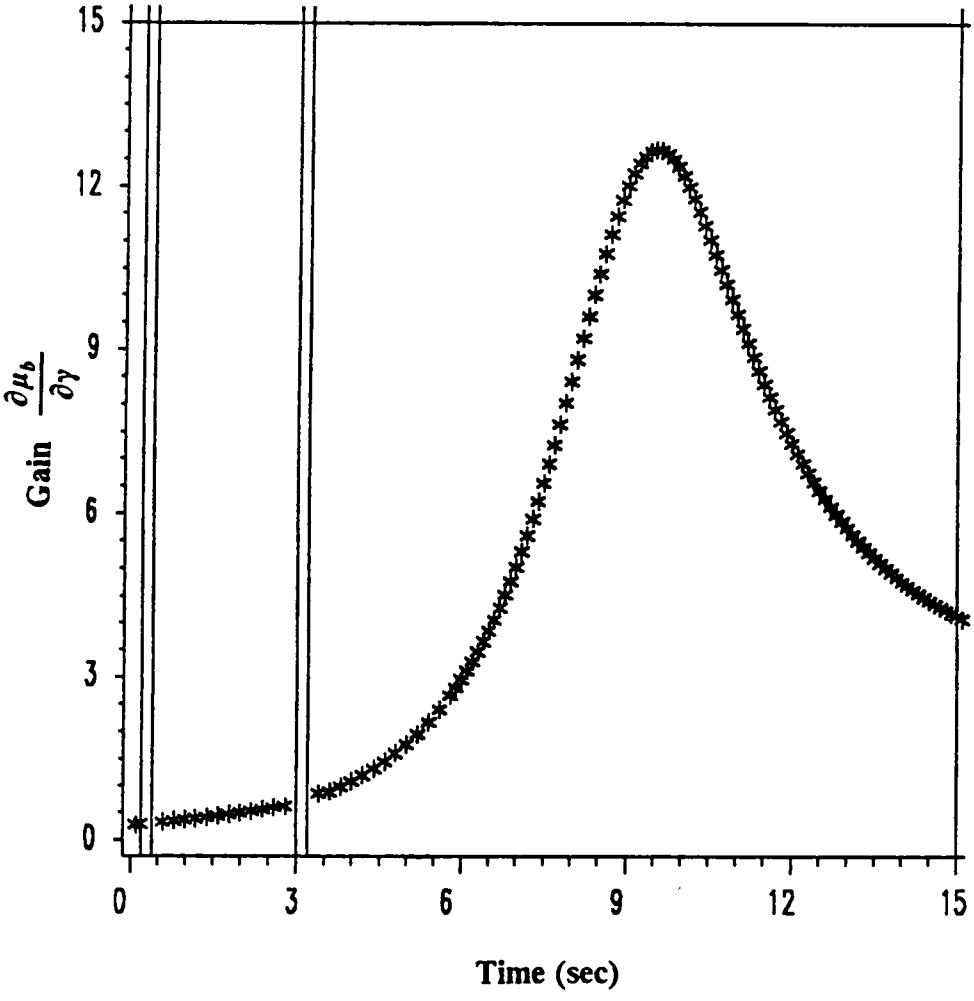

Fig. 5.22: Gain $\frac{\partial \mu_b}{\partial \gamma}$ history - boost phase with active control constraint

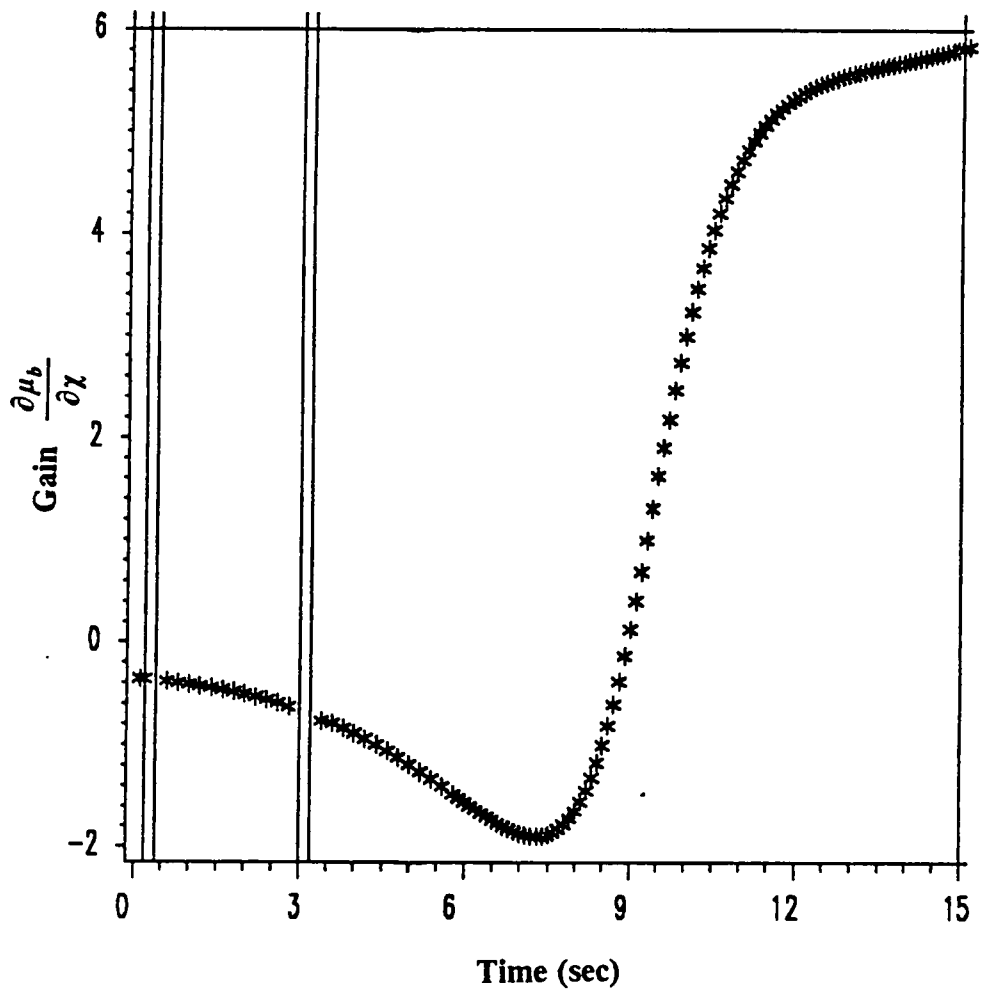

Fig. 5.23: Gain $\frac{\partial \mu_b}{\partial \chi}$ history - boost phase with active control constraint

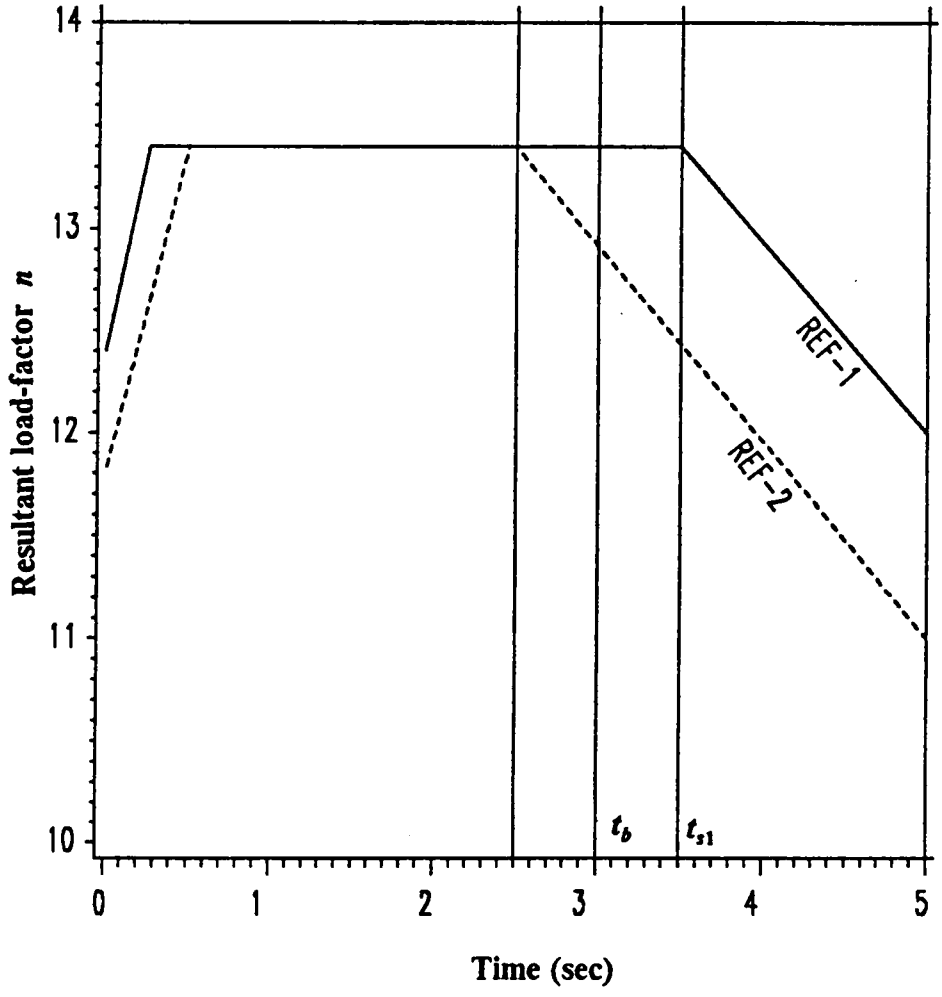

Fig. 5.24: Load-factor constraint and thrust switching interaction

Chapter 6: Midcourse Guidance

6.1: Overview

The guidance during the early phase of the trajectory encounters possible control constraint limits as indicated in the previous chapter. The midcourse guidance is initiated after the thrust phase where the trajectory is nearly ballistic. Transversal comparison [23,24,39,40] and other forms of performance augmentation have been employed during this phase where guidance is performed against a maneuvering target. Guidance in the presence of state perturbations and change of target set is considered. The midcourse guidance lasts for the longest duration in comparison to the boost-phase and terminal guidance.

6.2: Gain Evaluation

The reference solution is obtained as discussed earlier and the feedback gains are to be evaluated about these reference trajectories. Initially we assume that that

the target set is the extrapolated or predicted intercept point with an assigned final energy. Consider the general optimal control problem of Bolza as given in Chapter 2. The definition of the accessory minimum problem and the related matrices for the Riccati method of gain evaluations for the general category of free time problems are described in Chapter 6 of [21]. As discussed earlier the guidance is not performed about a fixed time maximum range extremal. The minimum time to intercept problem is solved and guidance is performed with this as the reference trajectory.

The perturbation in control vector is given by :

$$\delta u(t) = G_1(t)\,\delta X(t) + G_2(t)\,d\psi(t) \tag{6.1}$$

where $\delta X(t)$ is a vector of state perturbation from nominal at any time and $d\psi(t)$, a vector representing change in terminal conditions. The gains $G_1(t)$ & $G_2(t)$ are given by:

$$G_1(t) = -\mathscr{H}_{uu}^{-1}\,(\mathscr{H}_{uX} + f_u^T(\overline{S} - \overline{R}\,\overline{Q}^{-1}\overline{R}^T)) \tag{6.2}$$

$$G_2(t) = -\mathscr{H}_{uu}^{-1}\,f_u^T\overline{R}\,\overline{Q}^{-1} \tag{6.3}$$

where, $\mathscr{H}$ is the variational-Hamiltonian, $\overline{S}$, $\overline{Q}$ and $\overline{R}$ are time-varying matrices which are stored after integrating backwards in time the Eqs. (4.3-4.8) and evaluating the above matrices from Eqs. (4.12,4.13,4.14) respectively.

The nominal optimal control problem being minimum time, the final time also gets perturbed and a good estimate of the change in final time is given by:

$$dt_f = K_1(t)\,\delta X(t) + K_2(t)\,d\psi(t) \tag{6.4}$$

where the gains K_1 and K_2 are given by:

$$K_1(t) = -\left(\frac{m^T}{\alpha} - \frac{n^T}{\alpha}\bar{Q}^{-1}\bar{R}^T\right) \tag{6.5}$$

$$K_2(t) = -\frac{n^T}{\alpha}\bar{Q}^{-1} \tag{6.6}$$

Again, the vectors m , n , and the scalar α are time-varying and are obtained by integrating Eqs. (4.6-4.8). These gains are evaluated prior to flight and stored onboard. It is worthwhile to discuss briefly the choice for the terminal surface vector $\psi[X(t_f), t_f] = 0$ for the reference solution. One choice would be:

$$\psi[X(t_f)] = \begin{bmatrix} x(t_f) - x_f \\ y(t_f) - y_f \\ h(t_f) - h_f \\ E(t_f) - E_f \end{bmatrix} \tag{6.7}$$

where the x_f, y_f are fixed numbers decided by the optimal intercept point co-ordinate obtained by linear extrapolation of the target flying at constant altitude h_f and E_f is the final energy desired by the missile for endgame.
An other choice would be:

$$\psi[X(t_f), t_f] = \begin{bmatrix} x(t_f) - [x_{T0} - V_T\cos(\lambda_T)t_f] \\ y(t_f) - [y_{T0} - V_T\sin(\lambda_T)t_f] \\ h(t_f) - h_f \\ E(t_f) - E_f \end{bmatrix} \tag{6.8}$$

where,

(x_{T0}, y_{T0}) is the target co-ordinate at initial time, V_T is the constant target velocity, and λ_T is the inertial bearing angle of target measured from the negative down-range axis of missile.

The first choice is superior to the second choice in the manner that the feedback gains can be evaluated prior to flight while the second choice requires the target velocity and bearing angle as boundary conditions for the matrix differential equations [4.3-4.8] which are integrated backwards in time to obtain the feedback gains. The advantage of the second choice is that for a benign target moving at constant velocity along a straight line, $d\psi(t) = 0$, even if state perturbations are made during the trajectory. This reduces the storage requirements for onboard use. The second method is advantageous for non-maneuvering or stationary targets.

If the gains are scheduled with a clock-time comparison, i.e., comparison between the states at the same time, then for case when $dt_f > 0$ one can run out of gains. The perturbation dt_f can be calculated from Eq. (6.4) by substituting $d\psi$ as follows,

$$d\psi = [\frac{\partial \psi}{\partial X} dX + \frac{\partial \psi}{\partial t} \delta t_f]_{t_f} \tag{6.9}$$

Once δt_f and $d\psi$ are obtained, then the closed-loop control vector evaluated using Eq. (6.1) becomes

$$u_{CL}(t) = u_{reference}(t) + \delta u(t) \tag{6.10}$$

The feedback gains can also be evaluated by using the same method of perturbation as in the boost phase guidance. These gains and the gains obtained from Riccati solutions about regular/regularized extremals, show little difference except at few points corresponding to the ill-conditioning of the matrix given in Eq. (5.1). Fig. {6.1} gives a good comparison for a sample gain evaluated by the two methods. The ill-conditioned nature of the matrix in Eq. (5.1) is seen clearly near final time. The perturbation method becomes attractive for the case when $\mathscr{H}_{uu}(t_f)$ becomes singular. This occurs when the missile flight-path-angle and heading-angle at final time are unspecified - the corresponding adjoint variables are zero at final time. When this happens, the accessory minimum problem is singular at t_f and the associated matrix Riccati differential equation is invalid. The gains can be calculated using "Riccati method" for the irregular reference solution by regularization with penalty terms similar to Eq. (4.21) with $\varepsilon_t \to 0$.

The gains become unbounded as $t \to t_f$. Since some of the states are fixed at terminal time and as the time-to-go becomes smaller, larger magnitudes of control efforts would be required to make corrections. Hence midcourse guidance must be followed by some terminal guidance scheme as discussed in Chapter 7.

6.3: Transversal Comparison

Since the problem has no explicit dependence on time, and to prevent the "running out of gains", the time-to-go, $(t_f - t)$ is really the important time and the gains are "keyed" to it [21,24]. The difficulty of unbounded gains is avoided

if the gain tables are entered at an "index time" determined so that the time-to-go on the closed-loop neighboring path is the same as the time-to go for the nominal path. This is the same idea as performance-index-to-go as suggested by Kelley in [23].

Since the time-to-go, t_f' , is to be the same on the neighboring and nominal paths one has,

$$t_f' = t_f - t = t_f^N - t_I \tag{6.11}$$

where t_f is the estimated final time of neighbor, t , the clock time, t_f^N is the terminal time of the nominal solution and t_I is the desired index time. The perturbation in final time ($t_f - t_f^N$) is estimated from Eq. (6.4) so that the implicit equation for the index time can be found as in [24]:

$$t - t_I = \frac{K_1(t_I)\,[X(t) - X_N(t_I)] + K_2(t_I)[d\psi]}{[1 + K_1(t_I)\,\dot{X}^N(t_I)]} \tag{6.12}$$

One starts with the estimate $t_I = t$. The gains K_1 , K_2 and $\dot{X}^N$ are evaluated at this index time. $d\psi$ may or may not be a function of time-to-go (or simply of t_I). A new t_I is evaluated using Eq. (6.12). This procedure is repeated until t_I converges. In other words, Eq. (6.12) may be re-written as $t_I = g\,(t_I)$ and a fixed-point iteration performed to obtain a root of this equation.

An explicit formula for the closed-loop control, assuming the control and states to be smooth [24] is given by:

$$u(t) = u^N(t_I) + G_1(t_I)[X(t) - X^N(t_I)] \tag{6.13}$$

$$+ [G_1(t_I)\,\dot{X}^N(t_I) + \dot{u}^N(t_I)][t - t_I] + G_2(t_I)\,d\psi(t)$$

The closed-loop control is used to simulate a real time flight situation of the missile with target maneuvers and state perturbations. Indexing with time-to-go for this problem shows better simulation results particularly during the later period of flight. Simulation was performed for an aggressive target, i.e., a target travelling at constant speed in a specified direction, and a run-away target and the guidance scheme performs better for both cases when index time is used. Simulation results are presented in Figs. {6.4-6.21}, using clock-time and index-time transversal comparison, with the missile using the performance augmentation as described below.

6.4: Performance Augmentation

It has been observed that for the afore-mentioned reference solution, the closed-loop guidance works well only for $d\psi$ (using ψ from Eq. (6.7)) small. If the target tries to turn away and the missile ends up in a tail chase, then $d\psi$ increases with time and the neighboring optimal scheme fails due to the linearization being inaccurate. The same is true if ψ defined in Eq. (6.8) is used. However, if the target continues to be aggressive with only small perturbations from the nominal (anticipated) target trajectory the closed-loop guidance works effectively.

In order to reduce the magnitude of $d\psi$ for all possible target maneuvers, the concept of aiming at the so-called center of attainability of the target is visualized. The center of attainability of the target is **defined** as the average value of the maximum range in forward direction and the maximum range in backward direction on the symmetric axis of the attainability set of the target moving in the horizontal plane.

The target is assumed to maneuver only in the horizontal plane with a constant velocity enabling simplified target dynamics. In Chapter 8, a target capable of acceleration and turning load-factor control using a missile avoidance guidance scheme [26] is also used to check the versatility of the neighboring guidance scheme. The simplified target dynamics are as follows:

$$\dot{x}_T = - V_T \cos(\lambda_T + \chi_T) \tag{6.14}$$

$$\dot{y}_T = - V_T \sin(\lambda_T + \chi_T) \tag{6.15}$$

$$\dot{\chi}_T = \frac{n_T g}{V_T} \tag{6.16}$$

where,

(x_T, y_T) are the target co-ordinates, V_T, χ_T, n_T are the target velocity, the heading angle (measured with respect to the nominal target direction with a right turn indicating positive χ_T) and the turning load-factor, respectively. λ_T is the inertial bearing angle as defined earlier. The load-factor in Eq. (6.16) is assumed to be the control variable for the target with an upper bound in magnitude.

It can be easily derived that the distance of the center of attainability of the target from its current position, along the line of the instantaneous velocity direction is given by $p(t_f')$;

$$p(t_f') = at_f' + b\sin(ct_f') \quad if \quad t_f' < \frac{\pi V_T}{gn_{Tmax}} \tag{6.17}$$

$$p(t_f') = \frac{\pi V_T^2}{2gn_{Tmax}} \qquad if \quad t_f' \geq \frac{\pi V_T}{gn_{Tmax}}$$

where,

$$a = \frac{V_T}{2}, \; b = \frac{V_T^2}{2gn_{Tmax}}, \; c = \frac{gn_{Tmax}}{V_T} \tag{6.18}$$

Here, n_{Tmax} is the maximum turn load-factor and V_T, the constant velocity of the target to be guessed by the missile. t_f' is the time-to-go for the missile/target intercept.

Fig. {6.2} indicates the attainable set of the target for assumed values of $V_T = 700 ft/s$, $n_{\max} = 2$ and $t_f' = 150\,\text{sec}$. This is obtained by solving the boundary of attainability by maximizing the range. The control n_T appears linearly in the system dynamics. One can easily verify that the extremal control is bang-bang between limits $+n_{Tmax}$ and $-n_{Tmax}$ or singular corresponding to zero control. This can be derived using the minimum principle and theory of singular arcs. Thus the boundary of attainability is obtained by using two switching structures. The bottom region of Fig. {6.2} is obtained by the control arcs $[n_{Tmax}, 0]$ with the switching time as the parameter. Similarly the upper

region is obtained by using $[-n_{T\max}, 0]$, varying the switching time. The symmetry of the attainable set about the velocity vector direction is noted. The variation of $p(t_f')$ with t_f' is shown in Fig. {6.3}.

This definition of center of attainability is simply an adhoc scheme to construct a new nominal terminal surface for the missile, such that the perturbation $d\psi(t)$ is kept within bounds for all possible target maneuver in the horizontal plane. Alternate statistical models for the pseudo-target behavior may be used [41].

The new nominal minimum time optimal intercept problem uses $d\psi$ obtained as follows. The reference trajectory used which leads to the nominal intercept point, is obtained using the following target set.

$$\psi[X(t_f), t_f] = \begin{bmatrix} x(t_f) - [x_{T0} - p(t_f') \cos(\lambda_T)] \\ y(t_f) - [y_{T0} - p(t_f') \sin(\lambda_T)] \\ h(t_f) - h_f \\ E(t_f) - E_f \end{bmatrix} \tag{6.19}$$

The terminal x,y target set of the missile is chosen so that at final time it intercepts the center-of-attainability of the target with the predicted time-to-go. Time-to-go (t_f') is as defined earlier. Since t_f^N for the reference solution is known, $d\psi = F(t_I)$. This functional relationship can be seen from Eq. (6.17) and Eq. (6.19). The index time t_I is solved by iterating Eq. (6.12) until convergence to the desired tolerance. Along with the converged value of t_I , we obtain the

corresponding values of t_f', $p(t_f')$, and $d\psi(t)$ which are then used for evaluating the closed-loop control.

The closed-loop guidance was simulated using the gains derived for the above nominal minimum-time intercept problem. Simulation of target behavior was first performed with a target moving with a maximum velocity of 700 ft/sec (approximately half the velocity of the missile velocity at launch) as shown in Fig. {6.4}. The prediction of time-to-go to obtain the center of attainability of the target and for gain indexing are obtained by fixed-point iteration up to desired tolerance. The closed-loop guidance worked very well with the index-time gain scheduling showing better performance than clock-time comparison, especially during the latter phase of flight. Figs. {6.4-6.12} show the nominal and closed-loop trajectories (index and clock-time).

Fig. {6.4} indicates a better heading direction for the AAM using performance-index-to-go transversal comparison. This is due to the fact that the index timing uses the gains at the same time-to-go of the nominal and these gains are of higher magnitude than the gains at clock time used without indexing. Comparison with re-solved TPBVP of the perturbed problem is useless, since it does not convey the instantaneous guidance behavior of AAM due to target maneuver. It would only show the optimal trajectory for intercepting the final prescribed target co-ordinate. The guidance scheme breaks down, due to increasing gains and increasing magnitudes of $d\psi$ and δX at about 136.47 seconds with an estimated time-to-go of 18 seconds indicating an approximate

overall time of 154.47 seconds. This final time is only 4.47 seconds more than the optimal trajectory which intercepts the target at 150 seconds. The heading and the flight-path-angle at the end of the midcourse guidance show the good performance of the scheme and also show the potential of hand-over to a terminal guidance scheme like proportional-navigation.

A second target maneuver used for simulation was as follows:
The target travels along a straight line in the horizontal plane with a constant maximum velocity of 700 ft/sec for the first 80 seconds, then turns around with maximum lateral acceleration in the horizontal plane in a direction such that the line-of-sight angle from the target is increased until it is 180° . The target then flees in a straight line as shown in Fig. {6.13}. The guidance scheme breaks-down at about 182.47 seconds with time-to-go 26.2 seconds. It should be noted here that the missile tries to conserve energy for the long flight as shown in Fig. {6.17}. The altitude management of the missile to cruise at low drag and thus save energy for the final game is seen in Fig. {6.16}. Figs. {6.14-6.19} depicts the nominal, closed-loop (index and clock-time) state histories. Hand-over to terminal guidance (Chapter 7) is done depending on the slopes and magnitudes of the control efforts - Figs. {6.20,6.21}. An approximate bound on slopes and magnitudes of control and time-to-go can be considered as the criteria for the hand-over.

In Chapter 8, midcourse guidance against a maneuvering target using a special missile avoidance guidance technique is detailed. An "improvement" in the

midcourse guidance using a method called **half-pn** and its potentials are also discussed. This is dealt in Chapter 8 in order to clearly picture the entire guidance scheme after elaborating on the terminal guidance scheme in the following chapter.

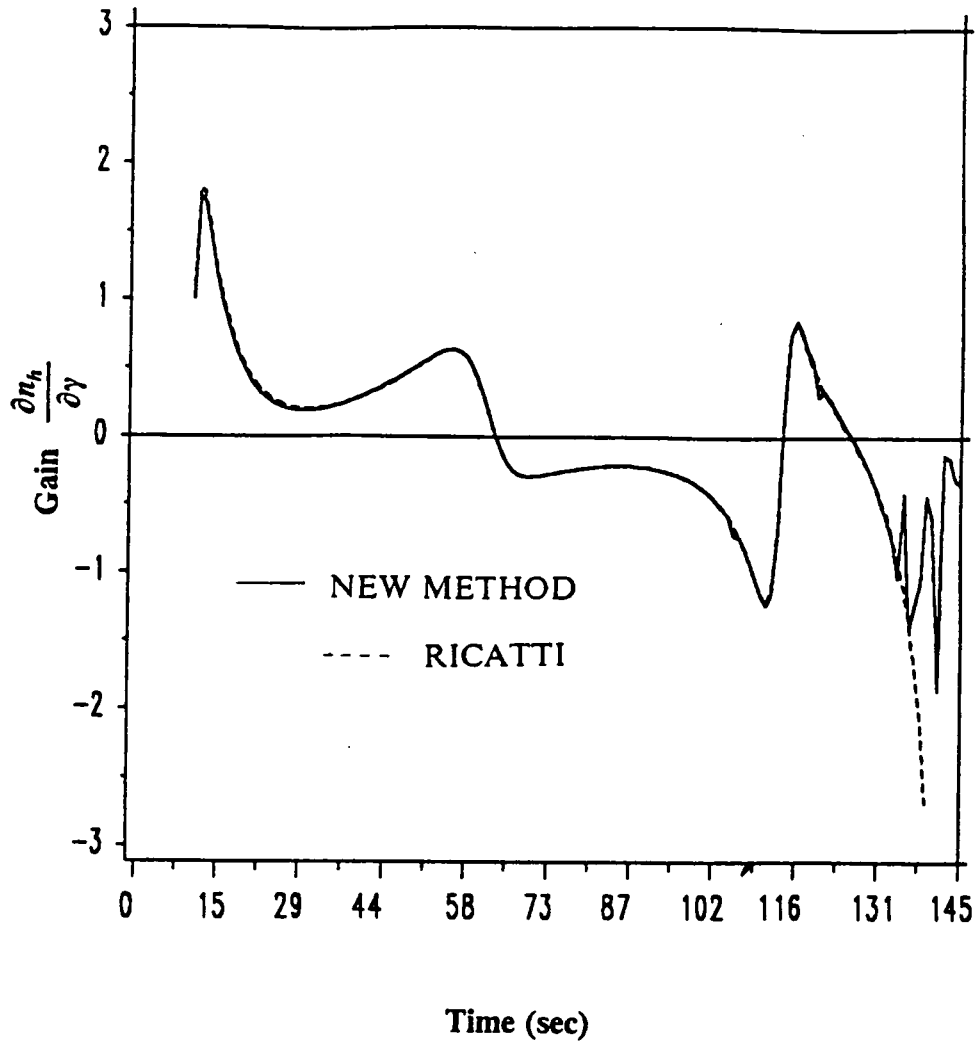

Fig. 6.1: Gain $\frac{\partial n_h}{\partial \gamma}$ comparison - Riccati method and new method

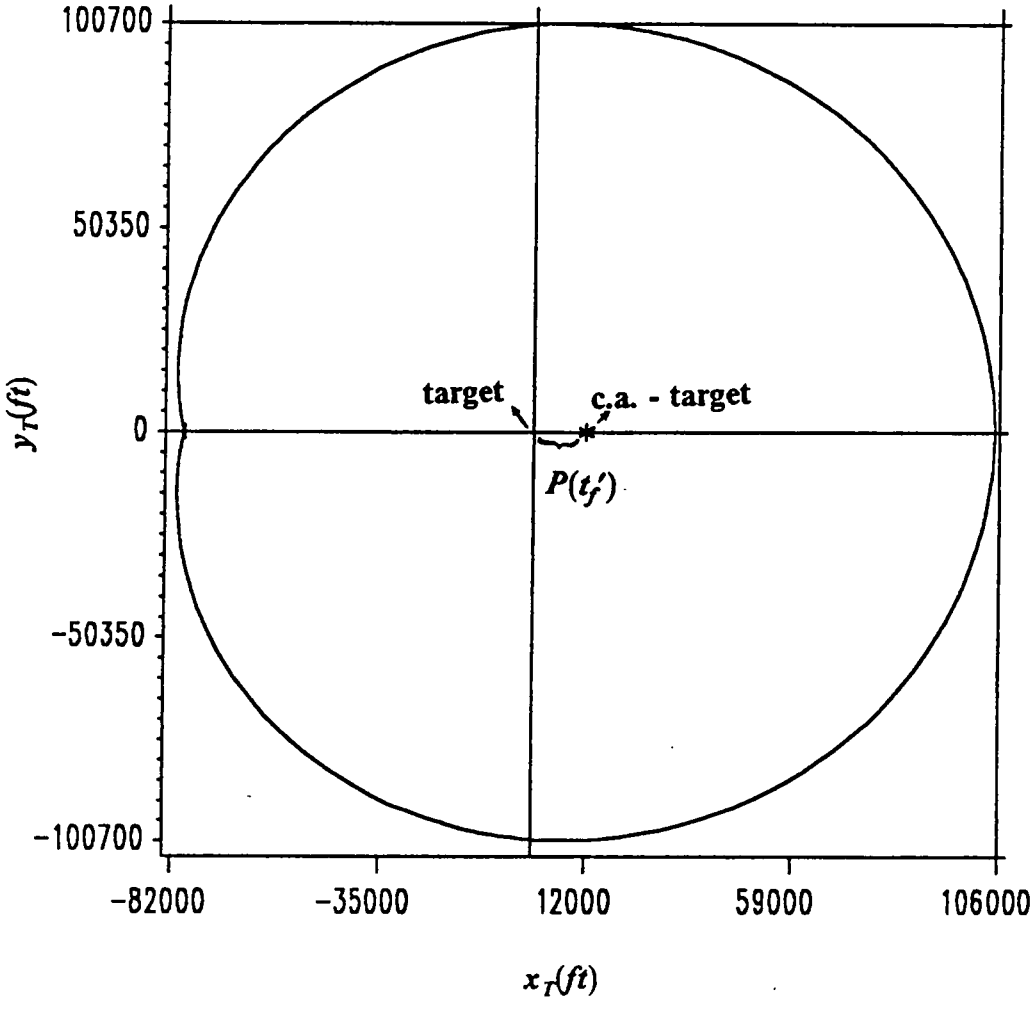

Fig. 6.2: Attainability set of target in horizontal plane

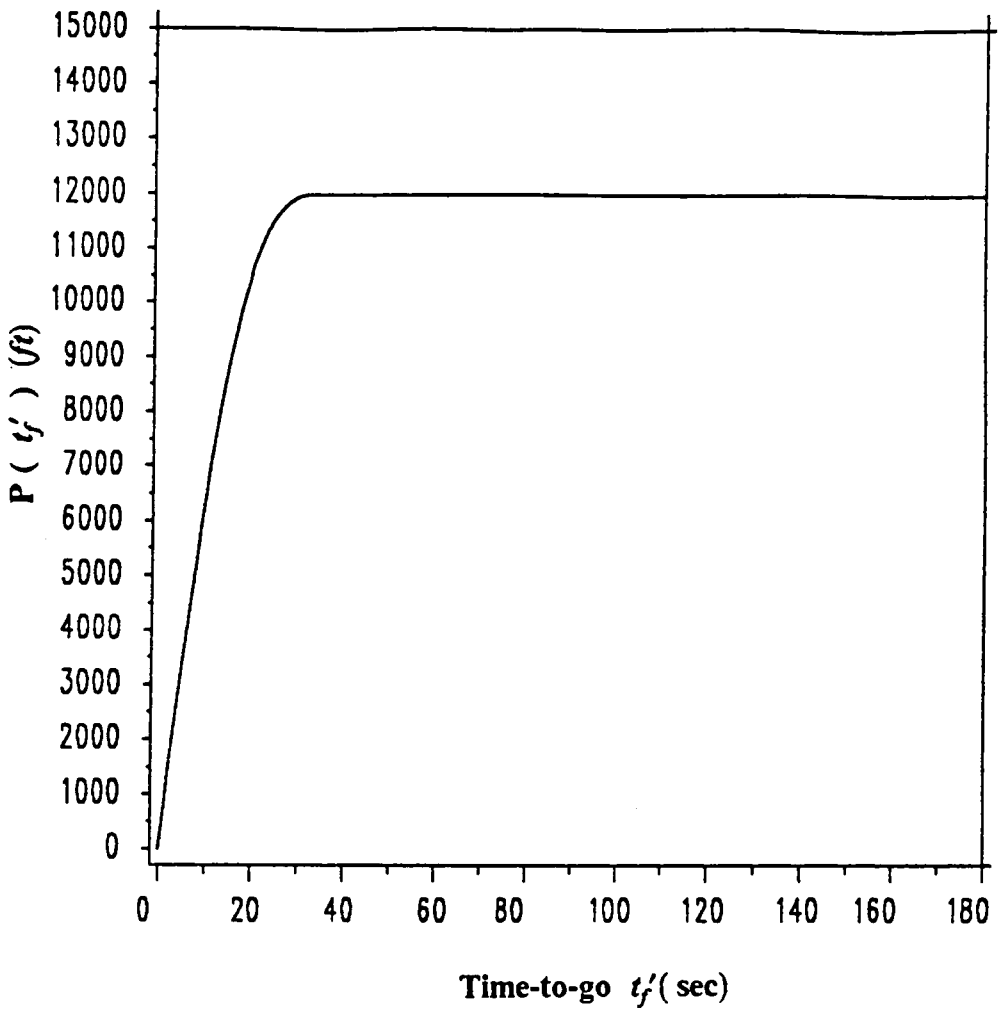

Fig. 6.3: Variation of $P(t_f')$ with t_f'

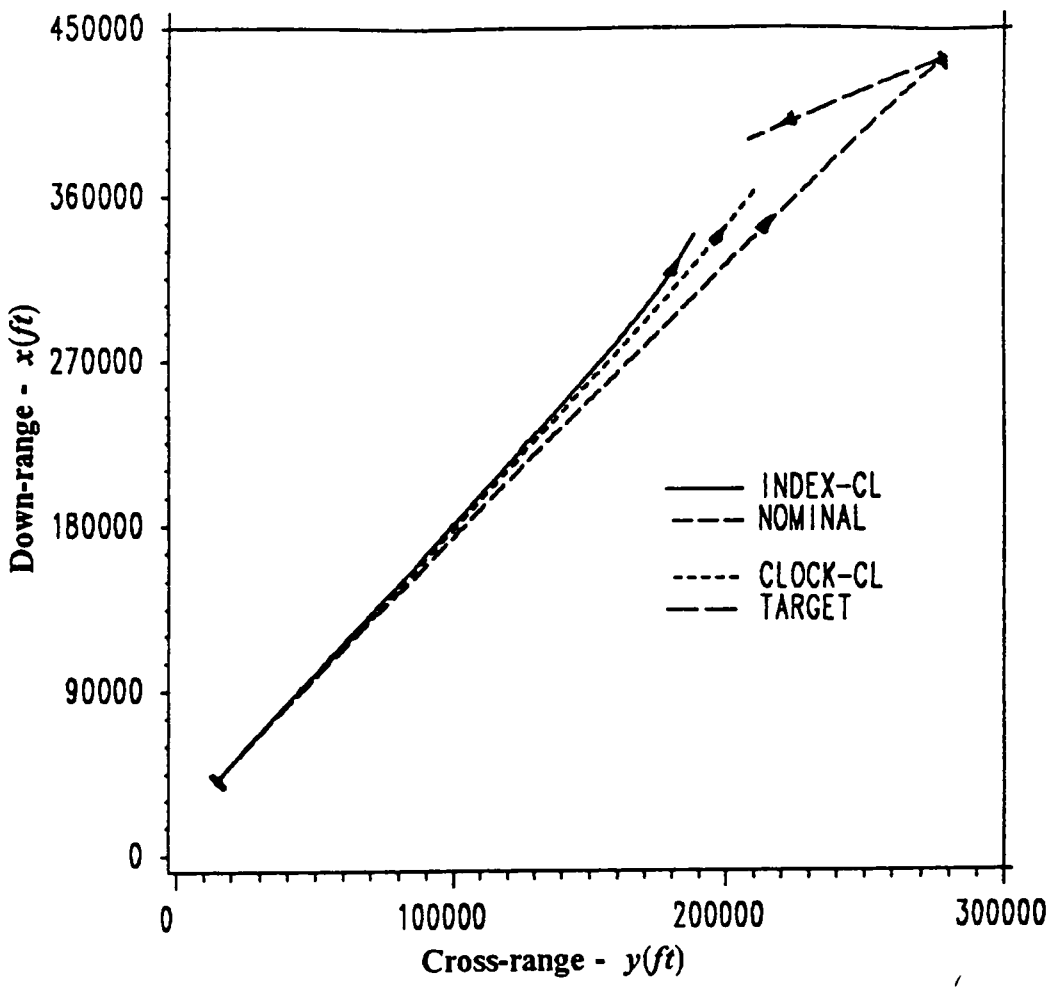

Fig. 6.4: $x - y$ projection of missile and aggressive target

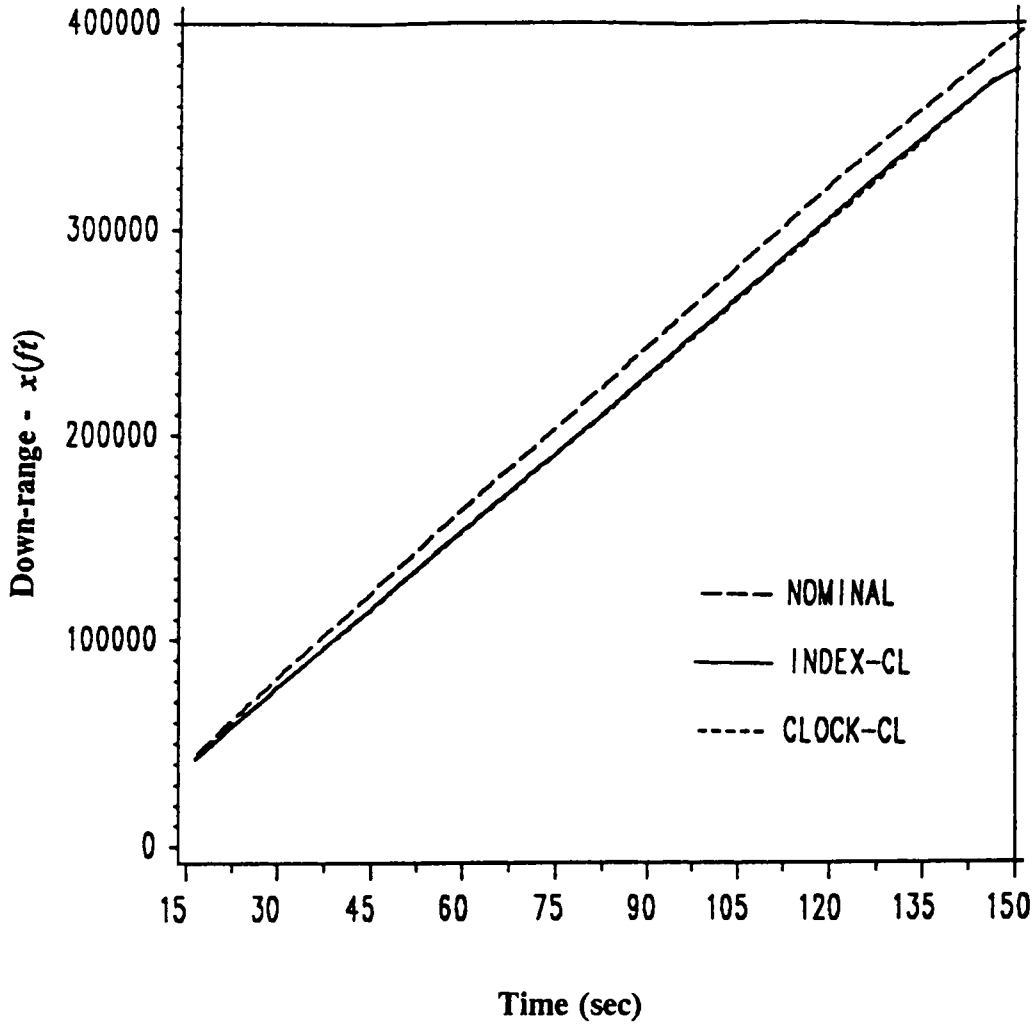

Fig. 6.5: Down-range time history of missile against aggressive target

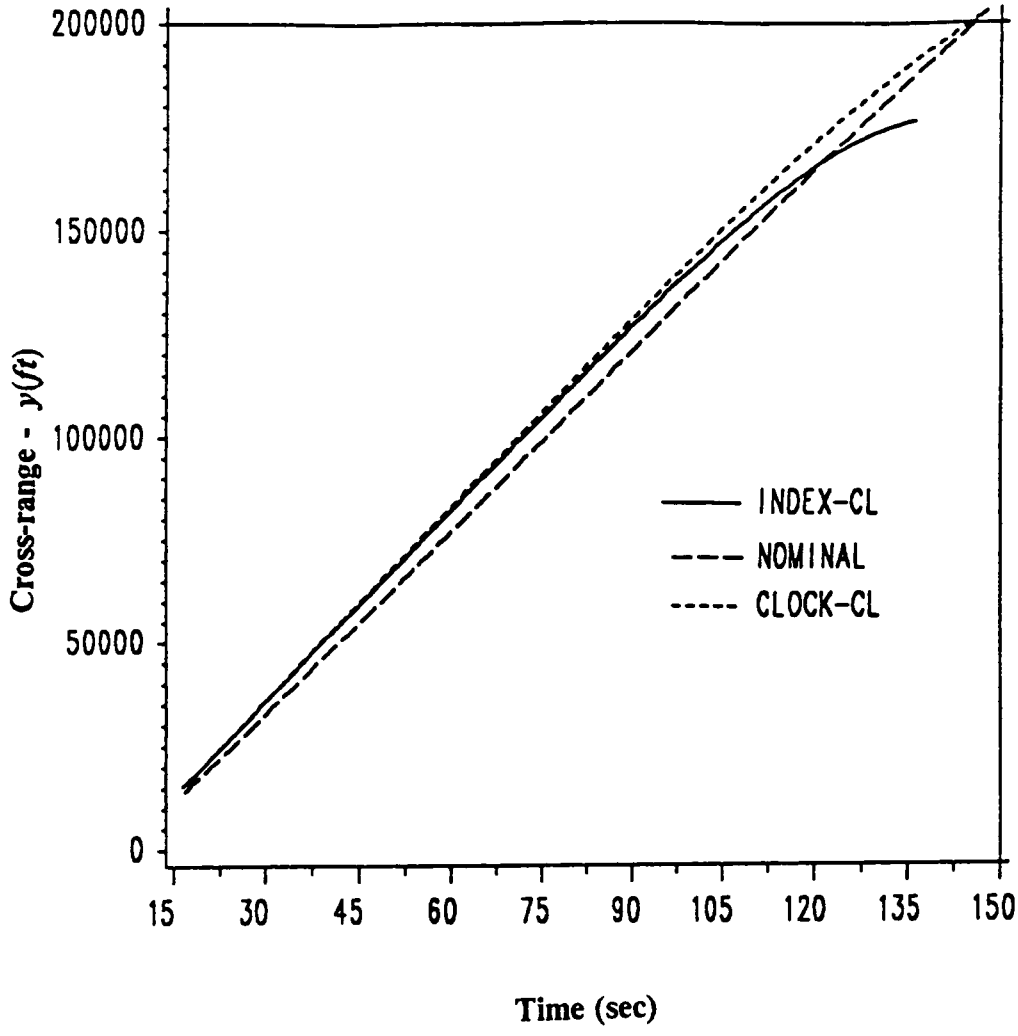

Fig. 6.6: Cross-range time history of missile against aggressive target

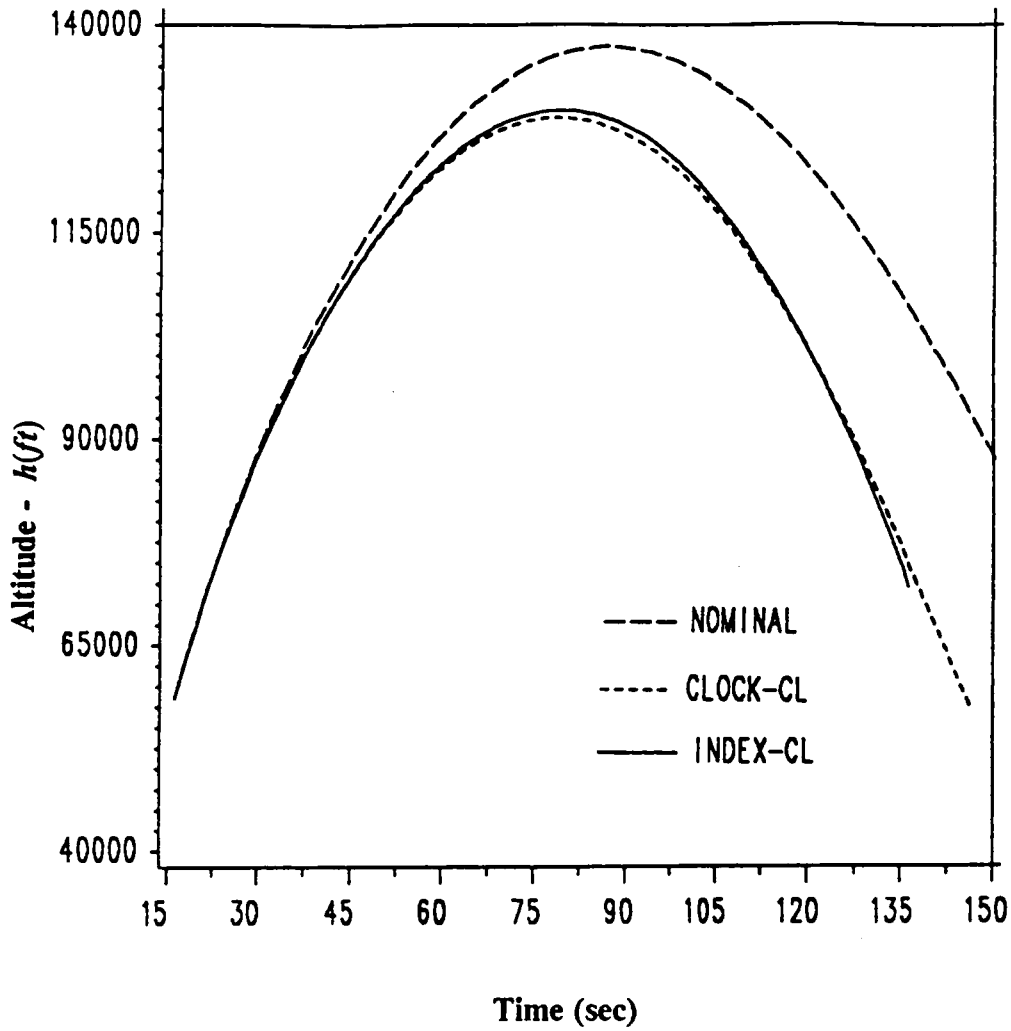

Fig. 6.7: Altitude time history of missile against aggressive target

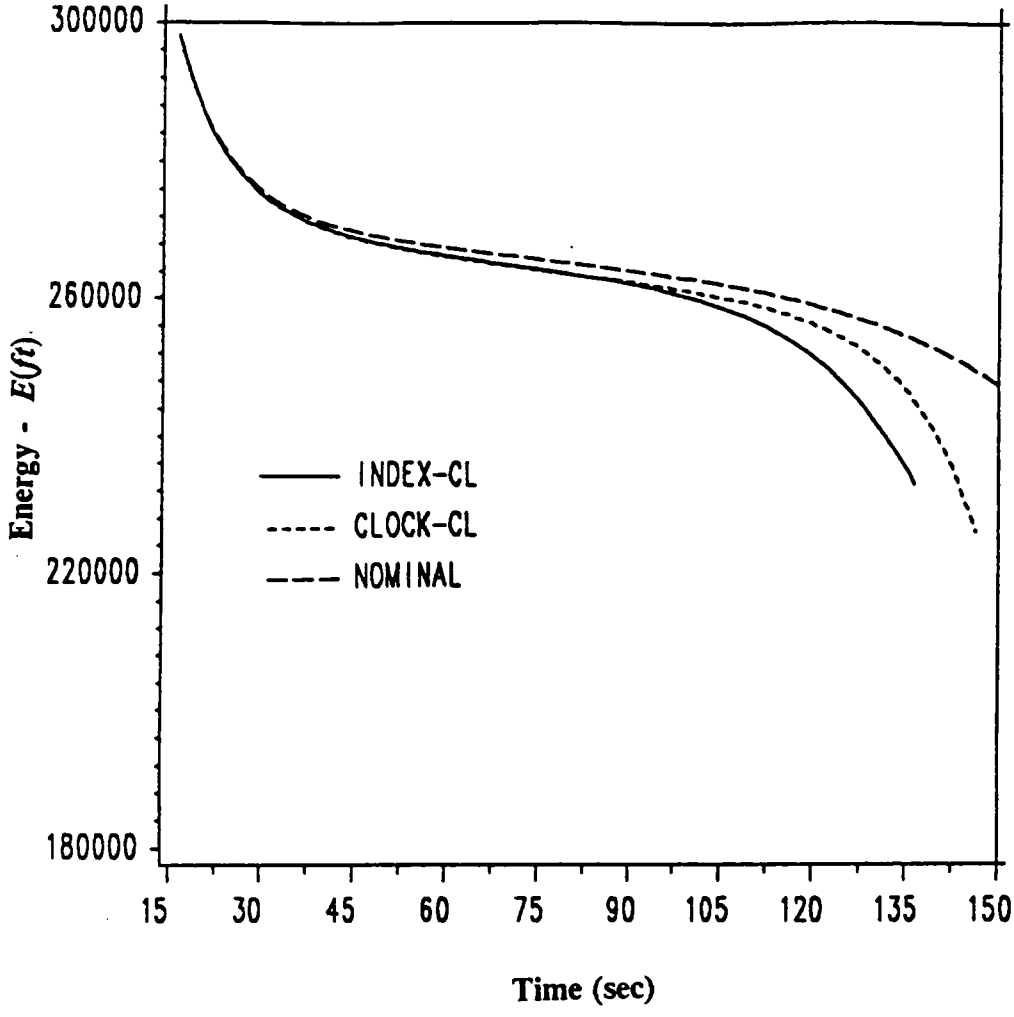

Fig. 6.8: Energy time history of missile against aggressive target

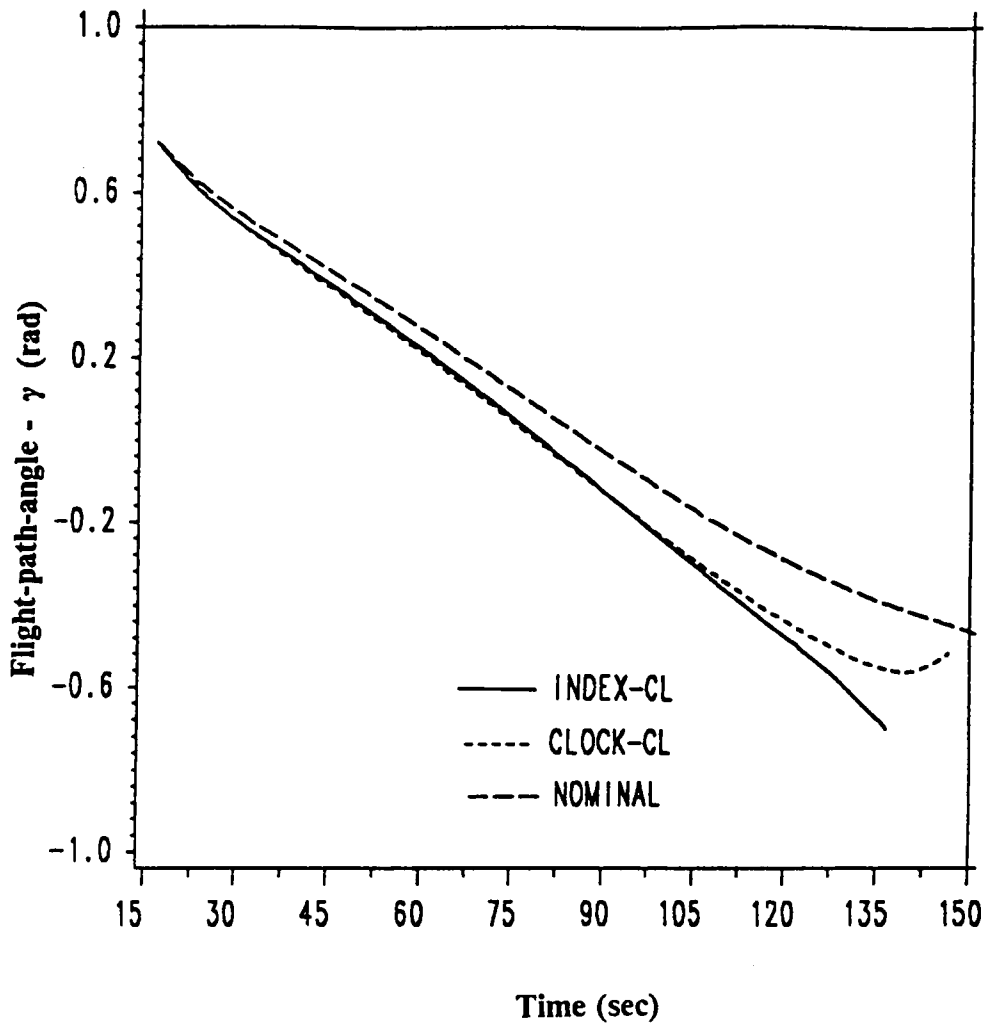

Fig. 6.9: Flight-path-angle time history of missile against aggressive target

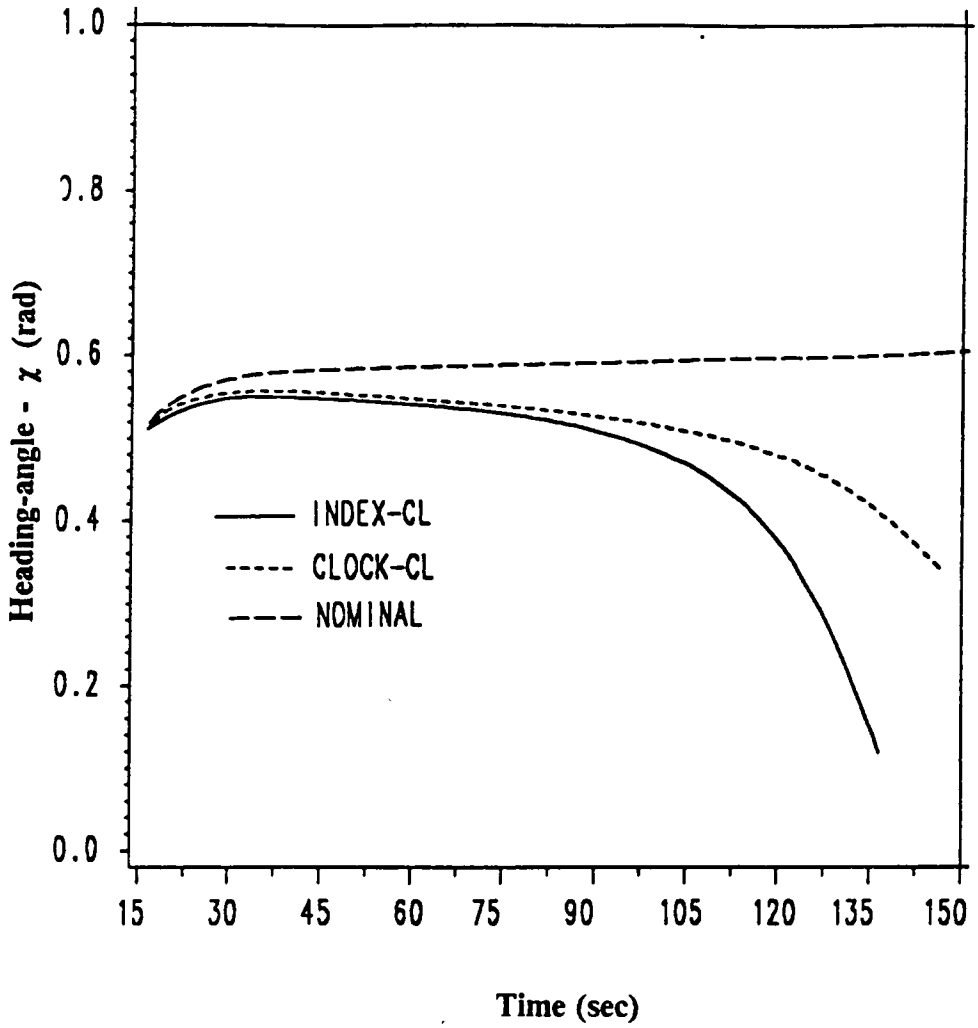

Fig. 6.10: Heading-angle time history of missile against aggressive target

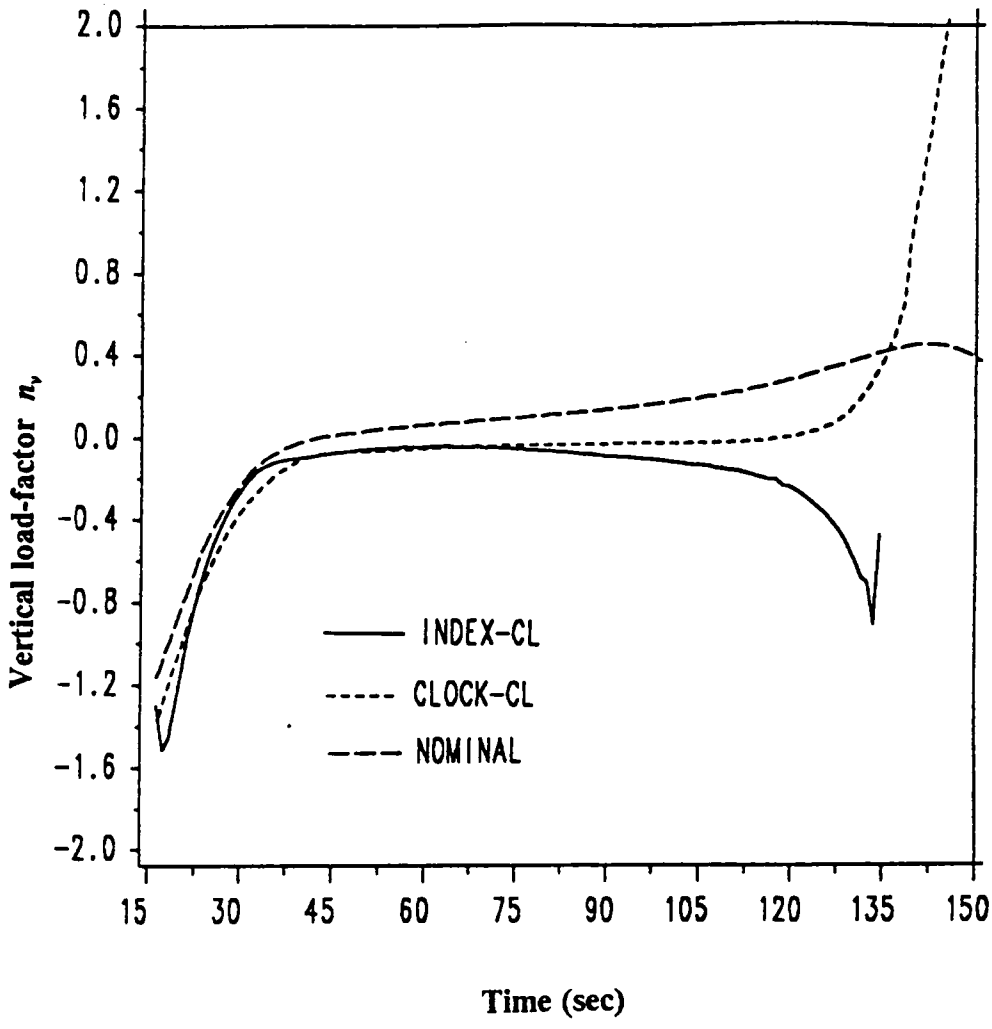

Fig. 6.11: Vertical load-factor time history of missile against aggressive target

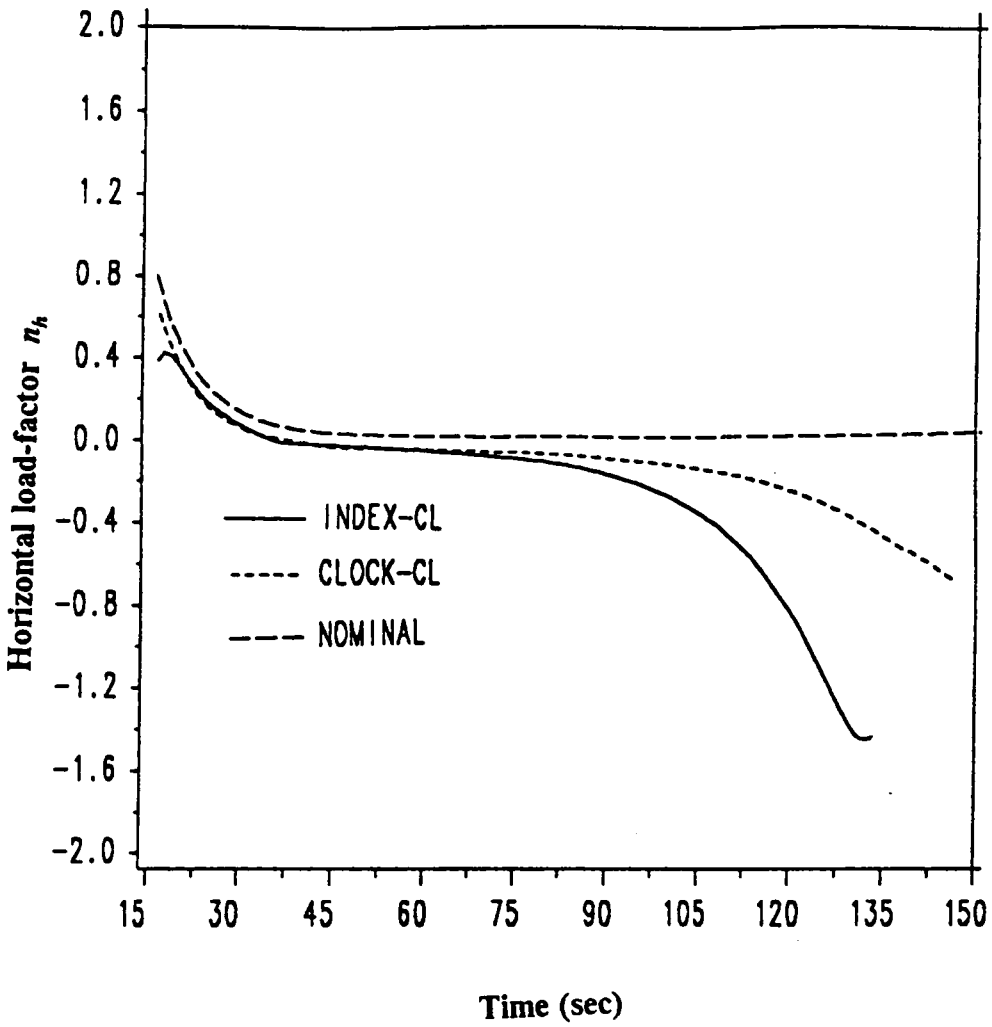

Fig. 6.12: Horizontal load-factor time history of missile against aggressive target

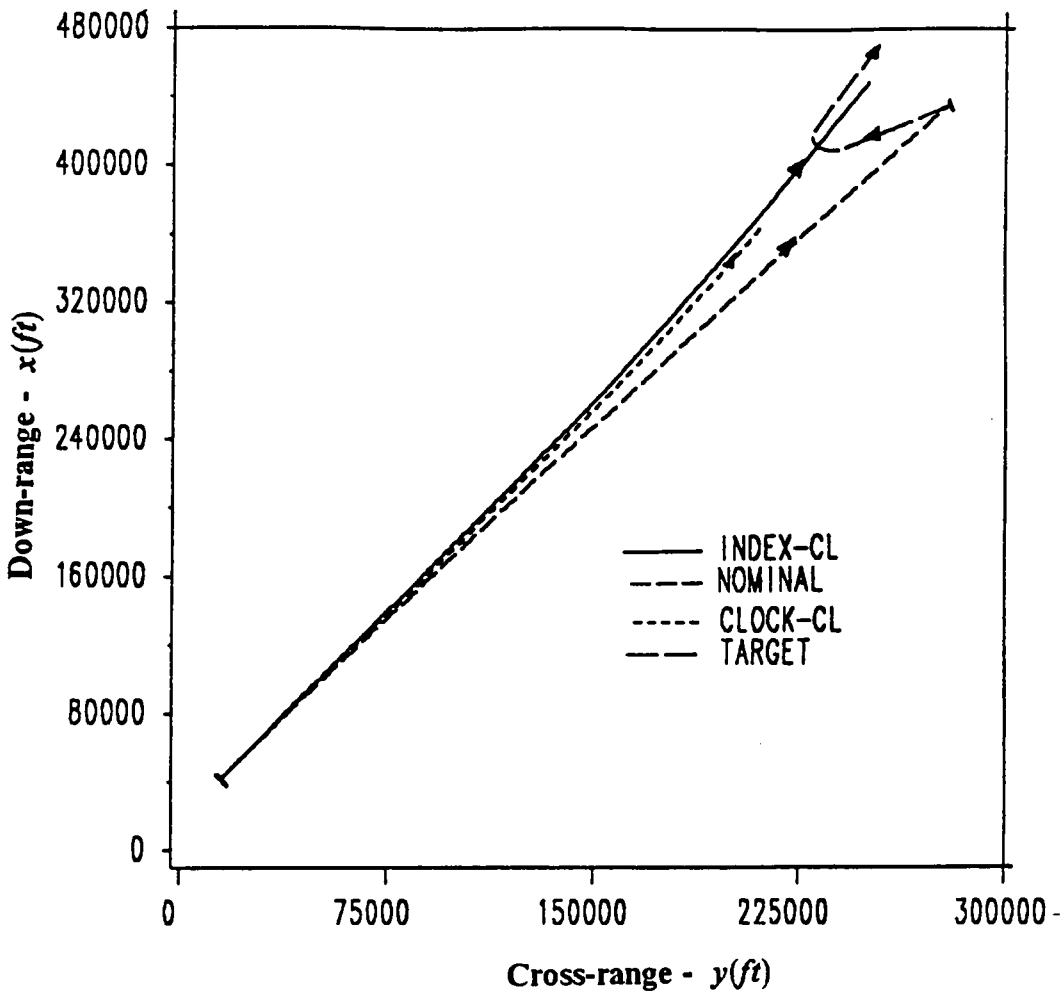

Fig. 6.13: $x - y$ projection of missile and run-away target

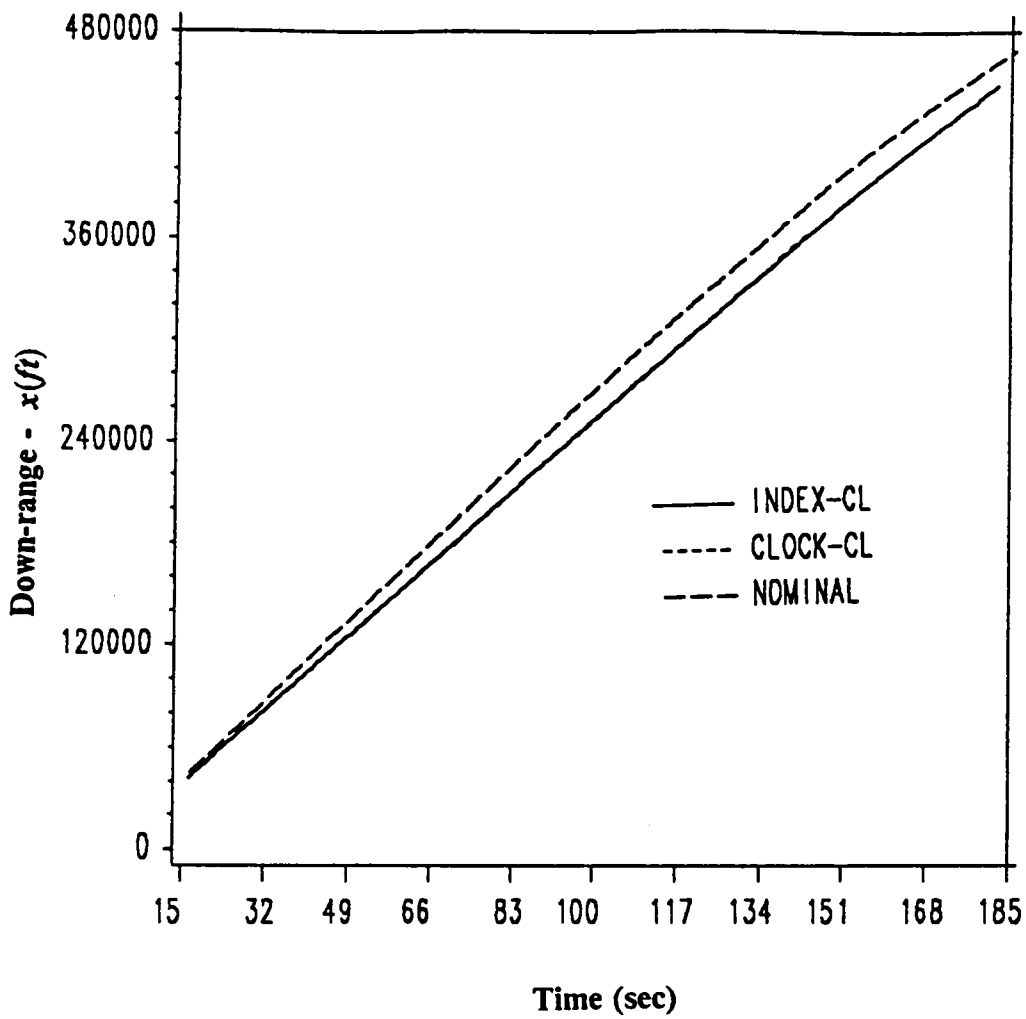

Fig. 6.14: Down-range time history of missile against run-away target

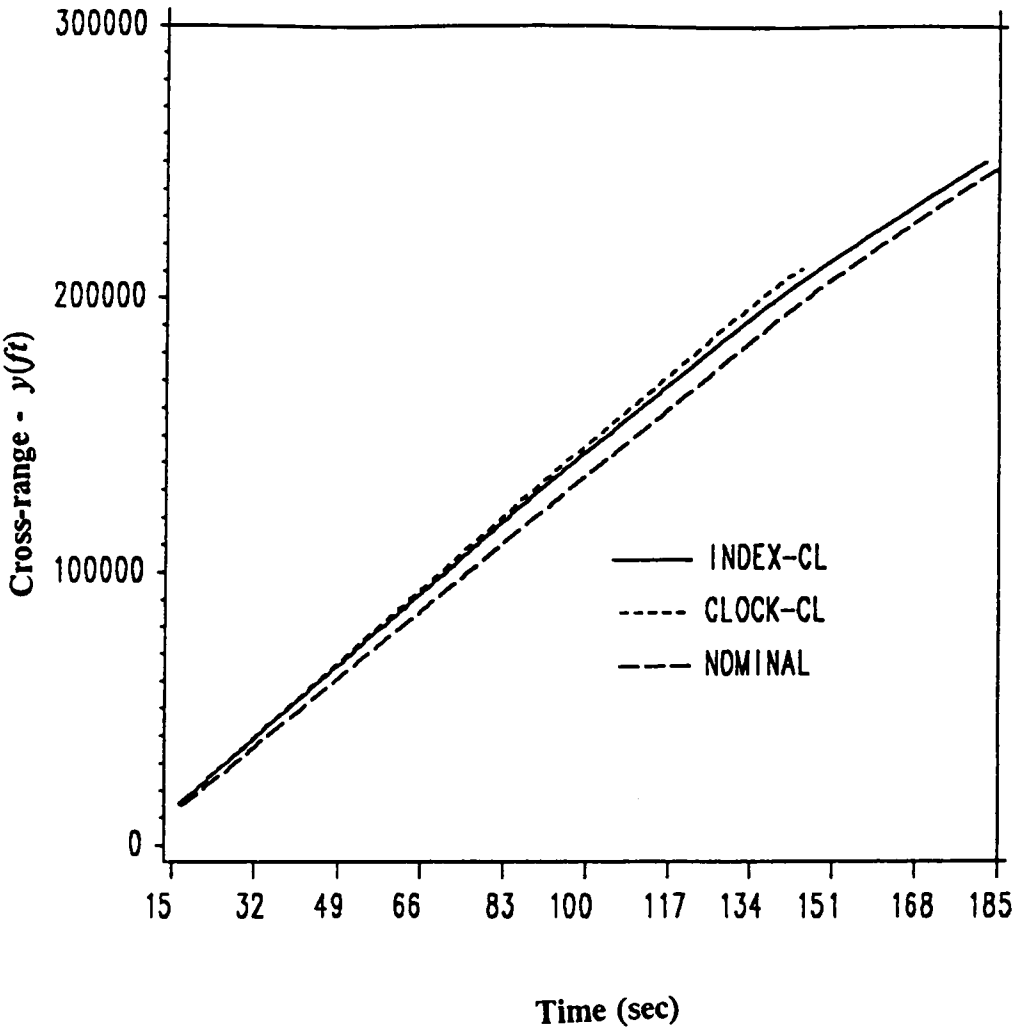

Fig. 6.15: Cross-range time history of missile against run-away target

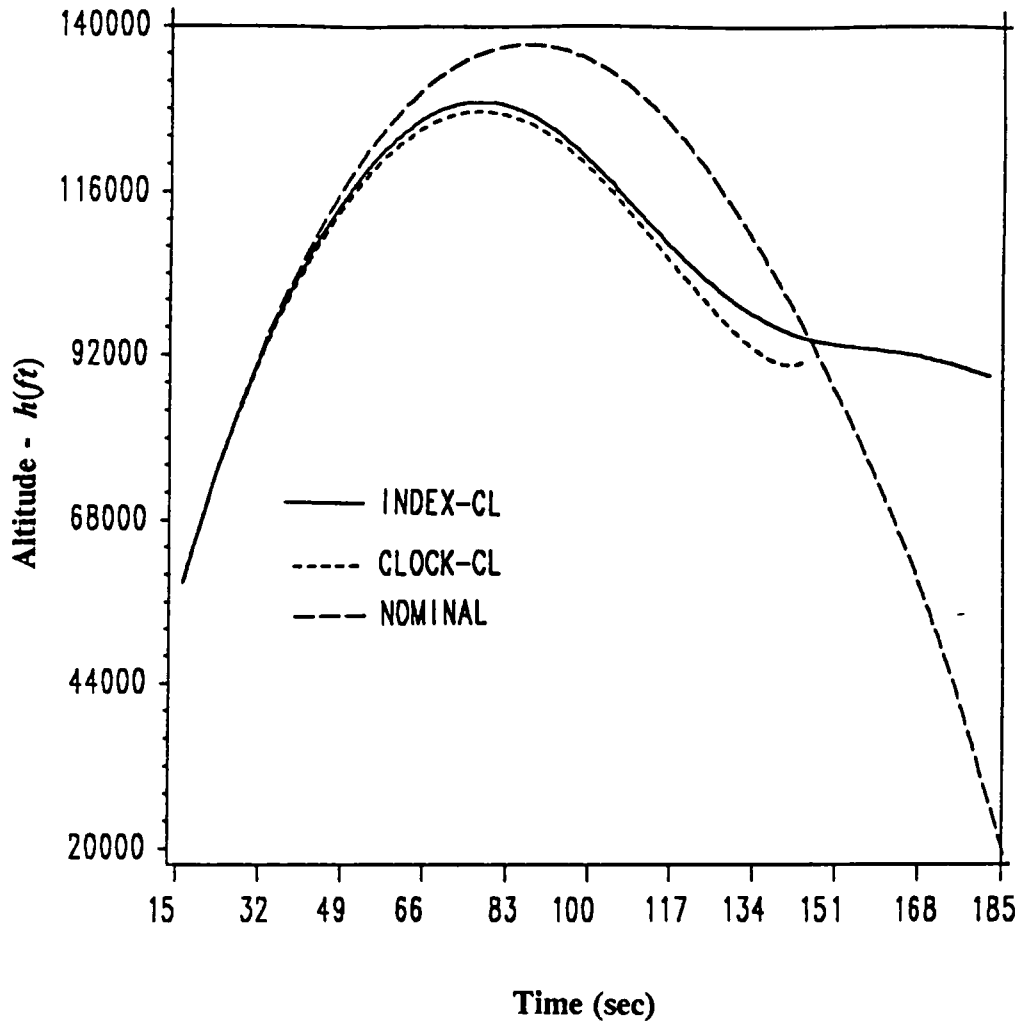

Fig. 6.16: Altitude time history of missile against run-away target

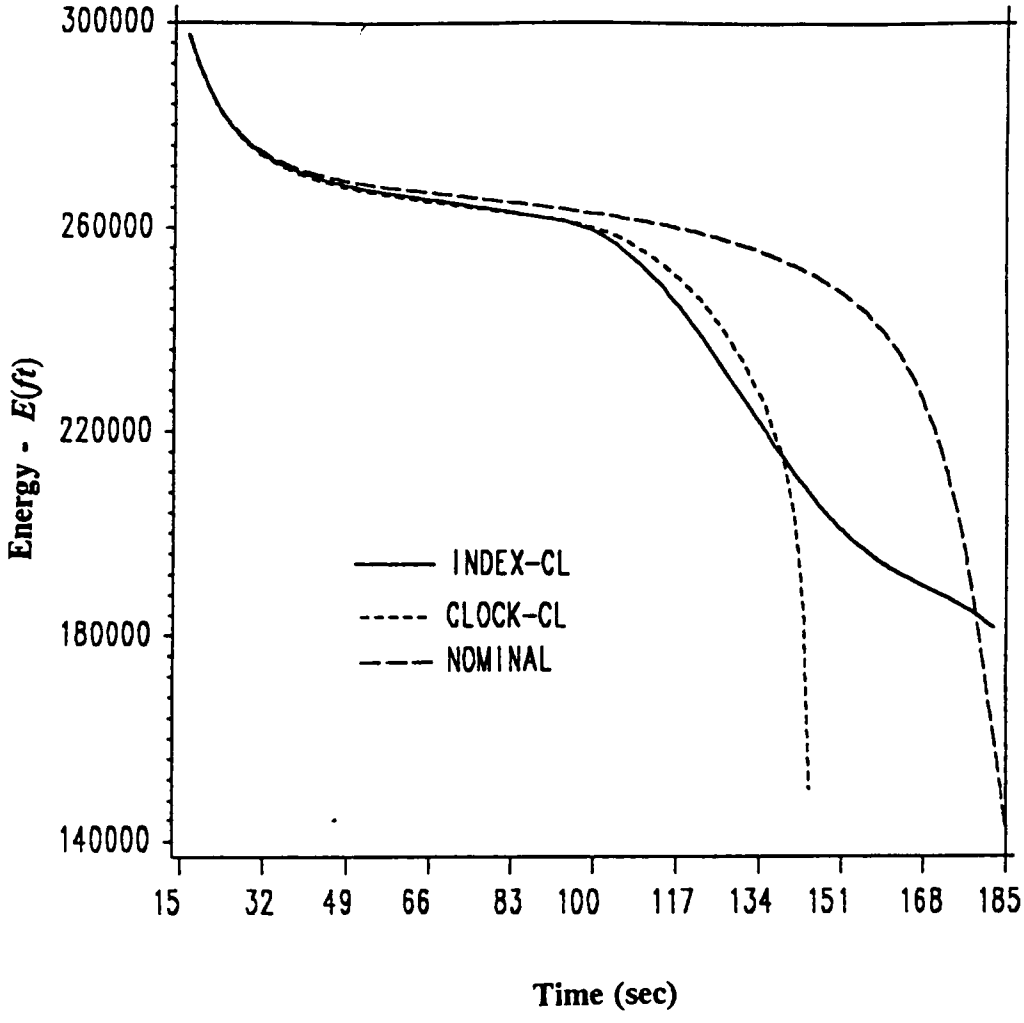

Fig. 6.17: Energy time history of missile against run-away target

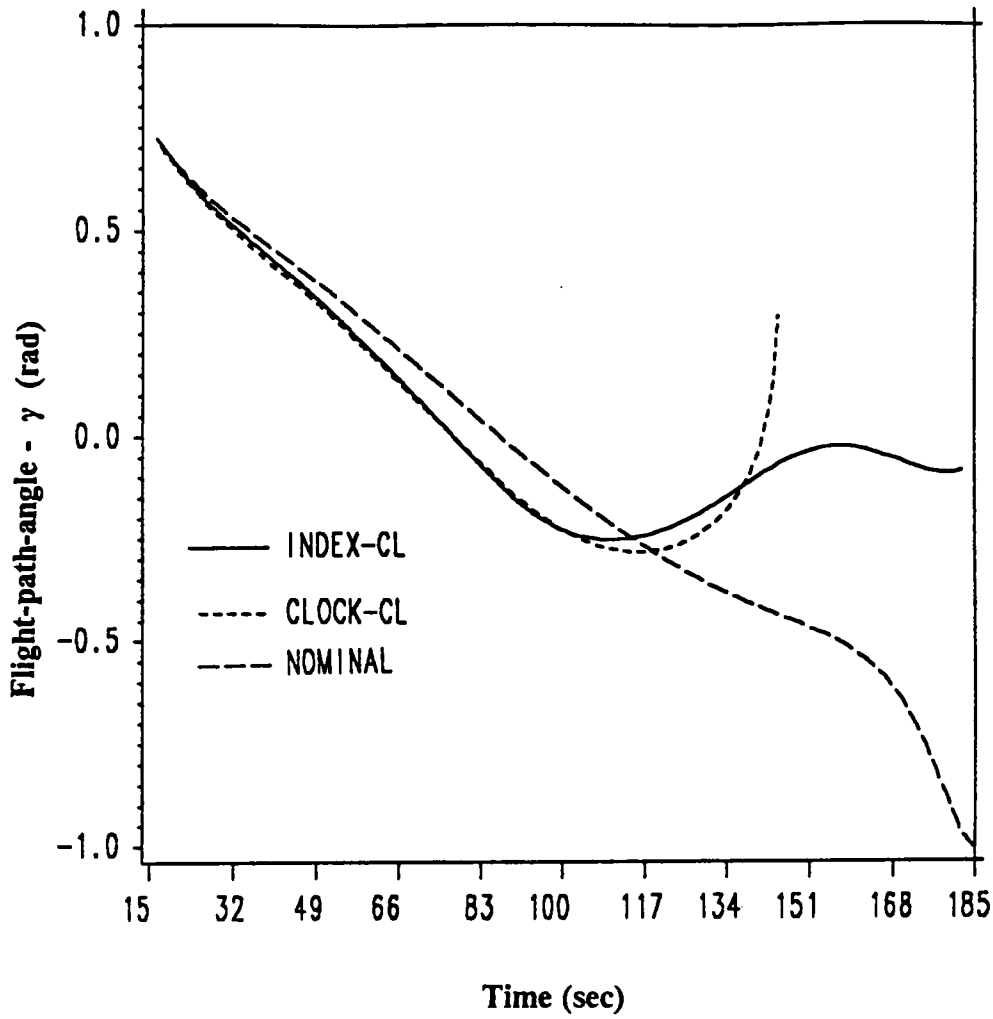

Fig. 6.18: Flight-path-angle time history of missile against run-away target

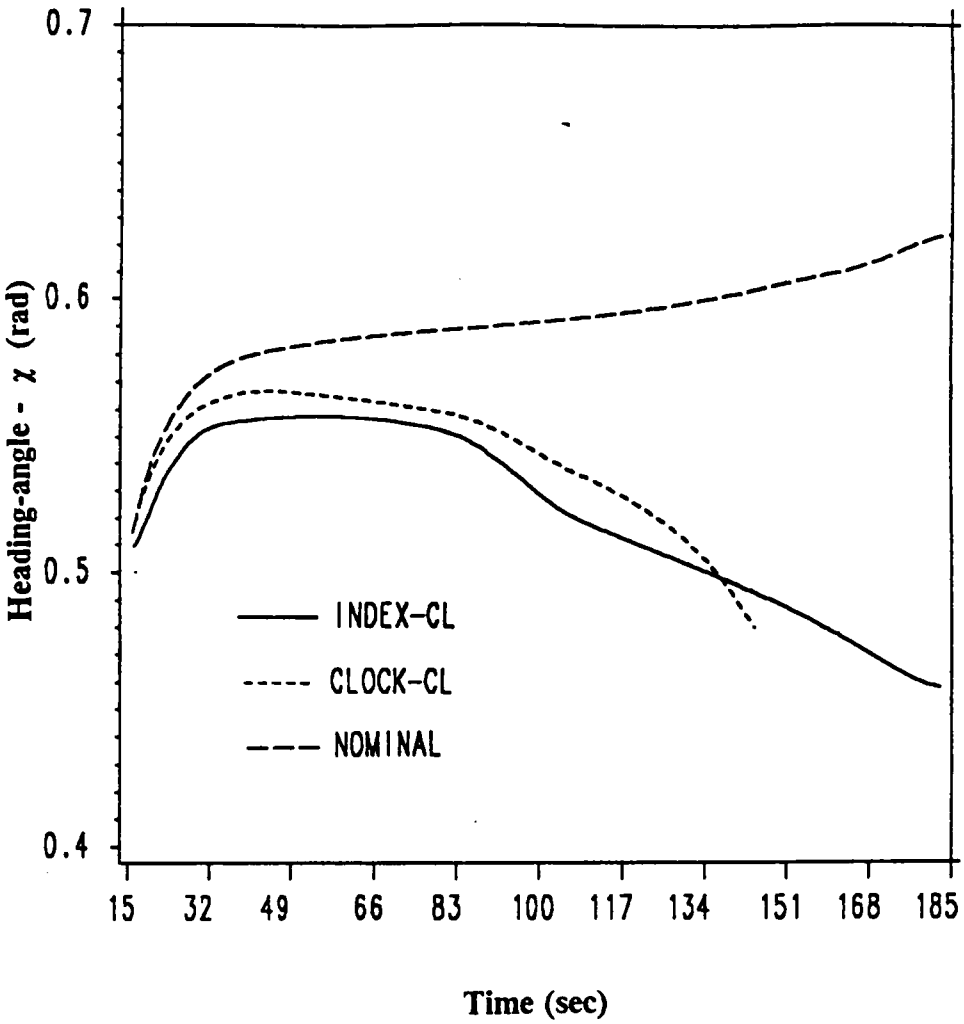

Fig. 6.19: Heading-angle time history of missile against run-away target

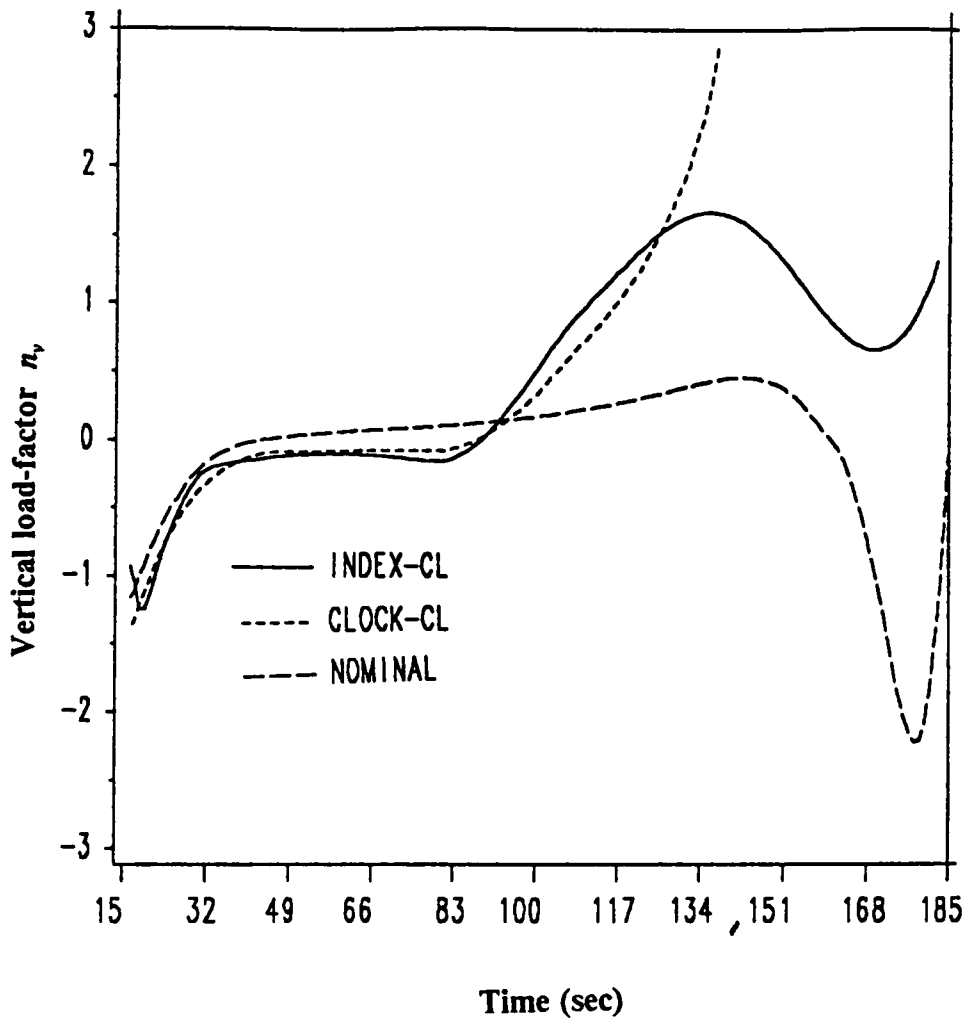

Fig. 6.20: Vertical load-factor time history of missile against run-away target

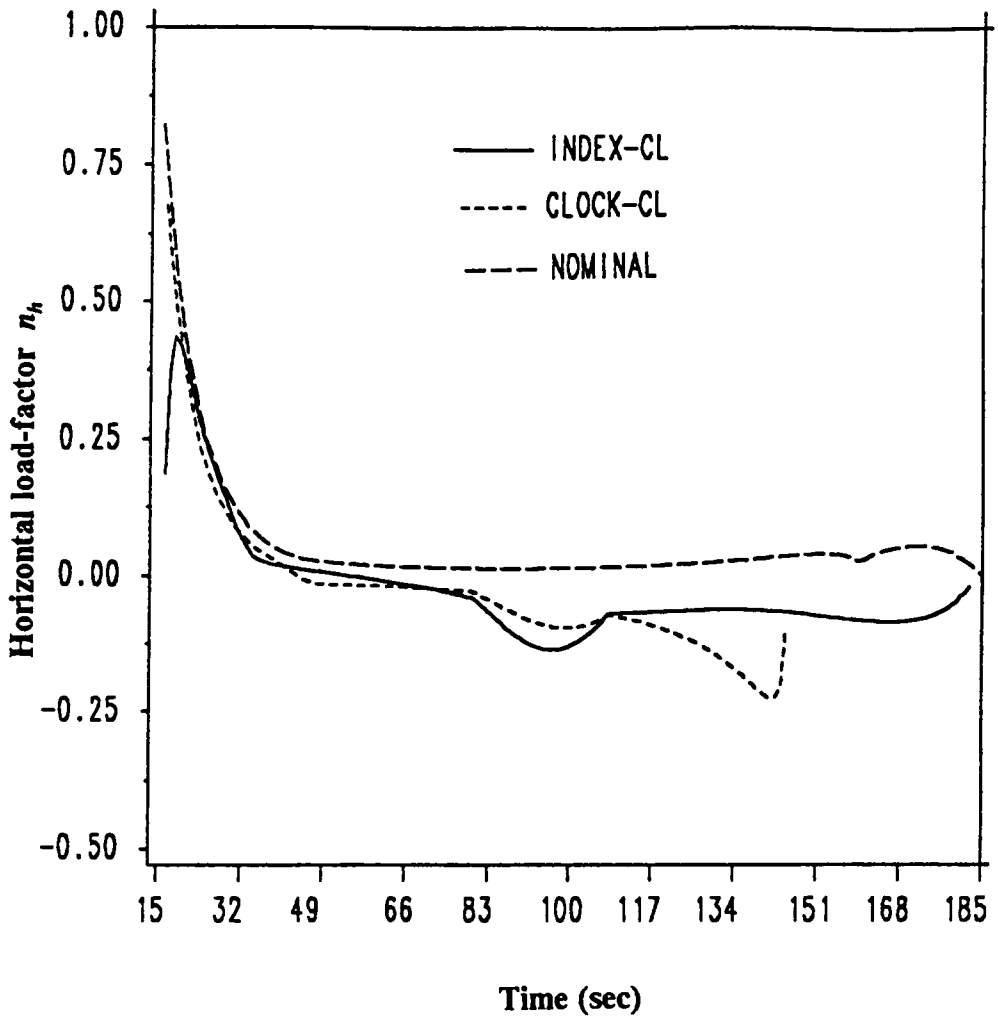

Fig. 6.21: Horizontal load-factor time history of missile against run-away target

Chapter 7: Terminal Guidance

7.1: Overview

The midcourse guidance phase must be terminated before intercept is encountered because the gains become unbounded. The guidance scheme is continued using terminal guidance in the form of proportional navigation (pro-nav) or one of its modifications. Chasing the center-of-attainability of the target, altitude shaping and drag resolution in conjunction with classical three-dimensional pure and true pro-nav are some of the schemes discussed in this section. Improvement in performance, i.e., time/energy, is the main objective in using the above modifications.

7.2: Classical Pro-nav in Three-Dimensions

Pure proportional navigation (PPN) in three dimensions as in [25] is defined in the following manner:

Construct the lead-angle-plane as shown in Fig. {7.1}, containing the velocity vector of the missile at a given time and the line-of-sight (LOS) to the target. The dynamics of the missile and target may induce a non-zero rate of change of the LOS. Let $\hat{e}_\sigma$ be the unit vector along the LOS from the missile to the target. The total time derivative of the unit vector is given by:

$$\hat{e}_\sigma = \dot{\sigma}_u \hat{e}_{\sigma u} + \dot{\sigma}_v \hat{e}_{\sigma v} \tag{7.1}$$

The rate of change is resolved into two orthogonal components - one, in the lead-angle-plane, normal to the LOS in the direction of $\hat{e}_{\sigma u}$ of magnitude $\dot{\sigma}_u$ and the other normal to the lead-angle plane along $\hat{e}_{\sigma v}$ of magnitude $\dot{\sigma}_v$. The inertial acceleration vector of the missile a_m can be composed as:

$$a_m = V \hat{e}_\gamma + g\,[-\frac{D}{W} - \sin\gamma]\,\hat{e}_\gamma \tag{7.2}$$

where $\hat{e}_\gamma$ is given by,

$$\hat{e}_\gamma = \dot{\gamma}_u \hat{e}_{\gamma u} + \dot{\gamma}_v \hat{e}_{\gamma v} \tag{7.3}$$

The quantities $\dot{\sigma}_u$ and $\dot{\sigma}_v$ can be obtained with the information on the target position, rate of change of position, and measuring the missile's own position and velocities. The PPN law states that:

$$\dot{\gamma}_u = K_1 \dot{\sigma}_u \tag{7.4}$$

and

$$\dot{\gamma}_v = K_2 \dot{\sigma}_v \tag{7.5}$$

The PPN law stated above is the simplest classical form of PPN as suggested in [25]. The quantities K_1 and K_2 are constants whose range varies from 2 to 5 in general. The usual practice is to consider $K_1 = K_2$ and to assign a constant value depending on the model and objective. It has been shown in [21], that a value of 3 for the constants is in fact optimal in the sense of minimizing a weighted sum of miss-distance and control (acceleration) cost for a simple intercept problem with a non-maneuvering target. The $\dot{\gamma}_u$ and $\dot{\gamma}_v$ are related to the controls n_v and n_h for the specific model which are instantaneously evaluated and used for the guidance. It is to be noted that the acceleration in the direction $\hat{e}_\gamma$ is fixed for a given n_v and n_h and hence not directly controlled by any criteria.

Another classical pro-nav scheme called true-proportional navigation (TPN) employs similar control logic. The rate of change of the LOS unit vector is resolved along the $\hat{e}_{\gamma u}$, $\hat{e}_\gamma$, and the out of plane direction $\hat{e}_{\gamma v}$ as follows:

$$\hat{e}_\sigma = \dot{\sigma}_{ut}\hat{e}_{\gamma u} + \dot{\sigma}_t\hat{e}_\gamma + \dot{\sigma}_{vt}\hat{e}_{\gamma v} \tag{7.6}$$

The TPN law states that:

$$\dot{\gamma}_u = K_1\,\dot{\sigma}_{ut} \tag{7.7}$$

and

$$\dot{\gamma}_v = K_2\,\dot{\sigma}_{vt} \tag{7.8}$$

The acceleration command along the direction of the missile velocity is obtained from the locus of all possible axial accelerations, as in Fig. {7.2}, allowed for the

missile model for prescribed lateral acceleration, due to the fact that there exists only two controls to match three acceleration components in the missile guidance.The lack of an axial control like thrust during the end-game shows the reduction in controllability of the missile to choose any acceleration vector. The terminal guidance is basically used in this study to check whether the midcourse guidance behaved satisfactorily. It is observed that the pro-nav scheme employing PPN or TPN is efficient in terms of time and energy at intercept for the aggressive target. The end of midcourse guidance terminates with the missile and target closely aligned in a collision course with a small time-to-go. Simulation of terminal guidance using PPN or TPN for a run-away target shows low energy at intercept time compared to the reference trajectory. The extended time-of-flight for the missile chasing the run-away target, supplemented by the fact that the thrust is zero, makes the lower energy at impact only obvious. However, one tries to improve the performance of this terminal phase to the limiting threshold.

7.3: Performance Augmentation

Any attempt to linearize the missile model as in [42] using a Brunovsky canonical form [43] and to solve a linear quadratic control problem to optimize final energy and miss-disance is rendered useless due to the absence of the third axial control. This simply implies the fact that any form of optimization would yield an acceleration command which may or may not be feasible.

It has been shown in Chapter 6 that the missile chasing the target center-of-attainability during the midcourse guidance dampens quick target maneuvers. Using the above idea for missile guidance, the midcourse guidance terminates with the missile chasing the pseudo-target. During terminal guidance, one could continue to chase the pseudo-target instead of the target. However, chasing the pseudo-target requires the missile to estimate the time-to-go and predict the center of attainability of the target. Chasing the center-of-attainability of an aggressive target or a target under "tail-chase" has a distinct advantage of slower dynamics of the pseudo-target because the distance of center-of-attainability from the target shrinks as time-to-go becomes smaller. The time-to-go during the midcourse guidance was evaluated by suitable linearization and prediction of the final time for the neighboring extremal. For the terminal guidance the time-to-go to intercept the target is obtained by a simple three-dimensional collision triangle. The following equations are used to linearly extrapolate a three-dimensional collision triangle.

$$x(t) + V(t) \cos \hat{\gamma}(t) \cos \hat{\chi}(t)\, t_f' = x_T(t) + \dot{x}_T\, t_f' \tag{7.9}$$

$$y(t) + V(t) \cos \hat{\gamma}(t) \sin \hat{\chi}(t)\, t_f' = y_T(t) + \dot{y}_T\, t_f' \tag{7.10}$$

$$h(t) + V(t) \sin \hat{\gamma}(t)\, t_f' = h_T(t) \tag{7.11}$$

Here it is assumed that the angles and velocities are constant for the linear extrapolation. The assumption that the target is travelling at constant altitude is also used. The equations (7.9-7.11) are solved for the three unknowns, namely,

$\hat{\gamma}(t)$, $\hat{\chi}(t)$, and t_f' . The two angles $\hat{\gamma}(t)$ and $\hat{\chi}(t)$ are the instantaneous angles used to define the collision triangle. A positive solution exists for t_f' as long as $V > V_T$. The center-of-attainability of the target is evaluated using Eq. (6.17) and the pro-nav scheme is used to chase this center-of-attainability of the target.

The results of chasing the pseudo-target show marginal improvement over the ordinary proportional navigation (PN) schemes. Figs. {7.3-7.5} compare the PPN scheme chasing the aggressive target and pseudo-target. The final energy is close to the reference final energy desired using either method. Fig. {7.3} compares the horizontal projection of the two trajectories. The pseudo-target chasing trajectory is "closer" to the collision triangle. The time and energy at intercept are nearly equivalent. Figs. {7.6-7.8} depicts the PPN scheme performed on a run-away target with the two methods. The pseudo-target chasing performs horizontal load-factor corrections closer to final time than the target chasing scheme as can be seen from Fig. {7.6} and hence better in the sense that for a given control effort, lesser energy is dissipated at lesser velocities attained towards final time. This can be inferred from the energy equation for the model. An increased final energy and a marginally shorter intercept time as seen in Figs. {7.8,7.6} ($\Delta E_f \simeq 3000ft$ and $\Delta t_f = -0.2s$) are obtained by chasing the pseudo-target.

TPN shows no or little improvement in final energy over PPN for either of the two target scenarios for given values of K_1 and K_2 . This can be observed from the energy state histories for the two cases as shown in Figs. {7.9,7.10}. For the

aggressive target they behave identically while for the run-away intercept the TPN is only marginally better than PPN in energy at intercept.

An attempt to increase the final energy at intercept of the run-away target is done using a scheme called **drag-resolution** . The lateral acceleration obtained from any of the pro-nav schemes above is obtained at a given time for a fixed value of K_1 and K_2 . Let this correspond to the point "P" in Fig. {7.2}. This direction is normal to the velocity vector direction or the axial direction. For this value of lateral acceleration there exists a unique axial acceleration, whose magnitude is given by the point "D3". This is due to the fact that an axial control is lacking in the missile model. To obtain a commanded acceleration closest to the desired lateral acceleration, one chooses the closest point in the "locus of all possible axial accelerations" denoted by "D2". This is done numerically by scanning the points close to "D1" and finding the point on the locus of all possible axial accelerations that minimize the distance "P-D2" in 2-norm. The resultant lateral acceleration is given by point "Q". $\vec{a}_{cr}$ is the new commanded acceleration of the missile with drag-resolution while $\vec{a}_c$ was the actual commanded acceleration of the missile without drag-resolution. Fig. {7.11,7.12} compares the energy histories for missile chasing the center-of-attainability of the run-away target. It is to be noted that this scheme of drag-resolution using PPN or TPN has only a marginally better effect on the final energy at intercept.

It can be clearly seen from the classical pro-nav schemes suggested until now, that the target altitude histories indicate an immediate steep dive towards the PIP.

The end of midcourse guidance against a run-away target shows an altitude management to fly at higher altitudes for less drag. For intercept, the missile has to perform a final dive. The time to initiate this depends upon the distances in the horizontal projection. As a trial to improve the performance of the missile characteristics, a method defined as **altitude-shaping** , necessarily an adhoc scheme, is simulated. The vertical load-factor is biased in such a fashion as to reduce the magnitudes of the negative vertical load-factor during the initial times of the terminal guidance. This is performed by using a simple adhoc scheme by defining a new vertical load-factor n_v' as defined below:

$$n_v' = n_v + | n_v | \frac{t_f'}{B} \tag{7.12}$$

where, n_v is the vertical load-factor obtained from classical pro-nav. B is a positive biasing factor and t_f' is the time-to-go. As the biasing factor is made smaller, the more the tendency of the missile initially to pull the nose up, as a result of higher vertical load-factors as in Fig. {7.15}. The altitude shaping thus performed shows small but noticeable improvement in the energy all along the trajectory. Fig. {7.13} shows the altitude histories for different values of the biasing factor. Fig. {7.14} shows energy state histories. For small values of B (i.e., $B < 60$) it should be noted that the energy improves for a given time, but the intercept time increases, thus reducing the energy at intercept. A lesser control effort may reduce the drag but can also increase the intercept time due to smaller "heading" corrections.

All the above methods used to improve the performance is performed with a basic objective to check the performance of the midcourse guidance especially against a run-away target (due to the poor energy at intercept). Only little improvement over the classical methods have been obtained by any of the suggested methods. Thus one concludes the fact that the long flight times associated with guidance against the target model and the limited energy of the missile is the fundamental reason for the same. Hence, the time of launch of the missile, optimal thrust to weight ratio of the missile, the targets of interest, no-escape envelopes, etc., are to be studied in detail to use the three-phase guidance scheme successfully in real combat scenario.

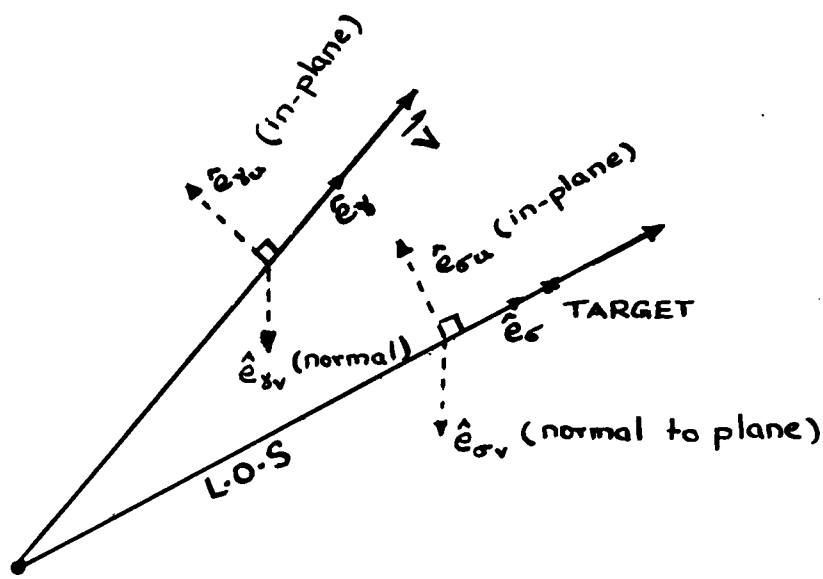

Fig. 7.1: Lead-angle-plane

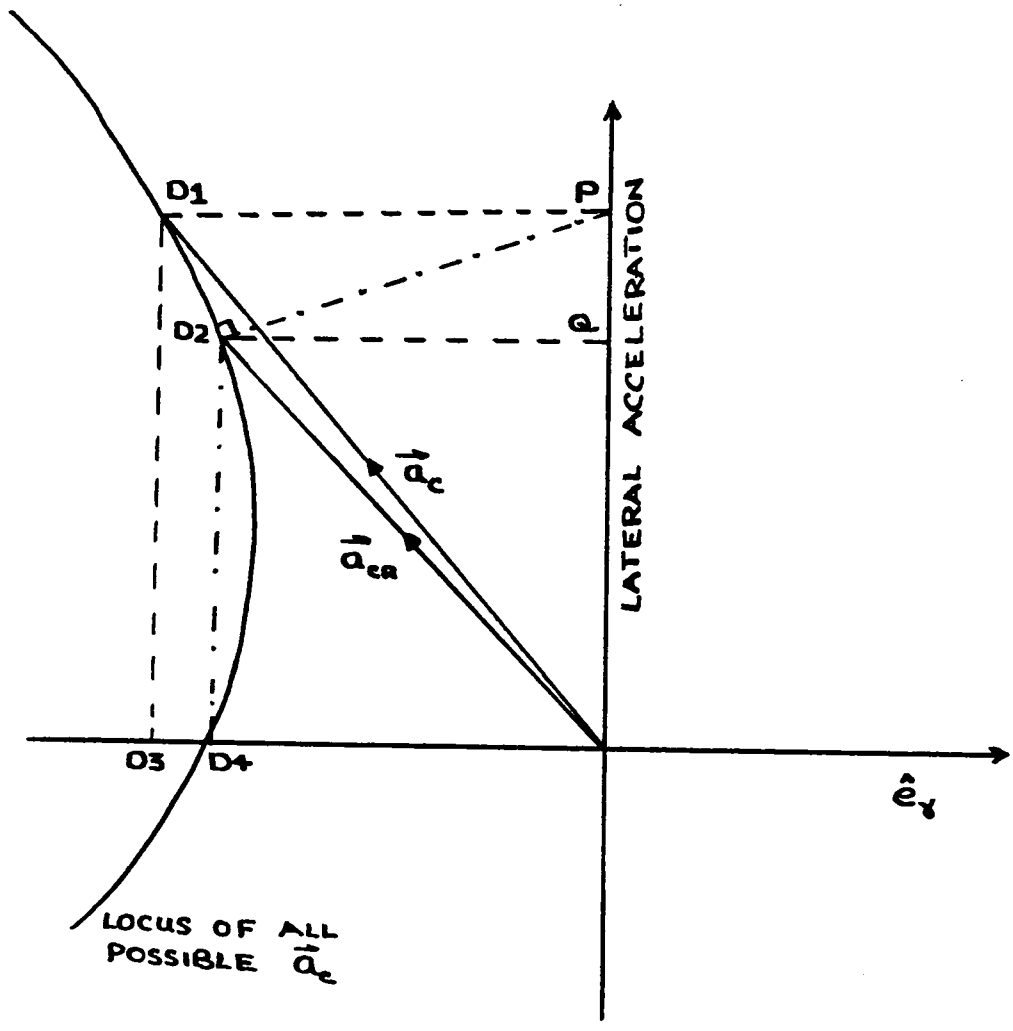

Fig. 7.2: Locus of all possible accelerations and drag-resolution

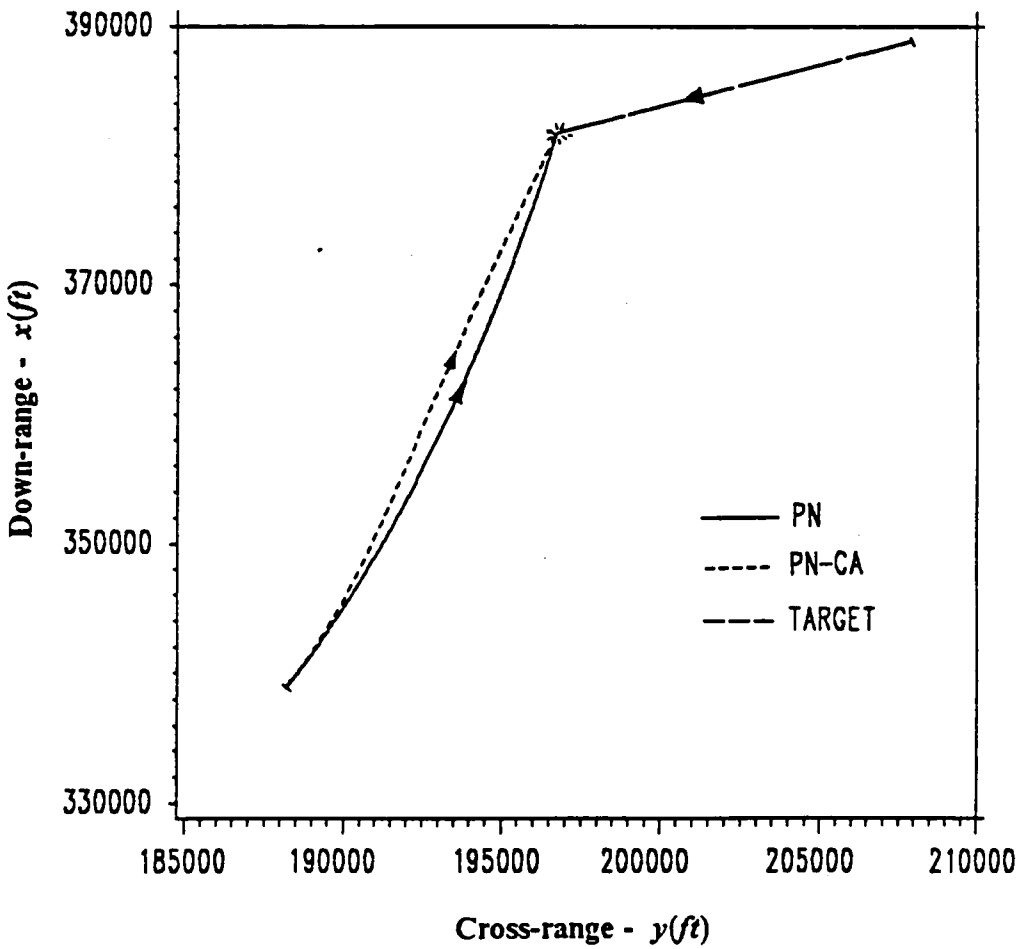

Fig. 7.3: $x - y$ projection of missile and aggressive target - terminal phase

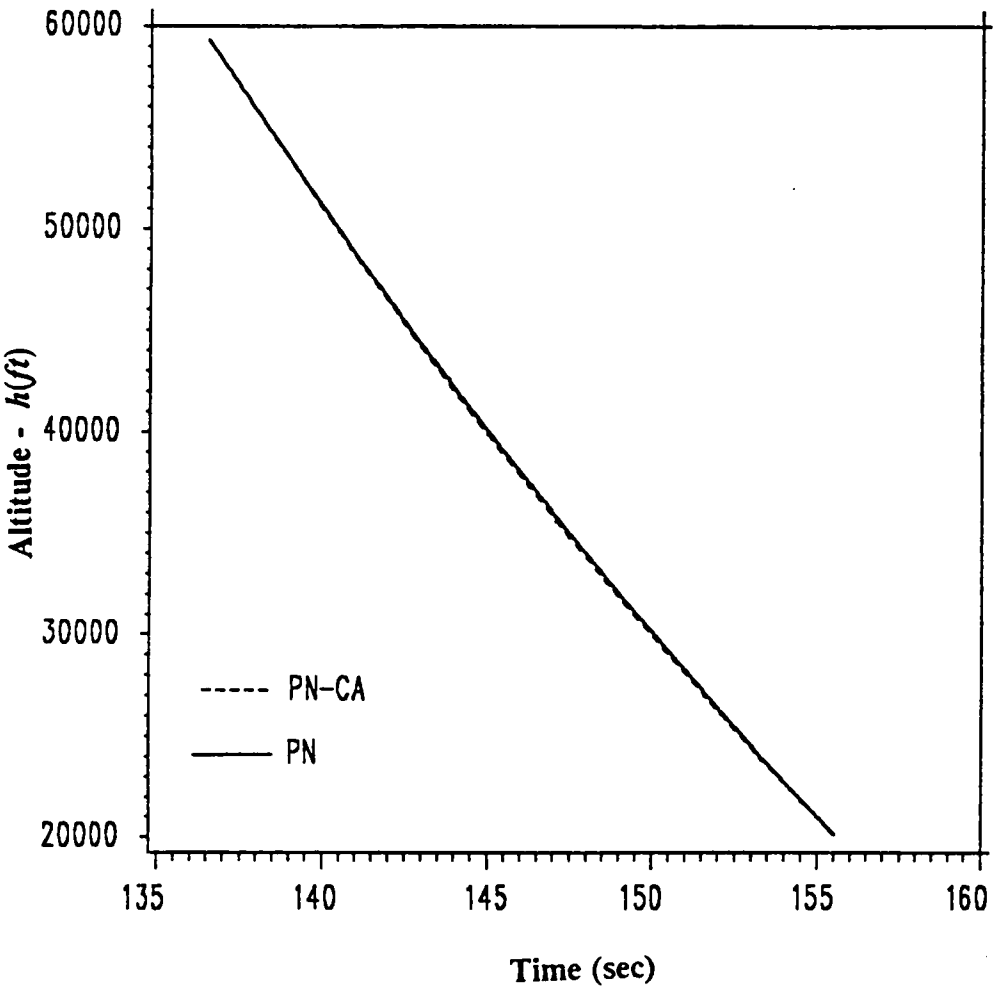

Fig. 7.4: Altitude comparisons of missile against aggressive target
- with/without chasing center-of-attainability

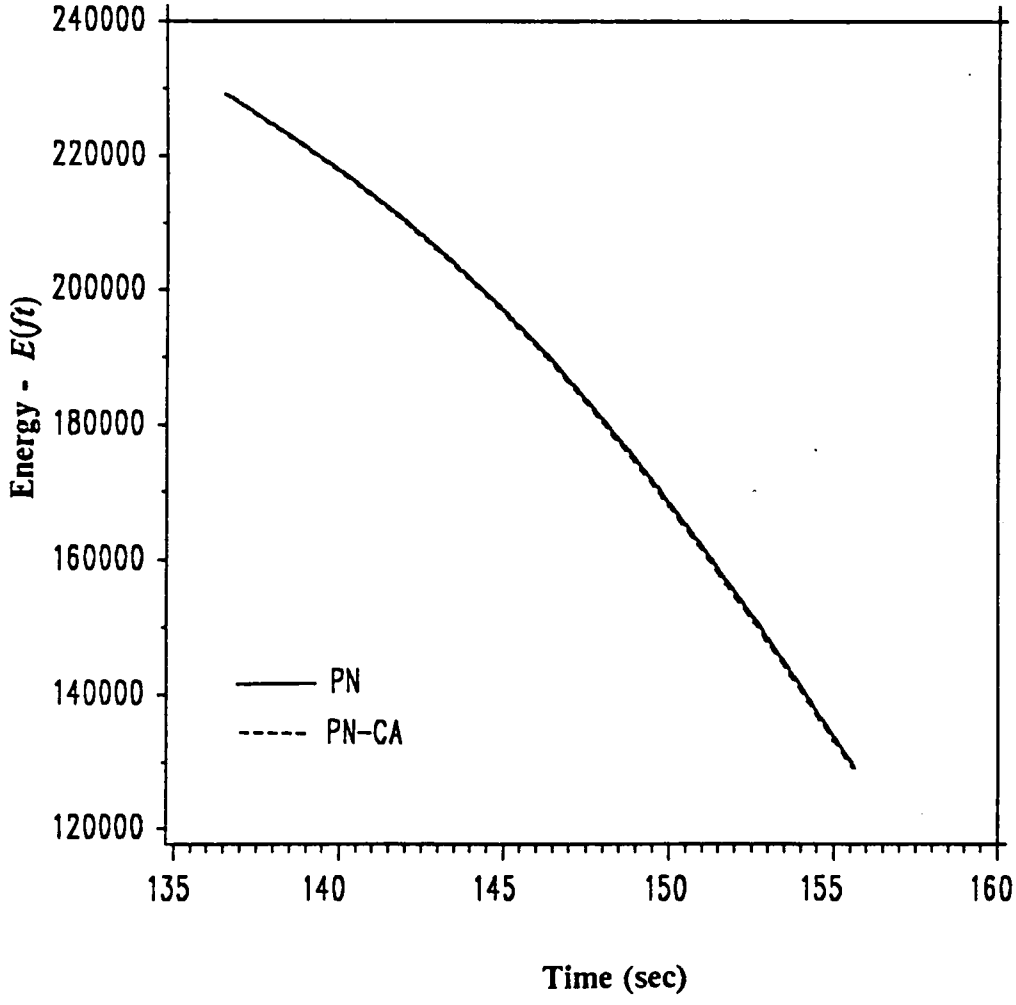

Fig. 7.5: Energy comparisons of missile against aggressive target
- with/without chasing center-of-attainability

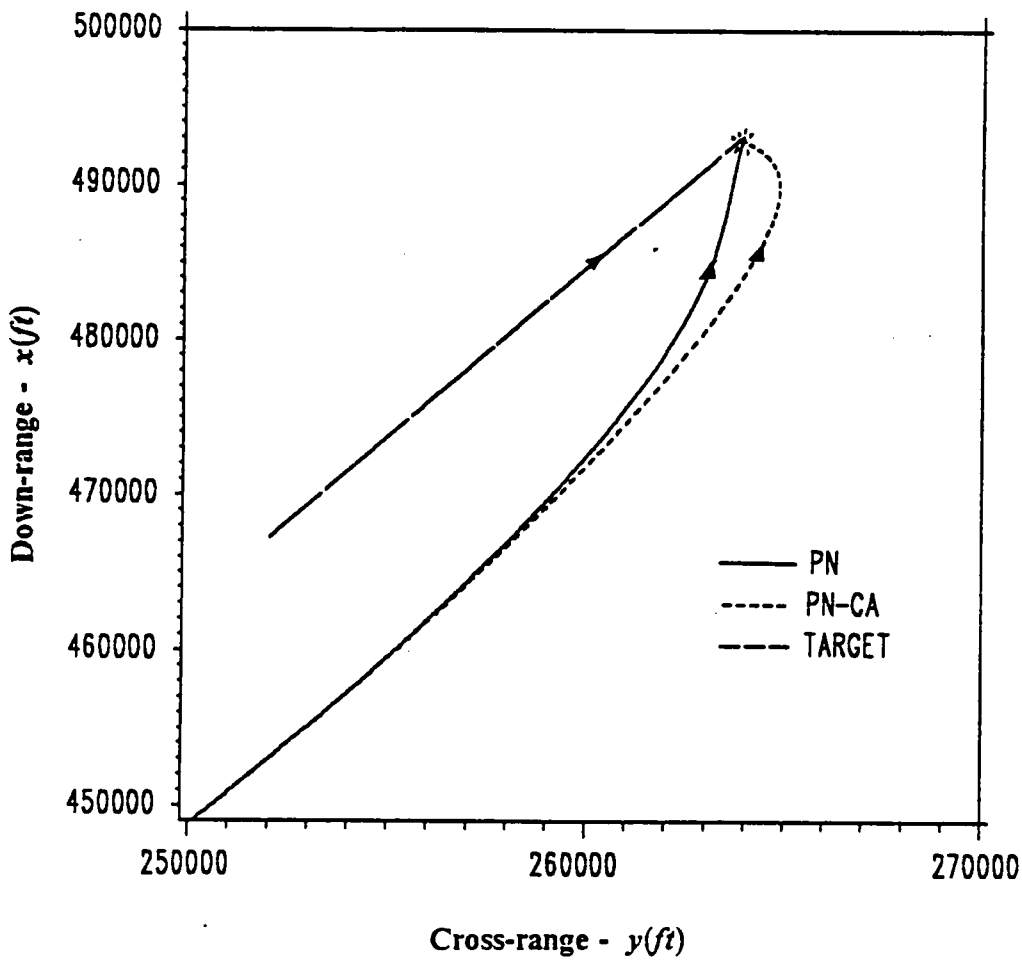

Fig. 7.6: $x - y$ projection of missile and run-away target - terminal phase

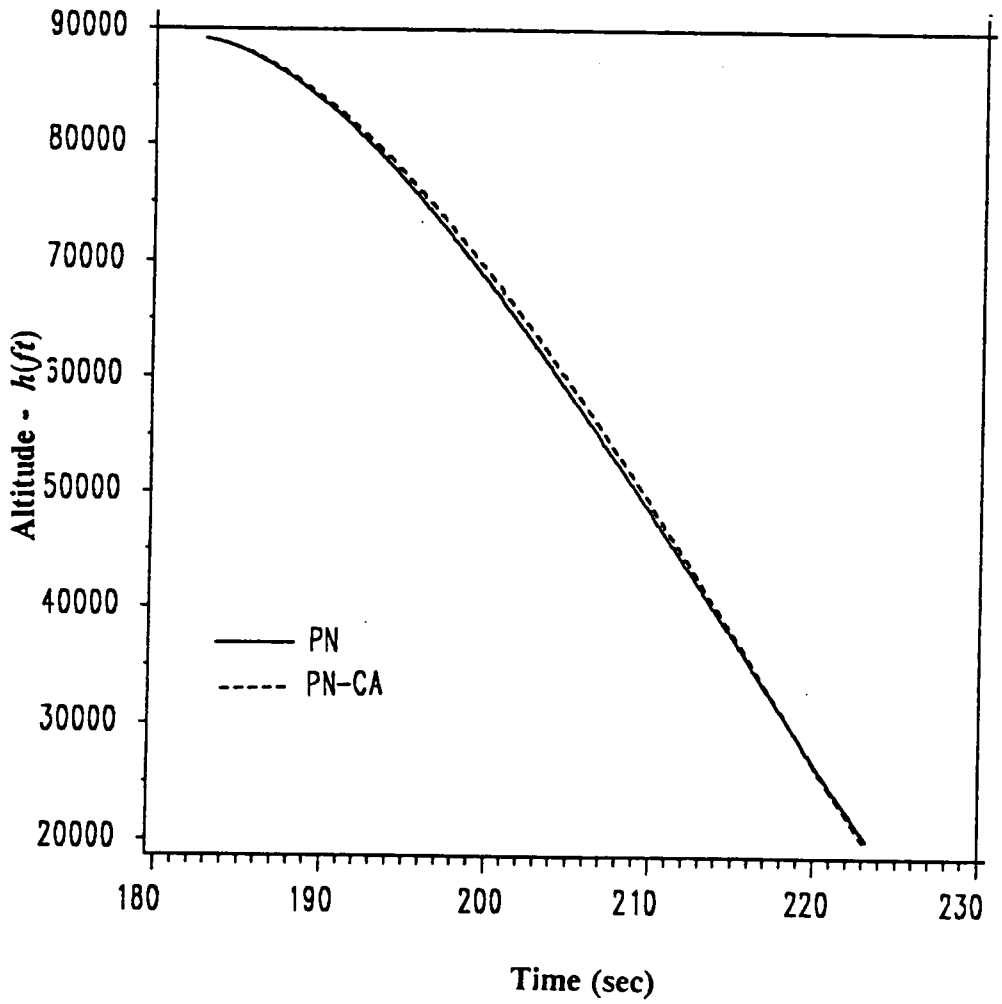

Fig. 7.7: Altitude comparisons of missile against run-away target
- with/without chasing center-of-attainability

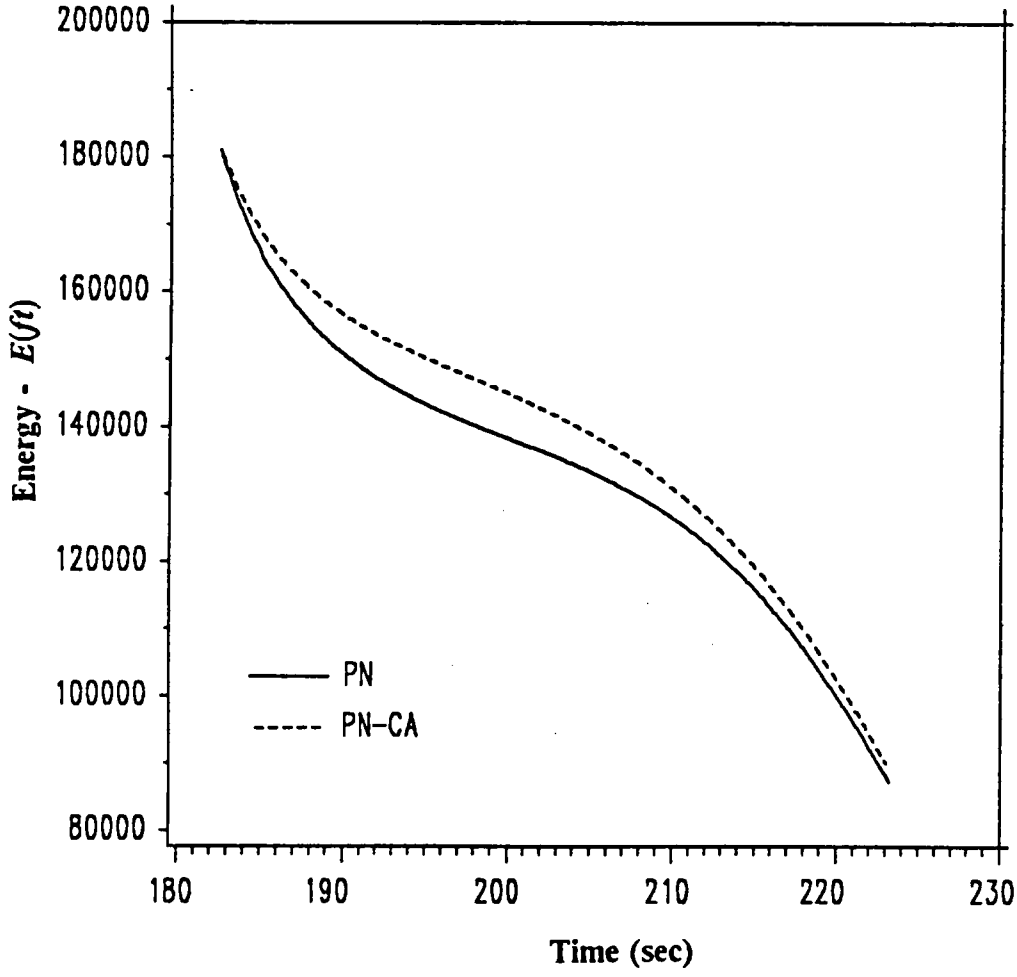

Fig. 7.8: Energy comparisons of missile against run-away target
- with/without chasing center-of-attainability

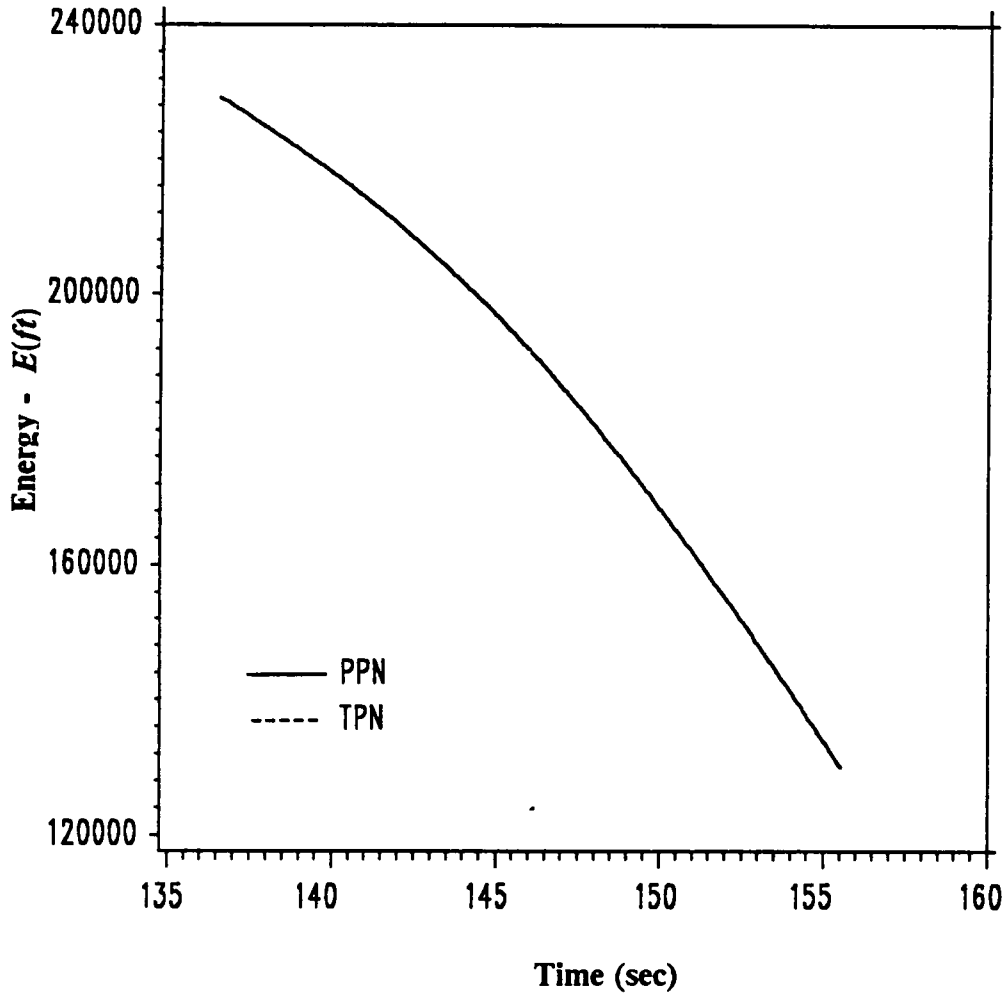

Fig. 7.9: Energy comparisons of missile chasing center-of-attainability of aggressive target - PPN vs TPN

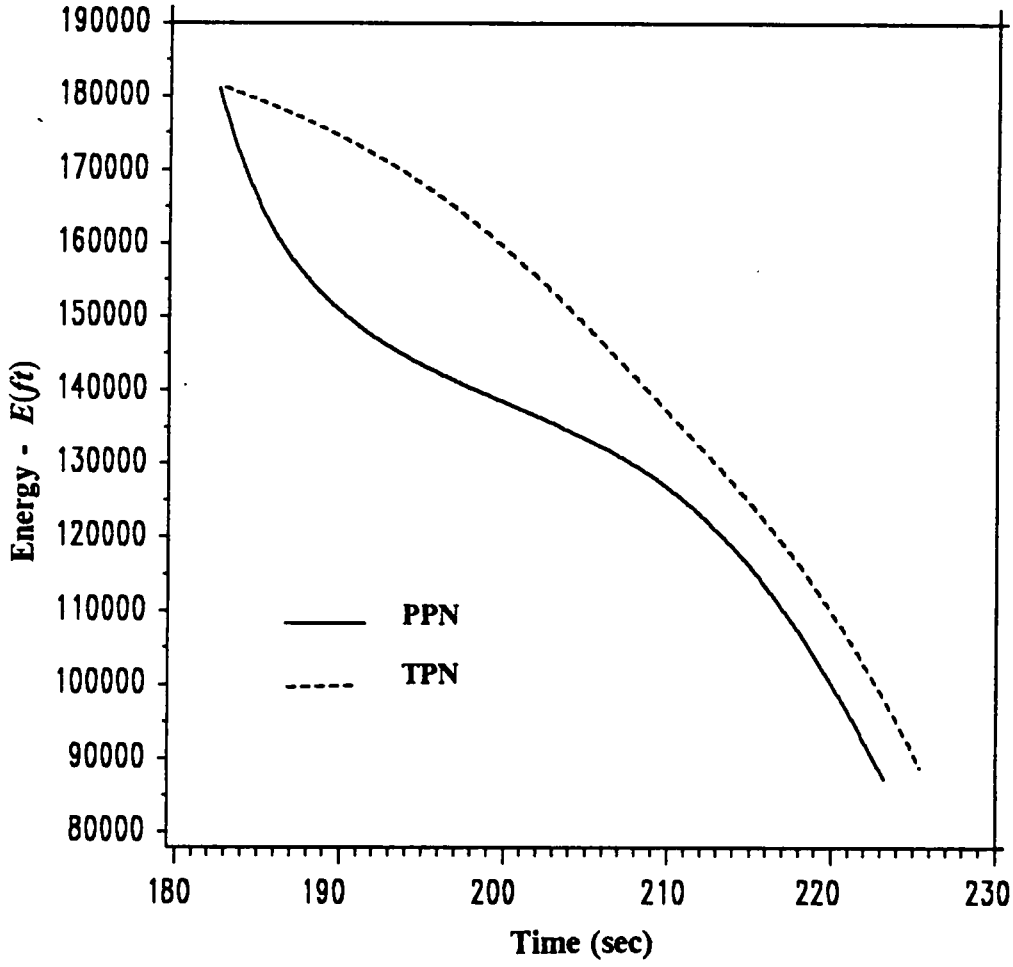

Fig. 7.10: Energy comparisons of missile against run-way target - PPN vs TPN

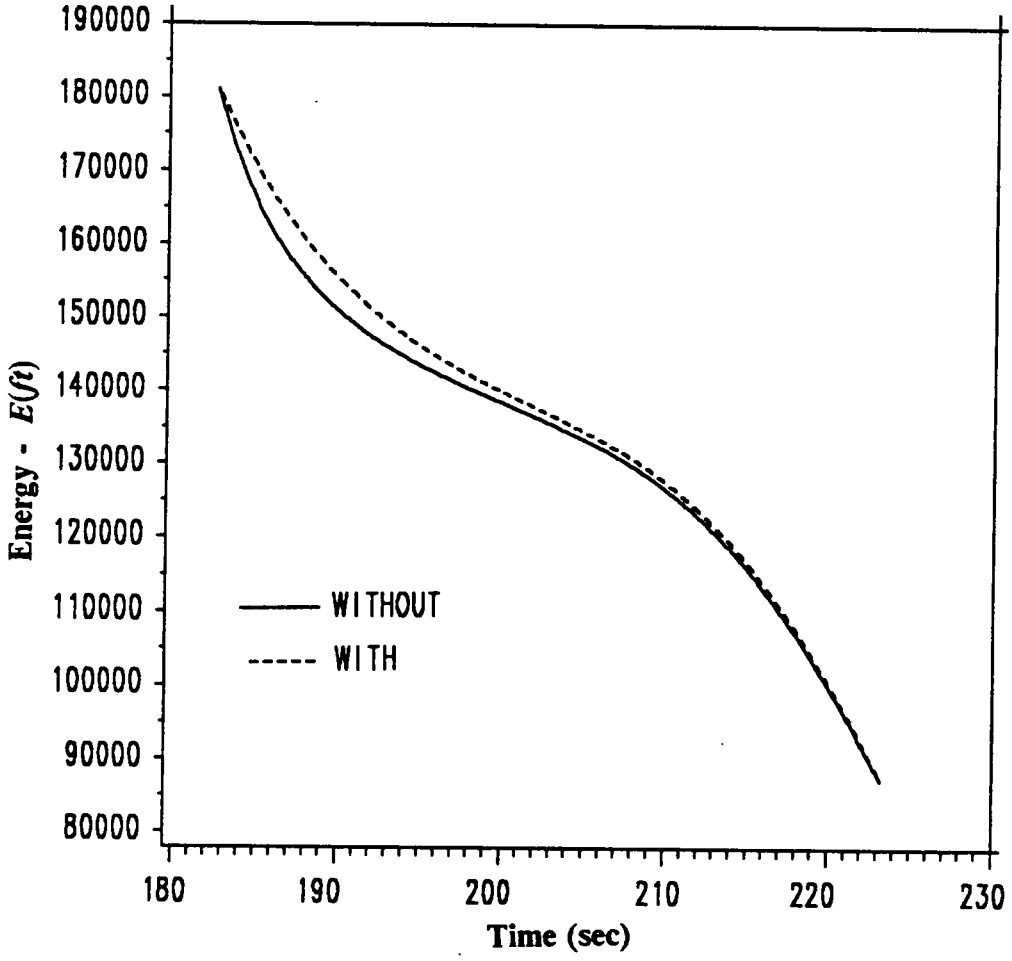

Fig. 7.11: Energy comparisons of missile using PPN chasing run-away target w/wo drag-resolution

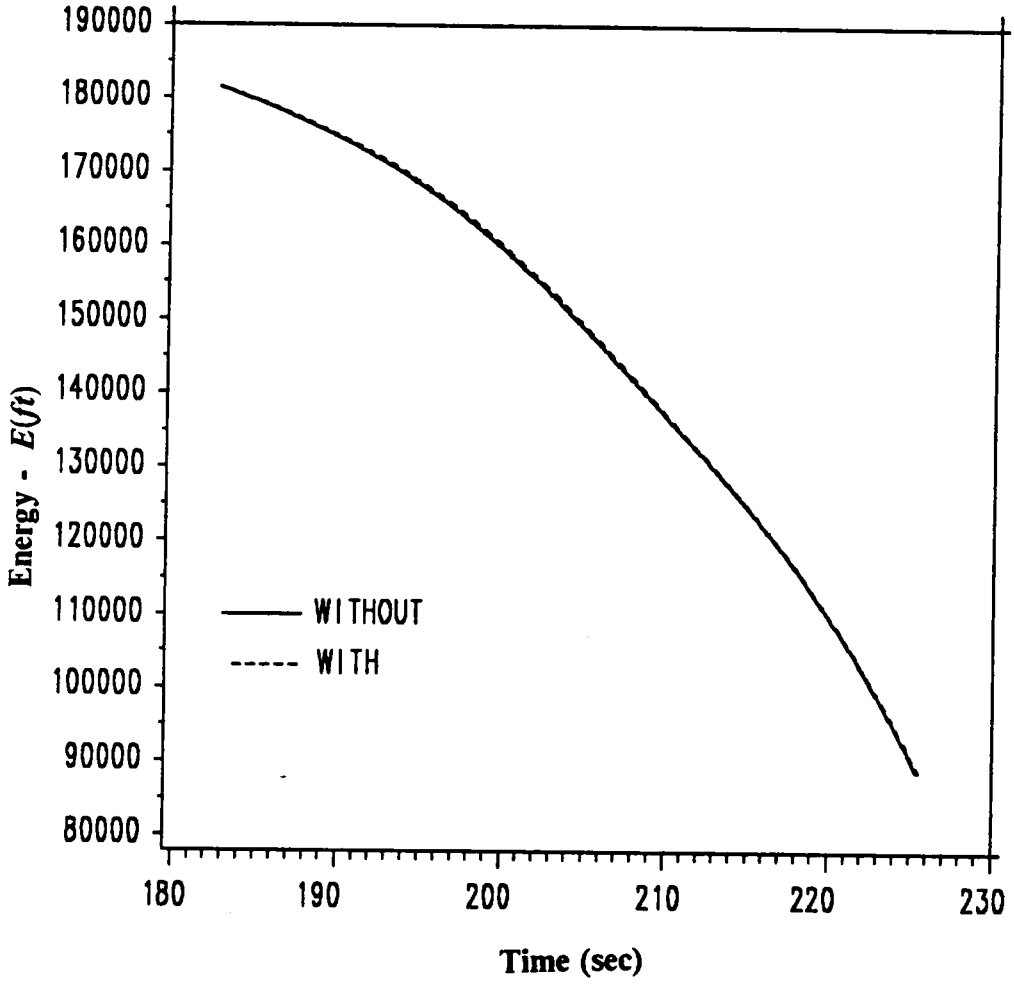

Fig. 7.12: Energy comparisons of missile using TPN chasing run-away target w/wo drag-resolution

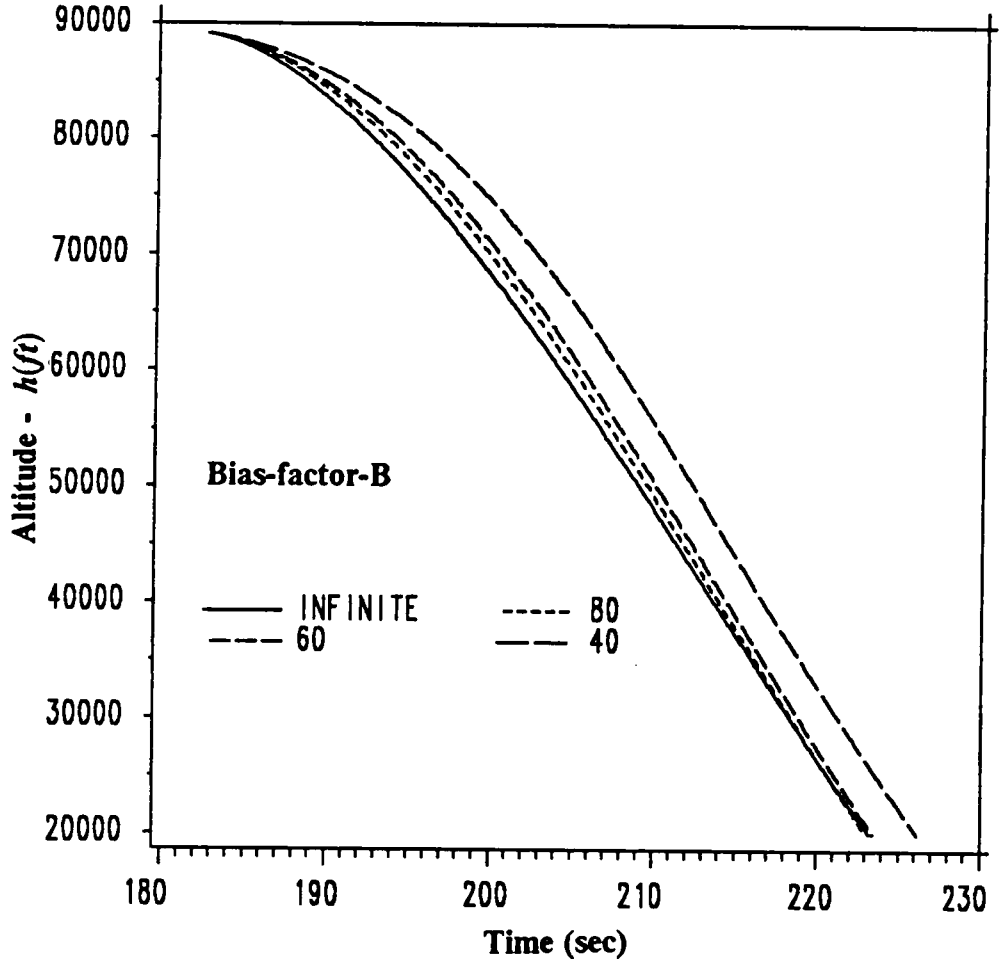

Fig. 7.13: Altitude histories of missile chasing run-away target with different biasing factors in vertical load-factor

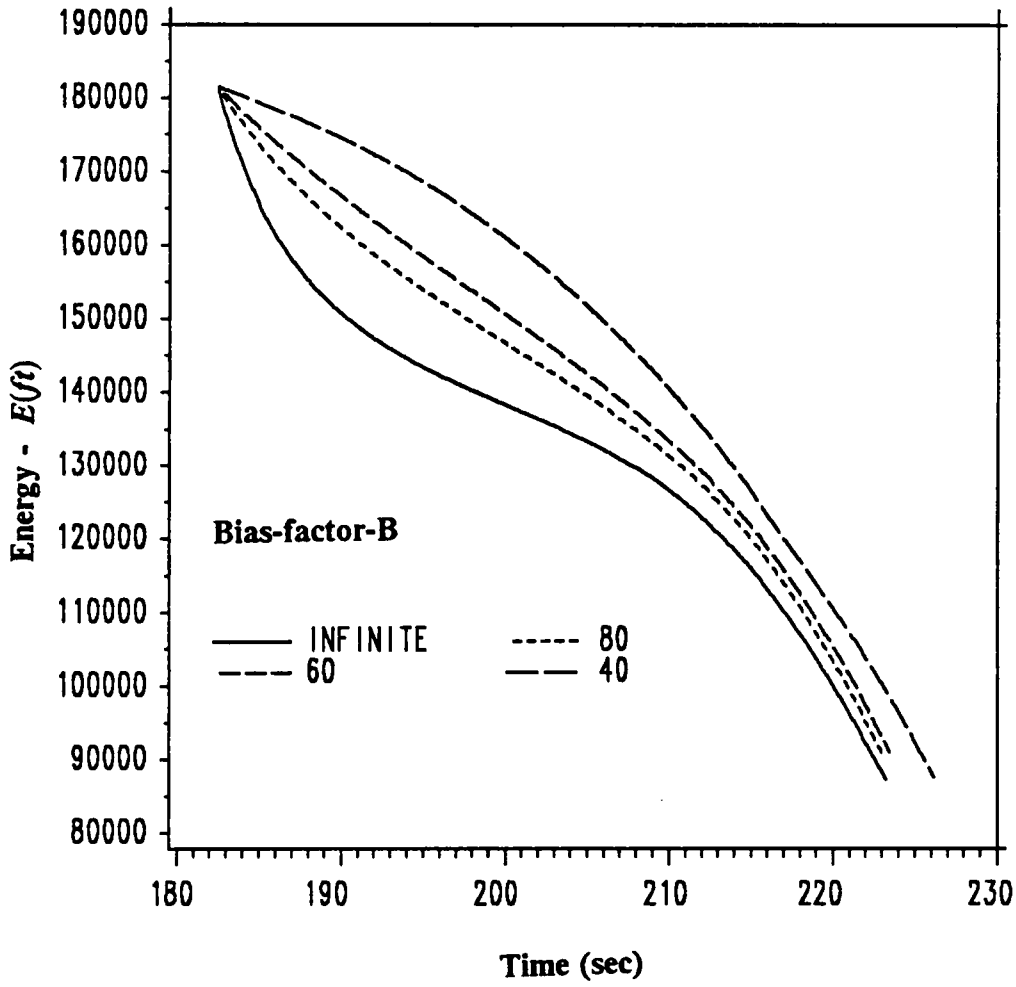

Fig. 7.14: Energy histories of missile chasing run-away target with different biasing factors in vertical load-factor

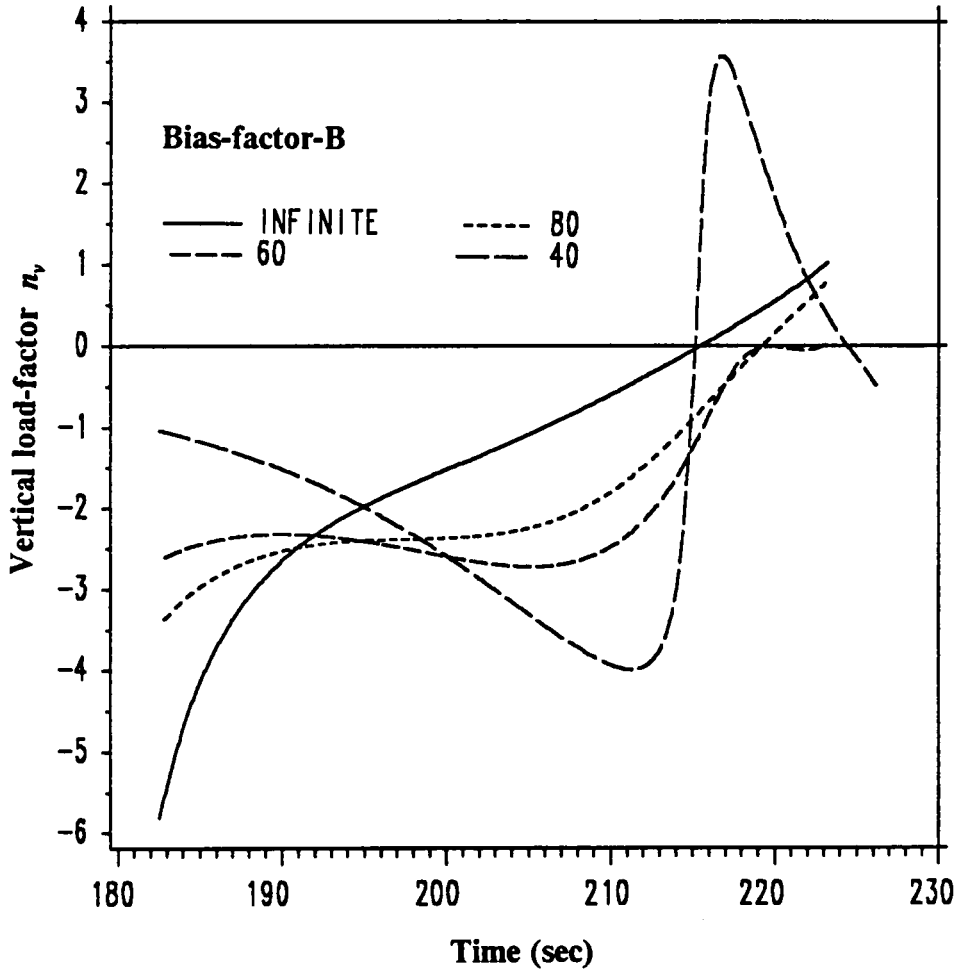

Fig. 7.15: Vertical load-factor histories of missile chasing run-away target with different biasing factors

Chapter 8: A Composite Guidance Strategy

8.1: Overview

Near-optimal guidance against a maneuvering target capable of acceleration and turning using Shinar's missile avoidance strategy is performed. Since near-optimal midcourse guidance cannot be sustained all the way to intercept, it is necessary that it be followed by some form of terminal guidance as in the previous chapter. Since the above is inevitable, a new scheme of midcourse guidance called **half-pn** is detailed which is extremely competitive to the previous schemes used and is more efficient in terms of on-board storage of data.

8.2: Shinar's Missile Avoidance Target Maneuvers

Simulation of the AAM is performed against a target aircraft guided by the laws suggested by Shinar's missile avoidance maneuvers of longer duration [26]. The missile-target dynamics is described in [26] using ordinary differential equations.

A zero-sum differential game with the pay-off function being the final miss-distance is considered. The missile is the pursuer trying to minimize the pay-off and the target is the evader whose objective is to maximize the pay-off. The controls for the target are the throttle and the turning load-factor. The throttle is bounded by an upper limit and the load-factor is bounded by an upper and lower limit. To simplify the scenario one considers the target to be maneuvering only in the horizontal plane.

The relevant target dynamics in the horizontal projection and the rate of change of relative positions are as follows:

$$\dot{R} = V_E \cos(\bar{\psi} - \chi_E) - V_P \cos(\bar{\psi} - \chi_P) \tag{8.1}$$

$$\dot{\bar{\psi}} = [- V_E \sin(\bar{\psi} - \chi_E) + V_P \cos(\bar{\psi} - \chi_P)] \; / \; R \tag{8.2}$$

$$\dot{V}_E = g \, [\xi \, (T_{\max})_E - (D_0)_E - (D_I)_E \; n_E^2] \; / \; W_E \tag{8.3}$$

$$\dot{\chi}_E = \frac{g[(n_E)_h]}{V_E} \tag{8.4}$$

where R is the distance between the missile and target in the horizontal projection, $\bar{\psi}$ is the LOS angle from the positive down-range axis of the missile in the horizontal projection, and V_E is the velocity of the evading aircraft with $(T_{\max})_E$ being the maximum thrust evaluated at the constant altitude. The $(D_0)_E$ and $(D_I)_E$ are the zero-lift drag and the induced drag of the target respectively. χ_E is the heading angle measured with respect to the positive

down-range axis of the missile and $(n_E)_h = [n_E^2 - 1]^{.5}$ is the load-factor control. The other control is ξ corresponding to the throttle setting. The weight of the evader is given by W_E. The subscripts P corresponds to the missile which is the pursuer. V_P is the horizontal component of the velocity of the missile. The maximum thrust limit, drag coefficients, and the weight are chosen from an aircraft model used in [44]. The atmospheric and aerodynamic properties are expressed analytically in the form of polynomials. The maximum thrust limit is suitably lowered so that the evader velocities are lower in comparison to the missile velocities for the end-game (for assumed missile thrust-to-weight ratio).

The horizontal feedback approximations as in [26] are obtained by using singular perturbations with two inner layers and one outer layer. The reduced-order outer solution is a "tail-chase" with maximum speed for the target. The two-inner layers are obtained by two time-stretches and the zeroth-order approximation of the optimal control in a feed-back form is obtained as given below.

Define the quantities r_E^2 and s_E as follows:

$$r_E^2 = [(T_{\max})_E - (D_0)_E] \;/\; (D_I)_E \tag{8.5}$$

$$s_E = \frac{g}{V_E}\,[(r_E)^2 - 1]^{0.5} \tag{8.6}$$

The uniformly valid feedback load-factor control is given by

$$(n_E)_h = \frac{V_E}{g}\; s_E\; (\frac{2\,V_E}{V_E^r - V_E})^{.5}\; \sin(\frac{\bar{\psi} - \chi_E}{2}) \tag{8.7}$$

It must be noted that the magnitude of the load-factor control is constrained by the limit of the form, $|(n_E)_h| \leq [(n_E)^2_{\max} - 1]^{0.5}$, where $(n_E)_{\max}$ is a prescribed maximum load-factor. The sign of $(n_E)_h$ is to be chosen such that if the missiles x,y co-ordinate is to the left of the target velocity vector, then the target turns right and vice-versa. The feed-back load-factor is only a function of the target parameters and the LOS angle. The quantity V_E^L is the maximum velocity that can be attained for the given altitude, corresponding to the thrust-drag equilibrium for $n_E = 1$.

The maximum principle governing the reduced order-game gives the throttle-setting parameter ξ to be unity identically. Thus at a given instant of time the two controls are determined and the target dynamics can be simulated. The simplicity of this scheme appears in the fact that the target uses only a simple parameter of the missile, $\overline{\psi}$, to determine its guidance law.

8.3: Introduction of a Composite Strategy

Simulation of the missile is performed, starting with midcourse guidance using near-optimal neighboring feedback with performance augmentation using pseudo-target (center-of-attainability) chasing, followed by a terminal guidance with pure-proportional navigation until intercept. For the center-of-attainability evaluation of the target $V_T = 700 ft/s$ and $n_{T\max} = 6$ is used. The target initially travels along a straight line with a constant velocity. At a fixed time of 80 sec ,

Shinar's guidance is initiated for the target. A maximum velocity of $V_E^r = 1065.33\,ft/s$ and $(n_E)_{\max} = 6$ is considered for target simulation.

Fig. {8.1} shows the x,y projection of the missile-target trajectories. Fig. {8.2} shows the velocity history of the evading target. Fig. {8.3} indicates the load-factor $(n_E)_h$ of the target. It is observed that the feedback control of the missile using neighboring guidance during midcourse has heading not aligned exactly with the target LOS. This is due to the fact that the gains are small initially, i.e., with a time-to-go transversal comparison, large control corrections are made only when the time-to-go is "small".

It is the above phenomena which prompted the use of a composite guidance strategy. The midcourse guidance is initiated using a feedback strategy as follows: The near-optimal feedback control is used for the vertical load-factor n_v and for the horizontal load-factor n_h of the missile one employs a proportional navigation scheme with or without modifications as suggested in Chapter 7. This guidance strategy is advantageous obviously in the fact that the set of gains $\frac{\partial n_h}{\partial X}$ and $\frac{\partial n_h}{\partial \psi}$ used for neighboring guidance can be eliminated from on-board storage. Thus, the data storage can be considerably reduced. The optimality of this guidance is the next question.

Simulation performed against Shinar's target with the data the same as explained in the preceding paragraphs using this mixed guidance strategy defined as **half-pn** is shown in Figs. {8.4-8.8}. Fig. {8.4} shows the horizontal projection of the

trajectory. The early heading corrections performed by the missile and the alignment of the missile heading with the LOS is desirable. The target-missile maneuvers resemble a tail-chase. Hand-over to terminal guidance is smooth and intercept occurs at the end of tail-chase. The velocity and load-factor histories of the target are shown in Figs. {8.5 & 8.6} respectively. The control histories of the missile are shown in Figs. {8.7,8.8}. The horizontal load-factor using half-pn shows transient behavior during the turn phase of the target. This is due to the rapid change in the center-of attainability of the target. The presence of large control efforts towards the end of midcourse guidance is not observed for n_h using half-pn. The control n_v is similar in nature for the two different midcourse guidance schemes.

Midcourse guidance using the two schemes showed that the time-to-go is higher using the half-pn scheme through out the trajectory. However since terminal guidance is required and since the heading at end of midcourse guidance is better for the half-pn scheme and since the target maneuvers are dependent on the missile position, the final energy and intercept time is better for the half-pn scheme at intercept. However, this does not reflect the non-optimality of the neighboring guidance, but indicates the following: since midcourse guidance cannot be continued until final time, and since terminal guidance is a necessity, the mixed guidance strategy is an efficient scheme.

Fig. {8.9-8.11} compares the half-pn scheme with neighboring guidance for the midcourse phase of the missile against an aggressive target moving along a

straight line at $700\,ft/s$. The control effort n_h is lower for the missile during the initial phase using neighboring guidance - Fig. {8.10}. However the increasing gains increase the control effort as time-to-go decreases. The energy at end of midcourse of the missile is nearly identical using either schemes. The vertical load-factor control n_v is identical for both schemes as seen in Fig. {8.11}. Better heading characteristics are depicted by the missile guided by half-pn as seen in Fig. {8.9}. The time-to-go or the performance-index-to-go is higher for the half-pn scheme all along the trajectory.

To check the optimality of the half-pn scheme for the midcourse guidance, one has to perform simulation comparing with an optimal trajectory. Hence midcourse guidance is performed against a stationary target using half-pn. The neighboring trajectory is same as the reference trajectory with $\delta X(t) = 0$ and $d\psi(t) = 0$. Half-pn midcourse guidance is employed to hit the same stationary target. Fig. {8.12} shows the change in cost, i.e., time to intercept using the two schemes. The dt_f is greater than zero all along the trajectory. However the change in cost is only very small, in the order of 0.26 seconds for a flight time of 175 seconds. This re-confirms the optimality of the reference solution but also indicates the potential of the half-pn scheme.

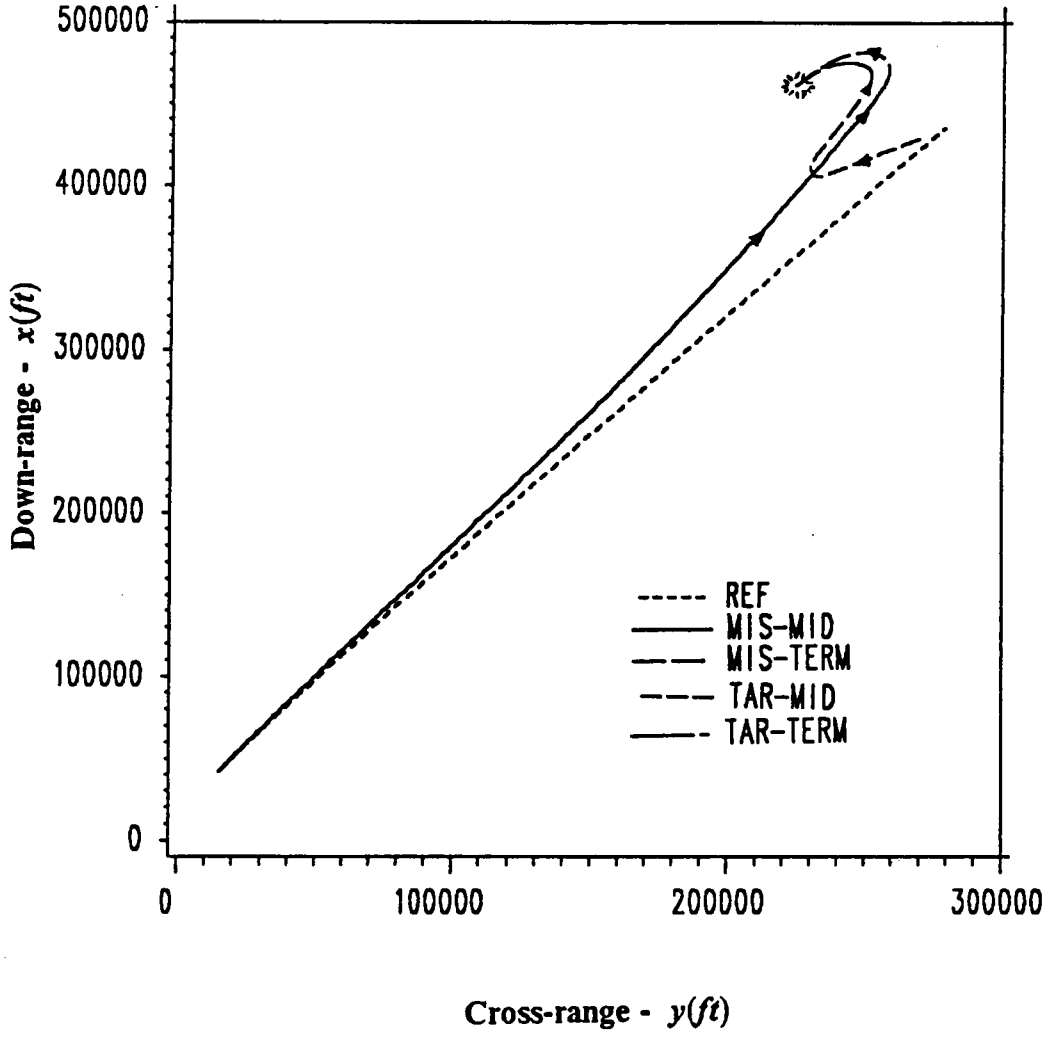

Fig. 8.1: $x - y$ projection of missile and Shinar's target

- near-optimal midcourse guidance and terminal guidance

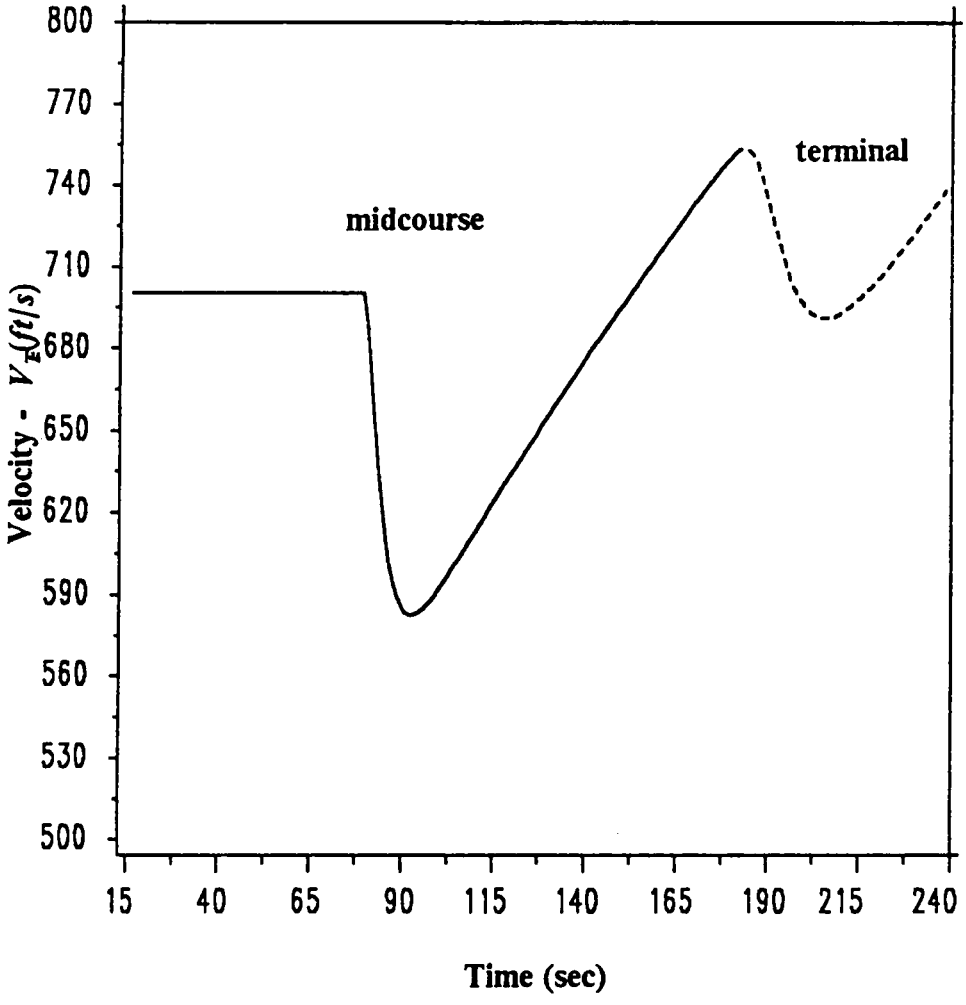

Fig. 8.2: Velocity history of Shinar's target during missile's near-optimal midcourse guidance and terminal guidance

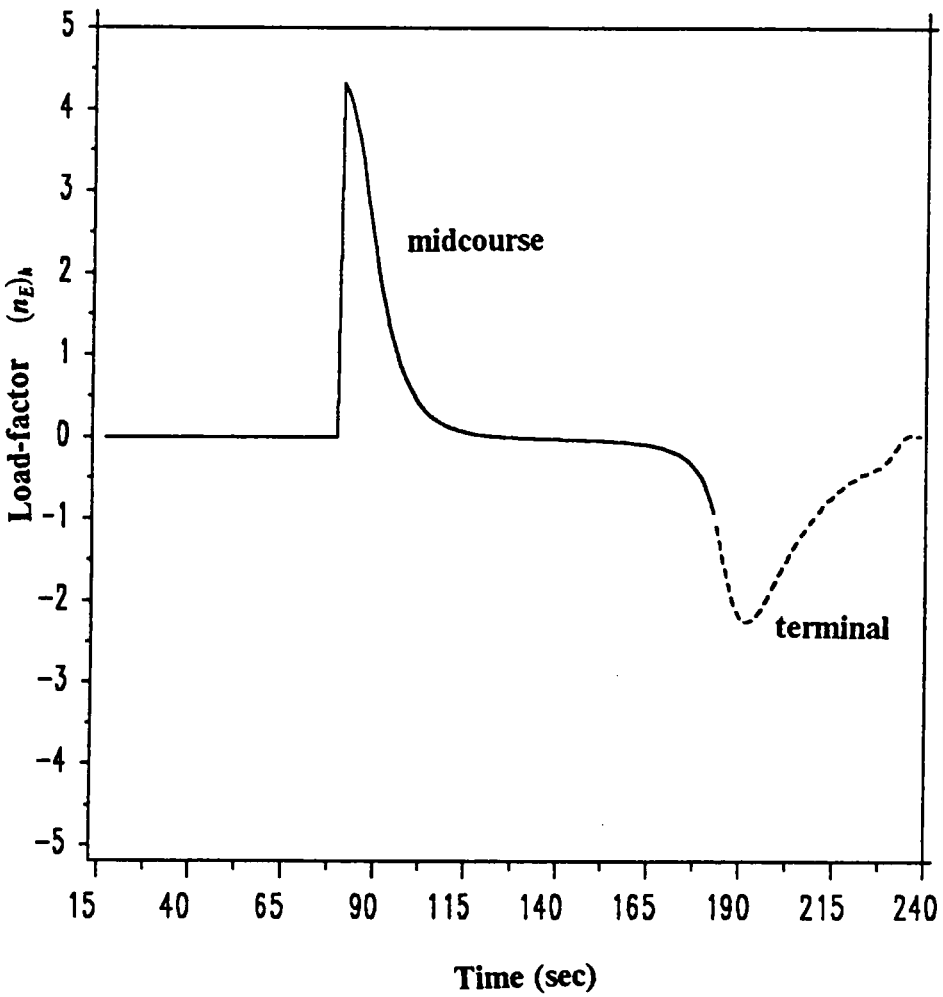

Fig. 8.3: Load-factor history of Shinar's target during missile's near-optimal midcourse guidance and terminal guidance

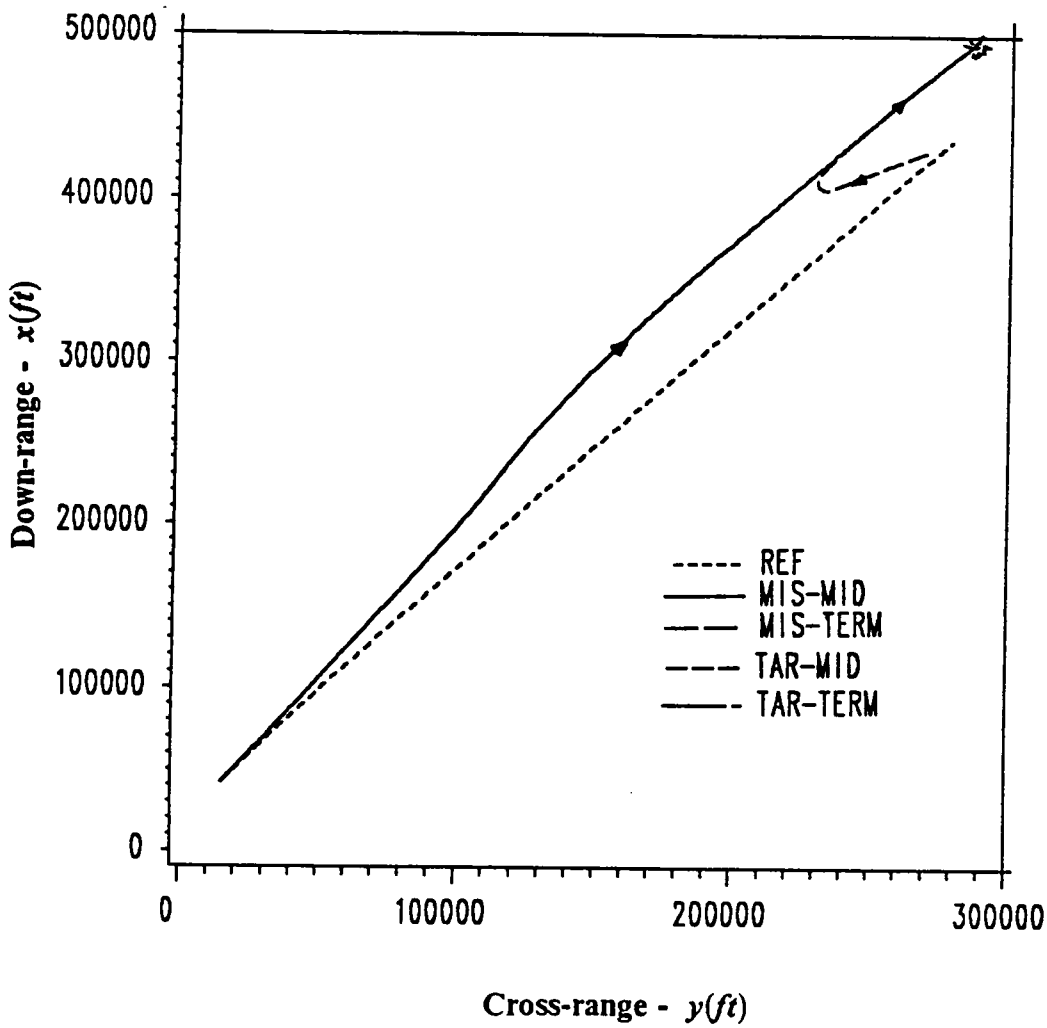

Fig. 8.4: $x - y$ history of missile and Shinar's target

- half-pn midcourse guidance and terminal guidance

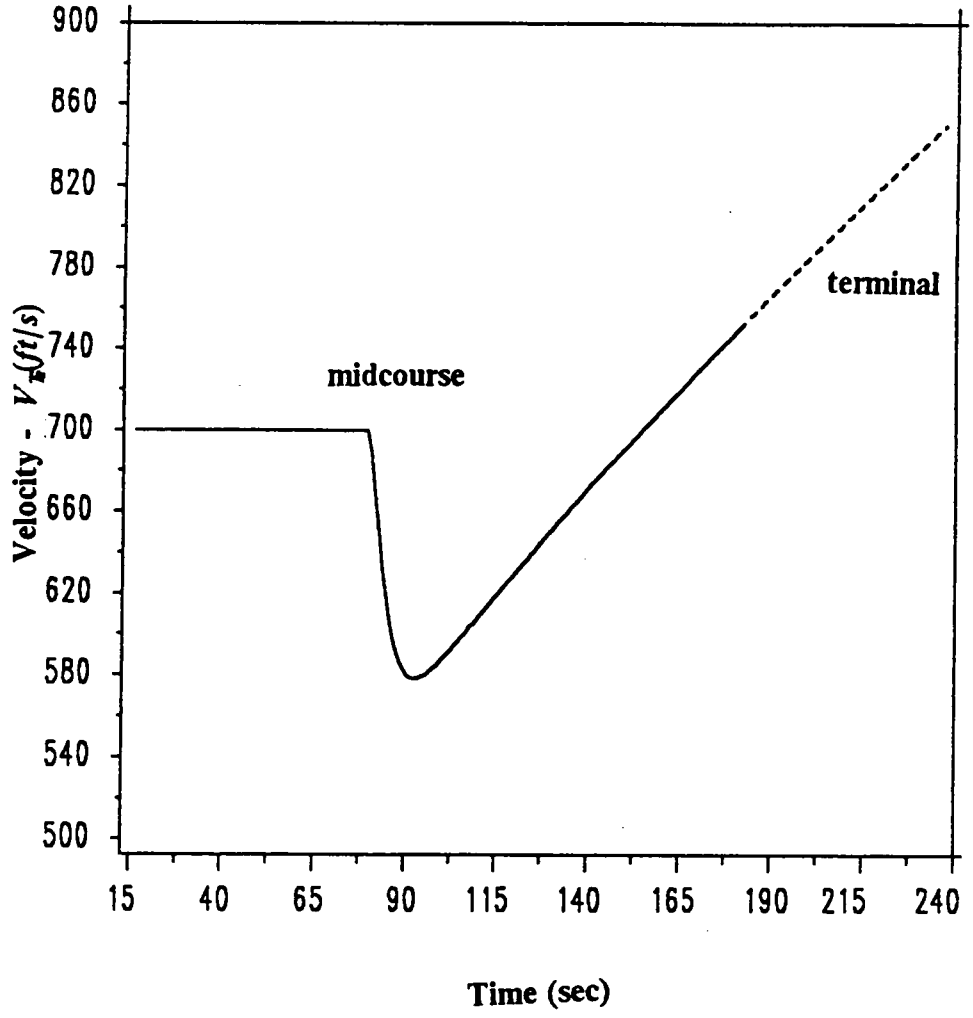

Fig. 8.5: Velocity history of Shinar's target during missile's half-pn midcourse guidance and terminal guidance

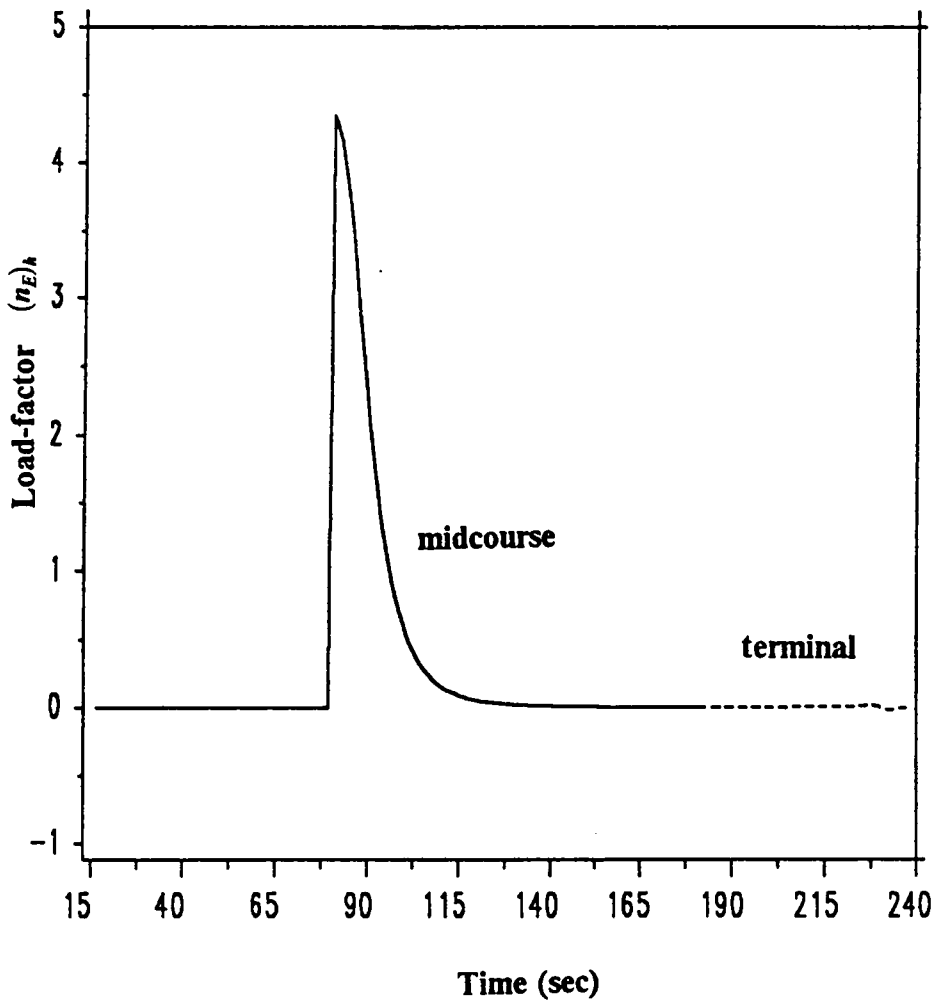

Fig. 8.6: Load-factor history of Shinar's target during missile's half-pn midcourse guidance and terminal guidance

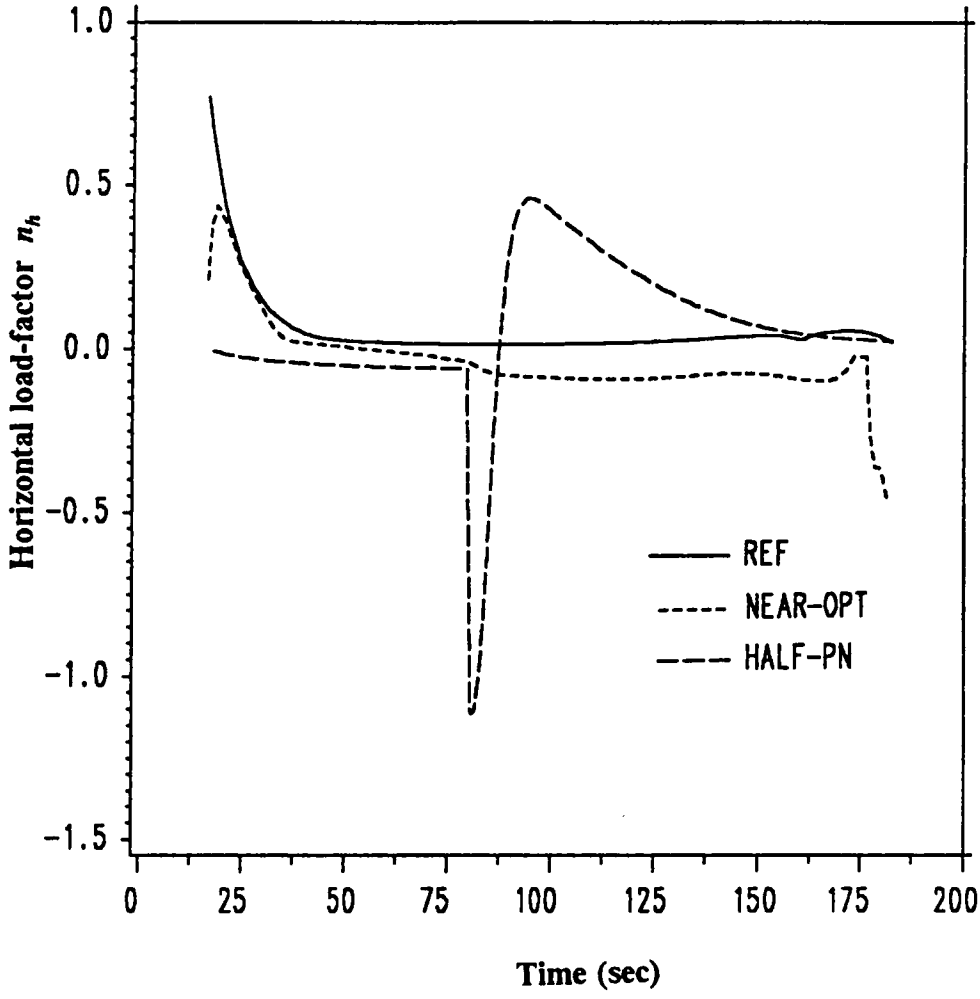

Fig. 8.7: Horizontal load-factor comparison between half-pn and near-optimal midcourse guidance of missile

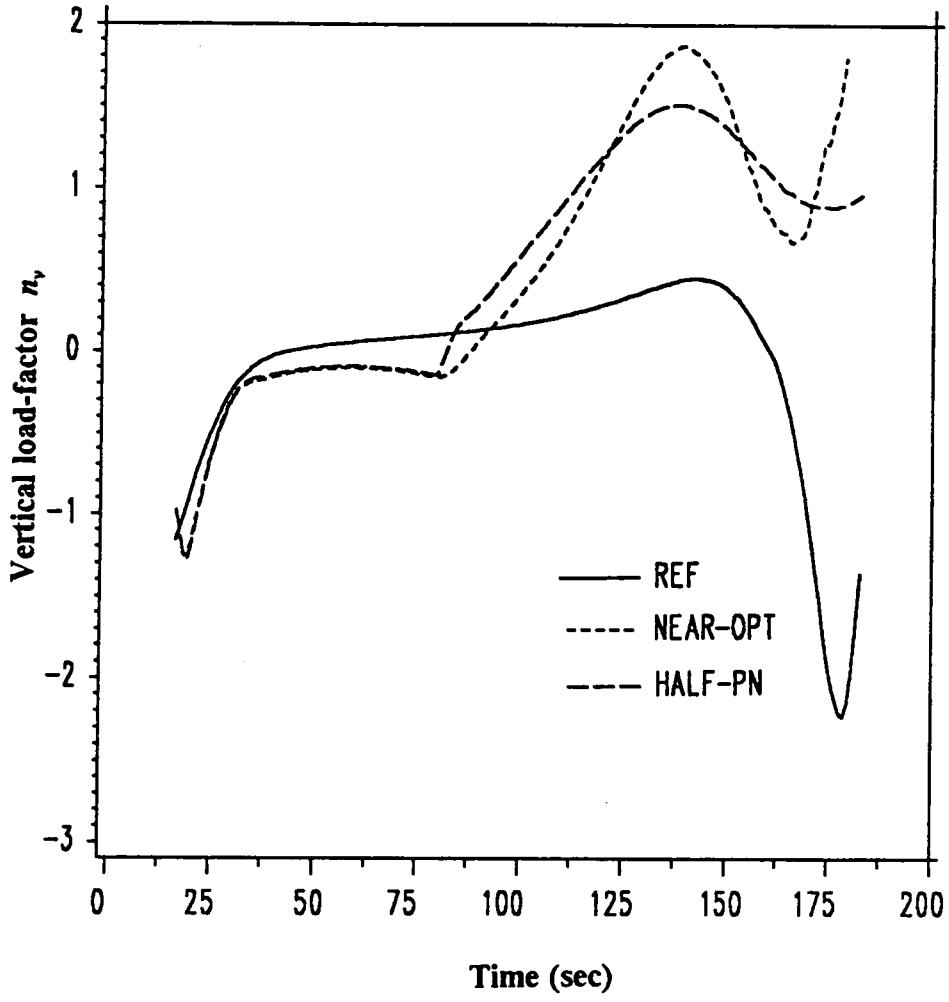

Fig. 8.8: Vertical load-factor comparison between half-pn and near-optimal midcourse guidance of missile

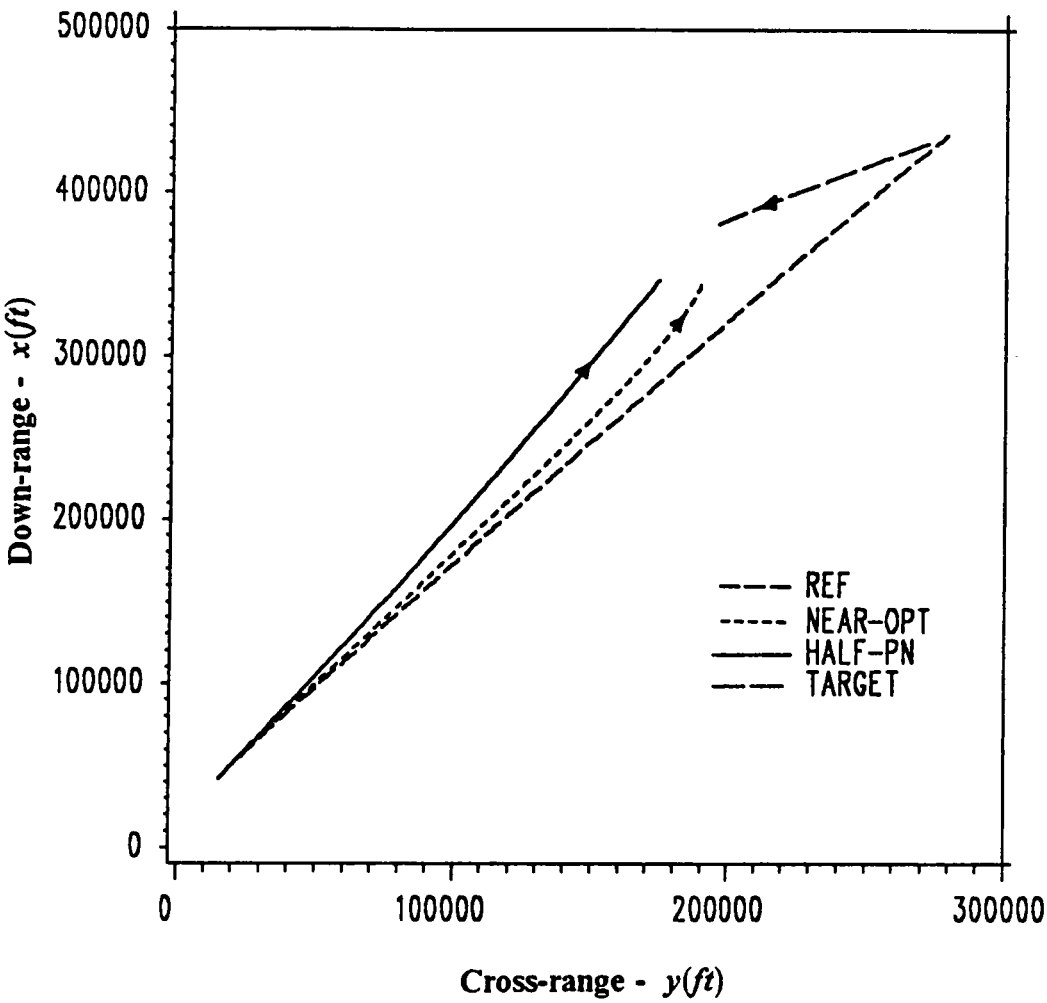

Fig. 8.9: $x - y$ projection of missile and aggressive target - near-optimal and half-pn midcourse guidance

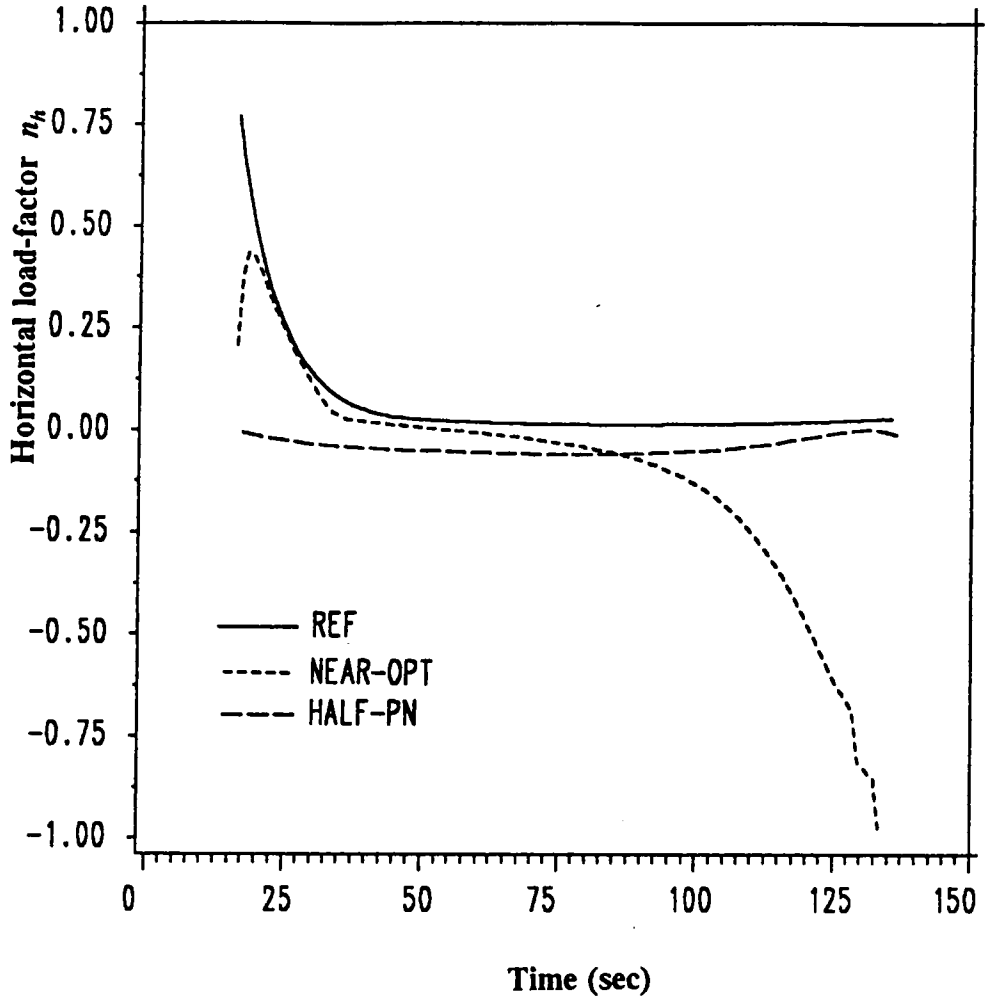

Fig. 8.10: Horizontal load-factor comparison between half-pn and near-optimal midcourse guidance against aggressive target

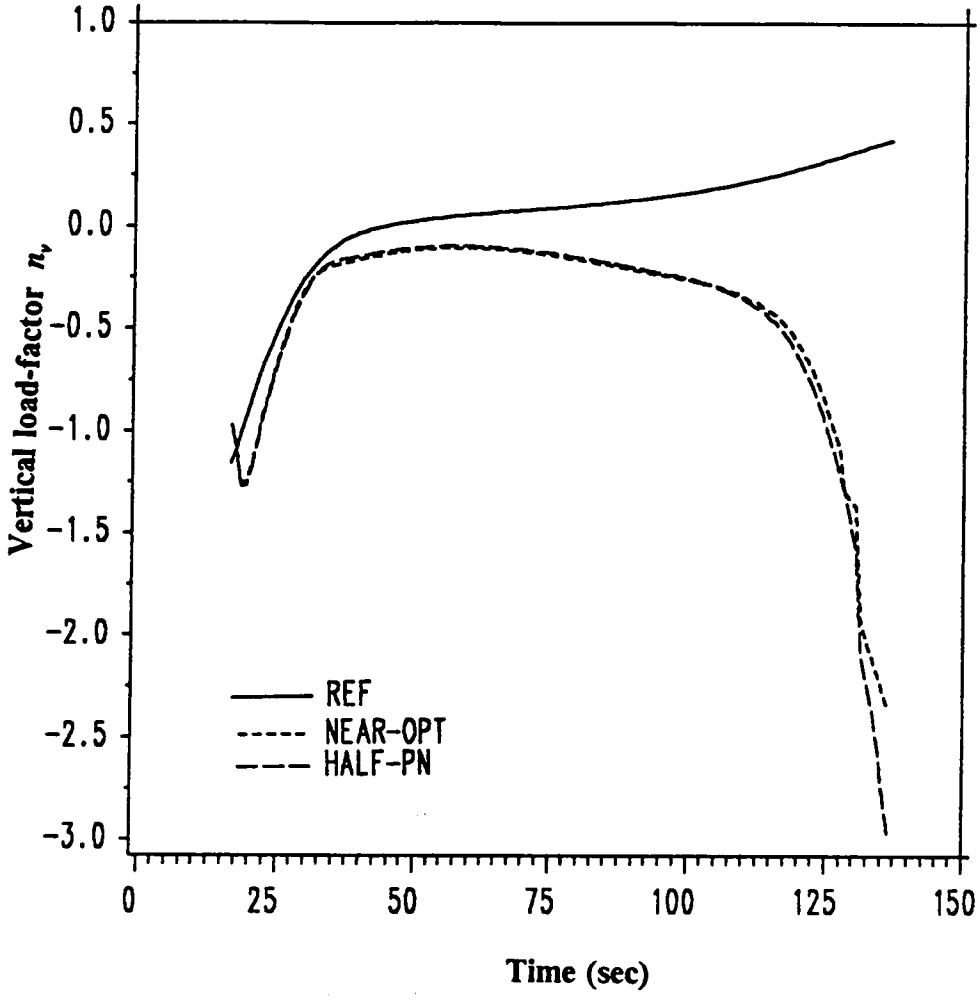

Fig. 8.11: Vertical load-factor comparison between half-pn and near-optimal midcourse guidance against aggressive target

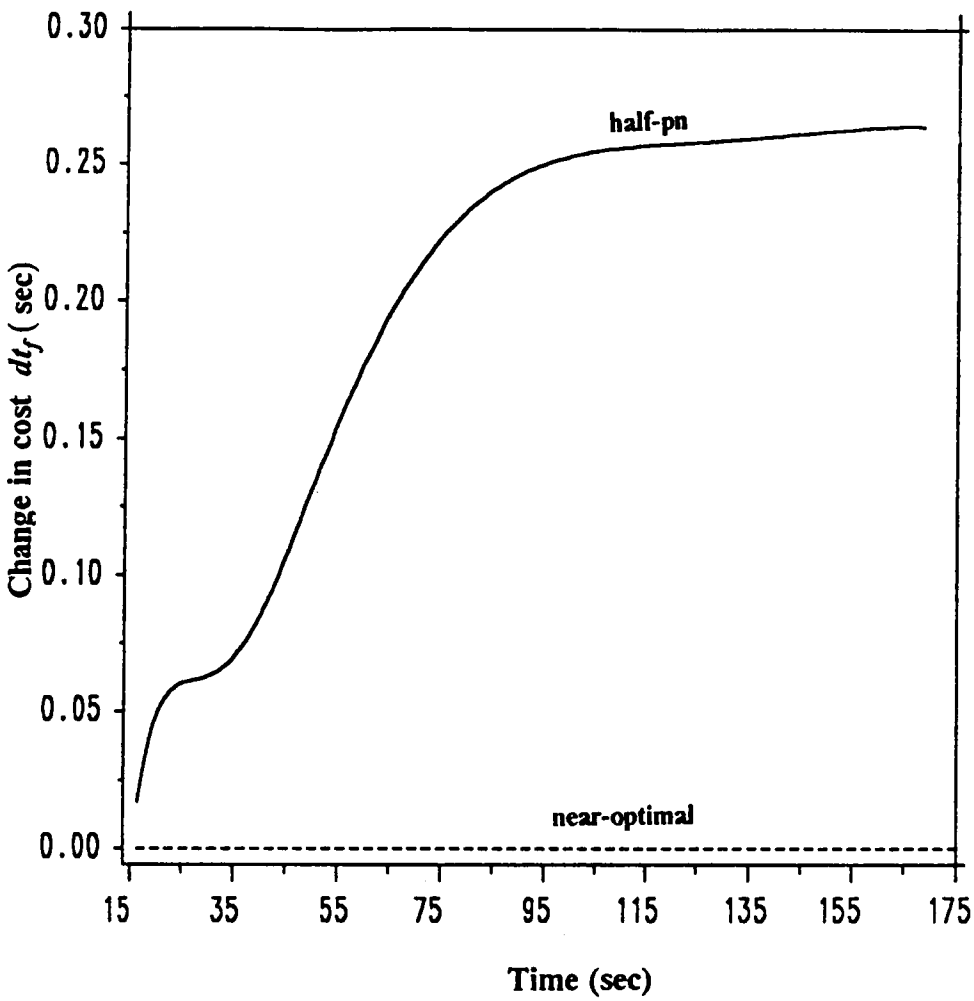

Fig. 8.12: Comparison of cost between half-pn and near-optimal midcourse guidance against stationary target

Chapter 9: Conclusions

9.1: Summary and Conclusions

A point-mass model of a boost-sustain-coast medium range air-to-air missile has been studied in detail. Open-loop optimal trajectories leading to "efficient" intercept in three-dimensional scenario is synthesized. Attainability sets of missile and intricate homotopy procedures to obtain these are understood. Regularization of non-regular extremals leading to the boundary of attainability and sufficiency conditions for optimality of these and regular test extremals are checked and are found to render a weak-local minimum. A new matrix Riccati differential equation is derived in this connection and boundary conditions suitably chosen to check for conjugate points along regular and regularized extremal trajectories.

A three phase guidance scheme for intercepting a target capable of maneuvering in the horizontal plane is used. An initial boost-phase guidance, involving

guidance in the presence of control constraints and thrust switching with possible state perturbations is simulated with excellent results. A new, more efficient method of gain evaluation is presented which in comparison to the usual methods of Riccati solutions etc. is computationally easier.

A midcourse guidance using neighboring optimal guidance with transversal comparison, as performance-index-to-go and its superiority with clock-time indexing is observed. Performance augmentation ideas to consider a larger domain of target maneuvers using the concept of center-of-attainability of the maneuvering target is found to yield better performance. The linearization scheme used in the near-optimal guidance works well using the combined effect of time-to-go-indexing and the pseudo-target chasing for different target scenarios!

Terminal guidance using classical 3-D proportional-navigation is modified to obtain marginally better energy/time/range at intercept. True and pure proportional navigation schemes are modified using the pseudo-target chasing ideas for a smooth transition from midcourse guidance of the missile chasing the center-of-attainability of target. Ideas of altitude shaping and drag-resolution were also implemented to improve the intercept performance against run-away targets. The improvement is attempted as required due to the large flight-times and limited energy resources of the missile. Altitude shaping and drag resolution gave only a marginal improvement in the performance.

An extremely competitive midcourse guidance scheme called half-pn is introduced which uses a composite guidance strategy using neighboring optimal guidance and pro-nav hand-in-hand. The improvement in heading direction at end of midcourse guidance, thus improving hand-over to terminal guidance and the reduction of storage requirements for onboard implementation, is remarkable. Simulations performed with Shinar's missile avoidance target strategies, aggressive targets, and stationary targets show near-optimal behavior of this scheme.

9.2: Suggestions for Future Research

In this analysis, possible pre-launch maneuvers of the launching aircraft are neglected. The difficulty in obtaining "range-charts" for all possible target directions may be overcome by suitably applying a pre-launch maneuver to correct the heading within prescribed tolerance and then applying a half-pn technique. This would reduce the χ variations of the missile and vertical load-factor gains evaluated for flight in the vertical plane may be alone necessary to obtain a good guidance scheme. Thus a study of efficient pre-launch maneuvers is critical and may provide added insight to near-optimal on-board guidance. Further, target maneuvers extended to three-dimensions should also be considered.

References

1. Locke A.S., Guidance, a Volume in the Series. Principles of Guided Missile Design, edited by Grayson Merrill, *Van Nostrand*, Princeton, 1955.

2. Yuan, C.L., "Homing and Navigational Courses of Automatic Target-Seeking Devices" , *J. of Applied Physics* , Dec. 1948, pp. 1122-1128.

3. Newell, H.E., "Guided Missile Kinematics" , Report No. R-2538, Naval Research Laboratory, Washington D.C., 5-22-1945.

4. Spitz, H., "Partial Navigation Courses for a Guided Missile Attacking a Constant Velocity Target" , Report No. R-2790, Naval Research Laboratory, Washington D.C., 3-26-1945.

5. Murtaugh, S.A., Criel, H.E., "Fundamentals of Proportional Navigation" , *IEEE Spectrum* , Vol.3, Dec. 1966, pp. 75-78.

6. Kishi, F.H., "Optimal and Sub-Optimal Designs of Proportional Navigation Systems" , in Lavi, A. and Vogl, T.P.(ed.), *Recent Advances in Optimization Techniques (Proc. of the April 1965 Symposium)* , John Wiley, 1965.

7. Bryson, A.E., "Linear Feedback Solutions for Minimum Effort Interception, Rendezvous, and Soft Landing", *AIAA J.* , Vol. 3, No. 8, 1965, pp. 1542-1544.

8. Bryson, A.E., "Application of Optimal Control Theory in Aerospace Engineering ", *J. Spacecraft* , Vol. 4, No. 5, 1967, pp. 545-553.

9. Kreindler, E., "Optimality of Proportional Navigation ", *AIAA J.* , Vol.11, No. 6, 1973, pp. 878-880.

10. Cottrell, R.G., "Optimal Intercept Guidance for Short-Range Tactical Missiles" , *AIAA Journal* , Vol. 9, July 1971, pp.1414-1415.

11. Cheng, V.H.L., Gupta, N.K., " Advanced Midcourse Guidance for Air-to-Air Missiles ", *Journal of Guidance, Control and Dynamics* , Vol. 9, No.2, 1986.

12. Menon, P.K.A., Briggs, M.M., " A Midcourse Guidance law for Air-to-Air Missiles ", *AIAA-87-2509, Proc. Guidance, Navigation and Control Conference* , Monterey, CA, 1987.

13. Kelley, H.J., "Aircraft Maneuver Optimization by Reduced-Order Approximation" , *Control and Dynamic Systems* , Vol.10, edited by Leondes C.T., Academic Press, New York, 1973, pp.131-178.

14. Katzir, S., "Optimal and On-Board Near-Optimal Midcourse Guidance", *Ph.D. Dissertation, VPI&SU* , Nov, 1988.

15. Katzir, S., Cliff, E.M., Kelley, H.J., "Best-Range Study for a Boost-Sustain Missile ", *Proc. of the ACC* , IEEE, 1988, pp. 145-149.

16. Kelley H.J., " Guidance Theory and Extremal Fields", *IRE Transactions on Automatic Control, AC-7, 75-82* , 1962.

17. Pontryagin, L.S., Boltyanskii, V.G., Gamkrelidze, R.V., and Mischenko, E.F., " The Mathematical Theory of Optimal Processes", *Wiley-Interscience*, New York, 1962.

18. Leitman, G., *An Introduction to Optimal Control* , McGraw Hill, New York, 1966.

19. Bulirsch, R., " Die Mehrzielmethode zur numerischen Losung von nichtlinearen Randwertproblemen und Aufgaben der optimalen Steuerung ", *Lehrgang Flugbahnoptimierung Carl-Cranz-Gessellschaft e.v.*, October, 1971.

20. Leitman, G., *The Calculus of Variations and Optimal Control* , Plenum Press, 1981.

21. Bryson, A.E. and Ho, Y.C., " Applied Optimal Control", *Hemisphere Publishing Corporation*, New York, pp. 177-211.

22. Breakwell, J.V., Ho, Y.C., "On the Conjugate Point Condition for the Control Problem ", *International Journal of Engineering and Science* , Vol.2, pp. 565-579, Pergamon Press Ltd. 1965.

23. Kelley H.J., " An Optimal Guidance Approximation Theory ", *Transactions of the IEEE, AC-9, pp. 375-380* , 1964.

24. Speyer, J.L. and Bryson, A.E., "A Neighboring Optimum Feedback Control Scheme based on Estimated Time-To-Go with Applications to Re-entry Flight Paths", *AIAA Journal 6* , May, 1968.

25. Adler, F.P., "Fundamentals of Proportional Navigation ", *Journal of Applied Physics, Vol. 27, No. 5*, May, 1956.

26. Shinar, J., "Missile Avoidance Maneuvers of Longer Duration ", *Dept. of Aeronautical Engineering , Technion, Haifa, Israel* , Final report, 1984.

27. Shinar, J., "On Applications of Singular Perturbation Techniques in Nonlinear Optimal Control ", *Automatica* , Vol. 19, No.4, 1983, pp. 203-211.

28. Isaacs, J., *Differential Games* , New York, Wiley, 1965.

29. Kaiser, F., Der Steigflug mit Stragflugzeugen - Teil I, Bahngeschwindigkiet fur Bensten Steigen, Versuchsbericht 262-02-L44, Messerschmitt A.G., Augsburg, April 1944 (Translated as Ministry of Supply RTP/TIB translation GDC/15/148T)

30. Ewing, G.M., "Calculus of Variations with Applications", *Dover Publications, Inc.*, New York, pp. 64-68.

31. Lee, E.B. and Markus, L., "Foundations of Optimal Control Theory", *Robert E. Krieger Publishing Company*, Florida.

32. Marec, J.P., "Optimal Space Trajectories", *Elsvier*, New York, 1979.

33. Vinh, N.X., "Optimal Trajectories in Atmospheric Flight", *Elsvier*, New York, 1981.

34. Hermes, H., LaSalle, J.P., *Functional analysis and Time Optimal Control* , Vol. 56, Mathematics in Science and Engineering, Academic Press, N.Y. and London, 1969.

35. Kelley, H.J. and Moyer, H.G., " Computational Jacobi-Test Procedure", Proceedings of Workshop, *Current Trends in Control* ,Dubrovnik, Yugoslavia, June 29-30, 1984, JUREMA, Zagreb, 1985.

36. Hymas, C.E., Cavin R.K. and Colunga D., " Neighboring Extremals for Optimal Control Problems ", *AIAA Journal 11, 1101-1109* , 1973.

37. Pesch, H.J., " Real-Time Computation of Feedback Controls for Constrained Optimal Control Problems", *Technische Universitat Munchen* , 1987.

38. Visser, H.G., "Energy Management of Three-Dimensional Minimum-time Intercept", *Ph.D. Dissertation, VPI&SU* , Aug, 1985.

39. Powers, W.F., " A Method for Comparing Trajectories in Optimum Linear Perturbation Guidance Schemes", *AIAA Journal Vol. 6, No. 12* , Dec, 1968.

40. Powers, W.F., " Techniques for Improved Convergence in Neighboring Optimal Guidance ", *AIAA Journal Vol. 8, No. 12* , Dec, 1970.

41. Cloutier, J.R., Evers, J.H., and Feeley J.J., "An Assessment of Air-to-Air Missile Guidance and Control Technology" , *Proceedings of the ACC*, IEEE, 1988, pp.133-142.

42. Menon, P.K.A., "Short-Range Nonlinear Feedback Strategies for Aircraft Pursuit-Evasion ", *Journal of Guidance, Control and Dynamics* , Vol.12, No.1, pp. 27-32, Jan- Feb 1989.

43. Meyer, G., Su, R., and Hunt, L.R., "Applications of Nonlinear Transformations to Automatic Flight Control ", *Automatica* , Vol.20, pp. 103-107, 1984.

44. Seywald, H., and Well, K.H., "Maximum Range aircraft Trajectory with Dynamic Pressure Constraint" , Research at DFVLR, West Germany, 1986.

45. Kumar R.R., Seywald H., Cliff E.M. and Kelley H.J., " 3-D Air-to-Air Missile Trajectory Shaping Study", *Proc., 1989 AIAA Guidance, Navigation and Control Meeting* .

46. Kumar, R.R., Seywald, H., Cliff, E.M., "Near Optimal 3-D AAM Guidance Against a Maneuvering Evader ", *Proc., 1989 AIAA Guidance, Navigation and Control Meeting* , Submitted.

Appendix A : Missile Model - Aerodynamic and Propulsive

DRAG MODEL

The drag-to-weight ratio of the missile is expressed as:

$$\frac{D}{W} = D_0 + D_i (n)^k$$

where,

$$D_0 = \frac{qS}{W} \; C_{D0}(M,h)$$

and

$$D_i = \left(\frac{qS}{W}\right)^{1-k} \; C_{Di}(M)$$

The altitude dependence in the zero-lift drag-coefficient is expressed as

$$C_{D0}(M,h) = \hat{C}_{D0}(M)\left[1 + \hat{a}\left(\frac{h}{h_m}\right)^m\right] + C_{Dc}(M) f(T)$$

where $\hat{a}, h_m$ and m are constants used in interpolation of the function to approximate experimental data. The values of $\hat{a}, h_m$ and m used for the specific missile model are 1.7742, 200000 ft and 1.833 respectively. The value of k is chosen as 1.8 rather than the usual 2.0, for a better approximation to the aerodynamic data of the drag-polar. $\hat{C}_{D0}$, induced drag-coefficient C_{Di} and base-drag-coefficient C_{Dc} being specified functions of Mach number are as given in Table 1. The C_{Dc} term accounts for the increased drag due to base pressure with the motor shut down. The $f(T)$ is a switch on/off designator and assumes unity with engine off and zero with thrust on. The functions $\hat{C}_{D0}(M)$, $C_{Di}(M)$, $C_{Dc}(M)$, air density $\rho(h)$ and sonic velocity $a(h)$ are constructed as cubic-spline interpolating polynomials.

$q = 0.5\,\rho(h)\,V^2$ is the dynamic pressure. The numerical value of reference area S is 0.3068 sq.ft. The weight of the missile and its variation during flight is discussed later.

THRUST MODEL

The propulsion is of **boost-sustain-coast** type in the same order. The thrust is given as a function of time as shown in Fig. {A.1}. The magnitudes of thrust and the switching time for the model has been selected from [14].

$$T(t) = \begin{Bmatrix} T_b & - & 0 \le t \le t_b \\ T_s & - & t_b < t \le t_s \\ 0 & - & t_s < t \le t_f \end{Bmatrix}$$

T_b and T_s are the boost and sustain thrust magnitudes with numerical values 7500 lbf and 2000 lbf respectively. t_b and t_s are the boost and sustain end times and are chosen as 3 seconds and 9.47 seconds respectively. It is worthwhile to mention here, that an intermediate coast phase between end of boost and initiation of sustain phase is non-optimal (in the sense of range-maximization for prescribed final energy) for the specific model. Morover, research has indicated that any reduction in t_s, keeping the total impulse the same also reduces the range [14]. The thrust magnitudes and its switching times are fixed and are not control variables.

WEIGHT MODEL

The weight at initial time is given as 375 lbf. The rate of change of weight is a constant in each of the phases. The weight history is as shown in Fig. {A.2}. The rate of change of weight is given by:

$$\dot{W}(t) = -W_i \quad (i = b,s)$$

where $W_b = 31.32047$ and $W_s = 8.352125$.

LOAD-FACTOR CONSTRAINTS

The resultant load-factor n is constrained by two limits, namely, the structural limit $n_{\max}$ and the lift-coefficient limit n_L given by:

$$n_L = \left(\frac{q\,S}{W}\right) C_{L\,\max}(M)$$

The control constraint is of the form:

$$n \leq \text{infimum}(n_L, n_{\max})$$

The numerical value of $n_{\max}$ used is 30. The variation of $C_{L\,\max}$ with Mach number is as tabulated in Table 2. The maximum lift-coefficient is also approximated by cubic-spline interpolations.

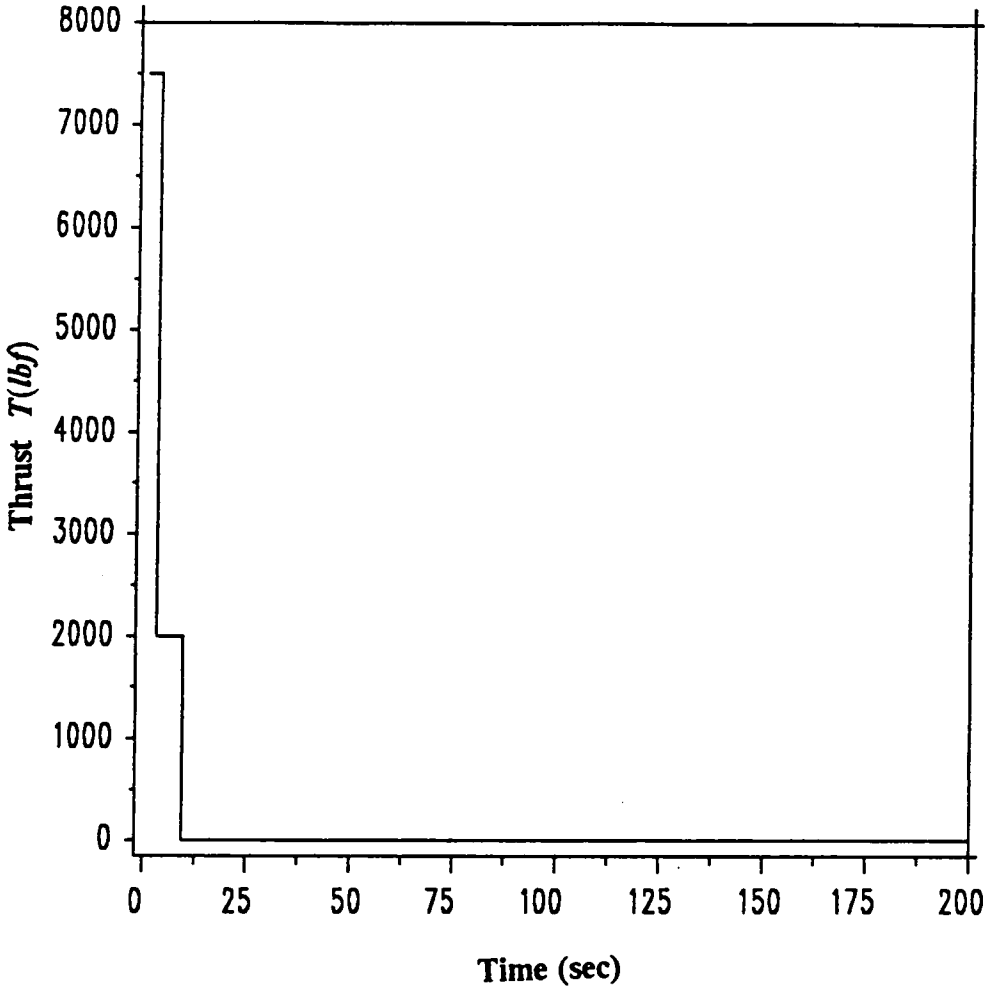

Fig. A.1: Thrust history of boost-sustain-coast missile

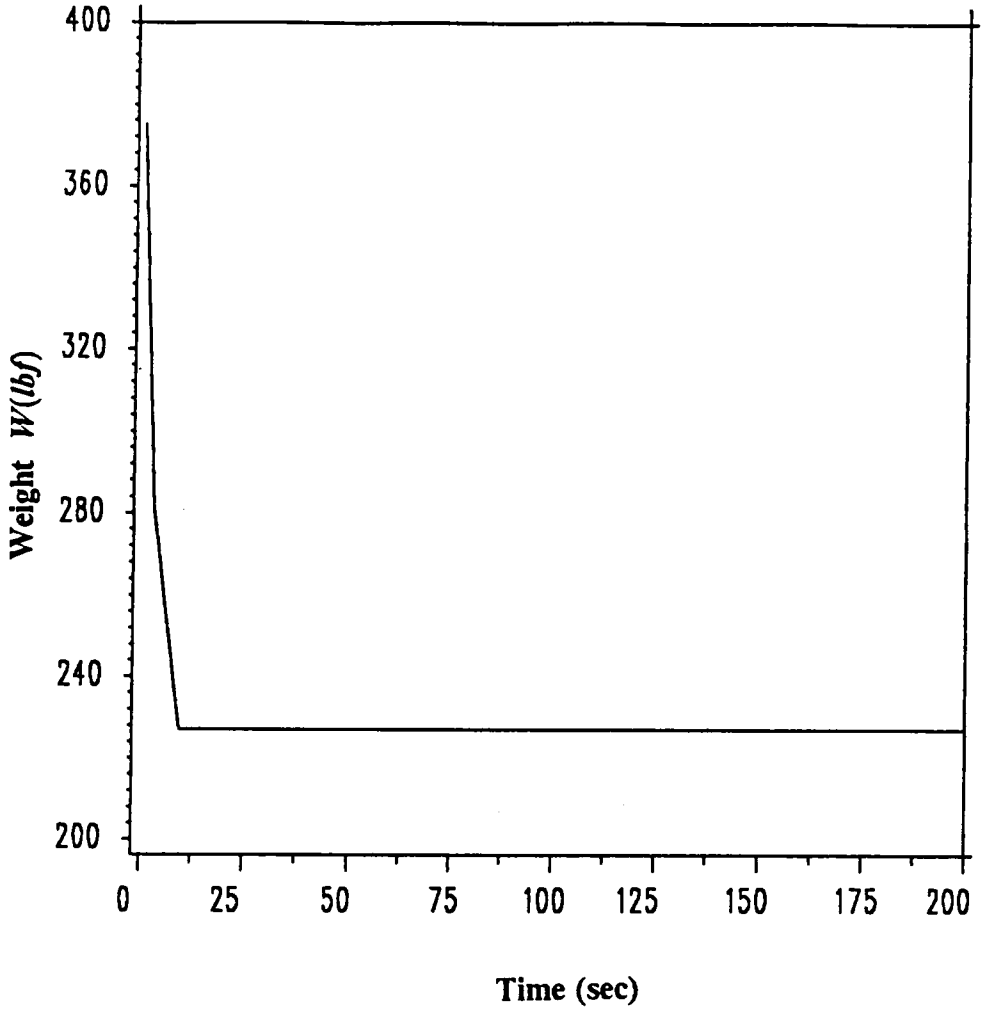

Fig. A.2: Weight history of boost-sustain-coast missile

Table 1: Variation of Drag-coefficients with Mach number

M	$\hat{C}_{D0}$ (M)	C_{DI} (M)	C_{DC} (M)
0.6	0.3350	0.0411	0.1245
0.9	0.3170	0.0392	0.1130
1.2	0.5104	0.0354	0.1813
1.5	0.4620	0.0354	0.1630
2.0	0.3926	0.0372	0.1380
2.5	0.3433	0.0411	0.1135
3.5	0.2513	0.0445	0.0780
4.5	0.2008	0.0495	0.0582

Table 2: Variation of $C_{L\,max}$ with Mach number

M	$C_{L\,max}$ (M)
0.6	19.743
0.9	20.983
1.2	23.620
1.5	23.640
2.0	22.446
2.5	20.926
3.5	18.274
4.5	15.957

Appendix B : Derivation of Riccati-type Differential Equations

FIXED FINAL TIME

The "no-conjugate point" condition as given in [21], requires the finiteness of the matrix $S - R\,Q^{-1}\,R^T$. It is possible during the testing of the same that the above matrix be still finite, but its components S and $R\,Q^{-1}\,R^T$ become infinite. This is illustrated in an example in Chapter 6 of [21]. However, the test matrix is evolved from the components which are governed by coupled ordinary differential equations - and hence the problem.

Suitably, the derivation to be followed, aims at obtaining a differential equation and suitable boundary conditions for the test matrix itself. Define a matrix $H = S - R\,Q^{-1}\,R^T$. This matrix H is not defined at the final time of the test extremal, since matrix $Q(t_f) = [0]$ and hence singular. This new matrix H is

introduced only from $t_f - \varepsilon$. The choice of $\varepsilon > 0$ is arbitrary. The absence of conjugate points at t_f is obvious. Otherwise, the Jacobian associated with the multi-point boundary-value problem would be singular and a converged nominal solution would not be obtained in the first place.

The derivation of the differential equation governing H is performed by formally differentiating H and using suitable substitutions as shown below.

$$\dot{H} = \dot{S} - \dot{R}\,Q^{-1}\,R^T - R\,(\dot{Q^{-1}})\,R^T - R\,Q^{-1}\,\dot{R}^T \qquad (a)$$

The differential equations and boundary conditions governing S, Q and R are given in [21]. The four terms in Eq. (a) are treated separately as shown below. The first term can be written as:

$$\begin{aligned}\dot{S} = & -HA - R\,Q^{-1}\,R^T A - A^T H - A^T R\,Q^{-1}\,R^T + HBH \\ & + R\,Q^{-1}\,R^T BH + HBR\,Q^{-1}\,R^T + R\,Q^{-1}\,R^T BR\,Q^{-1}\,R^T - C\end{aligned}$$

This is obtained by substituting $S = H + R\,Q^{-1}\,R^T$ in the matrix Riccati differential equation for S. The second term in Eq. (a) follows:

$$-\dot{R}\,Q^{-1}\,R^T = A^T R\,Q^{-1}\,R^T - HBR\,Q^{-1}\,R^T - R\,Q^{-1}R^T BR\,Q^{-1}\,R^T$$

The third term in Eq. (a) requires the first time-derivative of Q^{-1} .

$$\frac{d}{dt}\,[I] = [0]$$

implies,

$$\frac{d}{dt}[Q\,Q^{-1}] = [0]$$

which gives the following,

$$\frac{d}{dt}\,Q^{-1} = -\,Q^{-1}\,\dot{Q}\,Q^{-1}$$

Using the governing differential equation for Q, namely $\dot{Q} = R^T B R$,

$$\frac{d}{dt}\,Q^{-1} = -\,Q^{-1}\,R^T B R\,Q^{-1}$$

The third term of Eq. (a) takes the form:

$$-\,R\,(\dot{Q^{-1}})\,R^T = R\,Q^{-1}\,R^T B R\,Q^{-1}\,R^T$$

Using the fact that matrices S and B are symmetric, the fourth term of Eq. (a) takes the form:

$$-\,R\,Q^{-1}\,\dot{R}^T = R\,Q^{-1}\,R^T A - R\,Q^{-1}\,R^T B H - R\,Q^{-1}\,R^T B R\,Q^{-1}\,R^T$$

Adding up all the four terms and cancelling opposite terms it can be shown that the matrix H satisfies the Riccati matrix differential equation satisfied by S , i.e.,

$$\dot{H} = -\,H A - A^T H + H B H - C$$

A necessary condition for no conjugate point on the extremal is that $H(t)$ be finite for all $t_0 \le t < t_f$ The scheme for testing for conjugate points involve

integrating backward in time the $\dot{S}, \dot{Q}$ and $\dot{R}$ differential equations (4.3-4.5) from t_f to $t_f - \varepsilon$, where ε is an arbitrarily small time-step. Evaluate $H(t_f - \varepsilon)$. Integrate backwards in time the differential equation in H using above boundary condition and check for finiteness.

For problems of concern in the specific research, the component matrices for some sample extremals became unbounded near initial time (for final time of 150-200 seconds). Hence large values of ε (more than 10 seconds) could be used.

FREE FINAL TIME

The analysis of the previous section can be closely followed even for final time free with the note that the new matrix is defined as $\overline{H} = \overline{S} - \overline{R}\,\overline{Q}^{-1}\,\overline{R}^T$. The differential equations for $\overline{S}$, $\overline{Q}$ and $\overline{R}$ are the same as for S, Q and R respectively, but with different boundary conditions [21].

$\overline{H}$ follows the following differential equation:

$$\dot{\overline{H}} = -\overline{H}\,A - A^T\overline{H} + \overline{H}\,B\,\overline{H} - C$$

with similar boundary conditions as explained in the previous section.

The vita has been removed from the scanned document